Middle and Upper Pleistocene fluvial terraces in an abandoned valley in Upper Franconia (Germany): Chronology and driving forces

Thomas R. Kolb
geboren in Erlangen

Dissertation
zur Erlangung des akademischen Grades eines
Doktor der Naturwissenschaften
(Dr. rer. nat.)
an der Fakultät für Biologie, Chemie und Geowissenschaften
der Universität Bayreuth

Bayreuth, Germany
Dezember 2017

©2017 – Thomas R. Kolb
all rights reserved.
Typesetting by LaTeX

Die vorliegende Arbeit wurde in der Zeit von 08/2011 bis 12/2017 in Bayreuth am Lehrstuhl für Geomorphologie unter Betreuung von Herrn Professor Dr. Ludwig Zöller angefertigt.

Vollständiger Abdruck der von der Fakultät für Biologie, Chemie und Geowissenschaften der Universität Bayreuth genehmigten Dissertation zur Erlangung des akademischen Grades eines Doktors der Naturwissenschaften (Dr. rer. nat.).

Dissertation eingereicht am: 19.12.2017

Zulassung durch die Promotionskommission: 10.01.2018

Wissenschaftliches Kolloquium: 03.05.2018

Amtierender Dekan: Prof. Dr. Stefan Peiffer

Prüfungsausschuss:
Prof. Dr. Ludwig Zöller (Gutachter)
Prof. Dr. Dominik Faust (Gutachter)
Prof. Dr. Stefan Peiffer (Vorsitz)
PD Dr. Klaus-Martin Moldenhauer

(Weiterer Gutachter: Prof. Dr. Andreas Lang)

Middle and Upper Pleistocene fluvial terraces in an abandoned valley in Upper Franconia (Germany): Chronology and driving forces

Thomas R. Kolb

Abstract

Generally controlled by the development of the Rhenish drainage system, the fluvial history of northern Bavaria is characterized by a high complexity, which is reflected in the irregular spatial alignment of river courses. In particular, this applies to the headwaters of the Main River, which is, with a total length of about 530 km, the longest right-bank tributary of the Rhine River system.

This dissertation deals with the mid- and late-Pleistocene development of the drainage network in the vicinity of the city of Bayreuth. Dominated by the two headwater streams of the Main River, the Red Main River and the White Main River, and by the river Warme Steinach, the area has been the subject of scientific research for more than 100 years. So far, these investigations have focused mainly on the application of well-established methods from the field of sedimentology and lithology, which finally allowed deriving a complex landscape evolution model.

Up to now, however, investigations have been lacking that could provide reliable information on the timing and dynamics of these complex river deflections. The overall objective of this PhD-thesis is therefore to establish a reliable chronological framework for the mid- and late-Pleistocene evolutionary stages of the local drainage system, which is based on modern numerical dating methods.

Our study is located in the unusually wide Trebgast Valley, which is situated in the north of the city of Bayreuth and has been identified as a former valley of the

Red Main River. This valley and its well-preserved fluvial and slope deposits offered ideal conditions for palaeoenvironmental research. Besides additional lithological analyses of fluvial gravel and the evaluation of a high-resolution digital terrain model, the methodological focus was on the application of innovative methods of luminescence dating.

The results of this PhD-thesis partially contradict the age estimates of earlier studies and indicate a much more complex landscape evolution than previously assumed. Specifically, our findings suggest an additional evolutionary stage that spans the period from ~ 30 ka to ~ 20 ka. For the older fluvial terraces identified within the research area, new techniques of luminescence dating had to be applied, which allow a significant extension of the dating range. Our findings, however, prove serious methodological issues, which make the evaluation and classification of the determined ages considerably more difficult.

Finally, the luminescence ages derived for samples, which originated from the Upper Pleistocene fluvial terrace of the Steinach River, suggest a diachronic character of river incision processes. If this finding can be confirmed for other river systems and do not turn out as a mere local feature associated with the specific regional environmental setting, it will have a significant impact on the interpretation of age estimations for fluvial sediments in general.

Zusammenfassung

Generell gesteuert durch die Entwicklung des rhenanischen Abflusssystems, ist die Flussgeschichte Nordbayerns insgesamt durch eine hohe Komplexität gekennzeichnet, welche sich in der unregelmäßigen räumlichen Anordnung der Flussläufe widerspiegelt. Namentlich gilt dies für das Quellgebiet des Mains, der mit einer Gesamtlänge von etwa 530 km der längste rechtsseitige Zufluss des Rheinsystems ist.

Die vorliegende Doktorarbeit befasst sich mit der mittel- und spätspleistozänen Flussgeschichte des Entwässerungsnetzes in der unmittelbaren Umgebung von Bayreuth. Dominiert von den beiden Quellflüssen des Mains, dem Roten Main und dem Weißen Main, sowie dem Fluss Warme Steinach ist das Gebiet bereits seit mehr als 100 Jahren Gegenstand wissenschaftlicher Untersuchungen. Diese

Untersuchungen konzentrierten sich bislang hauptsächlich auf die Anwendung etablierter Methoden der Sedimentologie und Lithologie, welche schließlich die Erstellung eines komplexen Landschaftsentwicklungsmodells ermöglichten.

Bislang fehlten indes Untersuchungen, die verlässlich Auskunft über die zeitliche Einordnung und die Dynamik dieser komplexen Flusslaufverlagerungen geben konnten. Die übergeordnete Zielsetzung der vorliegenden Arbeit ist daher die Erstellung einer verlässlichen chronologischen Gliederung für die mittel- und spätpleistozänen Entwicklungsphasen des lokalen Abflusssystems, die auf modernen numerischen Datierungsmethoden beruht.

Das ungewöhnlich breite Trebgasttal im Norden Bayreuths, das als ehemaliges Tal des Roten Mains identifiziert werden konnte, bot mit seinen gut erhaltenen fluvialen Ablagerungen und Hangschuttsedimenten ideale Rahmenbedingungen. Neben der lithologischen Analyse fluvialer Schotter und der Auswertung eines hochaufgelösten digitalen Geländemodells lag der methodische Schwerpunkt auf der Anwendung innovativer Verfahren der Lumineszenzdatierung.

Die Ergebnisse der vorliegenden Arbeit stehen teilweise im Widerspruch zu Alterseinschätzungen früherer Untersuchungen und weisen auf eine deutlich komplexere Landschaftsentwicklung als bislang angenommen hin. Konkret legen unsere Befunde eine zusätzliche Entwicklungsphase nahe, welche den Zeitraum von etwa 30 ka bis 20 ka umfasst. Für die älteren Terrassen des Untersuchungsgebietes mussten neue Techniken der Lumineszenzdatierung eingesetzt werden, welche eine deutliche Ausweitung der Datierungsreichweite ermöglichen. Unsere Befunde belegen indes methodische Schwierigkeiten, welche die Auswertung und Einordnung der ermittelten Alter erheblich erschweren.

Die Lumineszenzalter für Proben der jüngsten pleistozänen Steinach-Terrasse deuten schließlich auf einen diachronen Charakter von Flusseinschneidungsprozessen hin. Sollte sich dieser Befund auch für andere Flusssysteme bestätigen lassen und sich nicht nur als lokale Besonderheit erweisen, hätte er erhebliche Auswirkungen auf die Interpretation von Alterseinschätzungen für fluviale Sedimente.

Preface

This dissertation is part of a regional research project entitled *Kultur- und Landschaftsgeschichte Oberfrankens – Das Trebgasttal und seine Entwicklung (Cultural and landscape development in Upper Franconia – The Trebgast Valley and its evolution)*. The project was generously funded by the Oberfrankenstiftung (Upper Franconia Foundation) ever since the year 2011. The general aim of the project was to gain new information on the late Pleistocene and early Holocene landscape evolution in the region of Upper Franconia, Northern Bavaria (Germany). Thereby, natural geomorphic processes triggered by changing climatic conditions as well as the special role and increasing importance of human settlers, who have had a lasting impact on Holocene landscapes ever since the first Neolithic settlements, were investigated.

In this context, information on palaeoenvironmental changes and on early human activities were derived from various sedimentary archives located in the Trebgast Valley and the adjacent Red Main Valley close to the city of Bayreuth. The reconstruction of palaeoenvironmental conditions based on sedimentary archives, however, requires the availability of precise and reliable regional chronologies. As those high-resolution chronologies have so far not been established in the study area, a major part of the project dealt with establishing a local chronostratigraphical framework as basis for further palaeoenvironmental and archaeological research.

By applying innovative dating techniques from the wide field of luminescence dating approaches, the present dissertation contributes to constraining time frames for different evolutionary stages identified in the research area. In particular, it is focusing on determining age information for the accumulation of a set of five distinct Pleistocene fluvial terraces. While aspects of human impact on landscape evolution are not part of this thesis, it significantly contributes to improve the knowledge about the regional landscape evolution in Upper Franconia during the mid- and late-Pleistocene period and additionally provides new insights into the timing of terrace formation and fluvial dynamics that go far beyond a merely local or regional focus.

Dedicated to my beloved wife

Contents

I Conceptual design 1

1 Introduction 3
1.1 Research area and research history 5
1.2 Central aims of this PhD-thesis 10
1.3 Thesis outline 12
1.4 List of manuscripts and own contribution 14

2 Methods and material 17
2.1 Fundamentals of luminescence dating 18
2.1.1 Basic principle 18
2.1.2 Physical background of the luminescence phenomenon 21
2.1.3 Dosimeters and measurement procedures 30
2.2 Determination of equivalent doses – measurement protocols . . 41
2.2.1 The multiple aliquot additive dose protocol (MAAD-protocol) 42
2.2.2 The single aliquot regenerative dose protocol (SAR-protocol) 46
2.2.3 The post-IR IRSL protocol at 225°C ($pIRIR_{225}$-procedure) and fading correction 54
2.3 Dosimetry 61
2.4 Applied workflow for luminescence dating in the present PhD-thesis 69
2.4.1 Sample collection and preparation 69
2.4.2 Measurement facilities 73

II Publications 77

3 Study One: Quaternary river terraces and hillslope sediments as archives for palaeoenvironmental reconstruction: new insights from the headwaters of the Main River, Germany 79
3.1 Introduction 81

3.2 Study area . . . 85
3.2.1 General information and river drainage system . . . 85
3.2.2 Geological and geomorphological setting . . . 86
3.2.3 Fluvial history . . . 89
3.3 Methods and materials . . . 91
3.3.1 Qualitative petrographic analyses . . . 91
3.3.2 Malacological analyses . . . 92
3.3.3 Sediment dating . . . 93
3.4 Results . . . 96
3.4.1 Petrographical analyses . . . 96
3.4.2 The composition of the mollusk assemblage at the Crottendorf site . . . 96
3.4.3 Dating results . . . 100
3.5 Discussion . . . 103
3.5.1 Petrographical analyses . . . 103
3.5.2 T2-terrace accumulation and timing of the final deflection of the Steinach River . . . 103
3.6 Conclusion . . . 107

4 Study Two: Deciphering fluvial landscape evolution by luminescence dating of river terrace formation: a case study from Northern Bavaria, Germany 109
4.1 Introduction . . . 111
4.2 Study area . . . 114
4.3 Sampling design . . . 117
4.4 Methods . . . 118
4.4.1 OSL sample preparation and measurement procedure 118
4.4.2 Luminescence properties and rejection criteria . . . 120
4.4.3 Insufficiently bleached samples and age calculation models . . . 120
4.5 Results – sample characteristics and age calculation . . . 121
4.6 Discussion . . . 126
4.6.1 The timing of the T2 terrace formation . . . 126
4.6.2 Diachronic character of river incision? . . . 129
4.7 Conclusion . . . 131

5 Study Three: Luminescence dating of pre-Eemian (MIS 5e) fluvial terraces in Northern Bavaria (Germany) – benefits and limitations of applying a $pIRIR_{225}$-approach 133
5.1 Introduction . . . 135
5.2 Study area and sampling locations . . . 140

5.3 Methodology . . . 146
5.3.1 Sample preparation and instrumental facilities . . . 146
5.3.2 Measurement protocols and setup for equivalent dose determination . . . 147
5.3.3 Fading measurements, dose recovery and bleaching experiments . . . 149
5.3.4 Dosimetry . . . 151
5.4 Results and discussion . . . 153
5.4.1 OSL and IRSL properties . . . 153
5.4.2 Dose response curves and equivalent dose distributions 157
5.4.3 Post-IR IRSL residual doses . . . 160
5.4.4 Fading rates and fading correction . . . 163
5.4.5 Luminescence ages . . . 166
5.5 Conclusion . . . 175

III Synthesis and outlook 177

6 Synthesis 179

7 Outlook 187

References 190

IV Appendix 219

Appendix A Radionuclide conversion factors 221

Appendix B Attenuation factors 223
B.1 Grain size attenuation factors . . . 223
B.2 Etch depth attenuation factors . . . 226
B.3 Water attenuation factors . . . 227

Appendix C Radioactive decay chains 229

Appendix D List of publications and presentations 233
D.1 Scientific articles . . . 233
D.2 Conference talks . . . 234
D.3 Invited talks . . . 235
D.4 Conference posters . . . 235

Appendix E Declarations 237

List of Figures

1.1 General map of Germany 6
1.2 General map of Upper Franconia and detailed map of the Trebgast Valley 7
1.3 3D-model of the research area 11

2.1 The principle of luminescence dating 19
2.2 Distribution of electronic states and band gap 23
2.3 Energy band model 25
2.4 Efficiency of sunlight bleaching for optical signals of quartz and feldspar separates 31
2.5 Three routes of luminescent electron-centre recombinations . . 35
2.6 Simplified schematic model of energy bands in feldspar minerals 37
2.7 MAAD growth curve 43
2.8 The single aliquot regenerative dose protocol (SAR) 48
2.9 SAR dose response curve 50
2.10 The post-IR IRSL 225°C protocol 56
2.11 Radioactive decay 63
2.12 Thick source alpha counting 74

3.1 Overview map of Upper Franconia 82
3.2 Geological map of Upper Franconia 84
3.3 Detailed map of the Trebgast Valley 87
3.4 Schematic cross-section of the Trebgast Valley 88
3.5 Evolutionary stages 90
3.6 Sampling locations 94
3.7 Results of the qualitative petrographic analyses 98
3.8 Compilation of the malacological results 100
3.9 The Crottendorf site 101

4.1 Study area in northern Bavaria (Germany) 115
4.2 Schematic cross-section of the Trebgast Valley 115
4.3 The Pleistocene terraces of the study area 116
4.4 Typical OSL shine-down curve, growth curve and equivalent dose distribution 122
4.5 Luminescence ages for sampling locations in the Trebgast Valley 127

5.1 Research area and sampling locations 138
5.2 Stratigraphic logs of the sampling sites 144

5.3 Photos of the sampling sites 145
5.4 Luminescence shine-down curves and additional information . 154
5.5 Quartz recuperation and recycling ratios 155
5.6 Quartz: dose recovery test (DRT) 155
5.7 Feldspar: dose recovery tests (DRT), recuperation and recycling ratios 156
5.8 Abanico plots and dose response curves 158
5.9 $pIRIR_{225}$ residual doses 160

6.1 Additional evolutionary stage 182
6.2 Marine isotope stages (MIS) and luminescence ages 186

C.1 ^{40}K- and ^{87}Rb-decay 229
C.2 ^{238}U-series 230
C.3 ^{235}U-series 231
C.4 ^{232}Th-series 232

List of Tables

3.1 Qualitative petrographic analyses results 97
3.2 Dosimetric data 102
3.3 OSL-dating results 104

4.1 Stratigraphically derived age estimations for different terrace levels 114
4.2 Dosimetric data 124
4.3 OSL-dating results 125

5.1 Basic information 142
5.2 Applied OSL and post-IR IRSL measurement protocols 148
5.3 Analytic dose rate data 152
5.4 OSL results for quartz samples 167
5.5 Results for $pIRIR_{225}$-measurements 172

A.1 Radionuclide conversion factors 222

B.1 Grain size attenuation factors for alpha particles 224
B.2 Grain size attenuation factors for beta particles 225
B.3 Etch depth attenuation factors for beta particles 226
B.4 Water content attenuation factors 227

Acknowledgments

This PhD-thesis is the result of more than five years of scientific research, particularly focusing on luminescence dating of fluvial archives and furthermore dealing with a wide variety of sedimentological, stratigraphical and geomorphological issues. During this time many people crossed my paths, influencing my specific points of view and supporting my work in many different ways.

First of all, I would like to thank my two supervisors Prof. Dr. Ludwig Zöller (University of Bayreuth) and Prof. Dr. Markus Fuchs (Justus-Liebig-University Gießen) for their steady and encouraging support. They never failed to emphasize the great importance of maintaining a critical point of view, especially when dealing with well-established scientific ideas. They showed me innovative and interesting ways of re-thinking specific geomorphological models as well as methodological approaches in the field of luminescence dating. Without their great experience in practical fieldwork and luminescence dating methodology this study would not have been possible. They were always able to support my work either by giving a helping hand during sampling procedures in the field or by long-lasting and interesting discussions on specific measurement parameters, alternative approaches and result interpretation.

Great thanks to my co-authors who were able to significantly improve the quality of the manuscripts by critical and comprehensive commands. Especially, I would like to thank Dr. Olivier Moine (UMR CNRS 8591) for doing the malacological analyses for the Crottendorf mollusk assemblage. Although I was seriously cursing while I had to prepare 30 kg of sampling material just to separate all those tiny little snails you needed for your analyses, the cooperation with you was really a great pleasure.

I also would like to thank Manfred Fischer for introducing me to the practical workflow of sample preparation in the luminescence laboratory at the University of Bayreuth. Especially, I have to thank him for explaining details of the technical facilities in the lab as well as for showing me innovative and sometimes fancy ways of coping with the various practical and technical problems that emerged during

my time at the Bayreuth luminescence laboratory.

Dr. Sebastian Kreutzer (Université Bordeaux Montaigne) and Dr. Christoph Schmidt (University of Bayreuth) are both thanked for fruitful discussions on specific luminescence dating problems as well as on general scientific developments. Furthermore, I would like to express my gratitude to PD Dr. Klaus-Martin Moldenhauer (University of Bayreuth). I really appreciated that I was able to use every single opportunity to join you on various fieldtrips to the vicinity of the city of Bayreuth. During these fieldtrips I was able to benefit from your great experience with practical fieldwork.

During my time at the University of Bayreuth I had the great pleasure to act as a (co-)supervisor for a large number of BSc- and MSc-thesis. Applying a wide range of either well-established or innovative methods, some of these thesis were really extraordinary. Although only a few of them had a direct impact on this PhD-thesis (e.g., parts of the petrographic analyses used for Study 1 have been performed by Julian Brindel), all of them somehow influenced the way this PhD-thesis was carried out. Therefore, I would like to thank all students involved in the Trebgast Valley project for their GIS-based landscape modelling approaches, their petrographic and sedimentological analyses, for digging trenches, counting fluvial gravels and keeping the Mastersizer busy by doing grain size analyses, for determining palaeomagnetic parameters and finally for luminescence dating of colluvial sediments and channel fills indicating changing human impact on landscape evolution.

Although not directly involved in the project from which this PhD-thesis arises I would also like to thank my great colleagues from the working group of Prof. Dr. Dominik Faust (Technical University of Dresden). Over the last few years, we were able to do several fieldtrips to Central Spain and Fuerteventura during which I had the chance to get to know your thrilling way of performing work in the field. The never-ending night-time discussions about aeolian and fluvial systems were really fascinating. Guys, it was always a great pleasure to have you around!

Finally, I would like to thank my family who enabled me to start my university studies and always encouraged me to continue my scientific career. In particular, this applies to my beloved wife Katja who not only never failed in providing huge amounts of chocolate and cheesecake whenever this appeared to be necessary but who was also always there whenever I needed a helping hand or someone to talk to. Our long lasting evening discussions about measurement procedures, data analysis,

R-codes and specific statistical problems were really elucidating. Although we were not always able to find a consensus which we both could agree on (what might be due to the fact that you as a climatologist are working on completely different problems concerning the atmospheric circulation whereas I spend most of my time digging in the dirt) it was always a great pleasure having those discussions. With your encouraging and loving smile and your fascinating eyes you have always been a bright light guiding me the way even through the darkest night.

Part I

Conceptual design

1

Introduction

Fluvial systems are regularly regarded as an essential part of the general geomorphological system and can be found in nearly all environmental settings all over the world (e.g., Vandenberghe, 2002; Charlton, 2008). Revealing an amazing diversity of forms (e.g., Charlton, 2008), rivers must always be interpreted as product of their specific landscapes (e.g., Fryirs & Brierley, 2013). Extremely sensitive to external and internal forcing, they reflect the particular characteristics of climatological and geological conditions as well as the site specific vegetation cover or the local and regional topographical and hydrographical settings, which as a whole are controlling the specific geomorphic processes occurring in a catchment area (e.g., Charlton, 2008).

Thereby, fluvial systems are always characterized by inherent complexities (e.g., Fryirs & Brierley, 2013), not only including process-response relationships on the valley floors, but also hillslope and other processes that exert a primary control on fluvial activity by means of sediment supply and water retention. Moreover, fluvial systems also reflect temporal changes of environmental conditions to which they adjust in very specific ways. These adjustments are regularly preserved in depositional series (e.g., Vandenberghe, 2002) whose varying sedimentary characteristics can be attributed to palaeoclimatic variations and corresponding changes in fluvial discharge and sediment load. The sedimentary records of rivers, which are

often referred to as valuable climatological and palaeoenvironmental archives, are crucial sources of information for the reconstruction of fluvial landscape evolution.

Besides research projects dealing with drainage network response to tectonic uplift and providing new insights on the relation between fluvial systems and tectonic activity (e.g., Demoulin et al., 2017), many studies focused on analysing the increasing anthropogenic impact on landscape evolution and fluvial dynamics (e.g., Mishra et al., 2007; Antoine et al., 2010; Wolf et al., 2014). As sedimentary bodies of fluvial systems regularly contain a considerable amount of archaeological artefacts, they are important sources of geoarchaeological research, providing essential information on human occupation, agricultural activities and even on changes in ancient human societies (Cordier et al., 2015).

In summary, fluvial archives provide a palaeoenvironmental record, comprising the historical period, the Holocene as well as the Pleistocene (e.g., Cordier et al., 2015) and, at least in some fluvial systems, even a large part of the Cenozoic (e.g., Schoorl & Veldkamp, 2003; Maddy et al., 2007). Apart from their essential importance for palaeoenvironmental research, many studies highlight the particular relevance of studying fluvial archives in order to understand present-day fluvial systems and to assess the potential impacts on these systems triggered by the future global change (e.g., Gregory et al., 2006; Herget et al., 2007).

What applies to fluvial sediments in general, is even more true for river terraces. River terraces are widespread geomorphic features, known from various landscapes and climates all over the world. They allow the investigation of fluvial systems on different temporal (e.g., Gibbard & Lewin, 2009; Westaway et al., 2009; Hobo et al., 2010; Wallinga et al., 2010) and spatial scales (e.g., Bridgland et al., 2007; Bridgland & Westaway, 2008a). However, although intensely investigated, many aspects of river terrace formation, such as the specific boundary conditions, the exact mechanisms and its dynamics, are still not completely understood, revealing the great need for further systematic fluvial research. This is specifically true for the complex river drainage system in Northern Bavaria, Germany, for which our research project intended to derive new information on river dynamics and on the timing of terrace formation.

1.1 Research area and research history

The research area is a small abandoned valley in the headwaters of the Main River and is located in a region named Upper Franconia (Oberfranken), which is situated in the north-east of Bavaria, Germany (see Figure 1.1). The valley was named after the small Trebgast Creek, which is a tributary to the White Main River (see Figure 1.2). With a total length of only ~18 km, the Trebgast Creek reveals an average discharge of ~0.421 m^3/s (Bayerisches Landesamt für Umwelt, 2017c).

According to the Köppen-Geiger climate classification the climate of the research area can be classified as *Cfb-climate* (marine west coast climate/oceanic climate). The average annual precipitation is ~745 mm and average temperatures are about 8.7°C[1].

The fluvial system in the vicinity of the city of Bayreuth is dominated by two headwater streams of the Main River. The *White Main River* originates in the nearby crystalline basement area of the Fichtel Mountains ('Fichtelgebirge') east of our study area. It has a total length of ~52 km and shows an average discharge of ~4.07 m^3/s (Bayerisches Landesamt für Umwelt, 2017b). The *Red Main River's* source is located 10 km to the south of the city of Bayreuth in an area characterized by mesozoic sedimentary rocks. At first, the southernmost part of the Red Main Valley is showing an overall south-north alignment. Near the city of Bayreuth, however, the Red Main River is sharply bending to the west, flowing through the Bayreuth Basin and changing its course to a general north-western direction (see Figures 1.2 and 1.3). With a total length of ~72 km and an catchment area size of ~520 km^2, the Red Main River reveals an average discharge of ~3.14 m^3/s measured at the gauging station in Bayreuth (Bayerisches Landesamt für Umwelt, 2017a).

Also originating in the Fichtel Mountains, a third river, important for the local drainage system, is the river *Warme Steinach* which hereafter is normally mentioned as *Steinach River*. Although the distance between source and mouth is only ~25 km, the Steinach River overcomes a pronounced difference in elevation of ~450 m and is, therefore, characterized by a steep slope. Despite the rather low average discharge of ~1.21 m^3/s (Bayerisches Landesamt für Umwelt, 2017d), the Steinach River

[1] Ten-year-average values calculated for the period 1998-2007; http://www.bayceer.uni-bayreuth.de/mm/de/klima/5407/BotGar/Klima_BotG.php [accessed online 2017-11-30].

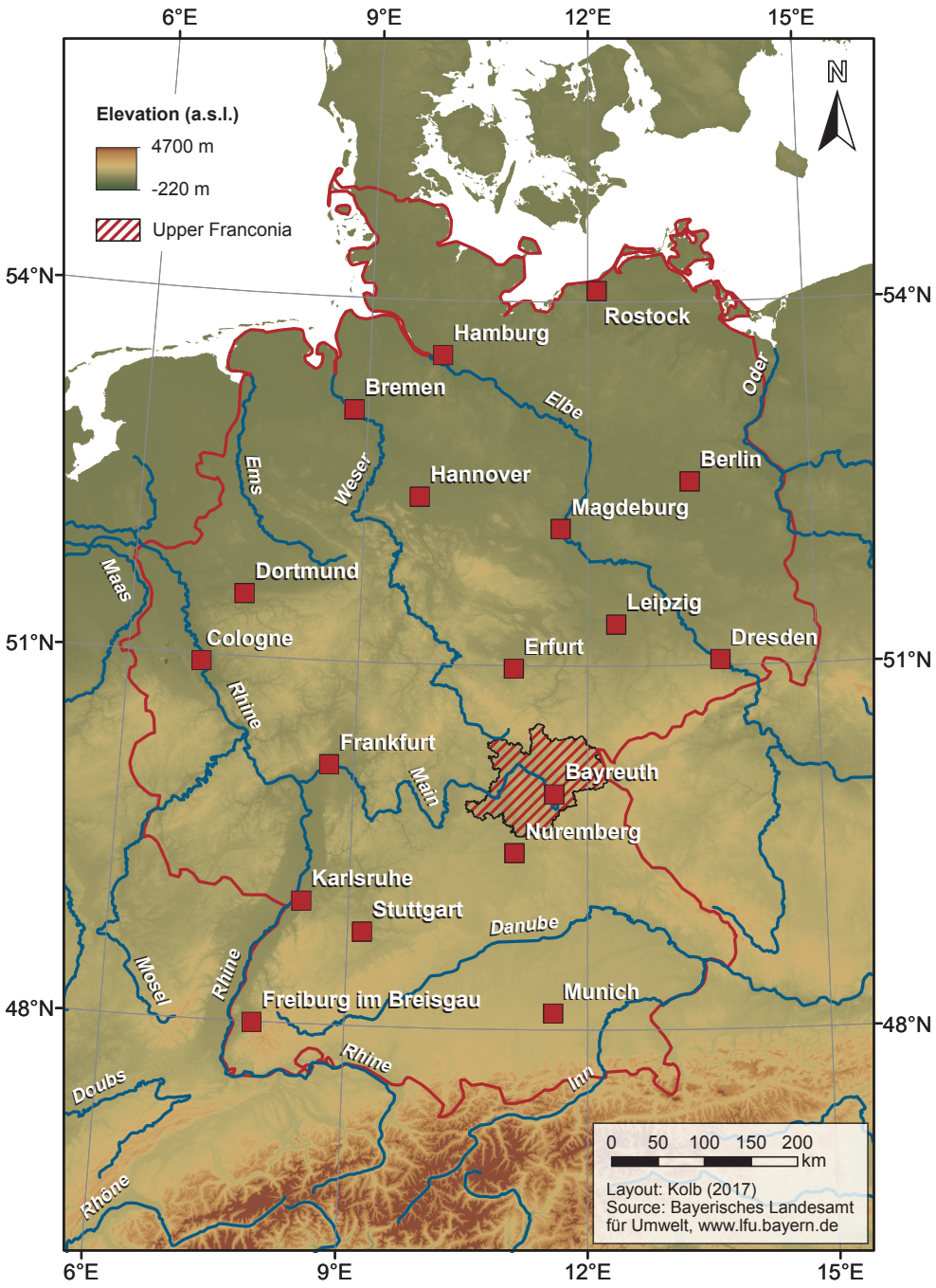

Figure 1.1: General map of Germany. The region of Upper Franconia is located in the north-eastern part of Bavaria and highlighted in the map.

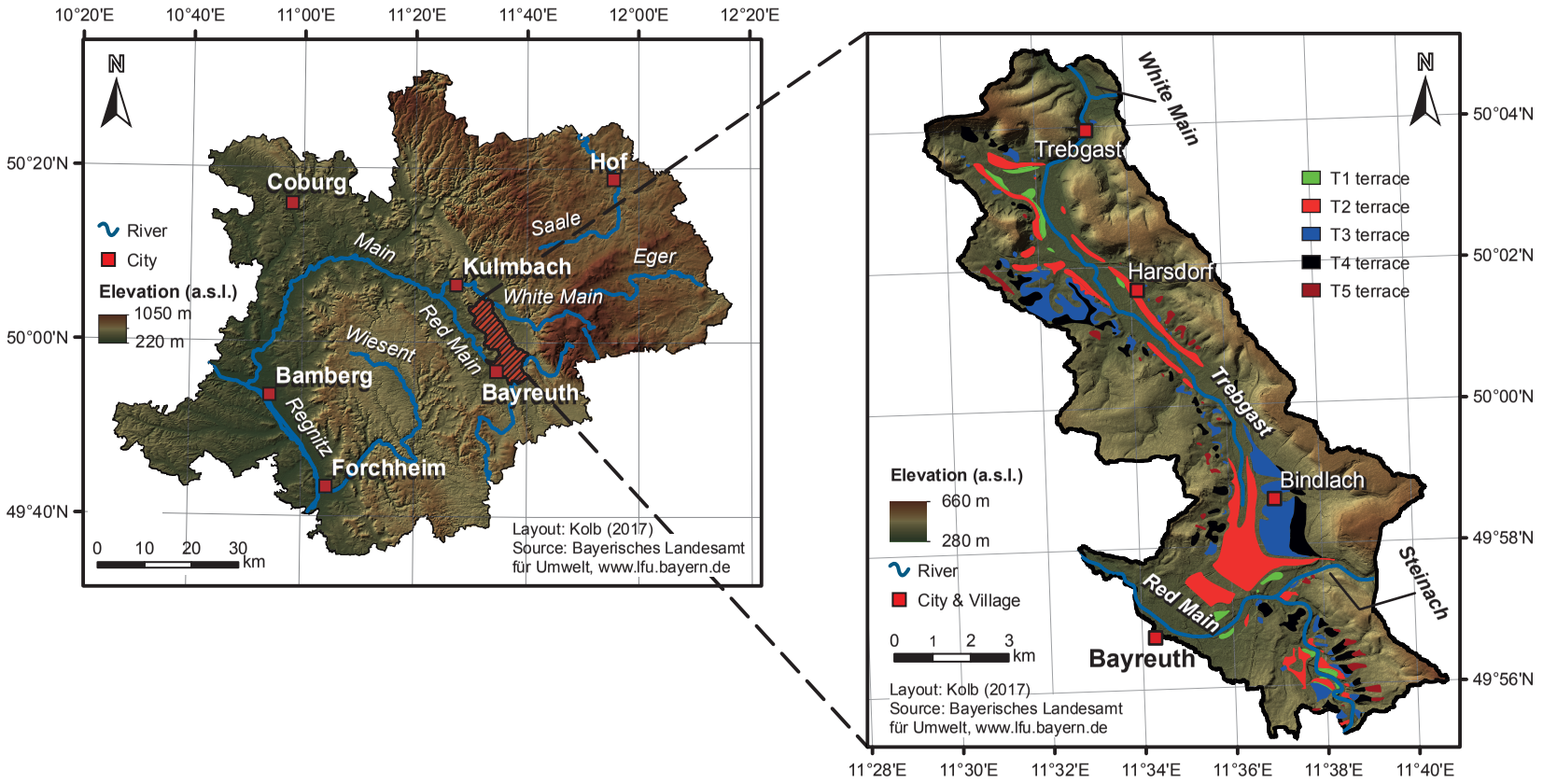

Figure 1.2: General map of Upper Franconia (left side) and detailed map of the Trebgast Valley (right side). Important cities/towns and rivers are highlighted. The detailed map of the research area on the right side also illustrates the five Pleistocene terrace levels identified by Kleber & Stingl (2000).

reveals a high transport capacity. For further details on the geology of the surroundings and on the geomorphological setting of the Trebgast Valley, the reader is referred to the explanations given in Study 1 on page 85.

The evolution of the river drainage system in Northern Bavaria since the onset of the Neogene can be characterized as a process of great complexity, which was generally controlled by the development of the Rhine system. Whereas the present Main River is a tributary of the Rhine River, the primal Main River was initially established on a south-dipping peneplain, reaching from the Franconian Forrest in the north to the Molasse Basin in the northern Alpine Foreland (e.g., Schirmer, 1984, 2010, 2014). In order to clearly discriminate between early stages of the progressively extended present-day course of the Main River and this overall south-directed stream, Schirmer (1984) introduced the name '*Moenodanuvius*' to characterize the latter, a term which may be translated as '*Main-Danube-River*' (e.g., Zöller et al., 2012a,b).

Due to the subsidence of the Upper Rhine Graben, the Rhine River was able to enlarge its catchment area by stepwise headwater erosion and river deflections (e.g., Eberle et al., 2010; Schirmer, 2010, 2012). Thereby, more and more originally south directed rivers and creeks were deflected to the more erosive Rhine system. As a result, the watershed between the Rhine and the Danube river systems was gradually shifted further to the southeast, leaving behind an irregular drainage system characterized by various triangular and rectangular changes in the courses of the involved rivers. A striking example for this development can be seen in the shape of the present-day course of the Main River. More and more headwater streams of the south-directed Moenodanuvius were deflected, finally resulting in the Moenodanuvius to vanish till the end of the Pliocene (e.g., Schirmer, 2012, 2014). Meanwhile the overall establishment of the River Main as the longest right bank tributary of the Rhine drainage system was more or less completed by the onset of the Pleistocene (e.g., Zöller et al., 2012a,b).

After that, there were still further second order river deflections occurring in the headwaters of the Main River during the Quaternary. The latest of these Upper to Middle Pleistocene river deflections took place in the so called Trebgast Valley, an oversized valley in the north of the city of Bayreuth, Bavaria, Germany (e.g., Zöller et al., 2012a,b). Within this dry valley, five well-preserved Pleistocene terraces can be distinguished. These river terraces are interpreted as the result of a

very complex landscape evolution, characterized by an at least twofold river deflection involving two important headwater streams of the Main River (e.g., Kleber & Stingl, 2000; Zöller et al., 2007).

The evolution of the Trebgast Valley has been discussed among geoscientists for over a century. A first scientific publication by Reck (1912) was the reason for a long lasting and controversial debate on the landscape evolution in the headwaters of the Main River in general and on the Red Main River's significance to the development of the Trebgast Valley in particular.

Mainly based on morphological and lithological evidence as well as on the spatial alignment of the valleys (see Figure 1.3), Reck (1912) and others (e.g., Seefeldner, 1914; Stadelmann, 1924; Körber, 1962) concluded that the Trebgast Valley was originally drained by the Red Main River. This opinion was first contradicted by Henkel (1917) and Henkel (1920), whose point of view was picked up by Emmert & Weinelt (1962) as well as by Emmert (1977). They doubted the lithological evidence provided by Reck (1912) and others and, on the contrary, interpreted the Trebgast Valley as a former valley of the primary Steinach River. According to their opinion, only the primary Steinach River drained the Trebgast Valley to the north, before it was deflected to its present-day course as tributary of the Red Main River.

It was not until recent time that new studies (e.g., Kleber et al., 1988; Kleber & Stingl, 2000; Zöller et al., 2007) were able to prove the participation of both rivers in the evolution of the Trebgast Valley and to derive the complex landscape evolution model (e.g., Kleber & Stingl, 2000), which was the starting point of this PhD-thesis. With a palynological study, conducted by Ertl (1987) during the 1980s, and a study focusing on sedimentological and palaeopedological issues of loess-loam bearing cover sediments by Veit (1991), there have been approaches from which first evidence could be derived to determine a chronological framework for the different stages of the valley's evolution. However, these palynological and morphostratigraphical evidence could just be used to approximate the timing of the river deflections (e.g., Zöller et al., 2007) and strongly depend on specific assumptions and individual interpretations. So far, there has always been a considerable lack of numerical datings for the research area.

1.2 Central aims of this PhD-thesis

With respect to the long lasting research history of more than 100 years, it is of crucial importance to highlight the central aims of this study. As already mentioned above, fluvial sedimentary records and especially river terraces provide valuable climatological and palaeoenvironmental archives. The importance of fluvial terraces in geomorphology, archaeology and modern river engineering is well documented by a huge and still growing number of studies spanning a wide range of climatic and regional settings (e.g., Buch, 1988; Houben, 2003; Knox, 2006; Schirmer, 1983; Schirmer et al., 2005; Vandenberghe, 2015).

However, the information gained from fluvial terraces and their significance for paleoenvironmental research strongly depend on an accurate dating of the terrace formation (e.g., Fiebig & Preusser, 2003). Numerical ages are of fundamental importance for interpreting sedimentological, morphological or stratigraphical findings. They are essential for assessing the influence of various driving forces (e.g., Cordier et al., 2015) and for providing insights into river adjustments over differing timeframes (e.g., Fryirs & Brierley, 2013). Without a reliable chronological framework, reconstructing past fluvial environments would not be possible.

Although our study area has long been the subject of geoscientific research, all age estimations proposed for the different evolutionary stages are only based on indirect conclusions, derived from sedimentological or stratigraphic findings. With regard to numerical dating, the entire region of Upper Franconia and specifically the area in the vicinity of the city of Bayreuth is characterized by considerable gaps.

Taking into account the previous considerations, the central aim of the present PhD-thesis is to establish a reliable chronology for the individual evolutionary stages proposed for the local drainage system by previous studies (e.g., Kleber et al., 1988; Kleber & Stingl, 2000). Based on the numerical approach of luminescence dating, this chronological framework is intended to provide the basis for future investigations, deriving conclusions on boundary conditions, driving forces and dynamics of fluvial processes in the research area.

With respect to this central aim, the present PhD-thesis addresses two major research questions:

1. Is it possible to confirm findings of previous studies, which derived age estimations on the distinct evolutionary stages from sedimentological and stratigraphical evidence, when numerical dating procedures are applied?

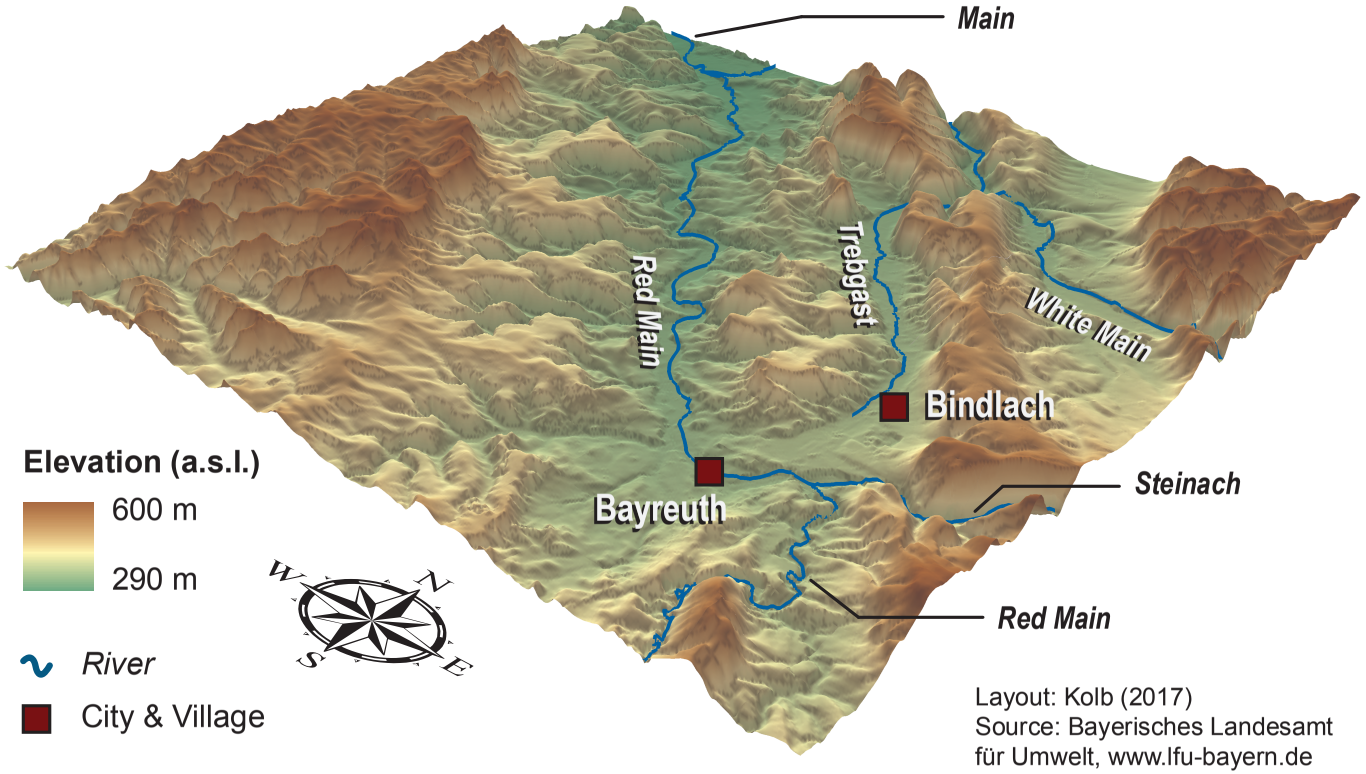

Figure 1.3: 3D-model of the research area illustrating the spatial alignment of the valleys near the city of Bayreuth. Coming from the south, the Red Main River is not continuing its north directed course any more, but is suddenly bending to the west when it reaches the city of Bayreuth. Due to this very specific spatial alignment of valleys and additionally supported by lithological evidence, Reck (1912) was the first to conclude that the Trebgast Valley represents a former Red Main Valley interconnecting the Red Main/Steinach system in the south and the White Main system in the north.

2. Can innovative techniques of luminescence dating (post-IR IRSL procedures) successfully be used to derive age information on fluvial sediments which are assumed to reveal ages that have so far been beyond the dating range of standard luminescence approaches?

1.3 Thesis outline

After this short introduction, a methodological chapter (*Chapter 2*) is introducing the basic principles of luminescence dating as well as its physical background. The workflow of sample preparation is described and measurement procedures, which were applied in this PhD-thesis, are illustrated. Thereby, this chapter is focusing on those topics and issues relevant for the studies in Part II of this thesis.

The chapters of Part II comprise three manuscripts that form the centrepiece of the PhD-thesis. These chapters represent individual studies dealing with specific aspects of our research project. All of them reveal their own introduction, methodological explanations and discussion. In order to integrate the results derived from the studies, the central scientific outcome is summarized at the end of this thesis.

With respect to the already published manuscripts (Chapter 3 and Chapter 4), I would like to point out that there are minor modifications compared to the published versions. These modifications do not affect the scientific contents of the studies, but are restricted to layout issues, such as size, resolution and exact position of figures and tables. Furthermore, references were not considered in the individual chapters, but summarized at the end of this PhD-thesis.

Chapter 3 represents the starting point of our research project. Besides summarizing the results of previous studies, this chapter gives a rather comprehensive introduction into the geological and geomorphological setting of the research area. The study deals with the youngest Pleistocene fluvial terrace which was found to be accumulated by the primary Steinach River (T2-terrace)[2]. Indirect age estimations for the terrace formation are derived from luminescence dating of hillslope sediments. Apparent contradictions to older studies are discussed and a possible solution is derived from lithological investigations.

[2] Since the T1-terrace was identified as local form accumulated by the Trebgast Creek, it does not reveal any information relevant for determining a chronological framework for the river deflection in our research area. Therefore, the T1-terrace is not considered in this PhD-thesis at all.

Chapter 4 is further investigating the timing of the T2-terrace accumulation. Unlike in the first study (*Chapter 3*), optically stimulated luminescence dating is applied to sample material directly originating from the T2-terrace gravels. Thereby, various sites located throughout the river's longitudinal course are analysed. The findings presented in this chapter point to a fluvial history which is characterized by a much higher complexity than so far expected. Based on our results, an additional evolutionary stage is proposed which refines the so far established landscape evolution model. Furthermore, our data provide evidence for a diachronic response of fluvial systems to climatically or tectonically triggered changes of environmental conditions.

For the study described in *Chapter 5*, we focus our attention on the older fluvial terraces (T3-, T4- and T5-terrace levels), which were assumed to be of pre-Eemian (MIS 5e) age. In order to derive a chronological framework for these older evolutionary stages, innovative techniques of luminescence dating are applied. The results summarized in the manuscript are ambivalent. On the one hand, they partially confirm results of previous studies and allow to derive a (preliminary) chronology for the Middle Pleistocene terraces in the research area. But on the other hand, they also reveal significant methodological problems associated with the applied post-IR IRSL procedure.

The final part of this PhD-thesis (Part III) summarizes the essential results, which could be derived from the individual studies, in a *Synthesis* (*Chapter 6* on page 179) and gives a short *Outlook* (*Chapter 7* on page 187) on still unanswered questions and possible future research activities.

Finally, tables and figures in the *Appendix* provide additional information relevant for this PhD-thesis as well as a list of publications and presentations (orals and posters) related to our research project.

1.4 List of manuscripts and own contribution

According to the examination regulations for achieving the academic degree of a Doctor of Natural Sciences (Dr. rer. nat.) of the Faculty of Biology, Chemistry and Geosciences at the University of Bayreuth, the author of a PhD-thesis is required to provide information on his own contribution to the manuscripts which are the centrepiece of the thesis. The following tables quantify the approximate contributions of all co-authors to the manuscripts compiled in Part II of this PhD-thesis. The author of this PhD-thesis was corresponding author for all these studies.

Manuscript 1 – Chapter 3

Quaternary river terraces and hillslope sediments as archives for paleoenvironmental reconstruction: new insights from the headwaters of the Main River, Germany

Thomas Kolb, Markus Fuchs, Olivier Moine & Ludwig Zöller

Zeitschrift für Geomorphologie, Vol. 61 (2017), Suppl. 1, 53-76

Individual contributions to the manuscript

	TK	MF	OM	LZ
Field work	70%	10%	–	20%
Sampling	70%	10%	–	20%
Sample preparation	100%	–	–	–
OSL measurement	100%	–	–	–
Manuscript preparation	95%	–	5%	–
Comments to improve the manuscript	–	50%	20%	30%
Review handling	100%	–	–	–

Manuscript 2 – Chapter 4

Deciphering fluvial landscape evolution by luminescence dating of river terrace formation: a case study from Northern Bavaria, Germany

Thomas Kolb, Markus Fuchs & Ludwig Zöller

Zeitschrift für Geomorphologie, Vol. 60 (2016), Suppl. 1, 29-48

Individual contributions to the manuscript

	TK	MF	LZ
Field work	70%	10%	20%
Sampling	70%	10%	20%
Sample preparation	100%	–	–
OSL measurement	100%	–	–
Manuscript preparation	100%	–	–
Comments to improve the manuscript	–	70%	30%
Review handling	90%	10%	–

Manuscript 3 – Chapter 5

Luminescence dating of pre-Eemian (MIS 5e) fluvial terraces in Northern Bavaria (Germany) – benefits and limitations of applying a $pIRIR_{225}$-approach

Thomas Kolb & Markus Fuchs

Geomorphology – under review

Individual contributions to the manuscript

	TK	MF
Field work	100%	–
Sampling	100%	–
Sample preparation	100%	–
OSL measurement	100%	–
Manuscript preparation	100%	–
Comments to improve the manuscript	–	100%
Review handling	100%	–

2

Methods and material

For the present PhD-thesis, a wide range of different methods was applied. This is particularly true for Study One (see chapter 3 on pp. 79–108), in which petrographic analyses, malacological investigations and classical geomorphological approaches were used side by side with luminescence dating methods. Although the other studies were more focused on luminescence methodology, the results from stratigraphic investigations as well as findings of modern computer based GIS analyses of high-resolution Digital Terrain Models (DTM) provided important input for the interpretation of the calculated luminescence ages.

However, the main purpose of this thesis was clearly to establish a regional chronology for the research area in Northern Bavaria that is mainly derived from the results of various luminescence dating approaches. From a methodological point of view the focus is, thus, on luminescence dating techniques and their specific issues. The explanations given in the following chapter, therefore, will concentrate on luminescence dating methods. Thereby, the general aim is to give a short overview of the fundamental principles of luminescence dating with a special focus on those techniques applied in this PhD-thesis. In fact, the following methodological explanations are not intended to give an exhaustive description of luminescence methods, they only address to introduce those basic information on the physical background of the luminescence phenomenon that are indispensable for understanding

the methods applied in the studies of Chapter 3 to 5.

For very elucidating and extensive summaries of the theoretical background of the luminescence phenomenon, the interested reader is referred to the still groundbreaking works of Aitken (1985) and Aitken (1998) as well as to the more recent and comprehensive overviews given by e.g. Bøtter-Jensen et al. (2003), Chen & Pagonis (2011) and Yukihara & McKeever (2011) with additional information on various applications of luminescence techniques in earth sciences, archaeology or personal and medical dosimetry.

2.1 Fundamentals of luminescence dating

2.1.1 Basic principle

Over the last decades, luminescence dating has become a widespread method in earth sciences and archaeology, extensively applied to date different kinds of sediments and other materials. Together with ESR-dating it belongs to the so called *dosimetric dating methods*, which are based on the time-dependent accumulation of radiation damages in the crystal lattices of certain minerals, such as quartz and feldspars (e.g., Wagner, 1998; Walker, 2005).

Thereby, luminescence dating makes use of the fact that these minerals act like rechargeable batteries (e.g., Duller, 2008a) that are able to store energy which is induced by ionising radiation, originating either from the decay of natural radioisotopes omnipresent in natural sediments or from the cosmic radiation (e.g., Wagner, 1998). As this storage of energy is based on electrons trapped within defects of crystal lattices, ESR and luminescence dating are also referred to as techniques of *Trapped Charge Dating* (e.g., Grün, 2001).

In nature, sedimentary mineral grains are constantly exposed to a low level of ionising radiation. This radiation is primarily caused by the decay of naturally occurring radionuclides as part of the decay chains of uranium (^{238}U & ^{235}U), thorium (^{232}Th) and potassium (^{40}K). A minor contribution arises from the β-decay of ^{87}Rb (e.g., Aitken, 1985). An additional source of natural radiation is the cosmic radiation mainly consisting of high energetic protons and alpha-particles (e.g., Prescott & Hutton, 1994).

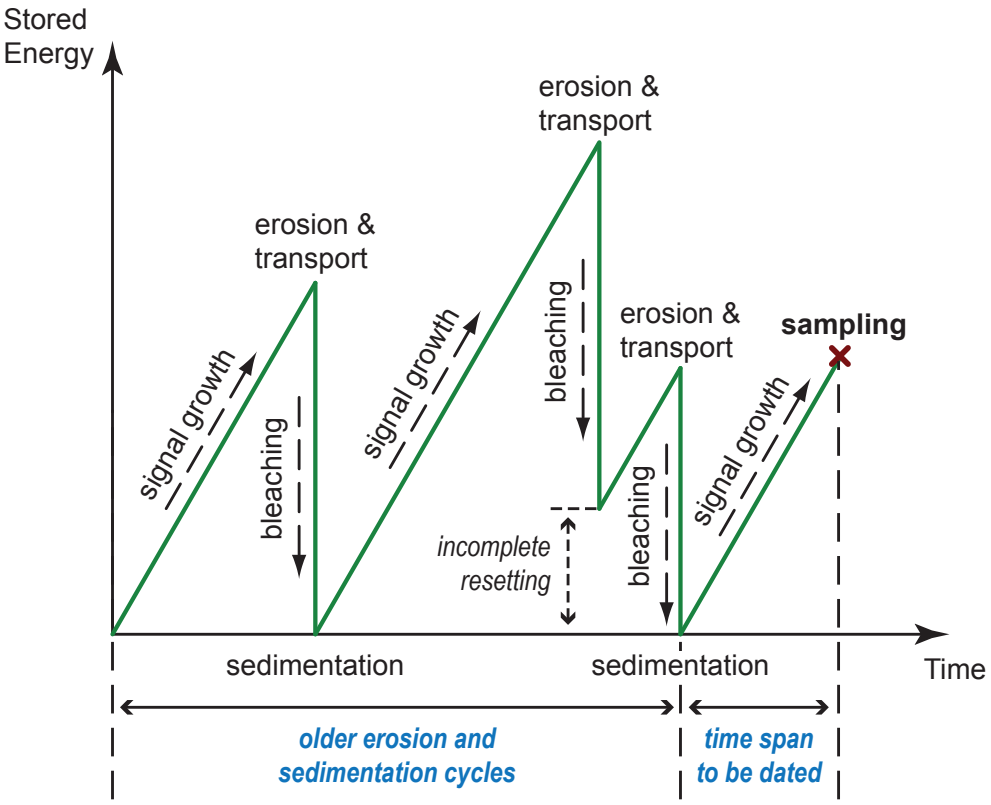

Figure 2.1: The principle of luminescence dating illustrated for sediments. As long as the sample material is shielded from sunlight, energy is accumulated in the crystal lattice with time. In nature, this latent luminescence signal is erased by sunlight exposure when the sample material is eroded and transported. This process is commonly termed '*bleaching*'. After the material is deposited and sealed from daylight by covering sediments, the signal starts to build up again. A sample may experience several of these erosion and sedimentation cycles. By measuring the amount of energy stored in the crystal lattice, luminescence dating is able to determine the time elapsed since the last sunlight exposure. As illustrated in the figure, bleaching during transport can either occur as complete zeroing of the signal or as an incomplete resetting. If not detected, this '*partial bleaching*' will result in serious age overestimations.

When the sample material is shielded from sunlight, the natural ionising radiation causes redistribution of electrons in the crystal lattice from low but stable energetic levels to excited metastable levels. Thereby, the number of electrons trapped in these metastable energetic states increases over time, as long as the dosimeter is exposed to the natural ionising radiation. When the sample material is exposed to sunlight, the trapped electrons are able to absorb additional energy and are released from their traps. Commonly termed '*bleaching*' (e.g., Duller, 2008a; Thiel, 2011), this de-trapping is accompanied by the release of energy in form of photons, resulting in a light emission referred to as *luminescence*. Thereby, the latent luminescence signal, i.e. the stored energy, is either completely reset or at least reduced to a negligible level. In nature, sunlight exposure of sediments may most probably occur during relocation processes. Erosion, transport and deposition of sediments will erase the latent luminescence signal and, thus, set the '*luminescence clock*' to zero (e.g., Duller, 2008a). When the relocated material is deposited and covered by other sediments shielding the material of interest from daylight, the latent luminescence signal starts to grow again. The fundamental cycle of energy accumulation during burial, signal resetting due to transport and renewed accumulation of energy after deposition is illustrated in Figure 2.1.

The intensity of the luminescence signal depends on the amount of stored energy, which itself is a measure of time during which the sample had been affected by the continuing influence of ionising radiation without being exposed to sunlight. With the intensity of the luminescence signal being a function of storage time, it can be used to estimate the time elapsed since the last deposition.

Thereby, two parameters have to be quantified in order to be able to calculate sedimentation ages for luminescence samples. The first of these parameters is called '*palaeodose*'. It is defined as the total amount of energy accumulated per mass unit of sample material during burial. Its unit of measurement is Gray (Gy), with 1 Gy = 1 J kg^{-1} (Aitken, 1998). The second parameter is a measure of the location specific strength of natural ionising radiation and is either termed '*natural dose rate*' (e.g., Aitken, 1985; Wagner, 1998) or '*environmental dose rate*' (e.g., Liritzis et al., 2013a; Durcan et al., 2015). It is defined as '[...] *the rate at which energy is absorbed by a grain from the flux of radiation to which it is exposed*' (Aitken, 1998) and often shortened to the term '*dose per time unit*' (Wagner, 1998). In palaeoenvironmental research, it is commonly expressed either as Gray per thousand years

(Gy ka^{-1}) or given as annual dose (mGy a^{-1}). More detailed information on dose and dose rate determination are given subsequently in sections 2.2 and 2.3.

When both parameters are known, the depositional age of a sample can be calculated by applying the following (simplified) formula:

$$Age\ [ka] = \frac{Palaeodose\ [Gy]}{Environmental\ dose\ rate\ [Gy/ka]} \tag{2.1}$$

2.1.2 Physical background of the luminescence phenomenon

The mechanism of energy storage in crystal lattices is commonly explained by the energy band model. Meanwhile, a large selection of models have been proposed which only slightly differ in details concerning the involved traps and centres (one trap/one centre models vs. multiple trap/multiple centre models) and the various paths of charge transitions (electron/trapped hole recombination vs. electron/mobile hole recombination) (e.g., McKeever, 1985; Bailey, 2001). For details the reader is referred to Bøtter-Jensen et al. (2003) and Yukihara & McKeever (2011). The following remarks will concentrate on illustrating the basic concepts of energy storage and release in crystal lattices and will thereby refer to a strongly simplified model depicted in Figure 2.3 which is characterizing the energy band structures commonly assumed for quartz minerals. As feldspar minerals show a greater variety of chemical compositions including various differences in crystal structures and bonding angles, the situation for feldspars is more complex (e.g., Poolton et al., 1994, 1995, 2002b,a; Jain & Ankjærgaard, 2011; Kars et al., 2013). However, although characterized by a larger complexity, indicated for example by the important role of band tail states, the storage and release of energy in feldspar minerals in principle follows the same mechanisms described for quartz in the following paragraphs.

Unless the energies of free electrons, those of electrons in crystal lattices do not show a continuous distribution, but are characterized by discrete energy levels. These sharply defined energetic states can be attributed to the interference with the electrical field originating from the regular arrangement of ions building up the crystal (e.g., Kittel, 2005). The electronic energy levels in crystal solids can be calculated by solving the Schrödinger equation applying the Bloch function for a

periodic potential which yields bands of allowed energies, separated by zones of forbidden energies, for which no solution of the Schrödinger equation can be found (e.g., Kittel, 2005). Electrons progressively fill the available energy levels, starting with the lowest energy level and continuing with levels of increasing energies (e.g., Yukihara & McKeever, 2011). The band representing the highest energetic state occupied by electrons is called *valence band*, the first empty level above the valence band is termed *conduction band* (e.g., Yukihara & McKeever, 2011; Wagner, 1998).

In crystalline solids, the edges of valence band and conduction band are clearly defined and both levels are separated by a more or less pronounced forbidden zone ('*energy gap*' – see Figure 2.2). The width of this band gap can be characterized by the energy E_g that would be necessary to overcome the gap and excite an electron from the valence band to the conduction band (e.g., Chen & Pagonis, 2011). The majority of natural occurring crystalline solids are either insulators or semiconductors, for which the energy gap E_g is commonly regarded to be > ~2.5 eV (for insulators) (e.g., Yukihara & McKeever, 2011) or in the range of ~1-2.5 eV (for semi-conductors) (Kittel, 2005). With particular respect to quartz minerals, the energy gap between valence and conduction band has been reported to be ~8.5 eV (e.g., Kreutzer, 2014; Schmidt, 2013, with further references therein).

All natural occurring crystalline structures are characterized by a more or less huge number of imperfections, disturbing the otherwise regular configuration of atoms in the well-ordered periodicity of the crystal lattice. Energy storage in crystal lattices is based on the presence of such defects. Thereby, a great variety of imperfections is reported in quartz minerals, including either intrinsic defects due to structural irregularities, such as Si or O vacancies, or extrinsic defects which are related to impurity atoms (e.g., substitution of Si^{4+} by Al^{3+}) (e.g., Bøtter-Jensen et al., 2003). Although many studies point to the complexity of defect structures (e.g., Preusser et al., 2009; Bøtter-Jensen et al., 2003; Schmidt, 2013), commonly three main types of defects are distinguished (e.g., Mahesh et al., 1989; Wagner, 1998; Yukihara & McKeever, 2011):

- *Interstitials (Frenkel defects)* – These point defects are characterized by interstitial atoms in between lattice points. They can either be caused by extra atoms integrated in the lattice structure or by atoms replaced from nearby lattice positions.

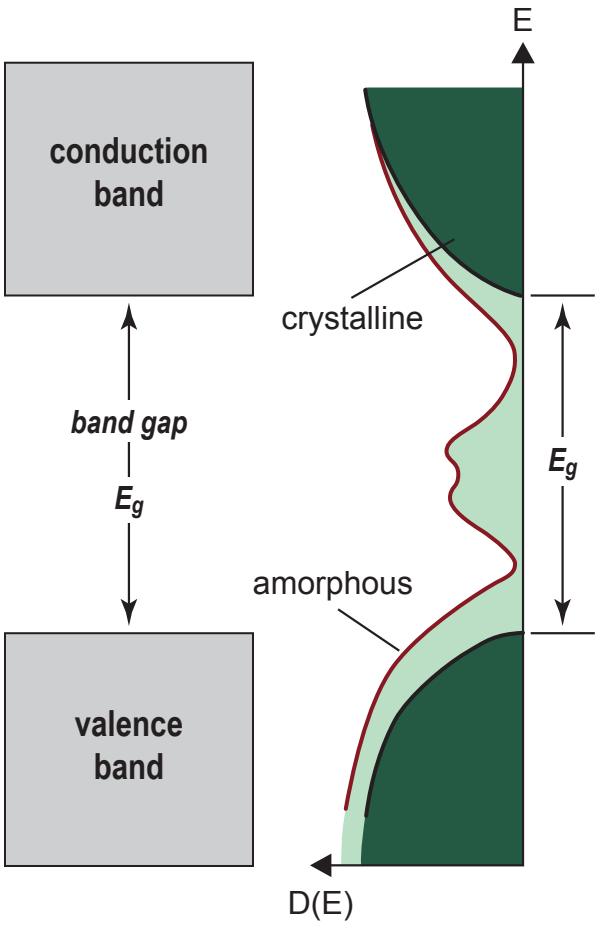

Figure 2.2: Distribution of electronic states in amorphous and crystalline solids. For crystalline solids, valence band and conduction band are characterized by distinct band edges and separated by the band gap E_g. Due to the existence of additional energetic states within the band gap (band tail states), the configuration of amorphous solids is much more complex. Modified after Demtröder (2016).

- *Vacancies (Schottky defects)* – Vacancies are non-occupied lattice positions which can be attributed to missing atoms. They either occur during the initial mineral formation or are caused by subsequent displacement of atoms from their inherent lattice positions. Interstitials and vacancies may appear as defect pairs and are then sometimes referred to as 'Schottky-Frenkel type defects' (e.g., Wagner, 1998, please note that the terminology is not always coherent).

- *Substitutions due to impurities* – A third type of point defect is attributed to the replacement of lattice atoms by foreign atoms of a similar ionic radius. A very common example is the substitution of Si^{4+} by Al^{3+} or by other ions showing similar size (e.g., Ga^{3+}, Fe^{3+} or Ge^{4+}). These substitutions are often accompanied by complex secondary changes in the crystal lattice necessary for charge compensation (e.g., Schmidt, 2013).

Irregularities in crystal structures are commonly characterized by either positive or negative charge deficits. Therefore, they can act as traps on free charges, diffusing through the crystal lattice (e.g., Wagner, 1998). With respect to the energy band model, the presence of crystal defects causes local changes in the otherwise periodical system of the lattice structure and thereby introduces additional discrete energy levels within the forbidden zone (e.g., Chen & Pagonis, 2011). From an energetic point of view, these localized energy levels are situated either close to the conduction band or slightly above the valence band. While the latter act as so-called '*hole traps*' inducing a local electric field that is able to capture positive charges ('*holes*'), the defect levels close to the conduction band attract electrons and are, thus, named '*electron traps*' (e.g., Yukihara & McKeever, 2011). Without the presence of ionising radiation, non of these traps would be occupied as electrons are tightly bound to their respective parent atoms, revealing energy levels corresponding to the valence band. This basic configuration is illustrated in Figure 2.3a.

In nature, crystals are continuously exposed to a more or less strong flux of ionising radiation (for details see section 2.3 on page 61). When this radiation interacts with the atoms of the penetrated crystal lattice, energy is transferred to these atoms resulting in an excitation of electrons to higher energetic states. In detail, the mechanism of energy transfer is very complex, including a variety of quantum-mechanical processes such as photoelectric effects, Compton scattering or electron-

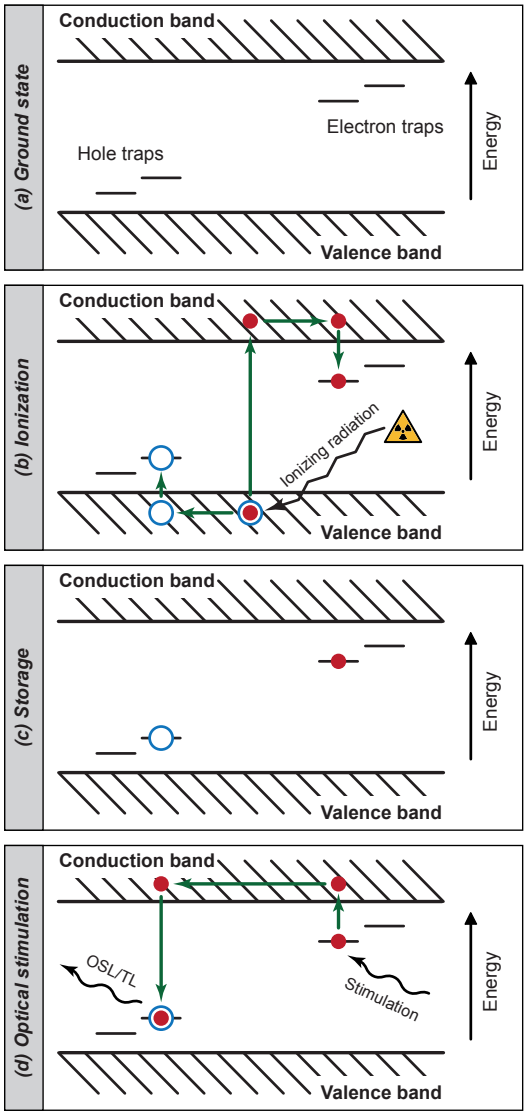

Figure 2.3: Energy band model illustrating the mechanism of energy storage and release in crystal lattices as source of the luminescence phenomenon. While filled red circles represent electrons, holes are depicted as open blue circles. The green arrows indicate possible trajectories for charge transitions. **(a)** Ground state with empty electron and hole traps situated in the forbidden band gap zone. **(b)** Ionisation and trapping process – when exposed to ionising radiation valence electrons can be excited to the conduction band, leaving behind positively charged holes. Electron and holes can be trapped at crystal defects acting as charge traps. **(c)** Configuration for long time storage – electrons and holes occupy metastable localized states either close to the conduction band or slightly above the valence band. With sufficiently large trap depths these form of energy storage can persist over geologically relevant periods. **(d)** Recombination mechanism – after optical or thermal stimulation, captured electrons are released from their traps and can recombine via conduction band with localized hole traps close to the valence band. Thereby the electrons' excess energy has to be carried off by the emission of photons, which are summing up to the luminescence signal.

positron-pair production (e.g., Yukihara & McKeever, 2011; Wagner, 1998). Regardless of the exact energy transfer mechanism, which depends on the type of radiation providing the initial energy, ionising radiation deposits energy in material by transferring the initial energy to secondary electrons termed δ-rays which disperse the energy throughout the mineral (e.g., Yukihara & McKeever, 2011). In summary, this triggers a cascade of excitation and ionisation processes which result in a large number of activated electrons detached from their atomic kernels and excited to the high energetic conduction band. The excited and delocalized electrons (negative charges) leave behind an excess of positive charges in the valence band which are referred to as '*holes*' (e.g., Wagner, 1998). Both, the excited electrons and the remaining holes, can migrate through the crystal lattice until they are trapped at either lattice defects with negative charge deficits (electron traps) or at defects with positive charge deficits (hole traps). This process of excitation and trapping of charges is depicted in Figure 2.3b.

Once trapped in such localized, metastable energetic states, electrons and holes may remain in their respective traps over geological timescales. Figure 2.3c illustrates this storage configuration. With time, an increasing number of electrons will be subjected to those excitation processes and captured at electron traps within the crystal lattice. This corresponds to an increasing amount of energy stored in the crystal lattice, associated with a growing latent luminescence signal. Since the number of crystal defects is limited, there will be an upper limit for the number of trapped electrons and holes. Thus, the latent luminescence signal will sooner or later reach a saturation level (e.g., Wagner, 1998; Preusser et al., 2008). As soon as this level is reached, further exposure to ionising radiation will not increase the luminescence signal any more. This will result in serious age underestimations. In this PhD-thesis, signs of luminescence signal saturation were identified for the quartz samples investigated in Study 3, for which the determined ages were regarded to be unreliable and only interpreted as minimum age estimates.

With respect to dating applications and age determinations, another crucial point is the stability of energy storage. This strongly depends on the potential energy of Coulombic attraction exerted on the captured electrons by the specific traps. As there are different types of crystal defects, there are also different types of traps characterized by differing stabilities, which can be described by the specific thermal lifetimes τ of the traps. τ is defined as the average residence time an electron is ex-

pected to spend in a trap (e.g., Aitken, 1985) and is strongly determined by the amount of energy required to overcome the Coulombic attraction of the trap (e.g., Schmidt, 2013). The thermal lifetime can be calculated according to the following formula (e.g., Aitken, 1985):

$$\tau = s^{-1} \cdot e^{\frac{E}{kT}}. \tag{2.2}$$

Thereby, s is a frequency factor, which depends on the trap type and is usually in the range of 10^9 to 10^{16} s^{-1} (e.g., Aitken, 1985). T represents the absolute temperature given in Kelvin [K] and k is the Boltzmann's constant. E (in eV) is the activation energy required to release a captured electron from the trap to the conduction band and is regularly termed '*trap depth*' (e.g., Aitken, 1985, 1998). In order to ensure that the leakage of electrons over time is negligible, the lifetime of electrons in the traps has to be considerably higher than the age span to be dated (e.g., Aitken, 1998). Aitken (1985) points out that τ would have to be at least 10 times the age of a sample if the upper limit of tolerated signal loss was set to 5%. As the lifetime primarily depends in the trap depth E below the conduction band, shallow traps situated close to the conduction band should be avoided for dating purposes. In fact, Aitken (1998) proposed to restrict luminescence dating techniques, which are normally dealing with burial periods of several tens of years to several hundreds of thousand of years, to traps characterized by a trap depth of at least 1.6 eV. At natural storage temperatures, this corresponds to a lifetime of ~several millions of years and guarantees that the measured luminescence signal arises from traps sufficiently deep to ensure negligible leakage of electrons and, thus, reliable dating.

The source of luminescence emission in semiconductors and insulators is the release of trapped electrons from their metastable states, followed by recombination of electron-hole pairs at defects in the crystal lattice (e.g., Yukihara & McKeever, 2011). Thereby, the trapped electrons have to be stimulated with an adequate amount of energy which has to be sufficient to overcome the specific Coulombic attraction of the trap. This energy is either provided by heating (thermoluminescence – TL) or by optical stimulation with light of particular wavelenghts (optically stimulated luminescence – OSL). By this stimulation, the trapped electrons are evicted from their traps to the excited delocalized state of the conduction band where they can again migrate as free charges through the crystal lattice. Once the

electrons have been lifted to the conduction band, there are various charge transition trajectories showing characteristic probabilities. First, the released electrons might be recaptured either by the same trap or by a different type of trap, which will not result in a detectable luminescence emission (e.g., Aitken, 1998)[1]. Furthermore, the freed electrons can undergo a direct electron-hole recombination across the band gap from the conduction band to a migrating hole in the valence band. This electronic transition is in principle possible even in insulators, however associated with an extremely low probability (e.g., Yukihara & McKeever, 2011). Neither the recapture process nor the direct recombination from the conduction to the valence band is shown in Figure 2.3d, which only illustrates the main mechanism and basic principle of charge recombination and luminescence production.

This main mechanism can be described as a recombination of electron-hole pairs at crystal defects which are occupied by trapped holes and situated within the band gap. Thereby, hole traps which are located in the intermediate region of the band gap show a higher probability to act as recombination centres than those hole traps close to the valence band (e.g., Yukihara & McKeever, 2011). When such electron-hole recombinations take place, at first electrons are captured at excited states of the recombination defects before the recombined electron-hole pairs return to the ground state (e.g., Yukihara & McKeever, 2011; Schmidt, 2013). If this relaxation process from a high energetic state to the low energetic ground state occurs as radiative transition, the excess energy is carried off by emitting photons of specific energies. This flux of photons sums up to a detectable light emission that is the source of the luminescence phenomenon.

The details of this recombination process are again characterized by a great complexity. Apart from the fact, that there are various different possible transition pathways not mentioned in the text above, among others including thermally assisted eviction mechanisms and athermal quantum-mechanical tunnelling (e.g., Bøtter-Jensen et al., 2003; Yukihara & McKeever, 2011), the recombination process is additionally complicated by the existence of different types of recombination centres, normally referred to as '*luminescence centres*' ('*L-centres*'),

[1] In fact, there is some kind of light emission occurring during those recapturing processes as well as during the initial trapping process after the electrons were lifted to the conduction band (e.g., Preusser et al., 2008). This emission of light is characterized by low energy photons corresponding to light emission in the infrared wavelength band. While this IR-light emission is the signal investigated by the radiofluorescence method, it is not detected in conventional luminescence dating approaches.

'*killer centres*' ('*K-centres*') and thermally unstable '*reservoir centres*' (R-centres) (e.g., Aitken, 1985; Zimmerman, 1971). Only recombinations at luminescence centres will result in the emission of light, while recombinations at K-centres will occur as non-radiative transitions. The role of reservoir centres is even more complex as they are supposed to compete for holes with L-centres during irradiation. Thus, R-centres are a relevant factor for explaining sensitivity changes observed in the dosimeters during the measurement procedure. As a result, the relative abundance of L-, K- and R-centres and changes in their proportions have an important impact on the amount of luminescence detected during OSL measurements.

At this point, it has to be emphasized that all processes described in the previous paragraphs are stochastic phenomena associated with characteristic probabilities. Describing luminescence emission by means of mathematical formulas is, thus, challenging and often only possible under the assumption of specific simplifications such as the 'one trap/one centre model' (e.g., Bøtter-Jensen et al., 2003). Assuming first-order kinetics (i.e., no re-trapping) and a constant stimulation intensity, this strongly simplified model describes the intensity I of the luminescence signal with stimulation time t by a single exponential function according to the following formula (e.g., Bøtter-Jensen et al., 2003):

$$I_{OSL}(t) = I_0 \cdot e^{\frac{-t}{\tau_d}}, \tag{2.3}$$

where I_0 is to the initial luminescence intensity at $t = 0$ and τ_d represents the CW-OSL decay constant. For details on the derivation of mathematical formulas describing the luminescence phenomenon, the interested reader is referred either to the comprehensive explanations of Bøtter-Jensen et al. (2003) and Yukihara & McKeever (2011) or to the brief summary given by Schmidt (2013).

2.1.3 Dosimeters and measurement procedures

Although the number of synthetic and natural materials showing luminous effects is quite large (e.g., Bøtter-Jensen et al., 2003; Yukihara & McKeever, 2011), dating studies in palaeoenvironmental and archaeological contexts are typically based on measuring either quartz or feldspar separates. Compared to other natural minerals such as zircon (e.g., Smith et al., 1991; van Es et al., 2000), calcite (e.g., Gaft et al., 2008), halite (e.g., Bailey et al., 2000) or gypsum (e.g., Mahan & Kay, 2012), which are in principle also suitable for dating purposes (e.g., Strebler, 2013), quartz and feldspars are abundant in nearly all environmental settings and dominate the luminescence signals of most sedimentary and archaeological materials. With their luminescence properties well-documented, both of them show specific advantages and suffer from distinct shortcomings.

Ever since Murray & Wintle (2000) proposed the single aliquot regenerative dose (SAR) protocol (see Chapter 2.2.2), quartz has been the mineral of choice in the major part of luminescence studies. One reason for preferring quartz separates might be its abundance in nature. Showing a higher resistance to chemical weathering, quartz minerals are still preserved when feldspar minerals, which are generally prone to chemical weathering, might be scarce or even completely missing. Furthermore, feldspar minerals cover a wide range of chemical compositions, whereas quartz is a rather simple structured mineral. Thus, the luminescence emission spectra from feldspar separates are regarded to be much more complex than those of quartz samples (e.g., Duller, 2008a) which might crucially have impeded the development of a coherent theoretical model describing the luminescence properties of feldspar minerals.

The striking advantage of quartz separates over feldspars, however, is the excellent bleachability of its luminescence signal. By conducting sunlight bleaching experiments for a set of various luminescence signals, Godfrey-Smith et al. (1988) were not only able to prove that the bleaching characteristics of optical signals by far surpass those of TL signals, but also showed that OSL signals derived from quartz separates are reset more rapidly than those of feldspar minerals (see Figure 2.4a). Figure 2.4b, which was derived from the original diagrams of Godfrey-Smith et al. (1988), illustrates that the luminescence emission of quartz is reduced to a level of only ~1% of the initial signal intensity after the mineral was exposed to daylight for a very short time of only ~10 s (see also Godfrey-Smith et al., 1988).

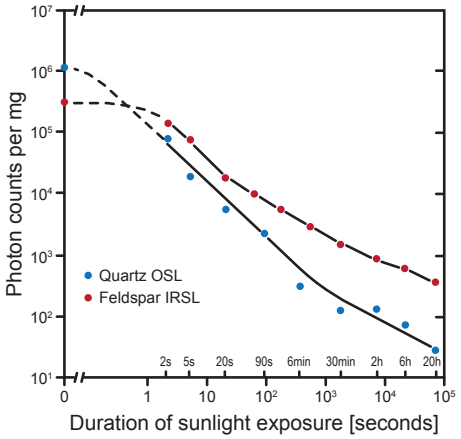

(a) Results from bleaching experiments summarizing different effects of sunlight exposure on the OSL signals of quartz and feldspar minerals. While the x-axis shows different exposure times, the y-axis depicts the intensity of unbleached luminescence signals. Note that both axis have logarithmic scales (redrawn with modifications after Godfrey-Smith et al., 1988).

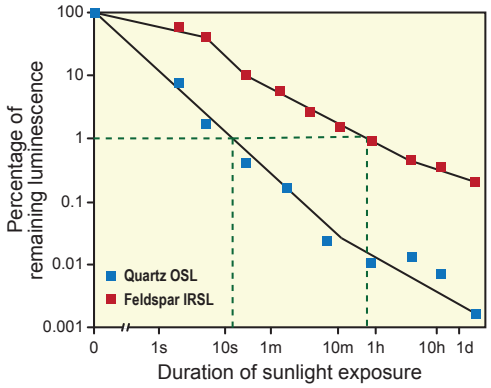

(b) Reduction of OSL signals from quartz and feldspar separates expressed as percentage of the initial signals remaining after various bleaching times (redrawn and slightly modified after Duller, 2008a). Note both axis showing logarithmic scales. The dashed green lines indicate the 1% level. For quartz, this level is reached after a short bleaching time of slightly more than 10 seconds, whereas it takes a prolonged time of sunlight exposure of ~1 hour to reach a similar level for feldspar dominated samples.

Figure 2.4: Efficiency of sunlight bleaching for optical signals of quartz (blue symbols) and feldspar (red symbols) separates. Both diagrams show that OSL signals of quartz are bleached with greater efficiency than those of feldspar samples.

Duller (2008a) points out that a sunlight exposure time of ~100 s is sufficient to reduce quartz signals to a negligible percentage of < 0.1% of its initial level. On the other hand, optical signals from feldspars are characterized by a much slower response to sunlight and, thus, need prolonged bleaching times to reach a level sufficient to be termed as complete resetting (see Figure 2.4b).

The aspect of bleachability is of special importance when dating sediments for which either only a short time of daylight exposure or a strongly reduced intensity of sunlight can be assumed during transport and sedimentation. This is particularly true for fluvial sediments such as those investigated in this PhD-thesis. Previous studies (e.g., Berger & Luternauer, 1987; Berger, 1990) have shown that solar resetting of waterlain sediments may significantly be limited by attenuation

due to either the water column or the suspended load. Other studies (summarized by e.g., Wallinga, 2002; Rittenour, 2008) point to the complexity of fluvial transport processes and identified other important controls on the bleaching of fluvial sediments, such as the transport distance, the mode of transport, the impact of high-discharge events and the direct admixture of non-bleached material due to river bed erosion.

However, quartz is also characterized by a series of more or less important limitations. First of all, some quartz samples show relatively low luminescence sensitivities. Revealing rather poor luminescence properties, this phenomenon has especially been reported for quartz extracts of sediments originating from geologically young orogens and is often attributed to a limited number of relocation cycles (e.g., Preusser et al., 2006; Klasen et al., 2006; Steffen et al., 2009). For these environments, thermal transfer of charge from light-insensitive traps to light-sensitive traps has been described as serious problem that might result in substantial equivalent dose overestimations (e.g., Rhodes & Bailey, 1997; Rhodes, 2000). With only ~5% of the grains contributing to the luminescence emission of a typical quartz sample (e.g., Duller, 2008b), the intensities of many quartz signals may also not be sufficient for dating young (i.e., Holocene) sediments in which only a low dose was accumulated since their deposition. Finally, due to crystal intergrowth of quartz minerals with various feldspar remnants it is sometimes impossible to separate pure quartz material (e.g., Preusser et al., 2008). Although some procedures have been suggested to deal with such feldspar inclusions (e.g., Wallinga et al., 2002), these approaches are still associated with a substantial number of unanswered problems.

The major disadvantage of using quartz samples for luminescence dating, however, is their low dose saturation. Normally this is regarded to lie in the range of 150-200 Gy (e.g., Roberts, 2008; Thiel et al., 2011b; Thiel, 2011), with some higher values reported for exceptional environmental settings (e.g., Buylaert et al., 2011). Depending on the location specific dose rate, the upper dating limit of quartz OSL measurements is, therefore, reached at ~50-150 ka (e.g., Buylaert et al., 2011; Li et al., 2014). With respect to sediments older than the last glacial-interglacial-cycle, this means that quartz samples are often in or at least close to saturation. Therefore, the results derived from such samples are less reliable and can only be interpreted as minimum estimates of the true deposition age.

Especially for dating old sediments, the use of feldspar minerals is therefore often advantageous and sometimes even indispensable. Due to much higher saturation doses of ~1500-2000 Gy (e.g., Huntley & Lamothe, 2001; Li et al., 2014; Thiel, 2011), IRSL-dating of feldspar separates and polymineral samples, in principle, provides the potential for significantly extending the range of luminescence dating far beyond the last glacial-interglacial-cycle. However, a major drawback of feldspar based luminescence dating is a well-documented (e.g., Aitken, 1985, 1998) phenomenon termed '*anomalous fading*' (e.g., Wintle, 1973). This phenomenon describes a loss of luminescence signal in feldspar minerals due to the eviction of electrons from thermally stable traps at ambient temperatures (e.g., Wintle, 1973; Aitken, 1985; Spooner, 1992, 1994a). Many aspects of this signal loss are still not fully understood. In particular, there has been a substantial and still ongoing debate about the question whether it is a universal phenomenon shared by all kinds of feldspar minerals (e.g., Duller, 2008a). Many studies provide clear evidence that the anomalous fading problem is of complex nature, indicated by strong inter-sample variations of fading rates as well as by the finding that signals of different wavelengths fade at different rates (e.g., Duller, 2008a). Although the exact mechanism of anomalous fading is still not completely understood, the signal loss is commonly attributed either to quantum-mechanical tunnelling of electrons from electron traps to nearby recombination centres without any stimulation or to 'hopping' of electrons from trap to trap, triggered and assisted by weak thermal stimulation (e.g., Visocekas, 1985; Visocekas et al., 1994; Guérin & Visocekas, 2015). Strongly depending on the specific configuration of the individual crystal structure (i.e., the electron-centre-distance and the density of crystal defects), these mechanisms, which are illustrated in Figure 2.5, can result in a significant loss of stored electrons.

If not corrected for, anomalous fading will, by all means, result in severe age underestimations. Therefore, different approaches have been suggested to cope with the problem and to be able to use feldspars as reliable dosimeters. From a general point of view, these approaches can be divided into two major groups. The first group consists of numerous correction models which apply specific mathematical algorithms to correct the measured values which were identified to be affected by fading. The most important of these models are the linear correction model introduced by Huntley & Lamothe (2001), the dose rate correction (DRC)

method of Lamothe et al. (2003) and the approach proposed by Kars et al. (2008) which is based on quantum-mechanical considerations. All of these three approaches were applied in this PhD-thesis (see Chapter 5) and are briefly described in section 2.2.3.

The second group comprises various attempts to identify and make use of luminescence signals from feldspar separates that do not suffer from anomalous fading. Therefore, either luminescence signals from different emission wavelengths are investigated or specific measurement protocols are proposed. One of these approaches is the *infrared radiofluorescence* procedure (IR-RF), which was originally introduced during the late 1990s (e.g., Trautmann et al., 1998, 2000; Krbetschek et al., 2000). Thereby, the radiofluorescence of K-feldspar separates emitted in the infrared wavelength spectrum at ~1.43 eV (865 nm) is measured during continuous β-irradiation (e.g., Erfurt & Krbetschek, 2003b; Erfurt, 2003). Based on a theoretical model, a single-aliquot regenerative dose procedure (IR-SAR) was proposed by Erfurt & Krbetschek (2003a), which has only been used in a small number of applied dating studies (e.g., Degering & Krbetschek, 2007; Wagner et al., 2010; Novothny et al., 2010; Lauer et al., 2011; Kreutzer et al., 2014). Although there are still major issues associated with radiofluorescence measurements (e.g., Buylaert et al., 2012a), new methodolocigal findings (e.g., Frouin et al., 2015; Huot et al., 2015) provide better insights into the mechanism of the radiofluorescence emission and resulted in some kind of methodological revival. Meanwhile, Frouin et al. (2017) proposed an improved radiofluorescence SAR protocol termed RF_{70} which might provide the potential to significantly increase the range of luminescence dating methods while avoiding problems arising from anomalous fading.

Other approaches to deal with the specific issues of anomalous fading involve various *isochrone dating* procedures (e.g., Zhao & Li, 2002; Li et al., 2007, 2008) as well as methods based on *pulsed stimulation* techniques (e.g., Tsukamoto et al., 2006). Especially Tsukamoto et al. (2006) were able to show that luminescence signals of K-feldspars and Na-feldspars can be disaggregated into distinct components when applying short-time stimulations using a fast photon counter and a pulsed IR LED stimulation unit. Based on the calculated recombination lifetimes (<1 µs, 3-4 µs and ~20 µs), they discriminated three distinct groups of signal components. Thereby, they found that the long lifetime (~20 µs) compo-

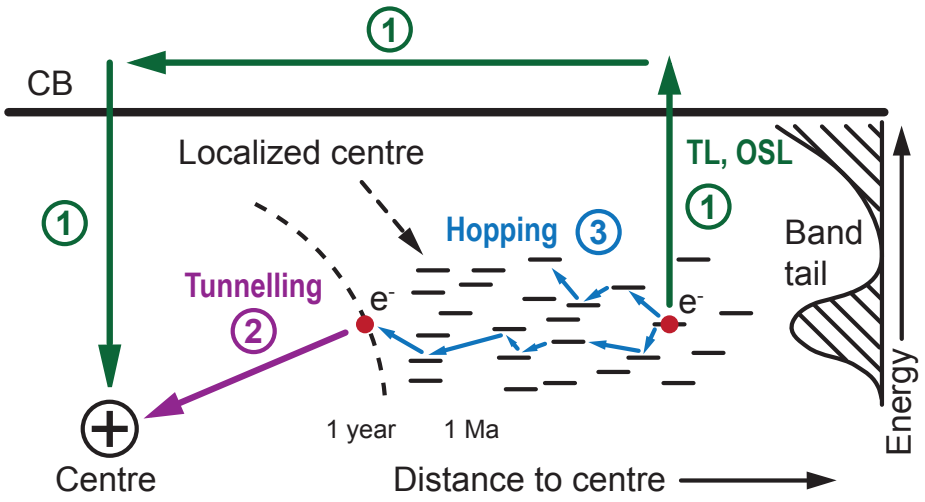

Figure 2.5: Schematic diagram showing three possible routes of electron-centre recombinations in feldspar minerals. (1) Electrons can be excited to the conduction band and recombine even with far distant centres. This requires a strong optical or thermal stimulation typically not given during burial in nature. Thus, this transition route cannot be the source of anomalous fading. (2) Direct quantum-mechanical tunnelling from the ground state of the electron trap to a nearby recombination centre. Not requiring any kind of stimulation, this transition strongly depends on the electron-centre distance and is therefore restricted to electron-hole pairs at small distances. (3) Thermally assisted hopping of electrons from trap to trap. As the probability of ground state tunnelling (process 2) decreases exponentially with increasing distance between electron and hole (e.g., Aitken, 1985), the major part of donor-acceptor-pairs (e.g., Poolton et al., 1994, 1995) would not be able to take part in tunnelling effects and could not contribute to the anomalous loss of luminescence signal in feldspar minerals. By the hopping mechanism, electrons from distant traps may migrate through the crystal lattice. Thereby, they can reach a trap close enough to a recombination centre that ground state tunnelling becomes possible. Ambient temperatures may provide sufficient energy to drive this process in nature. Transition pathways (2) and (3) are, therefore, regarded as possible quantum mechanical mechanisms responsible for the anomalous fading phenomenon. The right hand side of the diagram shows the density of band tail states. CB = Conduction band. Redrawn and slightly modified after Guérin & Visocekas (2015).

nent was significantly more stable than the shorter lifetime components. Equivalent doses derived only from the long lifetime component of the pulsed IRSL signal were consistent with D_es calculated for quartz separates of the respective samples. Therefore, Tsukamoto et al. (2006) concluded that the long lifetime component from feldspars might not suffer from anomalous fading at all. If this was true, pulsed stimulation would provide the potential to restrict equivalent dose determination to those signal components not affected by anomalous fading.

However, the most widely used approach to circumvent the fading phenomenon includes various so-called *post-IR IRSL* procedures, which are fundamentally based on the findings of Jain & Singhvi (2001) who investigated feldspar contaminations in quartz separates in order to improve accuracy and precision of equivalent dose determination, derived from blue-green light stimulated luminescence of quartz minerals. By analysing the effects of IR stimulation at different temperatures, Jain & Singhvi (2001) were able to conclude that there are at least two types of trap populations participating in the luminescence signals of feldspars. While the type A trap population can be stimulated by infrared light at low temperatures (125°C), the type B population is not affected by this low temperature treatment. However, IR stimulation of this type B population is successful at elevated temperatures of 220°C. Thus, as a by-product of their studies Jain & Singhvi (2001) could show that there is a residual IRSL signal in feldspars that is not affected by a low temperature (50°C or 125°C) IRSL readout, but can be accessed by a subsequent post-IR IRSL stimulation at elevated temperatures. A comprehensive summary of the complex structures characteristic for feldspar minerals and the resulting transition pathways for electrons is given by Jain & Ankjærgaard (2011).

Thomsen et al. (2008) systematically investigated this post-IR IRSL signal and found that IR-stimulated signals of feldspar minerals measured at elevated temperatures after a preceding IRSL readout at 50°C are less affected by signal loss due to anomalous fading. Based on these results, they proposed a two-step post-IR IRSL procedure, for which the basic idea can be described as follows: During a first IR stimulation at low temperature, electrons stored in unstable traps are released and recombine with nearby recombination centres. Thomsen et al. (2008) termed this step '*IR wash*'. As this low temperature stimulation is associated with the supply of low energy, this first step only affects traps that are close to recombination centres. In the donor-acceptor model of Poolton et al. (1994,

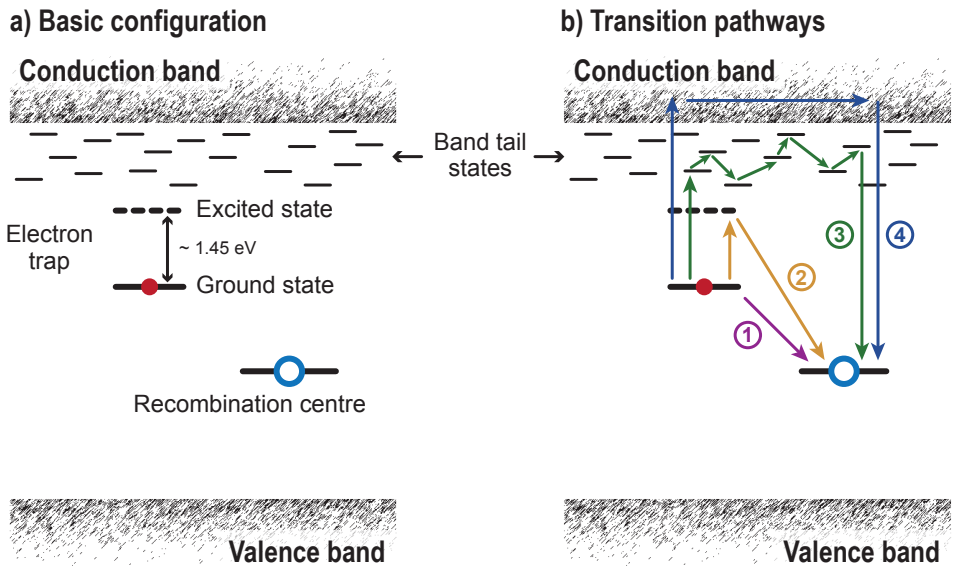

Figure 2.6: Simplified schematic model of energy bands in feldspar minerals. a) The left-hand side shows the basic configuration of energy storage in the crystal lattice, illustrating an electron trap (ground state and excited state) occupied by an electron (red circle), a recombination centre (blue circle) and band tail states below the conduction band. These band tail states can act as bridges, allowing far distance transport of electrons even if they are not able to reach the conduction band. b) Possible transition routes for donor-acceptor-recombinations: (1) Ground state tunnelling. This mechanism is regarded to be the main reason for anomalous fading (see explanations on page 35). (2) Excited state tunnelling. This transition is attributed to IRSL signals arising from an infrared stimulation at low (50°C) temperatures. The energy supplied by this weak stimulation is only sufficient to lift trapped electrons from the ground state to the excited state of a trap. However, this significantly increases the tunnelling probability to nearby recombination centres. As a result, IR stimulation at low temperatures empties the system of those nearby electron-hole pairs that are characterized by a high tunnelling probability in nature. (3) Thermally assisted hopping through the band tail states. This mechanism is suggested as explanation for the stable post-IR IRSL signal. Following the 'IR wash' step, a subsequent IR stimulation at elevated temperatures is able to excite all remaining electrons to excited energy levels below the conduction band. Although these electrons do not reach the conduction band, they can migrate through these band tail states and recombine with distant recombination centres. (4) Recombination via conduction band transport of electrons after a strong optical (blue/green light) or thermal stimulation. Inspired by the diagrams presented in the studies of Kars et al. (2013) and Jain & Ankjærgaard (2011).

1995, 2002b,a), these traps give raise to IRSL signals that are attributed to direct donor-acceptor pair recombinations due to quantum-mechanical tunnelling from the excited state of the IRSL trap to nearby holes (see transition route (2) in Figure 2.6b). As already mentioned above, ground state tunnelling between spatially close donor-acceptor pairs (transition route (1) in Figure 2.6b) are also regarded to be the main reason for anomalous fading (e.g., Jain & Ankjærgaard, 2011; Buylaert et al., 2012b, also see explanations on page 33). As a result of the '*IR wash*' step at 50°C, the major part of those electron-hole pairs that can be assumed to be prone to anomalous fading is empty and cannot contribute to subsequently measured IRSL signals anymore (e.g., Buylaert et al., 2012b). The first IR stimulation at 50°C is followed by a second IR stimulation at elevated temperatures (commonly > 200°C) (e.g., Li et al., 2014), which supplies a larger amount of thermal energy assisting the IR stimulation which allows the trapped electrons to reach the band-tail states right below the conduction band (see transition route (3) in Figure 2.6b). During this second stimulation the post-IR IRSL signal is recorded, which is dominated by electron-hole-recombinations at distant recombination centres after the electrons were transported through the band-tail states (e.g., Thomsen et al., 2008). As quantum-mechanical tunnelling strongly depends on the distance between traps and recombination centres (Aitken, 1985; Guérin & Visocekas, 2015), anomalous fading can be expected to be of little importance for this long distance recombinations. Therefore, the post-IR IRSL signal should be more stable than the IR_{50} signal and much less affected by anomalous fading (e.g., Buylaert et al., 2012b; Thiel, 2011).

Meanwhile, a great variety of different post-IR IRSL procedures have been proposed and tested in numerous applied dating studies on feldspar separates from many different environmental settings. Based on the same fundamental principles, these approaches include various versions of two-step post-IR IRSL methods using different combinations of IR stimulation temperatures. With the $pIRIR_{225}$-protocol (e.g., Buylaert et al., 2009; Alappat et al., 2010; Sohbati et al., 2012) and the $pIRIR_{290}$-protocol (e.g., Thiel et al., 2011a,b; Buylaert et al., 2012b), the most commonly applied protocols make use of a combination of a low temperature readout at 50°C for the first IR stimulation step and a high stimulation temperature of > 200°C for the subsequent pIRIR-step. However, some studies showed that such high temperature post-IR IRSL approaches may be prob-

lematic for younger samples originating from specific environmental settings (e.g., Kars et al., 2014). Therefore, alternative approaches were suggested using post-IR IRSL stimulation at moderate temperatures of either 150°C or 180°C (Madsen et al., 2011; Reimann et al., 2011; Reimann & Tsukamoto, 2012; Reimann et al., 2012; van Gorp et al., 2013).

As an alternative to these two-step post-IR IRSL approaches, Li & Li (2011) introduced a multi-step post-IR IRSL procedure which they named multi-elevated-temperature post-IR IRSL (MET-pIRIR) protocol. In this protocol, the fading component of the IRSL signal is progressively eliminated by applying multiple IR stimulations with increasing stimulation temperatures from 50°C to 250°C (e.g., Li & Li, 2011; Li et al., 2014). One advantage of this MET-pIRIR approach is the possibility of illustrating the effect of anomalous fading in D_e-temperature plots (D_e-T-plots), in which the determined equivalent doses are plotted against the specific post-IR stimulation temperatures. In such a plot, the depicted D_e will increase with increasing stimulation temperature until a D_e-plateau is reached at higher temperatures. This plateau can be used as an internal diagnostic tool indicating the D_e-region not affected by anomalous fading any more (e.g., Li & Li, 2011; Li et al., 2014). The MET-pIRIR approach has so far only been tested by a rather limited number of applied studies (e.g., Fu et al., 2012; Fu & Li, 2013; Li & Li, 2012; Thomsen et al., 2012).

In summary, there is a large variety of different approaches applied either to quartz samples or feldspar separates. With respect to dosimeters and measurement procedures, many considerations have to be made in order to ensure that both of them fit to the specific requirements of the environmental context for which the dating is done. In this PhD-thesis, I primarily worked with either fluvial sediments or hillslope material, for which the resetting of luminescence signals is commonly regarded to be a major problem (e.g., Fuchs & Lang, 2009; Preusser et al., 2008, 2011; Rittenour, 2008; Wallinga, 2002). In this respect, quartz minerals, in principle, seem to be advantageous over feldspar dominated samples, as they clearly show better bleaching properties. Thus, quartz was the preferred dosimeter in this PhD-thesis, as long as its application was considered to be possible. Quartz based OSL dating, therefore, was applied to all younger samples, originating either directly from gravel beds of the youngest Pleistocene Steinach terrace (T2-level) or from hillslope sediments superimposing the T2-terrace gravels.

With respect to the older evolutionary stages (i.e., > MIS 5e) and their associated terrace levels, dating attempts using quartz separates for two locations of the T3-terrace level provided evidence that these samples had already reached the saturation level (see Study 3 in Chapter 5). The calculated quartz based OSL-ages are, therefore, assessed to be unreliable and can only be interpreted as minimum age estimates (see page 159). As the quartz fraction proved not to be appropriate for dating these older sediments, I had to shift my attention to feldspars, even though the feldspar luminescence signals may most probably suffer from both, anomalous fading, which causes age underestimation, and partial bleaching, resulting in significant age overestimation. In order to reduce at least the effects of anomalous fading, a post-IR IRSL protocol and fading correction methods were applied. Detailed information on the specific parameters used for the post-IR IRSL measurements and the fading correction procedures applied to all older samples originating from the T3-, T4- and T5-terrace levels are summarized in section 2.2.3.

2.2 Determination of equivalent doses – measurement protocols

A crucial point in luminescence dating is the determination of energy stored in the crystal lattice of the investigated dosimeters since the sample material was last exposed to sunlight. This energy is commonly termed '*palaeodose*' or '*natural dose*' and is either described as the dose that the sample received during antiquity (Aitken, 1985) or more formally defined as the total amount of energy accumulated per mass unit of sample material during burial (Aitken, 1998). A fundamental issue, thereby, is the fact that there is no way to determine the palaeodose by means of direct measuring.

With respect to the explanations on the physical background of the luminescence phenomenon given in section 2.1.2 on page 21, it should be obvious that the intensity of measured luminescence signals strongly depends on the individual properties characteristic for the particular mineral grains under investigation. As these properties are determined by the individual configurations of the crystal structures of the involved minerals, different mineral grains will exhibit different luminescence signals even if they have been exposed to the very same amount of ionising radiation. Thus, there is no clearly defined and universally valid relationship between luminescence signal intensity and stored energy that could generally be applied to derive palaeodoses from the measured OSL signals.

In order to determine the palaeodose of a sample, a reference system has to be established that is able to evaluate the luminescence sensitivity of each subsample individually. Thereby, subsamples (aliquots) are artificially irradiated with different known laboratory doses. By measuring the intensity of luminescence signals induced by these known doses, an empirical function can be derived which describes the relationship between measured luminescence and administered dose. This empirical relationship is commonly called '*dose response curve*' or '*growth curve*' (e.g., Aitken, 1998; Schmidt, 2013). By comparing the natural luminescence signal induced during burial in nature to those signals induced by the artificial irradiation, a laboratory dose can be identified that is able to produce a signal intensity equal to that of the natural luminescence signal (e.g., Lomax, 2009). This laboratory dose is termed *equivalent dose* (D_e) and can be used as measure of the palaeodose, although it has to be emphasized that equivalent dose (laboratory conditions) and

palaeodose (natural conditions) are not identical.

With additive dose and regenerative dose procedures, in principle there are two major approaches for equivalent dose determination. Based on these basic configurations, a wide variety of different measurement protocols have been proposed for luminescence dating over the last decades, typically adapted to the special requirements of specific dating contexts. For this PhD-thesis three different OSL measurement procedures were applied. The structure of each procedure is described in the following sections and depicted in detail in Figure 2.8 and 2.10.

2.2.1 The multiple aliquot additive dose protocol (MAAD-protocol)

After originally being used in thermoluminescence dating for many years, *multiple-aliquot approaches* were also adopted to OSL dating and were dominating the major part of luminescence studies up to the mid and late 1990s (e.g., Duller, 2008b; Preusser et al., 2008). For the present PhD-thesis the multiple aliquot additive dose (MAAD) protocol was applied to polymineral and quartz separates of one fine grain sample (sample BT 737 – see Study 1 on page 79 and Study 2 on page 109). In this procedure, the equivalent dose determination is based on the construction of dose response curves derived from the measurements of several aliquots of the same sample. Thereby, the sample is divided into different groups of aliquots. While one of these groups is used for determining the natural luminescence signal, the other groups are given additional, group-specific radiation doses before luminescence measurements are performed. After measuring the luminescence signals of all groups of aliquots, a growth curve can be fitted, including data points for both, natural dose aliquots and natural+additive dose aliquots (see Figure 2.7). The equivalent dose is determined by extrapolating this growth curve to the intercept with the dose-axis (e.g., Wintle, 1997; Wagner, 1998; Bøtter-Jensen et al., 2003).

The fact that dose response curve construction is based on multiple aliquots of the same sample can either be interpreted as a considerable advantage or as a major drawback of multiple aliquot procedures. As every single aliquot is only measured once, the MAAD-protocol is able to avoid changes in the luminescence sensitivity of the sample investigated. Such changes, which are assumed to be caused by re-

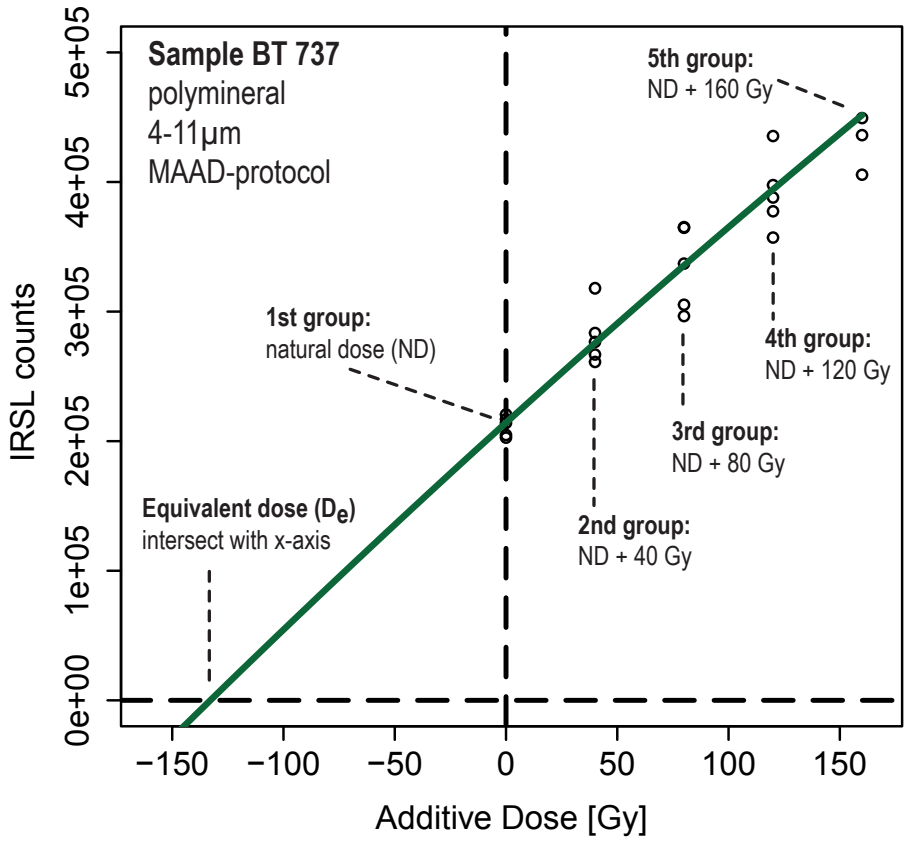

Figure 2.7: MAAD growth curve for sample BT 737 (polymineral fine grain fraction). Five different sub-samples each consisting of five aliquots were used. Additional doses of 40 Gy, 80 Gy, 120 Gy and 160 Gy were given to the different additive dose groups. In this example, a single saturating exponential function was used for growth curve fitting. After extrapolating the growth curve, the equivalent dose can be derived from the intersect of the constructed growth curve with the dose axis.

peated thermal treatment and irradiation of the same aliquot, have been reported as serious limitation of single aliquot protocols applying regenerative doses (e.g., Wintle, 1997).

However, the MAAD-protocol is also faced with a set of considerable methodological problems. One of them is the fact that multiple aliquot dating requires a large number of aliquots and is, thus, only possible for samples that are providing a sufficient amount of suitable material (e.g., Duller, 1995). Another disadvantage may arise from the extrapolation of the dose response curve. As there are no measured datapoints for the low dose region (i.e., doses lower than the natural dose), the exact shape of the growth curve is not known, which can cause severe uncertainties in determining the precise position of the intercept with the x-axis. In thermoluminescence dating, dose response curves have been reported to show a supralinear signal increase for the low dose region that have to be taken into account when equivalent doses are determined (e.g., Aitken, 1985; Schmidt, 2013). Although such low-dose supralinearities are commonly assessed to be of less importance for optically stimulated dating (e.g., Aitken, 1998), they cannot completely be excluded. Together with the uncertainties arising from non-linear curve fitting, which is regularly required for older samples, the low reliability of extrapolation procedures may significantly hamper the determination of accurate estimates for equivalent doses (e.g., Preusser et al., 2008).

The most important limitation of MAAD-procedures, however, arises from the mechanism of luminescence production itself, which has already been described in section 2.1.2 on page 21. Different aliquots should normally contain a variety of grains showing a great diversity of mineral structures. As a consequence, different aliquots will exhibit different luminescence sensitivities even if originating from a homogeneously irradiated bulk sample (e.g., Duller et al., 2000). In MAAD approaches, dose response curve construction is based on datapoints derived from averaging the single measurements made for the individual aliquots of each group (e.g., Lomax, 2009). Thereby, the scatter of data will introduce serious uncertainties to mathematical growth curve fitting and to equivalent dose determination (e.g., Preusser et al., 2008).

This major limitation of MAAD-protocols requires normalisation procedures that provide the possibility to correct for such inter-aliquot variations in luminescence sensitivity. In fact, several normalisation procedures have been proposed for

TL and OSL dating, amongst others including '*weight normalisation*', '*short shine normalisation*' and '*equal total dose normalisation*'[2] (e.g., Aitken, 1985; Wintle, 1997). The weight normalisation is achieved be weighing each measured disc and calculating a correction factor that is applied to normalise the luminescence signal derived from the respective disc to standardized amount of mass (e.g., Wintle, 1997). For fine grain samples, such a time consuming procedure is usually considered not to be necessary, since a sufficient uniformity of sample deposition on each disc is assumed to be guaranteed by the procedure which is applied to produce the discs (e.g., Aitken, 1985; Wintle, 1997). For short shine normalisation, each disc is exposed to a short light stimulation (normally $\leq$ 0.1 s), during which the luminescence emission is recorded. Since this initial part of the natural signal is measured prior to any laboratory treatment, it can be used as normalisation factor (e.g., Wintle, 1997). The equal total dose normalisation is based on the measurement of OSL response to a fixed test dose, which is applied to the aliquots after the OSL readout for equivalent dose determination. This approach includes a series of bleaching, preheat and artificial irradiation steps applied to each aliquot before the test dose irradiation in order to ensure identical pretreatment histories for each aliquot (Wintle, 1997; Schmidt, 2013).

In order to account for inter-aliquot scatter, a weight normalisation was applied to the polymineral and quartz separates of the fine grain fraction of sample BT 737, which were measured by applying the MAAD-procedure. Thereby, the amount of grains dispensed on each disc was quantified by weighing the material using a high precision balance. For preparing 100 discs, 206.2 mg of sample material were suspended in 25 ml of de-ionised water. 200 µl of this suspension were pipetted onto each disc, resulting in a constant amount of ~2 mg sample material uniformly dispersed on each disc. The samples were divided into 5 different groups of subsamples, each consisting of 5 aliquots. Four of these groups were β-irradiated using increasing additive doses, whilst the fifth group was used for measuring the natural luminescence signal. After irradiation and prior to OSL readout, aliquots of polymineral material were stored in a drying chamber at 70°C for 7 days, whereas aliquots containing quartz were stored at room temperature. Indicated by low mathematical fitting errors, the best results for dose response curve construction

[2] Please note that in TL dating this approach is usually termed 'equal pre-dose normalisation' (e.g., Wintle, 1997).

were found by using single saturating exponential functions. Since low-dose supralinearity has been reported to be unusual in OSL dating (e.g., Aitken, 1998), we decided not to apply any kind of supralinearity correction.

2.2.2 The single aliquot regenerative dose protocol (SAR-protocol)

With the single aliquot regenerative dose (SAR) protocol introduced to luminescence dating by Murray & Wintle (2000) and refined by Murray & Wintle (2003), there is a well established standard procedure commonly used in quartz OSL dating. The basic idea of this approach is to derive the equivalent dose of a sample by determining individual equivalent doses for a large number of single aliquots of the sample. Since all measurements for D_e determination are carried out on a single aliquot, the SAR protocol is able to circumvent the above described problems arising from varying luminescence properties of grains from different aliquots which are used in MAAD procedures (e.g., Preusser et al., 2008).

However, the SAR protocol in principle follows regenerative dose techniques. Once the natural luminescence signal is measured, these techniques make use of repeated OSL measurements applied to the very same aliquot after administering different laboratory doses (*regenerative doses*) in order to construct dose response curves. As already mentioned above, such repeated irradiation and readout cycles may induce changes in luminescence sensitivities (e.g., Duller, 1991; Stokes, 1994; Chen & Pagonis, 2011). If not corrected for, these sensitivity changes will cause severe changes in the OSL response to the given doses, which will result in erroneous dose response curves.

The major breakthrough achieved by the SAR procedure proposed in Murray & Wintle (2000) is to monitor any sensitivity change that may occur during the measurement procedure by determining the OSL response to a constant test dose which is administered to the aliquot after each measurement of natural and regenerative signals (e.g., Preusser et al., 2008). Thus, each measurement cycle consists of two sub-cycles – a cycle to determine the natural or regenerative dose response and a subsequent cycle to detect the test dose response. Thereby, the test dose response T_x is used as measure for sensitivity changes induced by the preceding measurement of the natural or regenerative signal L_x. These changes in lumines-

cence sensitivity are corrected by normalising the L_x-signals to their corresponding T_x-signals which is done by dividing each L_x-value by the subsequent T_x-value. These sensitivity corrected luminescence signals (L_x/T_x) are used for growth curve construction (e.g., Preusser et al., 2008). The equivalent dose is determined by interpolating the sensitivity corrected natural luminescence signal (L_n/T_n) onto this dose response curve (e.g., Duller, 2008a)

Structural details of the used SAR protocol are illustrated in Figure 2.8 and the measurement routine applied in this PhD-thesis is described in the following paragraphs. In a first measurement cycle, the natural luminescence signal is determined by applying an optical stimulation at an elevated measurement temperature of 125°C (step 2), following a preheat treatment (step 1). Preheating the sample is of essential importance in order to guarantee that all unstable trap populations are empty and cannot contribute to the luminescence signals used for equivalent dose determination (e.g., Duller, 2008a). For each luminescence sample investigated in this study, the most adequate preheat temperature was individually derived either from *preheat plateau tests* (PPT) or from combined *dose recovery and preheat tests* (DRT), which will be described in detail on page 53. With respect to preheat plateau tests, the equivalent dose of different groups of aliquots is determined for a set of different preheat temperatures (e.g., Lomax, 2009). The determined equivalent doses are plotted against the respective preheat temperatures in order to identify a preheat plateau. As pointed out by Murray & Wintle (2000), such consistent D_e-values over a range of temperatures indicate a sufficiently successful isolation of stable signal components. Thus, any temperature from this plateau can be used as suitable preheat temperature for equivalent dose determination.

After measuring the natural signal, the sample is beta-irradiated using a small test dose (typically $\leq$ ~10% of the expected equivalent dose). This test dose remains constant throughout the whole measurement procedure. Again a preheat step is applied, followed by an optical stimulation to determine the test dose response. Unlike the preheat procedure prior to L_x-signal measurements, the preheat temperature prior to T_x-measurements is not held for 10 seconds, but carried out as short heating, commonly called '*cutheat*' (e.g., Cordier, 2010). This term implies that the sample is immediately cooled after the preheat temperature was reached (e.g., Murray & Wintle, 2000). With respect to this cutheat-step, a variety of approaches were suggested considering different combinations of preheat/cutheat-

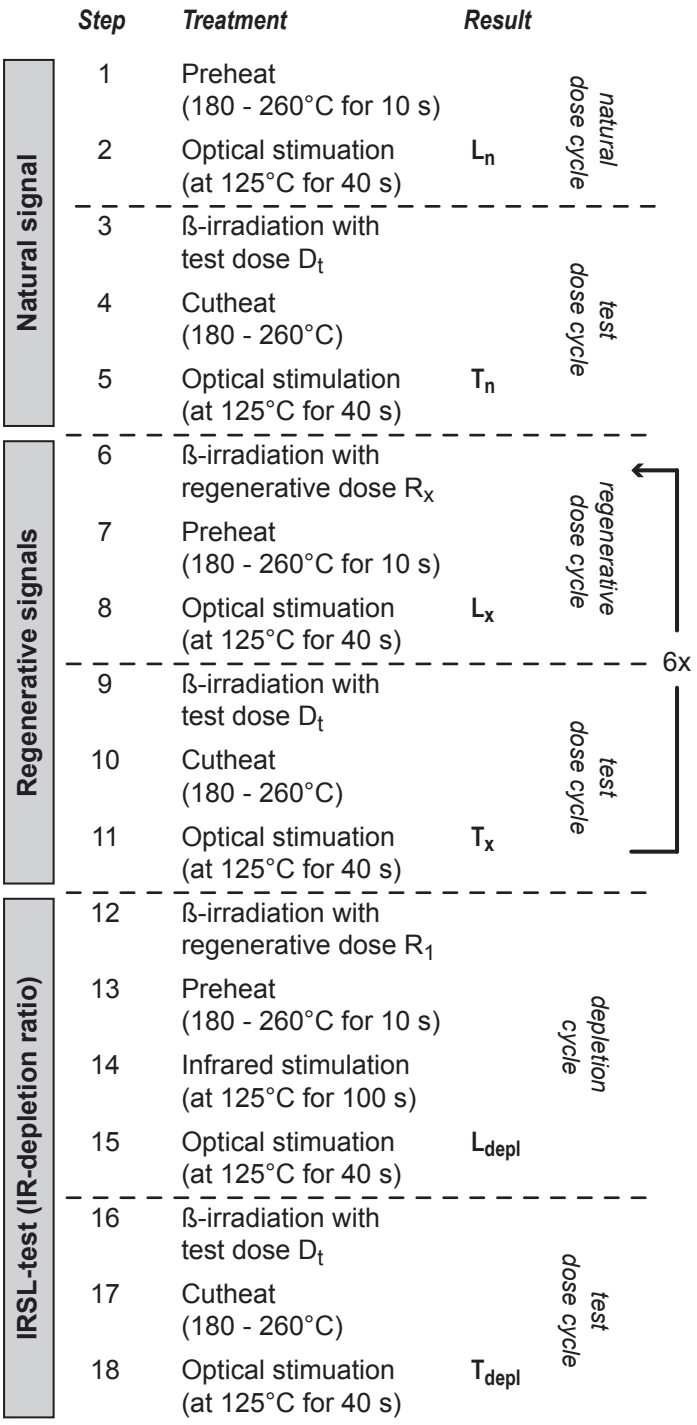

Figure 2.8: The single aliquot regenerative (SAR) dose protocol applied in this PhD-thesis. In principle following the basic protocol introduced by Murray & Wintle (2000), we applied several slight adjustments. First of all, we added an IR depletion test proposed by Duller (2003) at the end of the measurement sequence – please note that the IR-stimulation was performed at 125°C. Preheat temperatures were chosen according to the results of a combined dose recovery and preheat test. Cutheat temperatures used for the test dose cycles were always identical with the preheat temperatures.

temperatures, among others (e.g., Bailey, 2000) including a constant cutheat of 160°C independent of the preheat temperature (e.g., Murray & Wintle, 2000) and a cutheat temperature which is always 20°C lower than the preheat temperature (e.g., Murray & Wintle, 2003; Wintle & Murray, 2006). For this PhD-thesis, we decided to apply a cutheat temperature that was equal to the preheat temperature.

The second part of the SAR protocol comprises a set of several regenerative dose steps. Thereby, the aliquot is repeatedly irradiated with increasing doses supplied by an $^{90}Y/^{90}Sr$ β-source. For each regenerative dose, the induced luminescence signal is measured, followed by a test dose cycle to monitor sensitivity changes. In order to optimize growth curve fitting and to guarantee a precise interpolation of natural signals, regenerative doses should be chosen to bracket the expected equivalent dose. For the SAR protocol applied in this PhD-thesis a total of 6 regenerative dose points was used, including four regenerative doses corresponding to ~40%, ~70%, ~130% and ~160% of the expected equivalent dose, an additional zero dose step and a repeated 40%-step (recycling step) at the end of the regenerative cycles. This recycling step can be used as internal quality test.

The final part of the SAR protocol comprises an IRSL-test that intends to check the purity of the measured quartz separates. Although sample preparation aims at providing pure quartz extracts, there may still be some feldspar contaminations either due to remnants of feldspar minerals that could not completely be removed by the density separation and etching procedures or due to feldspar inclusions. Thus, an additional test is required to ensure that only those aliquots containing pure quartz grains are considered for equivalent dose determination. For this purpose, the respective aliquot is once more artificially irradiated administering the same dose as used for the last regenerative step (recycling step). After preheating, the sample is initially stimulated with infrared light before an optical stimulation using blue LEDs is applied, followed by a normal test dose cycle. Since the infrared stimulation will not or only slightly affect quartz grains on the disc (e.g., Spooner, 1994b; Duller, 2003), luminescence signals detected during this measurement step can merely arise from feldspar grains. These are more or less completely bleached by this procedure[3] and can, thus, not contribute to the subsequent

[3] Duller (2003) reported that the majority of feldspar grains in his experiment had less than 10% of their initial signal remaining after the initial IR stimulation.

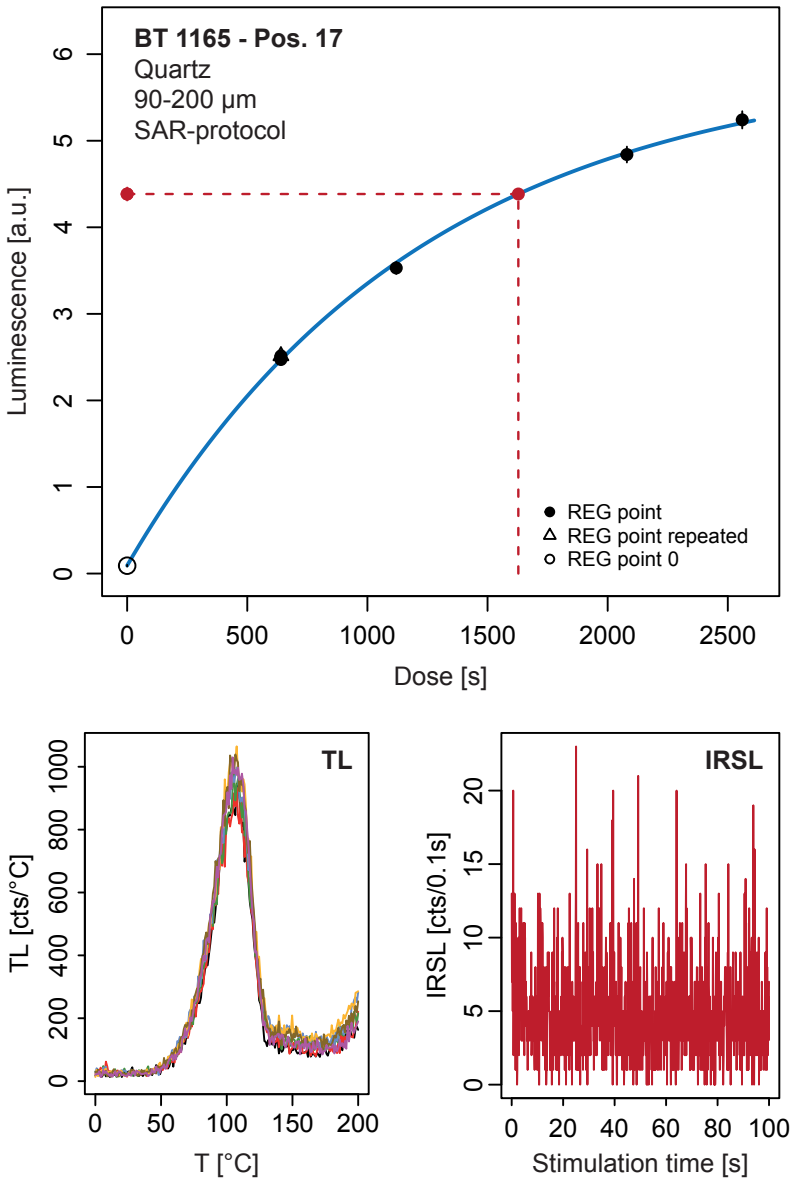

Figure 2.9: Upper part: SAR dose response curve for an aliquot of sample BT 1165. The black circles and triangles represent the sensitivity corrected luminescence signals for the administered regenerative doses (L_x/T_x). The red circles illustrate the sensitivity corrected natural signal (L_n/T_n). A single saturating exponential function was used for growth curve fitting (blue line). The equivalent dose is determined by projecting the L_n/T_n onto this curve. Lower part: TL measurement curves (left side) and IRSL shinedown curve (right side) for the same aliquot of sample BT 1165. The shape of the TL curves reveal an pronounced peak at ~110°C reported to be typical for quartz samples. The IRSL shinedown curve doesn't show any detectable signal, indicating an aliquot not contaminated with any relevant feldspar remnants.

blue light stimulation any more. Therefore, the OSL signal recorded during the second stimulation step will exclusively arise from the quartz grains on the disc.

As a result, feldspar contaminations can be detected by two distinct criteria. The first possibility is to examine the shape of the IRSL shine-down curve recorded during the IRSL stimulation. If there is no relevant feldspar contamination, this curve will reveal either no detectable IRSL signal at all or only a small signal slightly exceeding the measurement background. The second criterion is based on the comparison of two blue-OSL signals derived for the same administered dose. Thereby, the ratio of the OSL signal measured after a preceding infrared stimulation and the OSL signal without such a stimulation is calculated. This ratio, which was originally introduced for distinguishing feldspar and quartz grains in single grain dating, was proposed by Duller (2003) and is commonly termed '*OSL IR depletion ratio*' or in a shortened version '*IR depletion ratio*'.

For this PhD-thesis, the luminescence signal detected for the repeated regenerative step (recycling step) was compared with the blue-OSL readout following the IR-stimulation in the last part of the measurement sequence. In order to account for sensitivity changes, the IR depletion ratio was calculated based on the sensitivity corrected luminescence signals according to the formula (e.g., Duller, 2003; Kim et al., 2009)

$$IR\ depletion\ ratio = \frac{L_{IR-depletion}/T_{IR-depletion}}{L_{recycling}/T_{recycling}}. \tag{2.4}$$

If there is no feldspar contamination, the OSL signal measured after IR stimulation will not significantly deviate from the signal measured without IR stimulation. The IR depletion ratio will, thus, be close to unity (e.g., Henshilwood et al., 2002). However, if there is a relevant contamination with feldspar minerals, these minerals will, in fact, contribute to the recycling signal, but not to the post-IR blue signal. For such a case, the preceding IR exposure causes a considerable reduction of the intensity of the subsequent OSL signal (e.g., Duller, 2003; Mauz & Lang, 2004) which will result in an IR depletion ratio significantly differing from unity. By defining a threshold for the IR depletion ratio, it is possible to exclude those aliquots showing luminescence signals characterized by an unwanted feldspar contribution that is assessed not to be acceptable any more.

With respect to this threshold, there is no commonly accepted value. Frequently, values of 10%, 15% or 20% are suggested (e.g., Anechitei-Deacu et al., 2013;

Gaar et al., 2013; Rémillard et al., 2015; Trauerstein et al., 2017). For this thesis, we followed these suggestions and used the IR depletion ratio as additional rejection criterion, applying threshold values of 10% to 20% (for details the reader is referred to the studies in Part II of this PhD-thesis).

As suggested by Murray & Wintle (2000), the performance of the SAR procedure is evaluated by external and internal quality tests. The internal tests comprise two important criteria: *recuperation rate* and *recycling ratio*. The first criterion is based on the zero dose measurement. In theory, this zero regenerative dose should reveal a sensitivity corrected luminescence signal (L_0/T_0) close to zero. In reality, however, there are several mechanisms during previous irradiation, preheating and optical stimulation that are able to trigger a transfer of charges from optically insensitive traps to optically sensitive traps (e.g., Jain et al., 2003; Murray & Wintle, 2003; Wintle & Murray, 2006). Thus, even if administering a zero dose, a sample will most probably exhibit a small, but still detectable luminescence signal. This signal is commonly termed *recuperation* (e.g., Aitken & Smith, 1988). Whilst recuperation values slightly above zero do not necessarily correspond to methodological issues, those significantly exceeding zero may, however, indicate unwanted signal components that were induced by previous measurement steps. High values of recuperation are regularly regarded to as evidence for potentially unreliable measurement procedures (e.g., Preusser et al., 2008) which require modifications of the originally proposed protocol (e.g., Murray & Wintle, 2003).

The degree of recuperation, termed *recuperation rate*, is commonly expressed as percentage of the natural sensitivity corrected signal (e.g., Wintle & Murray, 2006) and calculated according to the following formula (e.g., Kim et al., 2009):

$$\textit{Recuperation rate} = \frac{L_0/T_0}{L_n/T_n}. \tag{2.5}$$

Murray & Wintle (2000) suggested a meanwhile commonly accepted threshold value of 5% for this recuperation rate which was also applied to all measurements performed for this PhD-thesis. For the great majority of our investigated samples, recuperation proved not to be problematic.

A second internal performance test is called '*recycling ratio test*' (e.g., Wintle & Murray, 2006) and verifies whether the sensitivity correction applied during

the SAR protocol was successful (e.g., Preusser et al., 2008). Thereby, the luminescence response to a particular dose, which was administered at the beginning of the SAR procedure, is compared with the response to the same dose repeated at the end of the measurement sequence. Since sensitivity changes are typically reported to be progressive, the first and the last regenerative dose step will represent the widest spread in sensitivity change (e.g., Wintle & Murray, 2006). Therefore, the repeated dose is usually chosen to be identical to the first regenerative dose (e.g., Wintle & Murray, 2006; Lomax, 2009). The repeated luminescence step is regularly called '*recycling step*'. In order to assess the performance of the SAR procedure the '*recycling ratio*' (e.g., Murray & Wintle, 2000) is calculated according to the formula

$$Recycling\ ratio = \frac{L_{recycling}/T_{recycling}}{L_1/T_1}. \tag{2.6}$$

If the SAR correction for sensitivity changes was successful, the sensitivity corrected luminescence signals of both measurement steps should reveal equal values and the recycling ratio should be close to unity (e.g., Wintle & Murray, 2006; Preusser et al., 2008). In order to account for statistical uncertainties, Murray & Wintle (2000) proposed to discard all aliquots for which the recycling ratio exhibits a deviation of more than 10% from unity, corresponding to a range of acceptability from 0.90 to 1.10 (e.g., Wintle & Murray, 2006). This commonly used threshold values were also applied to the samples in this PhD-thesis (for details the user is referred to the studies in Part II).

An important external test to check the robustness of the measurement protocol is the so called '*dose recovery test*' (DRT) (e.g., Wallinga et al., 2000; Murray & Wintle, 2003; Wintle & Murray, 2006). This test aims at evaluating whether the applied SAR procedure is able to reproduce a known laboratory dose with sufficient accuracy (e.g., Preusser et al., 2008). Thereby, the DRT primarily checks whether the first test dose measurement (T_0) is able to provide an appropriate correction for the change in luminescence sensitivity induced by the measurement of the natural signal (e.g., Wintle & Murray, 2006).

After zeroing the natural signal by optical bleaching, aliquots are artificially irradiated with a known laboratory dose. This dose is treated as unknown and determined by applying a SAR protocol using the measurement parameters supposed to be adequate for a correct equivalent dose determination. By calculating the

measured-to-given dose ratio, frequently termed '*dose recovery rate*', the performance of the applied measurement procedure can be assessed (e.g., Murray & Wintle, 2003). Thereby, the dose recovery rate is calculated as

$$DRR = \frac{Measured\ dose}{Given\ dose}. \tag{2.7}$$

If sensitivity correction for the first measurement step is adequate, this measured-to-given dose ratio will be close to unity, indicating the suitability of the applied measurement procedure to recover the given dose with sufficient validity. Additionally, the dose recovery test provides information on the maximum precision that can be expected for the respective sample (e.g., Wintle & Murray, 2006; Preusser et al., 2008).

In this PhD-thesis, dose recovery tests were either carried out as 'normal' DRTs (feldspar samples) or as *combined dose recovery and preheat tests* (quartz samples). For the latter, the artificially bleached and irradiated aliquots were divided into several groups, each consisting of three aliquots. Dose recovery tests were carried out for each group, applying different preheat temperatures in the range of 180°C – 260°C in steps of 20°C. For each preheat temperature the measured-to-given dose ratio was calculated based on the mean D_e values. These group specific dose recovery rates were used to identify the preheat temperature for which the given laboratory dose could be reproduced at its best.

2.2.3 The post-IR IRSL protocol at 225°C ($pIRIR_{225}$-procedure) and fading correction

As already mentioned in section 2.1.3 on page 40, quartz separates proved not to be appropriate for dating the older terrace sequences, identified in the research area. Therefore, feldspars had to be used as dosimeters, providing the opportunity to constrain a chronological framework even for the older evolutionary stages.

In order to avoid the problems associated with anomalous fading in feldspar minerals or at least to minimize its effects, we decided to apply a post-IR IRSL procedure. Over the last years, the $pIRIR_{290}$-protocol, which was originally suggested by Thiel et al. (2011a), has become a very popular approach. Many studies reported fading rates of ~1%$_{decade}$ or less when applying this protocol (e.g., Buylaert et al.,

2012b; Colarossi et al., 2015; Li et al., 2014) and interpreted these low fading rates as mere laboratory artefacts (e.g., Thiel et al., 2011a; Buylaert et al., 2012b). Thus, the post-IR IRSL signal at 290°C is often regarded as a '*non-fading signal*' for which no fading correction is required at all (e.g., Thiel et al., 2011a; Buylaert et al., 2012b).

However, the $pIRIR_{290}$-protocol is also reported to be affected by a hard to bleach signal component. Thus, post-IR IRSL measurements at 290°C are typically characterized by a slow signal depletion and by relatively high unbleachable residual doses (e.g., Kars et al., 2014; Colarossi et al., 2015). For our samples, this was confirmed by preliminary test measurements not presented in this thesis. With particular respect to fluvial environments, which are revealing complex transport mechanisms, the bleachability of the luminescence signal is typically regarded as major problem (e.g., Wallinga, 2002; Rittenour, 2008; Kars et al., 2014).

In their study, Kars et al. (2014) dealt with the problem of signal resetting for different post-IR IRSL procedures under natural conditions, comparing subaerial and sub-aqueous bleaching. For sub-aqueous conditions, they were able to show that $pIRIR_{290}$-signals are significantly harder to bleach than under full sunlight exposure (similar results were reported for $pIRIR_{290}$- and $pIRIR_{225}$-signals by Lowick et al., 2012). Kars et al. (2014) also concluded that the difference between filtered (i.e., sub-aqueous) and the full spectrum bleaching will significantly increase with higher stimulation temperatures, which they attributed to large distance transport of charges within the crystal lattice during recombination processes at elevated temperatures.

As a result, the findings of Kars et al. (2014) and of other studies (e.g., Lowick et al., 2012; Colarossi et al., 2015) may be summarized in the following sense: Although higher stimulation temperatures significantly reduce the degree of anomalous fading, they are always accompanied by more difficult to bleach signals. Therefore, it is necessary to find a suitable balance between signal stability (i.e., absence of anomalous fading) and signal resetting during transport (e.g., Kars et al., 2014).

Since the complete resetting of luminescence signals is of crucial importance for reliable age estimations, we decided to apply a post-IR IRSL procedure at a stimulation temperature of 225°C. This procedure is reported to show a rather rapid signal bleaching (e.g., Colarossi et al., 2015) and is, however, still characterized

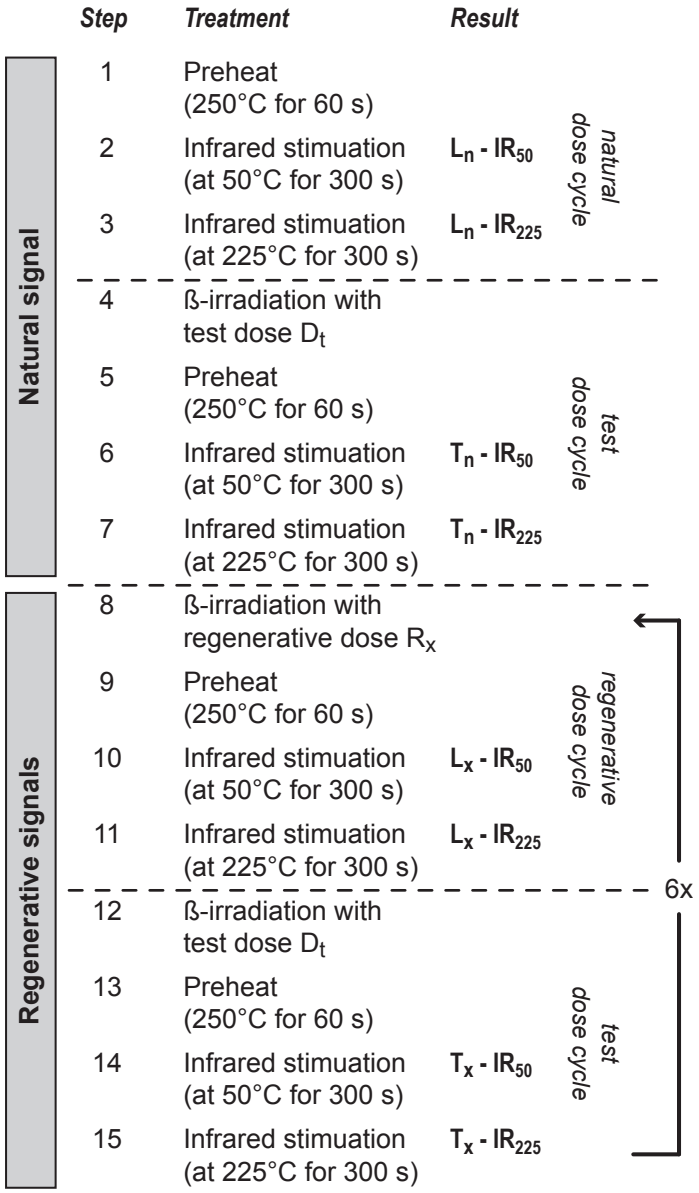

Figure 2.10: The post-IR IRSL 225°C protocol applied in this PhD-thesis. In principle following the $pIRIR_{225}$-protocol proposed by Buylaert et al. (2009), we slightly adjusted the measurement sequence. IR_{50}- and $pIRIR_{225}$-signals were recorded for a prolonged readout time of 300 s. Since recuperation proved not to be problematic, we decided not to apply any hot-bleach step.

by significantly reducing the degree of anomalous fading (e.g., Buylaert et al., 2009, 2012b).

The underlying mechanism of post-IR IRSL measurements has already been described in section 2.1.3 on page 36. Therefore, only the used measurement parameters are reported in the following paragraphs. The structure of the applied measurement sequence is additionally illustrated in Figure 2.10.

With minor adjustments, we followed the protocol proposed by Buylaert et al. (2009), which is in principle a single aliquot regenerative dose procedure including several regenerative and test dose cycles (see the explanations on page 46). After applying a preheat temperature of 250°C for 60 s, a first IRSL readout was performed at a stimulation temperature of 50°C, followed by a second infrared stimulation at 225°C. For this PhD-thesis, IR_{50}-signals as well as IR_{225}-signals were recorded for a total of 300 s, whereas Buylaert et al. (2009) applied a readout time of 100 s for both measurement steps.

Furthermore, Buylaert et al. (2009) suggested a '*clean out*' step, i.e. a high temperature IR-stimulation for 40 s at 290°C, at the end of each test dose cycle in order to reduce recuperation. This additional step is commonly termed '*hot bleach*' or '*hot wash*' step. Since recuperation proved to be negligible for all investigated samples in our study, we did not apply such a high temperature clean out. For further details, the reader is referred to the explanations in Study 3 on page 147.

Although post-IR IRSL procedures are often assumed not to be affected by anomalous fading, measurements performed to determine the degree of fading could not confirm this assumption for our samples. Laboratory fading rates ('*g-values*') of ~3%$_{decade}$ to ~4%$_{decade}$ (see Table 5.5 on page 172) revealed a significant loss of luminescence signal for all feldspar samples analysed in this PhD-thesis.

If not corrected for, anomalous fading will, by all means, result in severe age underestimations. Different approaches have been suggested to cope with the problem and to be able to use feldspars as reliable dosimeters. These approaches comprise numerous correction models based on the exact assessment of sample specific fading rates. In order to explore the extent of signal loss attributed to the fading phenomenon, laboratory fading experiments are performed. Thereby, repeated L_x/T_x measurements are carried out, applying various storage times between irradiation always administering the same β-dose and luminescence readout. The measured L_x/T_x-values are plotted against the time elapsed since the respective irradia-

tion, which is depicted on a log scaled x-axis. Applying a linear fitting function, a regression line can be constructed, for which the slope is derived. This slope quantifies the degree of anomalous fading and corresponds to the percentage of signal loss per decade of time, commonly referred to as '*g-value*' (e.g., Aitken, 1985). For details of fading test procedures, the reader is referred to the very informative explanations given by Auclair et al. (2003).

The determined '*g-values*' do not only characterize the amount of fading for the specific sample, but are also used to calculate fading-corrected luminescence ages derived from applying different mathematical algorithms. These correction models, however, are still controversially discussed (e.g., Wallinga et al., 2007; Lowick et al., 2012; Preusser et al., 2014), since all of them are affected by the major drawback that they are based on specific assumptions that cannot be verified (e.g., Thiel et al., 2011a; Thiel, 2011).

With the approach proposed by Huntley & Lamothe (2001), the dose rate correction (DRC) method of Lamothe et al. (2003) and the model introduced by Kars et al. (2008), a total of three correction procedures were applied to the samples in this PhD-thesis. However, the latter two methods failed in our study due to so far unknown reasons. In fact, it was not possible to apply an adequate mathematical function which allowed to fit the corrected values to a suitable growth curve. First preliminary results of systematic test measurements indicate two possible sources of error.

One of them is the precision of fading measurements, which are required to determine the laboratory fading rates (g-values) and to derive the recombination centre densities (ρ'). While the latter is used in the algorithms of Kars et al. (2008), the first parameter is essential for the DRC method of Lamothe et al. (2003). Systematic investigations showed that both approaches are very sensitive to slight modifications of these parameters. Thus, the precision of fading experiments, which is strongly affected by the specific measurement settings, might be the limiting factor.

A second possible source of error may be attributed to the specific measurement parameters used for the post-IR IRSL protocol. As already mentioned, the post-IR IRSL measurement sequence in principle is a regenerative dose procedure similar to the SAR-protocol applied to quartz samples. Therefore, we used the same regenerative dose points commonly applied for SAR-procedures at the luminescence

laboratories of the University of Bayreuth. Thus, regenerative dose points corresponding to ~40%, ~70%, ~130% and ~160% of the expected equivalent doses were used to construct the original dose response curves. The correction methods presented in Lamothe et al. (2003) and Kars et al. (2008), however, were always applied to dose response curves which were constructed from regenerative points reaching up to the high dose region near the saturation level of the samples. The serious problems, we were confronted with when applying the correction methods, may arise from the fact that our growth curves do not include this high dose region, which may cause an inappropriate mathematical data fitting.

To test both hypothesis, time consuming systematic measurements are required, including high-dose experiments and long lasting g-value measurements, which could not be considered for this PhD-thesis. Since the procedures of Lamothe et al. (2003) and Kars et al. (2008) could not be applied to derive fading corrected ages, they are not discussed here in detail. For further information, the interested reader is referred either to the original publications of Lamothe et al. (2003) and Kars et al. (2008) or to the short summary provided by Li et al. (2017a).

As a result, only the linear correction method of Huntley & Lamothe (2001) could successfully be applied. This method is in principle based on the following equation, which was introduced as equation [4] in Huntley & Lamothe (2001):

$$I = I_c \left[1 - \frac{g}{100} \cdot \log_{10} \left(\frac{t}{t_c} \right) \right] . \tag{2.8}$$

Thereby, I represents the luminescence intensity measured after a storage time of t, while I_c is the luminescence intensity at an arbitrary time t_c after artificial irradiation. The functionality of this correction method can easier be understood, when the formula is rewritten to the form of equation [1] proposed by Lamothe et al. (2003):

$$\frac{T_f}{T} = \frac{I_f}{I_0} = 1 - \kappa \cdot \left[\ln \left(\frac{T}{t_c} \right) - 1 \right] , \tag{2.9}$$

where T is the true age and T_f the apparent age affected by fading. I_f represents the fading affected luminescence intensity derived from the actual measurements of natural luminescence signals and I_0 equals the luminescence intensity expected if fading was not present. The sample specific constant κ is the fractional decay of

luminescence (e.g., Huntley & Lamothe, 2001; Lamothe et al., 2003) and can be derived from the determined g-values (e.g., Morthekai et al., 2011) by

$$\kappa = \frac{g}{100 \cdot \ln(10)}. \tag{2.10}$$

Assuming a linear relation between luminescence intensity and age, the true, i.e. fading corrected, sedimentation age is derived by iteration. As the basic assumption of this correction method is the linear relation of age and intensity, expressed as

$$\frac{T_f}{T} = \frac{I_f}{I_0}, \tag{2.11}$$

this method can actually only be applied to the linear part of the dose response curve and is, therefore, restricted to rather young samples (e.g., Lamothe et al., 2003; Huntley & Lamothe, 2001). However, some studies (Buylaert et al., 2008, 2011) were able to show that the procedure of Huntley & Lamothe (2001) could also successfully be applied to samples of Eemian (MIS 5e) age. Thus, they suggested that it might be able to apply the linear correction model to luminescence intensities even in the non-linear part of the dose response curve.

In such a case, the procedure of Huntley & Lamothe (2001) will, however, most probably only provide an insufficient fading correction. Even if the degree of age underestimation is significantly reduced, the corrected ages might still be affected by serious age underestimations. Since all feldspar samples investigated for this PhD-thesis revealed equivalent doses beyond the linear part of the dose response curve, this might be a major problem associated with the fading corrected ages presented in Study 3 (see Chapter 5).

2.3 Dosimetry

The second value needed for the calculation of luminescence ages is the environmental dose rate ($\dot{D}$) which is defined as the rate at which energy is absorbed by a grain from the flux of ionising radiation to which it is exposed (Aitken, 1998) and commonly expressed as the sum of its various components (e.g., Liritzis et al., 2013a):

$$\dot{D} = a \cdot \dot{D}_{\alpha} + \dot{D}_{\beta} + \dot{D}_{\gamma} + \dot{D}_{cosmic} \tag{2.12}$$

Thereby, α, β,γ and *cosmic* indicate the contributions of individual radiation components and *a* represents the alpha efficiency factor. The major part of the environmental dose rate originates from the radioactive decay of natural occurring radioisotopes either from the surrounding sediments (*external dose rate*) or from within the minerals to be dated (*internal dose rate*). The main sources of natural radioactivity are ^{40}K, ^{238}U, ^{235}U, ^{232}Th and to a minor part ^{87}Rb (e.g., Aitken, 1985). These nuclides emit α- and β-particles as well as γ radiation each of which characterized by different energies and penetration ranges (e.g., Wagner, 1998). While ^{87}Rb is a pure β-emitter, β-particles and γ-rays are emitted when nuclei of ^{40}K decay either into stable ^{40}Ca or ^{40}Ar. The ionising radiation from natural uranium and thorium is provided by radioactive decay chains in which the parent nuclides decay through a series of unstable daughter nuclides until final non-radioactive products (various stable lead isotopes) are reached. Thereby, the various members of these decay chains emit a variety of α, β and γ radiations (e.g., Aitken, 1985). Details of the radioactive series of uranium and thorium as well as on the decay of ^{40}K and ^{87}Rb are given in the Appendix on page 229.

Alpha particles consist of two protons and two neutrons (see Figure 2.11a) and can, thus, be regarded as accelerated He^{2+} nuclei (e.g., Preusser et al., 2008). Due to their large size and mass, α-particles interact heavily with atoms and molecules of the penetrated sediments. Thus, they lose their energy rapidly and are characterized by a limited penetration depth typically in the range of ~20 µm to 25 µm in material of an average density of 2.5 $^{g}/_{cm^3}$ (e.g., Grün, 1989; Aitken, 1998). As a result, the ionising effects originating from alpha particles are highly localized to the nearby surroundings of the emitting nuclei. Due to their huge mass, α-particles, furthermore, do not get scattered, but travel in straight lines (*tracks*) through the affected mineral grains. On their way, they produce secondary

electrons by ionisation processes which are concentrated in narrow cylinders with diameters of ~0.1 µm surrounding the tracks of the α-particles (e.g., Aitken, 1998). Along their tracks, α-particles are, therefore, characterized by a high ionisation density, i.e. electron traps close to the central core of the α-track are saturated rapidly and a large proportion of energy provided by α-particles gets wasted and cannot contribute to the accumulation of luminescence signals. As a consequence, heavily ionising alpha particles are less effective in inducing luminescence than the lightly ionising β-particles and γ-rays, which get scattered in the penetrated mineral grains and therefore, tend to produce a continuously distributed ionisation within the internal structures of the affected grains.

The poor luminescence effectiveness of α-particles is normally considered by applying an *alpha efficiency factor* that reflects the lower ionisation efficiency. Thereby, different approaches have been proposed (k-value system, a-value system, b-value system; see Aitken, 1985, 1998; Schmidt, 2013). For this PhD-thesis, the a-value system was applied when the contribution of α-particles had to be considered for dose rate determination. This had to be done for fine grain separates which are completely penetrated by all radiation components and for coarse grain feldspar separates that have not been etched (see explanations on page 71). However, the determination of a-values is a time-consuming procedure. As a-values are regularly reported to show only modest inter-sample varieties, the a-values used for in this PhD-thesis were not individually measured for each sample, but derived from literature. For coarse grain feldspar samples (see Study 3) a-values of 0.07 ± 0.02 (e.g., Preusser et al., 2014, 2016) were used for considering the alpha attenuation in the non-etched samples. For fine grain samples (see Study 1 and Study 2) a-values of 0.07 ± 0.02 (polymineral separates) and 0.04 ± 0.02 (quartz separates) were adopted from Kreutzer (2014).

For sand sized quartz dosimeters, the problem of reduced alpha efficiency is of minor importance as long as an etching procedure is applied. For coarse grain luminescence dating, sand sized grains with diameters of 90-200 µm are commonly used (see the explanations on page 69). These grains are rather large compared to the penetration range of ~20 µm characteristic for α-particles. Thus, the external alpha radiation can only affect the outer rim of these sand sized grains (e.g., Aitken, 1985). As quartz minerals are commonly regarded to be free of internal alpha emitters, the inner core of these grains can only be reached by beta, gamma

and cosmic radiation (e.g., Aitken, 1998). The external alpha contribution can be neglected if the outer alpha affected rim of the mineral grains is removed. This can be achieved by etching the quartz separates with concentrated hydrofluoric acid (HF) (e.g., Aitken, 1998).

All coarse grain quartz separates which were measured for this PhD-thesis were subjected to an etching procedure applying 40% hydrofluoric acid for at least 45-50 minutes. For some samples, this procedure was repeated several times as they still showed signs of a significant feldspar contamination. As a result, the contribution of alpha radiation was negligible for all coarse grain quartz separates in this study and was not taken into account when dose rates were determined for these separates.

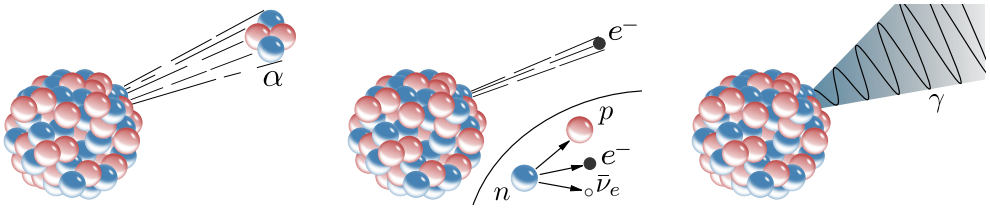

(a) Alpha decay – an atomic nucleus emits an alpha particle consisting of two protons and two neutrons. Showing an atomic weight of 4, α-particles carry two units of positive charge.

(b) Beta decay – due to nuclear disintegration a neutron is converted into a proton. Thereby, a negatively charged electron (black circle) and an antineutrino (white circle) are released.

(c) Gamma ray emission – excited atomic nuclei can relax to stable states by emitting high energetic electromagnetic waves which carry off the excess energy as gamma ray photon.

Figure 2.11: Diagrams of three main mechanisms of natural occurring radioactive decay. Protons are illustrated in red, neutrons in blue. Downloaded under public domain license from Wikimedia Commons (2016, 2017a,b).

Beta particles are high velocity electrons originating from nuclear disintegration in the nuclei of specific radioisotopes. Thereby, a neutron is converted into a positively charged proton, emitting a negatively charged electron of high energy, accompanied by an antineutrino (see Figure 2.11b). Showing a great variety of energies, β-particles are much lighter than α-particles and show penetration depths of up to ~2 mm in silicates (e.g., Grün, 1989). Just like γ-rays, β-particles can fully penetrate minerals of all grain size fractions commonly used for luminescence dating. Along their paths, β-particles experience a progressive loss of energy due to interactions with atoms of the crystal lattice (e.g., Wagner, 1998). This process is termed

beta attenuation and has to be considered when the beta contribution is calculated. Its amount strongly depends on the grain size as well as on the etching procedure, which accentuates this effect (e.g., Aitken, 1998). In order to account for the beta attenuation, grain size dependent beta attenuation factors are considered in the formulas applied for dose rate determination. Meanwhile, several datasets providing grain size specific attenuation factors were proposed including those of Mejdahl (1979), Brennan (2003) and Guérin et al. (2012).

For this PhD-thesis the updated beta attenuation factors provided by Brennan (2003) were applied along with the etch depth attenuation factors proposed in the same article. All calculations were done applying the 'Dose Rate and Age Calculator' (DRAC, version 1.2) introduced by Durcan et al. (2015). The used datasets can be found on the homepage of DRAC[4] and are summarized in the tables of the Appendix on page 223-227.

Gamma radiation can either be described as high energetic electromagnetic waves characterized by extremely short wavelenghts of less than 10^{-11} m or as constant flux of discrete photons of high energies in the range of 10^4 to 10^7 eV (e.g., Demtröder, 2017; Lomax, 2009). Gamma ray emission is a common byproduct of various nuclear processes, such as alpha or beta decay, neutron capture or nuclear fission (e.g., Demtröder, 2017). The emission of gamma rays does not alter the number of protons and neutrons in the nucleus. Gamma ray emission results in the relaxation of excited atomic nuclei from high (unstable) to low (stable) energetic states by carrying off the excess energy in form of gamma ray photons (see Figure 2.11c). Being electromagnetic waves, γ-rays do not have any mass and show only little interaction with atoms or molecules in the penetrated sediments. Thus, they are characterized by a low ionisation density as well as by a large average range of ~30 cm reported for silicates with a density of ~2.5 g/cm^3 (e.g., Grün, 1989; Aitken, 1998). Unlike β-particles, γ-rays experience only a negligible attenuation when penetrating sand sized grains. Therefore, no correction factor is needed for determining the gamma radiation contribution (e.g., Lomax, 2009).

A crucial point in dose rate determination, which is regularly regarded to be a serious limitation of the accuracy of luminescence dating (e.g., Aitken, 1985; Preusser et al., 2008), is the appropriate consideration of *interstitial water con-*

[4] https://www.aber.ac.uk/en/dges/research/quaternary/luminescence-research-laboratory/dose-rate-calculator/?show=datatables.

tents. Water in the pores of soils absorbs a considerable part of the radiation emitted by the naturally occurring radionuclides of the uranium and thorium decay chains as well as by ^{40}K. Thus, only reduced portions of the emitted radiation are able to reach the mineral grains where they can be absorbed and contribute to the accumulation of luminescence signals. As the determination of dose rate is based on measurements performed on dried sample material (see explanations on page 72), the water content has to be incorporated into the dose rate calculation (e.g., Duller, 2008a).

Thereby, the effects corresponding to the present day moisture content of a sample could easily be assessed and compensated by determining the degree of wetness measured as found (e.g., Aitken, 1998). However, the present day water content may not be representative for the burial period which might have been persisting over thousands of years and potentially comprising various climate and environmental conditions. Thus, an accurate and representative determination of environmental dose rates requires reliable estimations of average water contents over the whole burial period, considering significant variations due to climatic changes as well as due to natural or human interference with the drainage of the sampling location (e.g., Aitken, 1985).

As the knowledge of past climate and environmental conditions is rather limited, there is an undeniable lack of information concerning frequency and extent of water content variations in the past, which makes the water content a difficult parameter to be estimated (e.g., Duller, 2008a). Therefore, the water content is regularly regarded as the greatest source of systematic uncertainty in luminescence dating (e.g., Preusser et al., 2008).

For this PhD-thesis, the present day water contents were individually measured for each sample (see page 72) and used as guidelines for the estimation of *true water contents* which were used in dose rate determination. Apart from the present day water content and the saturation capacity derived from the porosity of the material, location specific information such as sedimentological properties, hydrological conditions and differences in the geographical settings of the locations were considered in order to gain well-founded estimates of the average water contents regarded to be representative for the respective burial period. With respect to the considerable uncertainties related to this approach, large absolute errors were assumed for the water contents in this study.

The explanations given in the paragraphs above focused on illustrating the so-called *external dose rate*, i.e. those components of the total environmental dose rate originating from the surrounding sediments of a sample. With respect to dating applications, the *internal component*, i.e. the contribution of radiation emitted from within a mineral grain, may also have a significant impact on the total dose rate and has to be considered under specific conditions. For quartz, the internal dose rate is usually assumed to be negligible (e.g., Aitken, 1998; Preusser et al., 2008), although some grains may exhibit a slight alpha activity (e.g., Aitken, 1998). Feldspar minerals on the other hand, commonly show significant amounts of potassium and at least small percentages of rubidium. As both elements exhibit radioactive isotopes (^{40}K and ^{87}Rb), there is a considerable internal contribution to the total dose rate. This is particularly true for potassium feldspars, for which internal contents in the range of 10-14% and 0.02-0.05% have been reported for potassium and rubidium, respectively (e.g., Aitken, 1998). Due to the attenuation of external radiation components, the proportion of internal radiation increases with grain size. For coarse grain feldspar minerals showing diameters of >100 µm, the internal beta contribution is undeniably significant (e.g., Aitken, 1998).

In this PhD-thesis, the internal dose rate had to be considered for all coarse grain feldspar samples that were used for post-IR IRSL dating in Study 3 (see page 133). Thereby, an internal potassium content of 12.5 ± 0.5% was not measured, but derived from literature (e.g., Huntley & Baril, 1997).

An additional source of natural radiation is the *cosmic radiation* mainly consisting of high energetic protons and alpha-particles (e.g., Prescott & Hutton, 1994). These primary components interact with molecules in the Earth's atmosphere and produce a cascade of lighter particles characterized by a wide variety of particle sizes, masses and energies. These *secondary cosmic rays* are divided into two subcategories termed *hard component* and *soft component* (e.g., Aitken, 1998). While the major part of the soft component is already absorbed by the Earth's atmosphere or at least by the top half-meter of sediment (e.g., Aitken, 1998), the hard component, dominantly consisting of muons, is able to penetrate to much greater depths below ground level and may, thereby, significantly contribute to the total environmental dose rate (e.g., Prescott & Hutton, 1994; Aitken, 1998).

The amount of cosmic rays reaching the surface is determined by two factors: the shielding provided by the Earth's magnetic field and the absorption of radiation in

the atmosphere. While the latter is dominated by the thickness of atmosphere and therefore by the elevation above sea level, the shielding from the Earth's magnetic field significantly varies with the geographical position. For assessing the cosmic component of the environmental dose rate, latitude, longitude and elevation a.s.l. have to be considered for each sampling location (e.g., Liritzis et al., 2013a).

However, the most important local factor is the thickness of sediment covering the sampled material and attenuating the cosmic radiation (Barbouti & Rastin, 1983; Prescott & Hutton, 1988). The effect of this sediment overburden can accurately be calculated if the burial depth is known. Thereby, it is regularly assumed that the sampled material has rapidly been buried following deposition and that the thickness of the overburden has remained fairly constant (e.g., Duller, 2008a). This assumption is justified in many cases, may, however, result in serious dosimetric problems if there have been significant changes in overburden thickness over time.

Apart from exceptional environmental settings where uranium, thorium and potassium concentrations are remarkably low, the cosmic contribution to the total environmental dose rate is only of little significance (e.g., Duller, 2008a, typically ~5% or less of the total dose rate).

For this PhD-thesis, cosmic dose rates were calculated according to Prescott & Hutton (1994) using the `'calc_CosmicDoseRate'`-function provided by the `R` package `'Luminescence'` (e.g., Kreutzer et al., 2012b, 2016). Thereby, the `'half.depth'`-option provided by the function to account for varying overburden thickness was not used for calculation.

All required calculations for dose rate determination were done by using the '`Dose Rate and Age Calculator`' (`DRAC`, version 1.2) introduced by Durcan et al. (2015). Thereby, I used the user interface from `R` to `DRAC` provided by the `R`-function '`use_DRAC`' implemented in the `R` package `'Luminescence'` (e.g., Kreutzer et al., 2012b, 2016). Input data were provided by using the '`template_DRAC`'-function of this package. As already mentioned, various conversion and attenuation factors were applied, which are summarized in the tables of the Appendix (see Table A.1 to B.4 on page 221 to 227). In detail, the following factors were used:

1. Radionuclide conversion factors: Guérin et al. (2011)
2. Grain size attenuation factor for alpha particles: Brennan et al. (1991)

3. Grain size attenuation factor for beta particles: Brennan (2003)
4. Etch depth attenuation factors: Brennan (2003)
5. Water content attenuation factors: Aitken & Xie (1990)

2.4 Applied workflow for luminescence dating in the present PhD-thesis

2.4.1 Sample collection and preparation

2.4.1.1 Luminescence material

All luminescence samples for this PhD-thesis were either collected under daylight conditions working with light-tight cylinders from stainless steel or at nighttime, storing the sample material in opaque plastic bags. For both approaches the profiles had previously been cleaned, photo-documented and described by means of stratigraphical and sedimentological categories. At nighttime sampling, OSL samples were collected after removing the outer rim of sediments that had been affected by sunlight. During this sampling procedure, headlamps were used which provided subdued red light ($\lambda = 640 \pm 20$ nm). For the daylight samples, the material at both ends of the steel cylinders, which was exposed to daylight during the sampling procedure, was removed in laboratory before proceeding with the sample preparation (e.g., Preusser et al., 2008).

Following standard procedures (e.g., Fuchs et al., 2010; Preusser et al., 2008), sample preparation was carried out at the luminescence laboratories of the University of Bayreuth. All laboratory preparation steps were done under subdued red light conditions ($\lambda = 640 \pm 20$ nm). In a first step all samples were wet sieved using standardized sieves with mesh sizes of 250 µm, 200 µm, 90 µm, 63 µm and finally 38 µm, in order to obtain specific grain size fractions. For samples showing huge amounts of coarse sand, also sieves with a mesh size of 1 mm were used. There are three grain size fractions typically used for luminescence dating. These fractions are called *coarse grain fraction*, *middle grain fraction* and *fine grain fraction*. As there is still no commonly applied definition of these terms, they are used with slightly different meanings, depending on the laboratory. At the Bayreuth luminescence laboratories *coarse grain samples* comprise fine sand material showing grain sizes of 90 - 200 µm. The *middle grain fraction* is used for grain sizes of 38 - 63 µm while the term fine grain fraction is restricted to the grain size region of 4 - 11 µm. Apart from two fine grain samples (quartz and polymineral separates of sample BT 737 – see Study 1 in Chapter 3), only coarse grain samples (90 - 200 µm)

were dated for this PhD-thesis. However, for all investigated samples all grain size fractions were prepared.

After sieving, all samples were treated with 10% hydrochloric acid (HCl) and 10% hydrogen peroxide (H_2O_2) to remove carbonates and organic matter (e.g., Fuchs et al., 2010; Preusser et al., 2008). For fine grain samples, the pH-value was permanently monitored during this procedure to avoid coagulation of clay sized particles in the low pH-region of < 3. In order to check whether all carbonates and organic material were completely dissolved concentrated (30%) HCl and H_2O_2 were added for a short time before the samples were repeatedly washed with de-ionised water.

After finishing the chemical treatment, the further preparation procedures differ for fine grain and coarse grain samples:

- *Polymineral fine grain samples (4-11 µm)* were separated by settling material of the <38 µm fraction in Atterberg cylinders applying specific settling times according to Stokes's law in order to remove grains > 11 µm and grains < 4 µm. This settling procedure was repeated as often as required to ensure the completeness of grain size separation (e.g., Mauz et al., 2002). For isolating fine grain separates of pure quartz, subsets of these polymineral fine grain samples were etched using pretreated fluorosilicic acid (H_2SiF_6) (e.g., Syers et al., 1968). In principle referring to the procedure described by Berger et al. (1980), the pretreatment followed the suggestions of Fuchs et al. (2005) who pointed out that optimal pretreatment results could be achieved by adding commercial quartz (100-500 µm) to the untreated acid at a ratio of 1:10 for a total of three days. After filtering out the commercial quartz, the pretreated H_2SiF_6 was used to etch each sample for a total time of six days intercepted by a washing step after three days (e.g., Fuchs et al., 2005). After etching, the quartz separates were washed in 10% HCl and de-ionised water before they were again settled in Atterberg cylinders.

- *The remaining coarse grain material (90-200 µm)* was subjected to density separation using sodium polytungstate solutions of various densities (2.70 g cm^{-3} and 2.62 g cm^{-3} to separate quartz from heavy minerals and feldspars and subsequently 2.58 g cm^{-3} and 2.53 g cm^{-3} to obtain the

potassium-rich feldspar fraction). For the potassium-rich feldspar fraction this heavy liquid density separation was repeated at least three times in order to increase the purity of the separates. The quartz separates were etched in 40% hydrofluoric acid (HF) for 45-50 minutes to remove the alpha-irradiated outer rim and to dissolve remaining feldspar contamination. All samples were rinsed with 10% HCl for 30 minutes and finally washed in de-ionised water before they were re-sieved using analytic sieves with a mesh size of 90 µm. As the effects of etching feldspar separates are still controversially discussed and with respect to recently published findings (e.g., Porat et al., 2015) which point to serious problems associated with HF etching of feldspar minerals, we decided not to apply any kind of etching procedure to the coarse grain feldspar separates measured for this PhD-thesis. Therefore, specific considerations had to be made in order to incorporate the contribution of alpha irradiation to the total environmental dose rate for these unetched samples (see explanations in section 2.3 on page 61).

At this stage, the purity of quartz extracts was checked by a postIR-blue measurement which allowed the calculation of IRSL/OSL-ratios (e.g., Kreutzer, 2014). Thereby, a minimum of five aliquots per sample consisting of unbleached quartz grains were measured, applying a two-step measurement protocol. After preheating to 220°C, these aliquots were first stimulated at 125°C using infrared LEDs, followed by a second stimulation at 125°C with blue LEDs. For both measurement steps, the emitted luminescence was recorded for 40 s using a Hoya U-340 filter which restricted the detection window to the UV band. OSL and IRSL signals were derived from the first 0.4 s of both shine down curves. Based on these signals, an IRSL/OSL-ratio was calculated which was used as rejection criterion. The etching procedure was regarded to be successful when the IRSL contribution was negligible compared to the OSL emission, which was assumed when the majority of aliquots revealed IRSL/OSL-ratios of less than 1% (for a similar approach see Kreutzer, 2014).

Additionally, the purity of each measured aliquot was permanently monitored during dating measurements by (1) determining the '*IR depletion ratio*' (e.g., Duller, 2003, also see explanations in section 2.2.2 on page 49) and (2) by visual inspection of the TL curve shape, i.e. the 110°C TL peak (e.g., Mauz & Lang,

2004). This included test measurements, dose recovery tests, preheat plateau tests and final measurements for equivalent dose determination.

For measurements, coarse grain samples were mounted on aluminium cups and fixed with silicon oil, using various circular templates ('*masks*') to define the quantity of grains per aliquot (e.g., Preusser et al., 2008). Thereby, the overall aim was to minimize the number of grains contributing to the luminescence signal by using so-called '*small aliquots*'. Although this term is not universally defined, it is frequently used to characterize aliquots with a diameter of up to 3 mm (e.g., Duller, 2008b). This procedure was suggested and successfully tested as approach to detect incomplete resetting of luminescence signals (e.g., Fuchs & Wagner, 2003; Duller, 2008b). For quartz samples either 2 mm or 3 mm masks, for feldspar separates only 1 mm masks were used. This restricted the number of grains to ~30-90 (1 mm masks), ~70-150 (2 mm masks) and ~100-300 grains (3 mm masks) (e.g., Duller, 2008b, the accuracy of this assumption was tested for a total of 15 of our samples by counting the number of grains per aliquot for five randomly picked aliquots of each sample). Fine grain samples were settled onto aluminium discs by carefully pipetting the material suspended in de-ionised water. Thereby, approximately 2 mg of sample material were settled on each disc.

2.4.1.2 Dosimetric material and water content

Sample material for dosimetric analyses was taken by bulk sampling of material from the surroundings (< ~30 cm) of the individual sampling positions. This material was also used for determining the present-day water content. After weighing the wet sample, the sample material was stored in a drying chamber at 105°C for at least five days and weighted again to determine the dry mass. The present-day water content was calculated by subtracting the dry mass from the wet mass and was expressed as percentage of dry mass according to the following formula:

$$water\ content = \frac{wet\ mass - dry\ mass}{dry\ mass} \cdot 100\% \tag{2.13}$$

After homogenization, the dried material was powdered by a ball mill (Retsch® MM 400), applying a frequency of 30 Hz for a total of 5 minutes. This procedure significantly contributes to avoiding α-overcounting, which was reported as seri-

ous problem for samples showing a considerable percentage of material with grain sizes larger than 20 µm (e.g., Zöller & Pernicka, 1989). A small amount of the powdered material was placed on top of a scintillation screen of zinc sulphide and gently compacted. It is important to use sufficient material to ensure complete coverage of the scintillation screen. After sealing the sample with a cover plate of acrylic glass, it was stored for at least 4 weeks to account for possible radon escape due to the grinding of sample material (e.g., Aitken, 1985) before it was used for thick source alpha counting (TSAC) (see the explanations on page 73).

Subsamples of powdered material were separated and used for determining the potassium contents of the samples. Further preparation steps were performed at the laboratories of the Bayreuth Center of Ecology and Environmental Research (BayCEER), including a hydrofluoric acid digestion, in order to prepare the sample material for ICP-OES measurements.

2.4.2 Measurement facilities

2.4.2.1 Luminescence measurements

All luminescence measurements were carried out at the luminescence laboratory of the University of Bayreuth using automated Risø-Reader TL/OSL-DA-15/20 systems. All readers were equipped with an built-in $^{90}Y/^{90}Sr$ β-source for artificial irradiation and a Thorn-EMI 9235 UV sensitive photomultiplier. For luminescence stimulation either blue LEDs ($\lambda = 470 \pm 30$ nm – applied to quartz separates) or infrared LEDs ($\lambda = 875 \pm 80$ nm – applied to feldspar and polymineral separates) were used. The luminescence signal for quartz samples was detected in the ultraviolette wavelength region, using a 7.5 mm U-340 Hoya filter. For feldspar and polymineral samples, the detection window was restricted to the blue-violet wavelength band by combining the photomultiplier with a 3 mm Chroma Technology D410/30x interference filter.

2.4.2.2 Dosimetric measurements

For dose rate determination, a great variety of analytic approaches have been proposed. Among the regularly applied methods are alpha and beta counting, (in-situ) gamma spectrometry, neutron activation analysis (NAA), atomic absorption spec-

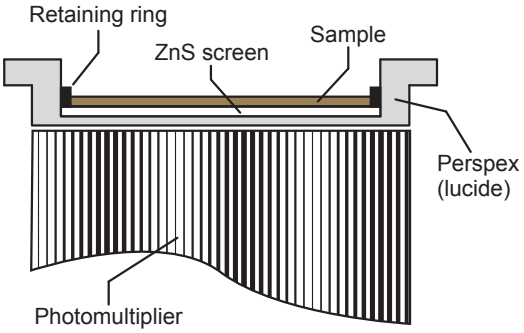

(a) Simplified schematic drawing of the principle measurement setup for thick source alpha counting (TSAC). The scintillator screen consists of a monograin layer of zinc sulfide and is carried by a sample carrier of acrylic glass. The scintillator screen is fixed by a retaining ring of stainless steel which restricts the circular area covered by the sample material to a standardized diameter of 42 mm. The powdered sample material is placed in direct contact with the ZnS screen and sealed by a cover plate of acrylic glass (not shown in this sketch). Redrawn and modified after Aitken (1985).

(b) Tools used for preparing samples for thick source alpha counting. A container of acrylic glass which serves as sample carrier can be seen on the right hand side of the photo.

Figure 2.12: Thick source alpha counting (TSAC) – tools and measurement device.

trophotometry (AAS), flame photometry, inductively coupled plasma mass spectrometry (ICP-MS) or ICP-OES (e.g., Duller, 2008a; Thiel, 2011).

In principle, three different basic procedures can be discriminated (e.g., Preusser et al., 2008):

1. The environmental dose rate can directly be measured in the sediment using dosimeters such as BeO or Al_2O_3:C.

2. Alpha, beta and gamma dose rates can be determined by radiation counting devices.

3. The concentration of radionuclides which have been identified as sources of the environmental dose rate can be determined and be used as base for dose rate calculation applying well-established conversion factors.

For this PhD-thesis, the radionuclide concentrations of uranium and thorium were detected by *thick source alpha counting* (TSAC), using a Littlemore Low Level Alpha Counter 7286 equipped with four photomultiplier tubes (PMT). A simplified schematic sketch of the basic measurement setup for this device and additional information are given in Figure 2.12a. Thick source alpha counting is based on scintillator techniques, which use the fact that ionising radiation produces light when interacting with specific materials which are termed scintillators (e.g., Mauz et al., 2002). Thereby, the powdered dosimetric material is placed on top of a scintillation screen consisting of a plastic plate impregnated with a monograin layer of zinc sulphide commonly dotted with either Al^{3+}- or Cu^{+}-ions (e.g., Aitken, 1985). The scintillator screen is standardized to a diameter of 42 mm and carried by a container of acrylic glass which is positioned on top of a photomultiplier.

Each alpha particle striking the scintillation screen produces a scintillation, i.e. a flash of light emitted by the scintillator material. Due to the photoelectric effect, each scintillation of light causes photoelectrons to be emitted from the photocathode of the photomultiplier. This small number of primary electrons is directed and accelerated towards the anode of the photomultiplier tube. Thereby, they have to pass the electron multiplier unit of the PMT consisting of a considerable number of positively charged electrodes, which are termed dynodes. Due to interaction with these dynodes, a cascade of electrons is produced characterized by an exponentially increasing number of electrons. When reaching the anode of the photomultiplier, this cascade of electrons sums up to a distinct electrical pulse that can be amplified and detected. By applying specific threshold values, it is possible to discriminate pulses of different voltages. Thus, electrical pulses corresponding to either beta particles or gamma rays can be rejected and the counting statistics can be restricted to alpha particles.

Based on the so-called '*Pairs Technique*' (e.g., Aitken, 1985), it is even possible to quantify the specific contributions coming from the uranium and from the thorium decay chains, respectively. This approach makes use of the fact that ~3% of the counts originating from the thorium decay chain occur in pairs due to the alpha emitter ^{216}Po which has a half-life of only 0.145 s (e.g., Aitken, 1985). Therefore, the 'pairs rate', i.e. the number of paired pulses detected within a time-slot of less than 0.21 s, is a measure of the thorium activity. However, as radioactive decay is a stochastic process, such short time alpha pairs may also be caused by random coin-

cidence of two independent alpha decays occurring in the uranium series. Furthermore, there are also fast pairs in the uranium decay chain due to the 0.002 s half-life of ^{215}Po (e.g., Aitken, 1985). Thus, these contributions have to be subtracted to get the '*true pairs rate*' (Aitken, 1985) or '*slow pairs*' which are used to assess the contribution made to the total alpha count rate by the thorium series. For details, the reader is referred to the elucidating explanations of Aitken (1985), providing additional information on technical specifications, specific adjustments of the device settings and, especially, on the mathematical derivations of exact formulas for alpha count rate calculation and slow pairs determination.

As a result, thick source alpha counting yields the total alpha count rate as well as the specific count rates associated with the uranium and thorium decay chains. Based on specific conversion factors, these count rates can be used to calculate the uranium and thorium concentrations (given as ppm) of the the investigated dosimetric sample.

As ^{40}K is a beta emitter, the potassium concentration cannot be determined by thick source alpha counting. Instead, inductively coupled plasma optical emission spectrometry (ICP-OES) was used for this purpose. The ICP-OES measurements for this PhD-thesis were performed at the laboratories of the Bayreuth Center of Ecology and Environmental Research (BayCEER) using a Varian Vista-Pro™ system. The determined potassium contents are given as per cent by weight and are summarized along with the uranium and thorium concentrations in the tables of the individual studies (Table 3.2, Table 4.2 and Table 5.3).

The determined concentrations were converted to individual contributions of alpha, beta and gamma dose rates applying conversion factors provided by Guérin et al. (2011). These conversion factors are depicted in Table A.1 which can be found in the Appendix on page 221.

Part II

Publications

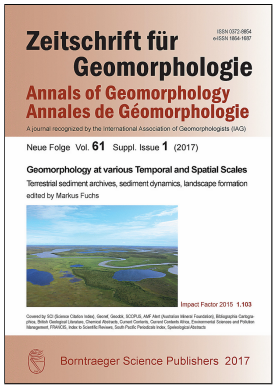

3

Study One: Quaternary river terraces and hillslope sediments as archives for palaeoenvironmental reconstruction: new insights from the headwaters of the Main River, Germany

Thomas Kolb, Markus Fuchs, Olivier Moine & Ludwig Zöller

Zeitschrift für Geomorphologie, Vol. 61 (2017), Suppl. 1, 53-76
published online December 2016
published in print March 2017

Quaternary river terraces and hillslope sediments as archives for palaeoenvironmental reconstruction: new insights from the headwaters of the Main River, Germany

Thomas Kolb, Markus Fuchs, Olivier Moine & Ludwig Zöller

Zeitschrift für Geomorphologie, Vol. 61 (2017), Suppl. 1, 53-76
with 9 figures and 3 tables

Summary

This paper deals with the analysis of hillslope sediments and fluvial terraces and how they are used as palaeoenvironmental archives for obtaining new information on the landscape evolution in a small dry valley in the headwaters of the Main River in northern Bavaria, Germany. Both, traditional geomorphologic approaches, such as field observations and qualitative petrographic analyses of fluvial gravels, and modern numerical dating techniques, are applied.

Qualitative petrographic analyses were used as a tool to identify the origin of fluvial terrace gravels and to draw conclusions on the genesis of the particular terrace aggradation. In order to establish a local chronological framework for the fluvial history during the Late Quaternary, luminescence dating techniques along with ^{14}C-dating methods are used to reassess age estimations for the Würmian T2-terrace made by previous studies.

Information on the palaeoenvironmental conditions of the research area are drawn from the malacological analysis of a unique community of fossil terrestrial mollusks with a surprising variety of species, so far not reported for the region of northern Bavaria. The presented results indicate that fluvial systems have always to be considered as individuals, responding in a very specific way to changes in environmental conditions and reflecting the unique settings of the investigated catchment.

Keywords: river terrace, OSL dating, Quaternary, river deflection, Northern Bavaria, mollusk assemblage, petrographic analysis, fluvial gravels

3.1 Introduction

River terraces are widespread geomorphic features. Their formation is mainly controlled by changing tectonic and climate conditions and therefore they can be used as archives for palaeotectonic and palaeoenvironmental reconstruction. River terraces are often interpreted as the expression of changing climates and especially as a result of numerous transitions between cold and warm conditions within the Quaternary and their corresponding changes in vegetation, sediment supply and transport capacity (e.g., Antoine et al., 2007; Bridgland & Westaway, 2008a; Busschers et al., 2008; Vandenberghe, 2008, 2015). However, the timing of incision and accumulation phases of fluvial systems and therefore the formation of river terraces in relation to climate is still not fully understood (e.g., Mol et al., 2000; Schulte et al., 2008; Vandenberghe, 2015; Viveen et al., 2013).

Before the 1990s, many studies on river terraces were primarily based on morphological analyses, such as extent and relative heights of terrace levels, and on their sedimentological characteristics, i.e. petrographic composition and weathering degree of the terrace gravels. Furthermore, classical field-based methods, such as field topographic measurements, grain size measurements and geomorphological mapping, together with quantitative approaches, like hydraulic geometry and formulae for bedload transport, were frequently applied in studies dealing with fluvial geomorphology (Piégay et al., 2015).

The informative value of fluvial archives and their significance for palaeoenvironmental research, however, strongly depend on a precise dating of the terrace formation. In the past, the lack of age determinations using numerical dating methods had often to be regarded as a serious limitation for palaeoenvironmental interpretations of fluvial archives in general and specifically of those investigated in the research area of the study in hand.

In southern Germany, the evolution of river drainage systems is on the whole greatly affected by the individual developments of two important river systems, those of Danube and Rhine rivers (e.g., Eberle et al., 2010). This is particularly true for the complex river drainage system of Northern Bavaria close to the European watershed. Due to the subsidence of the Upper Rhine Graben, the River Rhine was able to enlarge its catchment area by stepwise headwater erosion and river deflections, leaving behind an irregular drainage system characterized by var-

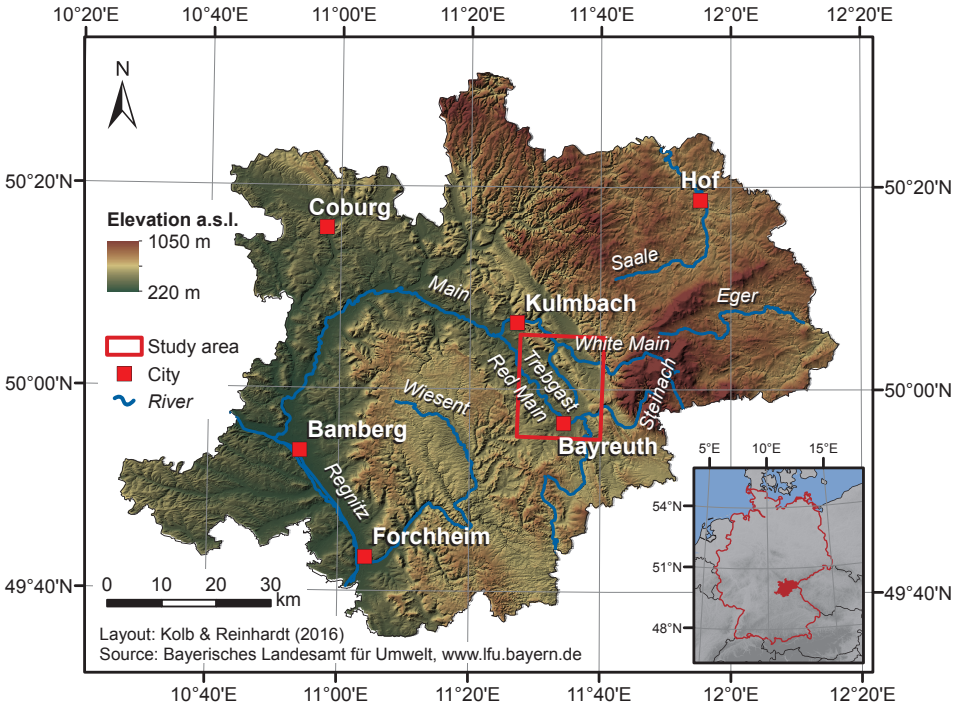

Figure 3.1: Overview map of Upper Franconia. The study area is highlighted by a red rectangular. The Trebgast Valley is a small valley located in the Main River catchment in northern Bavaria (Germany). It has been identified as former interconnection between the rivers Red Main in the south and White Main in the north.

ious triangular and rectangular changes in the courses of the involved rivers (e.g., Eberle et al., 2010; Schirmer, 2010, 2012). After the overall establishment of the Main River as the longest right bank tributary of the Rhine drainage system by the end of the Pliocene, there were still further river deflections occurring in the headwaters of the Main River during the Quaternary. The latest of these Upper to Middle Pleistocene river deflections took place in an oversized valley named Trebgast Valley in the north of the city of Bayreuth, Bavaria, Germany (Figure 3.1). Within this valley, five Pleistocene terrace levels were distinguished and interpreted as the result of a very complex landscape evolution in which two local rivers, the Red Main River and the Steinach River, were involved (e.g., Kleber & Stingl, 2000; Zöller et al., 2012a).

In order to understand the processes responsible for the recent drainage system, a precise local chronostratigraphy based on numerical dating methods should be established. Only this can provide a reliable database and chronological framework

for the reconstruction of palaeoenvironmental conditions associated with the formation of the different terraces in the research area.

Over the last two decades, luminescence dating, especially the optically stimulated luminescence (OSL) method, has become a commonly applied standard method for yielding sedimentation ages of fluvial deposits (e.g., Fuchs & Lang, 2001; Lauer et al., 2010, 2014). Despite several serious methodological challenges (e.g., incomplete resetting of the luminescence signal during fluvial transport or problems in dosimetry due to the heterogeneous composition of the fluvial sediments), the advantages of luminescence dating techniques are obvious: they enable the dating of (fluvial) sediments far beyond the last glacial-interglacial cycle and, by using quartz and feldspar minerals as dosimeters, suffer from almost no limitation of dateable material (e.g., Rittenour, 2008).

This paper gives an overview of the fluvial history and landscape evolution of the Trebgast Valley. We present new findings based on intensive fieldwork as well as on numerical dating approaches. As the timing of the final deflection of the Steinach River is of special interest for the reconstruction of the Late Pleistocene and Early Holocene landscape evolution, the study in hand was focused on attempts to date the aggradation of the youngest terrace level (T2 level) accumulated by the primary Steinach River, a tributary of the Main River. The presented OSL and radiocarbon dating results rise questions about the timing of the latest river deflection stated by previous studies (e.g., Kleber & Stingl, 2000; Zöller et al., 2007, 2012a) and, in general, highlight new questions regarding both, process and timing of gravel aggradation in fluvial systems in the northeastern part of Bavaria.

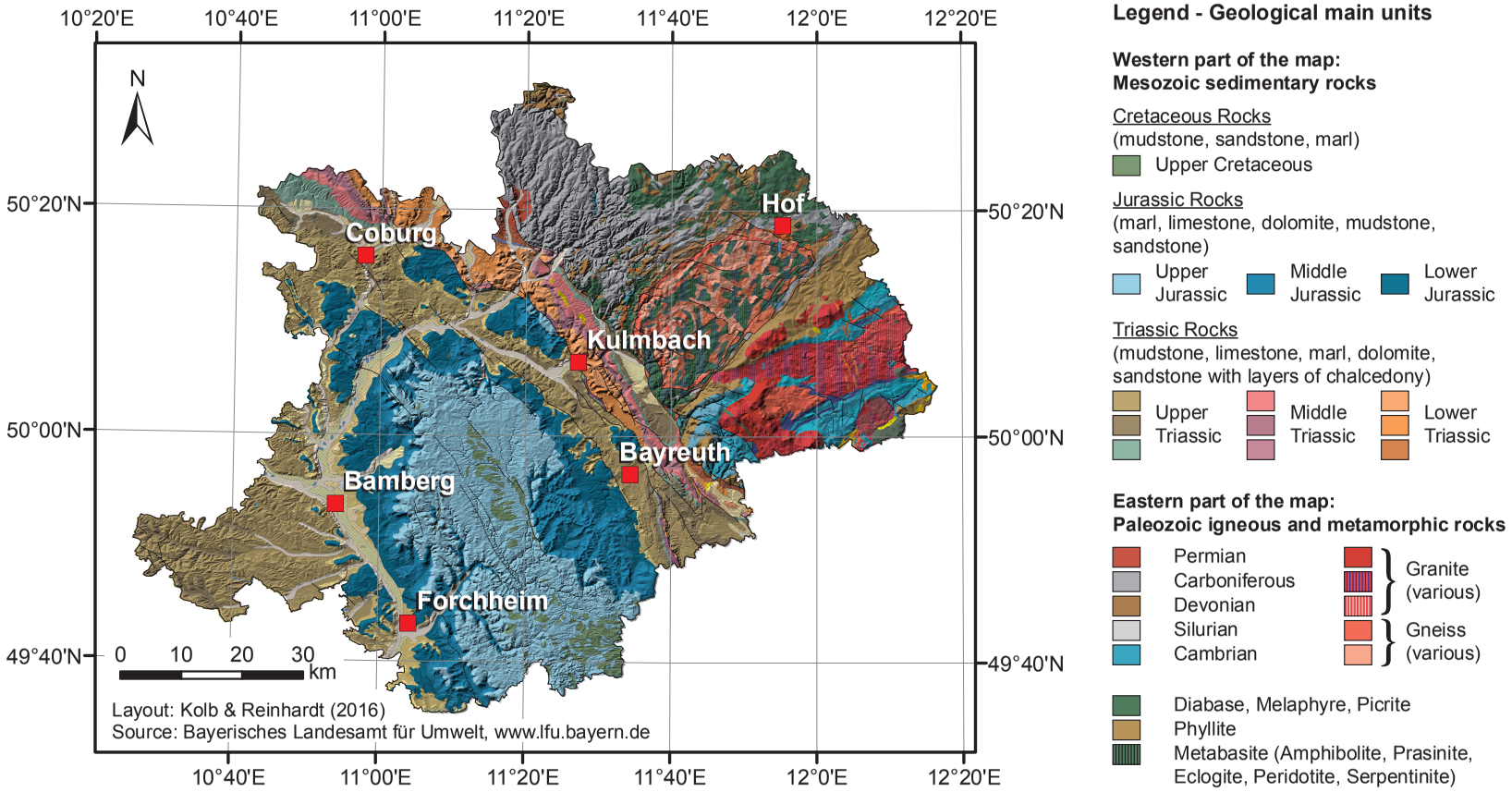

Figure 3.2: Geological map of Upper Franconia. The region is divided into two major geological units. The Nothern Franconian Alb in the west is built up of Mesozoic sedimentary rocks. In the eastern part, plutonites and metamorphic rocks dominate the lithology, exposed in the crystalline basement area of the Bohemian Massif. The Trebgast Valley itself is located in a transition zone developed within sandstone formations of Lower Triassic origin (orange color scheme).

3.2 Study area

3.2.1 General information and river drainage system

The research area, a small, oversized dry valley in the headwaters of the Main River, is situated in the north-east of Bavaria, Germany (Figure 3.1). Nowadays, the valley is drained by a small creek called Trebgast. The Trebgast Valley is a former interconnection between the Red Main/Steinach drainage system in the south and the White Main River in the north (e.g., Kleber & Stingl, 2000; Zöller et al., 2007, 2012a).

With the White Main River and the Red Main River, there are two headwater streams of the Main River dominating the drainage system of the study area. While the first originates in the Variscian basement area of the Fichtel Mountains, the latter has its origin in a Middle Jurassic sandstone area south of the city of Bayreuth. Both rivers join near the town of Kulmbach, forming the Main River, which is, with a total length of about 527 km, the longest right bank tributary of the River Rhine. A third river, important for the present-day drainage system as well as for the Quaternary development of the study area, is the river Warme Steinach (hereafter mentioned as Steinach River). It is a tributary to the Red Main River, with their confluence within the city of Bayreuth.

The evolution of the Trebgast Valley has been discussed among geoscientists since the beginning of the 20th century (e.g., Reck, 1912; Henkel, 1917). Mainly based on morphological and lithological evidence, this long lasting controversy focused on the question whether the Trebgast Valley was originally drained by the Red Main River (e.g., Reck, 1912; Seefeldner, 1914; Stadelmann, 1924; Körber, 1962) or whether it had to be interpreted as a former valley of the primary Steinach River (e.g., Henkel, 1917, 1920; Emmert & Weinelt, 1962). Other studies (e.g., Ertl, 1987; Veit, 1991) dealt with specific topics within the research area. But it was not until recently that new studies (e.g., Kleber & Stingl, 2000; Zöller et al., 2007, 2012a) were able to prove the participation of both rivers in the evolution of the Trebgast Valley and to derive the landscape evolution model described below (see section 3.2.3).

3.2.2 Geological and geomorphological setting

The research area is part of a transition zone between two major tectonic units (see Figure 3.2). The lithology of the valley is characterized by Triassic sandstone, claystone, marl and limestone formations. To the east, the surroundings of the valley are dominated by the crystalline basement of the Bohemian Massif, primarily exposing plutonites and metamorphic rocks. In the west, the study area is bordered by the Northern Franconian Alb consisting of Jurassic sedimentary rocks. The geology of the transition zone is dominated by the so called '*Franconian Lineament*', a NW to SE striking tectonic fault system, separating the Variscian Bohemian Massif from the adjacent South German Block and its Permo-Mesozoic sedimentary cover (e.g., Duyster et al., 1995). The study area itself belongs to the intermittent Upper Franconian Block-Faulted Zone, which exposes Triassic to Jurassic sedimentary rocks displaced by numerous anatomizing faults running more or less parallel to the Franconian Lineament.

The Trebgast Valley itself can be subdivided into four sections and is displayed in detail in Figure 3.3: (1) The uppermost reaches are characterized by a wide and flat valley bottom. This overall 4 km long section clearly shows a south-north orientation and is separated from the Red Main River valley by a steep slope of 10-15 m and a very flat watershed. No river or creek has been able to develop within this part of the valley so far. To the east, the valley slightly raises with three clearly distinguished steps from 355 m a.s.l. to 400 m a.s.l., indicating a staircase of at least three river terraces. To the west, the valley is bordered by slightly, but sometimes steeply ascending slopes developed in sandstone formations of Upper Triassic origin.

(2) Downstream the village of Bindlach, the valley overall bends to the northwest and generally follows the direction of the Middle Triassic limestone cuesta. After a short distance of narrowing, the valley floor widens again, revealing an oversized valley. This part of the study area is drained by the Trebgast Creek, which enters the abandoned valley floor at the village of Bindlach. The width of the valley is in contrast to the dimension of the creek. Within this approximately 8 km long section several river terrace staircases can be found on both sides of the valley. Overall five different Pleistocene terrace levels have been distinguished so far (Figure 3.3 & Figure 3.4).

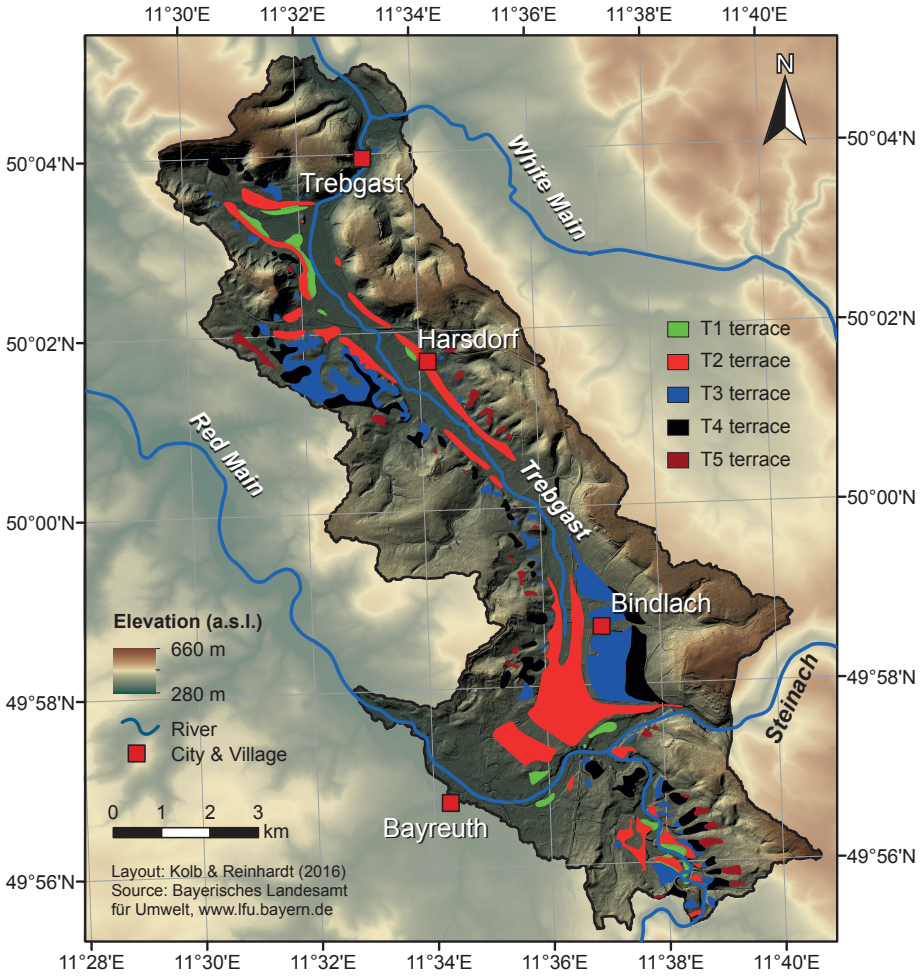

Figure 3.3: Detailed map of the Trebgast Valley showing the five Pleistocene terrace levels identified for the research area by previous studies. The alignment of the terraces was adopted from Kleber & Stingl (2000).

(3) Before bending to the north and entering the very narrow lowermost part of the valley, the valley floor broadens even more to a wide and flat basin, the so called '*Lindau Basin*' (Figure 3.6). Within this morphological depression several terraces are visible. The levels of these terraces correspond to those in the main part of the Trebgast Valley. Situated in the transition zone between the Lindau Basin and the present-day Trebgast Valley, a small fen, slightly surmounted by a humble hill, can be found. Previous studies (e.g., Zöller et al., 2007) interpreted this fen as a key site for the reconstruction of the Late Pleistocene and Holocene landscape

development of the Trebgast Valley and its surroundings.

(4) In the lowermost part of the research area the Trebgast Creek bends to a north-eastern direction, intersecting a ridge consisting of geomorphologically resistant Lower Triassic sandstone, before discharging into the White Main River near the village of Trebgast. Here, the valley can be described as a very narrow, even gorge-like valley, deeply incised into the sandstone formations and showing steeply ascending hill slopes. Within this section, no terrace staircases could be detected so far. Only the youngest river terrace of the T1 level was identified.

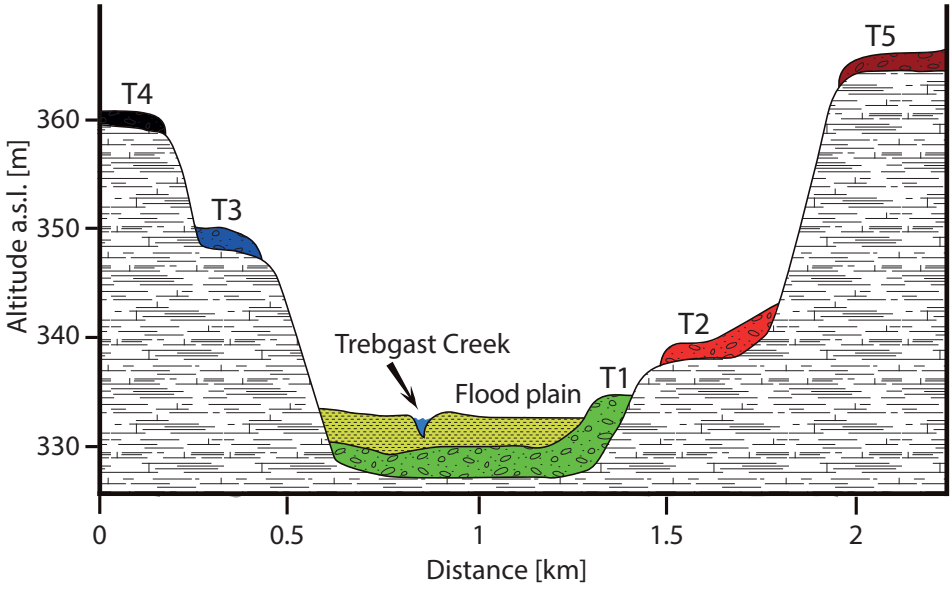

Figure 3.4: Schematic cross-section of the Trebgast Valley showing the five Pleistocene fluvial terraces of the research area.

3.2.3 Fluvial history

Based on intensive petrographic and geomorphologic analyses, Kleber & Stingl (2000) composed a detailed map of the different terrace levels (Figure 3.3 & Figure 3.4) and derived a very complex landscape evolution model. The evolution of the fluvial system within the study area is shown in Figure 3.5. Thereafter, the Steinach River and the Red Main River at first jointly flowed through the Trebgast Valley, depositing the river terraces of the two oldest levels (T5 and T4 levels). Presumably during an accumulation phase of the third last glacial period, a first river deflection took place, separating the Steinach River and the Red Main River.

After that, there followed a long lasting period during which the Steinach River solely drained the Trebgast Valley, whilst the Red Main River already used its present-day course. Derived from sedimentologic and morphostratigraphic evidence (Veit, 1991), Kleber & Stingl (2000) concluded that this evolutionary stage persisted for approximately 300,000 years, beginning at the end of the third last glacial period and ending with the final deflection of the Steinach River some time after the Last Glacial Maximum (LGM). This long lasting intermediate stage comprised the penultimate glacial period, which Kleber & Stingl (2000) assigned the forming of the T3-terrace to, and the Würmian glacial period, during which the T2-terrace gravels were deposited.

As a result of the Steinach River's deflection, the Trebgast Valley fell dry, with the Trebgast Creek using the abandoned valley downstream of the village of Bindlach. During this last stage, the youngest fluvial terrace (T1 level) was able to develop, restricted to the lowermost part of the valley.

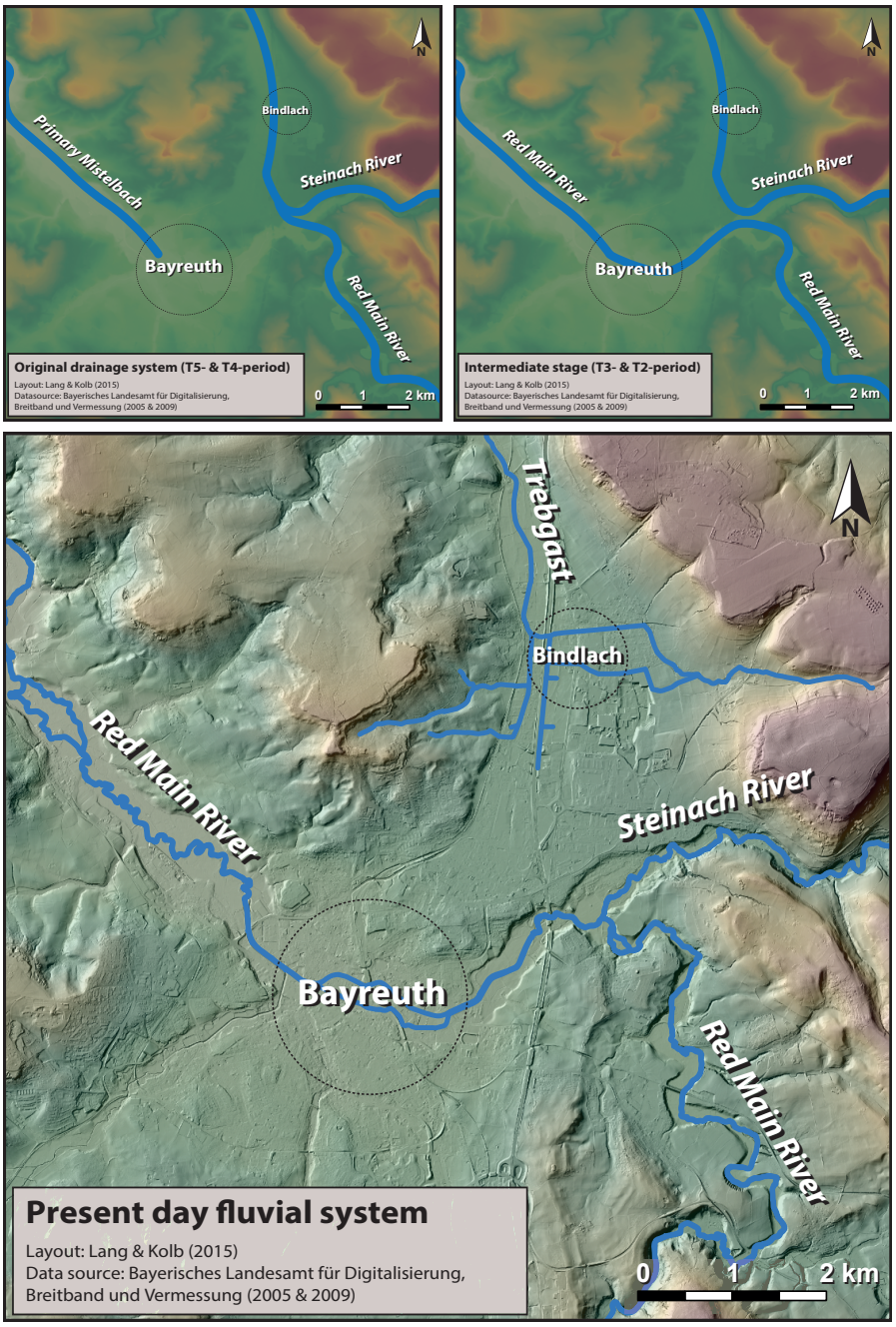

Figure 3.5: The different evolutionary stages of the Trebgast Valley. The maps are based on the complex multi-stage landscape evolution model proposed by Kleber & Stingl (2000).

3.3 Methods and materials

In order to shed light on the fluvial history and the landscape evolution of the Trebgast Valley, intensive fieldwork was combined with laboratory analyses. The results from qualitative petrographic analyses of previous studies (e.g., Kleber et al., 1988; Zöller et al., 2012a) were compiled and expanded by new petrographic studies of fluvial gravel deposits. To gain additional information on the palaeoenvironmental conditions, the composition of the malacofauna, extracted from periglacial slope deposits, was analyzed. The study in hand makes a first step to establish a chronological framework for the different phases of fluvial evolution by determining indirect age information for the aggradation of the upper Würmian terrace (T2) based on dating hillslope sediments by applying luminescence dating techniques along with radiocarbon AMS dating.

3.3.1 Qualitative petrographic analyses

Qualitative petrographic analyses of terrace gravels are used as an important tool to characterize different terrace levels und draw conclusions on their catchment areas.

While the Steinach River originates east of the research area within the crystalline basement of the Fichtel Mountains, the Red Main River's headwaters can be found further to the south, within an area covered by Mesozoic sedimentary rocks (see Figure 3.2). Therefore, the composition of the terrace gravel deposited by these rivers should be significantly different and can thus be used to draw conclusions on the participation of these two rivers in the terrace accumulation.

Besides the ubiquitous quartz gravels, specific lithologies are indicative of the different headwater areas. Phyllite, metamorphic and granite gravels are characteristic for the Steinach River. Although the Middle Jurassic sandstones are commonly prone to weathering, some iron agglutinated and, thus, weathering resistant gravels can be found in certain layers of these sandstone formations (Dogger β formation). These so called limonite crusts can, thereby, be transported over long distances and used as gravels indicative of the catchment area of the Red Main River.

For the presented study, the results of extensive petrographic analyses, made during the 1980s and previously summarized by Kleber et al. (1988), were compiled with results gained during various fieldtrips regularly performed with students of the University of Bayreuth over the last two decades (e.g., Zöller et al., 2007)

and analyses from new sites investigated for the study in hand, over all resulting in a very reliable database concerning the composition of the terrace gravel. The new sampling sites for the presented study were located in the middle and lowermost part of the valley (see Figure 3.6). At least one petrographic analysis per investigated terrace was performed on material directly originating from the respective gravel beds.

On every site a number of at least 300 gravels was sampled and subdivided into seven petrographic classes (phyllite, metamorphic, limonite sandstone, granite, quartz, quartzite, other sandstones; see Table 3.1 and Figure 3.7). As proposed by Müller (1964), the analyses were restricted to gravels showing a diameter from 2 cm up to 20 cm, separated by dry sieving. Gravels with a diameter bigger than 20 cm were registered but not used for counting. For every petrographic class of gravels, abundance was counted and relative frequency was calculated.

3.3.2 Malacological analyses

With terrestrial mollusks being strongly sensitive to variations in temperature and moisture, fossil mollusk communities have proved to be extremely useful for palaeoenvironmental and palaeoclimatic research (e.g., Rousseau, 1987). In order to gain additional information on the palaeoenvironmental conditions for the deposition of the loess-bearing slope detritus at a location in the middle part of the valley (49° 59' 49'' N, 11° 36' 15'' E, 362 m a.s.l., hereafter named the Crottendorf site), a malacological analysis was performed on a mollusk assemblage detected in the oldest lens of loess-like material. A sample of about 30 kg of sediment was taken, sieved and washed to extract the mollusk shells. Thereafter, the shells were counted, identified and classified following the classifications established by Ložek (1964) and Puisségur (1976). As analyses of mollusk samples are normally carried out based on a standardized sample volume of about 10 liters, the absolute frequencies yielded in the presented study have to be divided by three in order to be comparable with the results of other studies.

For the three dominant species, the juvenile/adult ratios (J/A) were either calculated according to Moine (2008) for *Pupilla muscorum* or visually estimated for *Succinella oblonga* and *Trochulus hispidus* owing to a more difficult distinction of juveniles and broken adults (absence of a particular ornamentation of the lip

marking the adult age) for the first and to the hazardous aperture recovery for the later. Variations of this ratio reflect changes in the reproduction rate and in the juvenile survival. With both strongly depending on the temperature during the reproduction season (Moine, 2003), the J/A ratio allows qualitative conclusions on the seasonal development of temperatures in the study area.

3.3.3 Sediment dating

3.3.3.1 Luminescence dating

OSL and IRSL dating techniques were used for the presented study. OSL dating was applied to the coarse grain quartz fraction (90-200 µm), using a single aliquot regenerative-dose (SAR) protocol (e.g., Murray & Wintle, 2000). In order to avoid an age overestimation due to incomplete resetting of the luminescence signal during the last process of transportation and deposition, small aliquots of about 100-300 grains were used, enabling to detect incompletely depleted samples (e.g., Fuchs & Wagner, 2003). Furthermore, the age model of Fuchs & Lang (2001) was applied. The IRSL approach was carried out on fine grain material (4 - 11 µm), using both, the SAR protocol for a fine grain quartz sample and the multiple aliquot additive-dose (MAAD) protocol (e.g., Mauz et al., 2002) for a polymineral sample.

Following standard procedures for sample preparation (e.g., Fuchs et al., 2010), all luminescence measurements were carried out at the University of Bayreuth on an automated Risø-Reader TL/OSL-DA-15, equipped with a $^{90}Y/^{90}Sr$ β-source for artificial irradiation and blue LEDs (470 ± 30 nm) for OSL stimulation as well as infrared light-LEDs (875 ± 80 nm) for IRSL stimulation. The luminescence signal was detected using a Thorn-EMI 9235 photomultiplier, combined with a 7.5 mm U-340 Hoya filter for the OSL measurements and a 3 mm Chroma Technology D410/30x interference filter for the IRSL measurements, respectively. All luminescence ages (OSL and IRSL) are given as thousand years (ka) with their 1σ-errors.

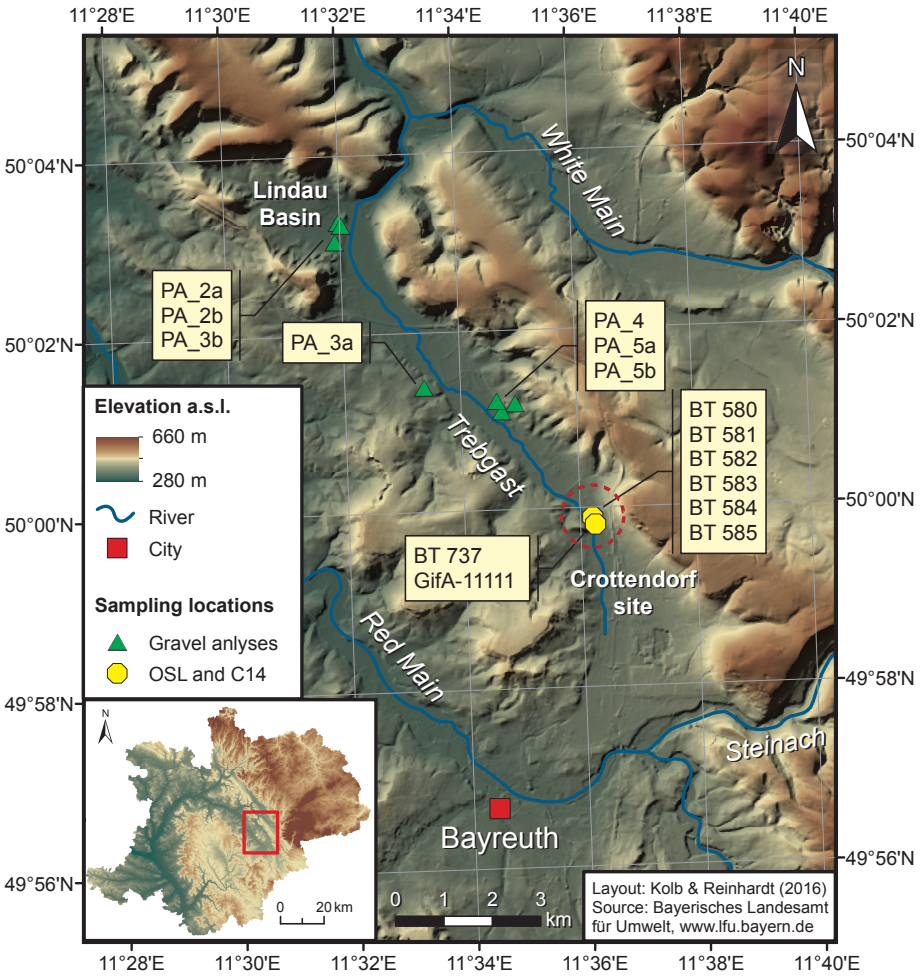

Figure 3.6: Detailed map of the research area. The sampling sites for the qualitative petrographic analyses are highlighted by green triangles. The outcrops which both, the OSL and the ^{14}C-samples, along with the material for the malacological analyses were taken from are marked by yellow hexagons.

3.3.3.2 ^{14}C-DATING

The ^{14}C-analysis of mollusk material was handled by the LSCE, Gif-sur-Yvette, France, on unidentified whorl fragments of shells from *Pupilla genus*. Indeed, Pigati et al. (2004) showed that the North American taxa *Pupilla blandi* has a modern ^{14}C-activity similar to that of the vegetation. However, for a reliable evaluation of the calculated radiocarbon age in this study, it is essential to emphasize that Pigati et al. (2010) showed that species of *Pupilla genus* may sometimes in-

clude dead carbon leading to age overestimations reaching up to 1 ka. The yielded conventional age, given as years before present (a BP), was calibrated using the calibration software Calib 6.1 based on the calibration curve IntCal09 (Reimer et al., 2009). This calibrated age is given as calendar years before present (cal BP) considering a 2 sigma error. With the mollusk samples taken from slope deposits originating from the Upper Triassic limestone cuesta, furthermore a significant hard-water effect has to be reconsidered for these samples. This hard-water effect may cause an age overestimation of several hundred years (Wagner, 1998). Therefore, the yielded radiocarbon age can merely be interpreted as a maximum sedimentation age.

3.3.3.3 Sampling strategy (see Figure 3.6 & Figure 3.9b)

All dated luminescence samples (OSL and IRSL) were taken at the Crottendorf site and originate from layers or lenses of loess-like material, embedded into heterogeneous periglacial slope sediments. Here, these slope sediments were exposed over a total length of several hundred meters, superimposing the T2 terrace gravels with a minimal thickness of about 6 meters. Most of the identified layers and lenses were found to be strongly affected by cryoturbation (see Figure 3.9a). The radiocarbon sample was taken from the oldest discovered lens consisting of gleyed loess-like material that contained numerous mollusk shells suitable for ^{14}C-dating.

3.4 Results

3.4.1 Petrographical analyses

Qualitative petrographical analyses were performed on gravels from a total of 6 sites that have not been investigated in previous studies. The results of these analyses are shown in Table 3.1 and in the diagrams of Figure 3.7.

Thereafter, all terrace levels are characterized by a dominant abundance of quartz and quartzite gravels. Combined, these two categories show relative frequencies between 56% (PA_5a) in minimum and 69% (PA_3b) in maximum. Furthermore, all investigated terraces show high amounts of phyllites (up to 38.8%) and considerable percentages of other metamorphic rocks (6.7% in maximum). On the contrary, Middle Jurassic limonite crusts were just found in gravels originating from sites of the T5 level (12% for location PA_5a and 22% for location PA_5b, respectively). Concerning the fact that all sandstones that could not clearly be identified to be of Middle Jurassic origin were assigned to the category "Other Sandstones", the proportion of limonite crusts for these sites may, by all means, be even higher than displayed in the diagrams. Limonite crusts are either completely missing or show negligible proportions in the investigated gravels originating from the T2 and T3 sites.

The results of the qualitative petrographic analyses partially confirm the findings of previous studies (e.g., Kleber et al., 1988; Kleber & Stingl, 2000; Zöller et al., 2007). However, our findings also show discrepancies to the results of previous studies. We tried to take samples from a site that has so far been interpreted as a part of the T4 level (location PA_4, 50.020°N, 11.577°E, 358 m a.s.l.). At this site, gravels, which showed the typical spectrum of the T4 level, were found to be densely distributed on a flat, slightly inclined surface. After trenching, however, we were not able to find any gravel bed and, thus, could not determine the composition of the T4-gravel for this location.

3.4.2 The composition of the mollusk assemblage at the Crottendorf site

Based on our observations, the mollusk fauna from the Crottendorf site is the first terrestrial loess fauna detected in Upper Franconia. With a total of nine species it is

Table 3.1: Results of the qualitative petrographic analyses for different fluvial terraces – sample codes, sampling locations, elevation a.s.l. and gravel composition.

Sample	Sampling location			Relative frequencies of the gravel composition grouped by petrographic classes							
	Latitude [°N]	Longitude [°E]	Elevation a.s.l. [m]	Phyllite[b]	Metamorphic[b]	Limonite sandstones[c]	Granite	Quartz	Quartzite	Other sandstones	Others
T2-Terrace level											
PA_2a	50.051	11.532	330	38.8%	2.3%	0.0%	0.5%	28.2%	29.5%	0.8%	0.0%
PA_2b	50.054	11.534	327	28.8%	3.6%	0.0%	0.3%	37.6%	29.7%	0.0%	0.0%
T3-terrace level											
PA_3a	50.023	11.556	344	22.7%	3.9%	0.3%	1.3%	41.8%	26.5%	3.6%	0.0%
PA_3b	50.054	11.533	342	26.5%	2.6%	0.0%	0.0%	36.1%	32.9%	1.3%	0.6%
T4-terrace level[a]											
PA_4a	50.020	11.577	358	NA	NA	NA	NA	NA	NA	NA	NA
T5-terrace level											
PA_5a	50.020	11.582	360	15.7%	6.7%	12.3%	0.0%	29.3%	26.7%	9.3%	0.0%
PA_5b	50.018	11.578	363	10.0%	3.5%	21.7%	0.0%	33.7%	24.6%	6.2%	0.3%

[a] Although showing a densely distributed surficial accumulation of gravels, no gravel bed could be found at this site. The surficial gravels were interpreted as the result of a local displacement of material originating from a higher terrace level. Therefore, no petrographic analysis was performed for this location.

[b] Phyllite and metamorphic gravels are indicative of the headwater area of the Steinach River.

[c] Originating from a Middle Jurassic sandstone area in the south of the city of Bayreuth, iron agglutinated limonite sandstones are indicative of the catchment area of the Red Main River.

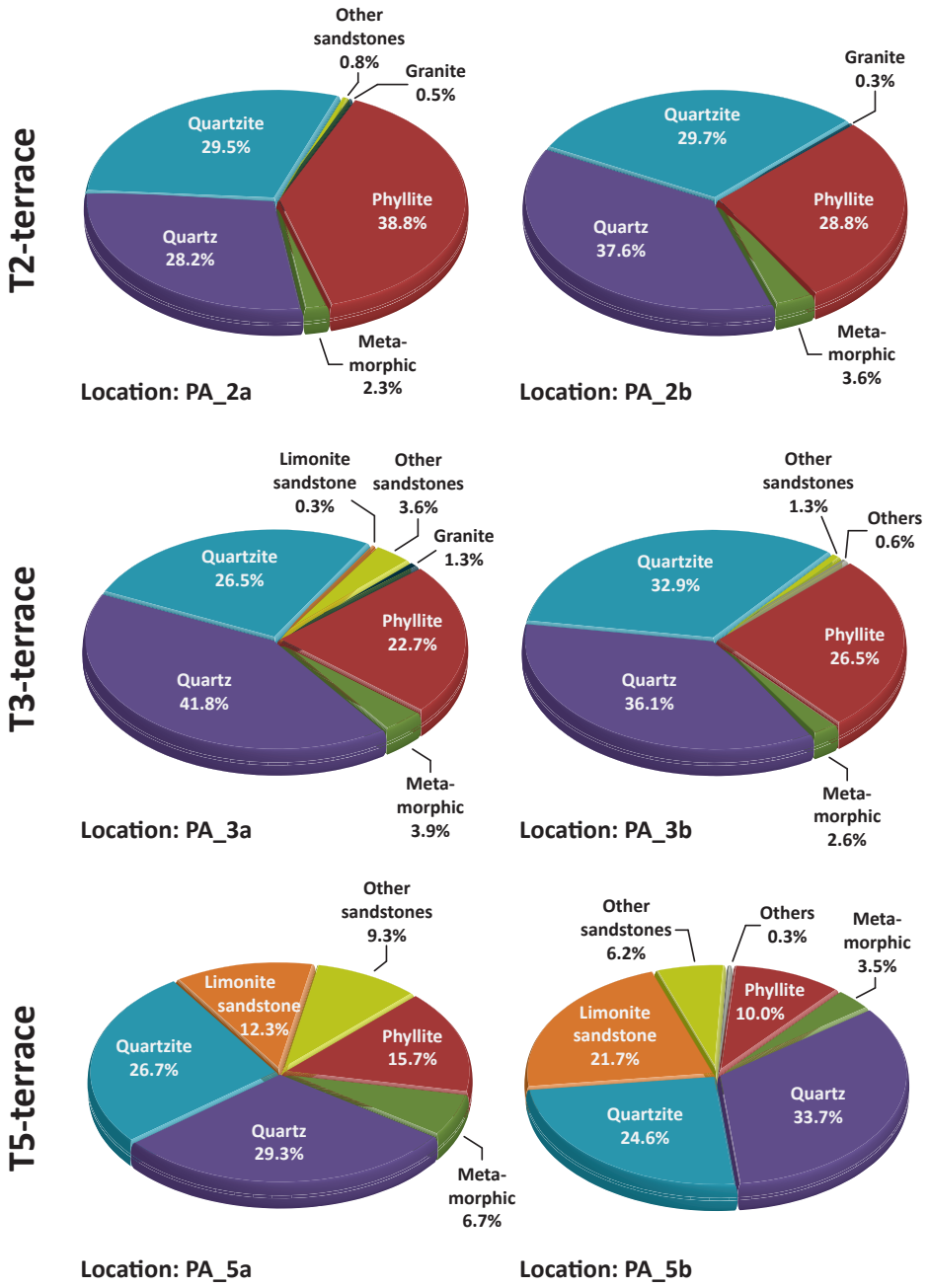

Figure 3.7: Results of the qualitative petrographic analyses for six sites representing three different terrace levels. With the gravels of the T2- and T3-terrace sites showing similar compositions, they can clearly be distinguished from the gravel compositions of the T5-terrace sites. Only the latter show a considerable proportion of limonite sandstones.

richer than those from the Danube valley loess (Brunnacker & Brunnacker, 1956) and characterized by a great variety rarely encountered outside of the Rhine Valley in Upper Weichselian loess deposits (Moine, 2008). A total abundance of 5534 individuals was counted for an investigated mass of about 30 kg of material. Even divided by three, this total abundance would by far outrange that of pure loess samples, in which abundance rarely reaches 200-300 individuals. The total abundance at the Crottendorf site equals that reported for mollusk samples originating from cryoturbated tundra gleys (Moine et al., 2008, 2011). With the texture being quite sandy and no evidence for earthworm granules being found, the mollusk bearing sediments at the Crottendorf site could have been affected by flood deposit dynamics, resulting in a concentration of mollusk shells in the sample location. However, the complete lack of aquatic species and the good state of shell preservation point to a short and smooth transportation process rather than to a displacement over long distances (Zöller et al., 2012b).

Figure 3.8 shows the absolute and relative frequencies of the counted mollusk shells, population indices and the affiliation of individuals and species to different ecological groups. Thereafter, the mollusk assemblage is dominated by *Succinella oblonga* (65%) followed by *Trochulus hispidus* (15%) and *Pupilla alpicola* (14%). These species require humid conditions and are, therefore, indicative of moist to wet environments mainly covered by short vegetation (Kerney et al., 1983; Falkner et al., 2001). Slugs, which are generally abundant in loess deposits, are almost completely missing at the Crottendorf site, which may as well be attributed to quite moist conditions. Besides, the low frequency of *Pupilla muscorum* (5%), and the few individuals of *Columella columella*, *Vallonia pulchella* and *Vertigo pygmaea* suggest a more diversified vegetation cover and a slightly drier soil surface in the close surroundings of the sampled gully (Zöller et al., 2012b). Moreover, presently living at high elevation *Columella columella* and *Pupilla alpicola* are indicative of low temperatures.

The affiliation of individuals to their particular ecological group shows a distinct preference for hygrophilous and palustral species. On the contrary, the species' distribution clearly indicates the sporadic presence of some species typical of dry and open environments.

For *Pupilla alpicola* a juvenile/adult ratio of 5.36 was calculated. For *Succinella oblonga* and *Trochulus hispidus* respective values of about 6 and more than 6 were

Taxa	Frequencies	
	Absolute	Relative
Arianta arbustorum (2)	1	0.02
Columella columella (5)	4	0.07
Pupilla muscorum (5)	298	5.38
Vallonia pulchella (5)	1	0.02
Vertigo pygmaea (5)	3	0.05
Trochulus hispidus (7)	853	15.41
Slugs (7')	2	0.04
Succinella oblonga (7)	3606	65.16
Pupilla alpicola (9)	769	13.90
Total	5534	100

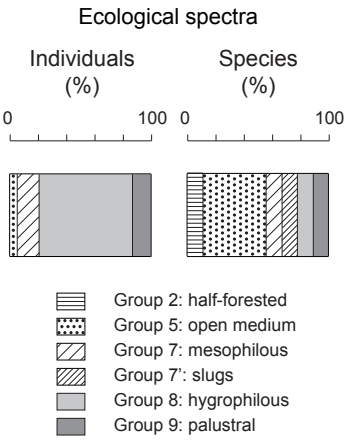

	Diversity	Equitability
Simpson	2.13	0.24
Shannon	1.46	0.46

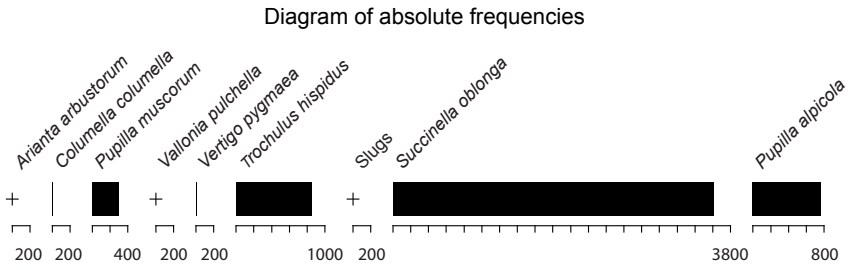

Figure 3.8: Compilation of the malacological results for the mollusk assemblage extracted from a lens of gleyed loess-like material embedded into hillslope sediments at the Crottendorf site (adopted from Zöller et al., 2012b).

estimated. These ratios point to convenient reproduction conditions, already been described in Nussloch (Rhine valley, Germany) and attributed to local increases in temperature during interstadial phases of the Upper Weichselian (Moine, 2008).

3.4.3 Dating results

3.4.3.1 Morphostratigraphical findings

Several drill cores, extracted from the slope detritus at the Crottendorf site, clearly showed that the periglacial cover sediments overlie the gravels of the T2 level with

a minimal thickness of about 6 meters. Therefore, the slope cover sediments were deposited after the aggradation of the T2-gravels and are, thus, younger than the latter. As there was no evidence for a significant, post-sedimentary erosion of the hillslope detritus by fluvial activity, we assume that the accumulation of the cover sediments took place after the final deflection of the primary Steinach River.

As mentioned above, most of the layers and lenses of loess-like material embedded into the slope detritus were strongly affected by cryoturbation (see Figure 3.9a). Hence, these lenses as well as the slope detritus on the whole should have been deposited not later than during the Younger Dryas (12,900 – 11,600 cal BP).

(a) Photo of a small lens of loess-like material embedded into the slope detritus at the Crottendorf site. Like others, this lens was affected by cryoturbation.

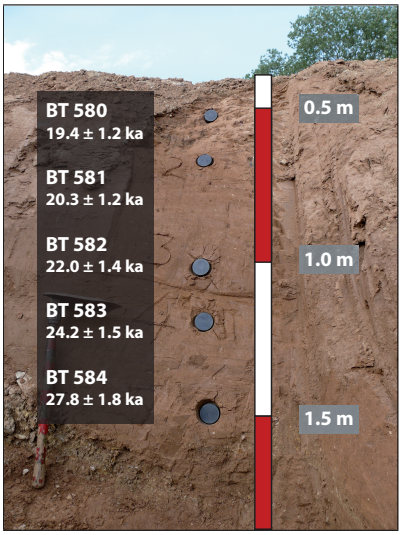

(b) The sampling situation for OSL-samples BT 580 to BT 584. This location was part of a several hundred meters long outcrop in periglacial slope sediments showing several distinct lenses and layers of homogeneous loess-like material. OSL-ages for coarse grain quartz samples are presented.

Figure 3.9: The sampling location at the Crottendorf site.

3.4.3.2 Numerical dating results

In order to ensure the above mentioned hypothesis derived from morphostratigraphical fieldwork, OSL, IRSL and ^{14}C-dating were applied on loess-like material sampled from the above described lenses. The analytic data for dose rate determination are listed in Table 3.2. The calculated luminescence and ^{14}C-ages are compiled in Table 3.3 and the OSL ages for the coarse grain quartz fraction of samples BT 580 to BT 584 are illustrated in Figure 3.9b.

Table 3.2: Radionuclide concentrations, cosmic dose rates and total dose rates calculated for the coarse grain quartz fraction.

Sample	Uranium [ppm][a]	Thorium [ppm][a]	Potassium [%][b]	$\dot{D}_{cosmic}$ [Gy/ka][c]	$\dot{D}_{total}$ [Gy/ka][d]
BT 580	4.63 ± 0.33	15.78 ± 1.09	2.55 ± 0.10	0.21 ± 0.01	4.26 ± 0.24
BT 581	4.51 ± 0.31	15.25 ± 1.04	2.43 ± 0.10	0.20 ± 0.01	4.11 ± 0.23
BT 582	4.07 ± 0.28	15.94 ± 0.93	2.37 ± 0.10	0.19 ± 0.01	3.98 ± 0.22
BT 583	4.69 ± 0.37	12.24 ± 1.21	2.49 ± 0.10	0.19 ± 0.01	3.99 ± 0.23
BT 584	4.51 ± 0.37	12.83 ± 1.24	2.31 ± 0.10	0.19 ± 0.01	3.83 ± 0.23
BT 585	3.37 ± 0.55	17.00 ± 1.86	2.35 ± 0.10	0.21 ± 0.01	3.90 ± 0.26
BT 737	4.26 ± 0.21	11.64 ± 0.71	2.53 ± 0.10	0.09 ± 0.01	3.78 ± 0.21

[a] Determined by thick source α-counting.
[b] Determined by ICP-OES.
[c] Cosmic dose rates were calculated according to Prescott & Hutton (1994).
[d] For dose rate calculation, a common water content of 15% was used for all samples. This value was derived using the average value of the possible water content range, based on the porosity of the samples and considering an error, which included the possible water content range (e.g., Fuchs et al., 2010, 2012; Prinz & Strauss, 2011; Scheffer et al., 2011).

AMS ^{14}C-dating yielded a conventional age of 26,810 ± 240 a BP, i.e. a 2σ-calibrated age of 30,974 - 31,500 cal BP. Within errors, all calculated OSL ages are in stratigraphic order, reaching from 19.4 ± 1.2 ka for the youngest investigated layer to 30.3 ± 1.8 ka for the oldest lens of loess-like material. Due to a lack of organic remnants, we were not able to gain ^{14}C-ages as independent age control, except for the mollusk bearing oldest lens. For this lens also an IRSL age was calculated. OSL and IRSL ages are identical within errors and both are in agreement with the calibrated ^{14}C age, when considering the fact that this calibrated ^{14}C age may most probably suffer from a distinct hard water effect and, therefore, overestimate the true sedimentation age by some hundred up to a few thousand years.

3.5 Discussion

3.5.1 Petrographical analyses

With all investigated terrace levels showing high amounts of phyllites and other metamorphic rocks, clear evidence could be found that the Steinach River was involved in the formation of all terrace levels. In the presented study, limonite crusts are restricted to the T5 level sites (PA_5a and PA_5b). The scarce occurrence of limonite crusts in the spectrum of location PA_3a can be explained by dislocation processes from higher terrace levels. Therefore, the Red Main River has only been engaged in the accumulation of the oldest so far detected terrace level.

Concerning the investigated T4-level site (PA_4) where no gravel bed could be found, the detected surficial gravels have most probably to be interpreted as the result of a local displacement from a higher terrace level. With no gravel bed being detected at site PA_4, we cannot confirm the existence of a T4 level terrace at this location. Furthermore, no other suitable location was found in the lowermost and middle section of the valley to be clearly identified as part of the T4 level. Thus, from our findings we are so far not able to confirm the existence of a T4 level in the middle and lower part of the research area at all. Up to now, we are not sure how these findings have to be interpreted. Maybe the discrimination of T4- and T5-terrace levels proclaimed by previous studies was not correct for the Trebgast Valley. If this was true all locations previously mapped either as part of the T4-terrace or of the T5-terrace would represent the very same terrace level. This interpretation, however, is strongly contradicted by findings gained in the Red Main valley. Here, both terrace levels (T4 and T5) were identified and could clearly be discriminated. Thus, this problem needs further investigation.

3.5.2 T2-terrace accumulation and timing of the final deflection of the Steinach River

Our findings at the Crottendorf site concerning the age of the aggradation of the youngest Steinach River terrace (T2 terrace) apparently conflict with results yielded by previous studies (Kleber & Stingl, 2000; Zöller et al., 2007).

Zöller et al. (2007) assumed the Lindau Moor to be a key site for the reconstruction of the Trebgast Valley's development since the deflection of the primary

Table 3.3: Sample codes, sampling locations, elevation a.s.l., sampling depths, number of aliquots, equivalent doses, OSL and ^{14}C ages.

Sample	Sampling location		Elevation a.s.l. [m]	Sampling depth [cm]	m[a]	n[b]	k[c]	D_e determination and age calculation	
	Latitude [°N]	Longitude [°E]						D_e [Gy]	OSL age [ka]
Coarse grain quartz - SAR protocol									
BT 580	49.998	11.603	356	50	48	25	19	82.44 ± 2.04	19.4 ± 1.2
BT 581	49.998	11.603	356	75	48	34	18	83.21 ± 1.97	20.3 ± 1.2
BT 582	49.998	11.603	356	115	71	34	17	87.73 ± 2.57	22.0 ± 1.4
BT 583	49.998	11.603	356	125	46	32	20	96.52 ± 2.49	24.2 ± 1.5
BT 584	49.998	11.603	356	150	47	38	17	106.59 ± 2.60	27.8 ± 1.8
BT 585	49.998	11.603	356	50	39	24	10	81.39 ± 2.67	20.9 ± 1.5
BT 737	49.997	11.604	355	450	94	44	31	114.41 ± 2.12	30.7 ± 1.8
Fine grain polymineral - MAAD protocol[d]									
BT 737	49.997	11.604	355	450	–	–	–	143.57 ± 7.40	29.0 ± 1.7
Fine grain quartz - SAR protocol[e]									
BT 737	49.960	11.601	355	450	24	20	13	139.65 ± 1.97	30.7 ± 1.1

^{14}C-*dating*

Sample Code	Conventional age	Calibrated Age
GifA - 11 111	26,810 ± 240 a BP	30,974 – 31,500 cal BP

[a] Number of measured aliquots.
[b] Number of aliquots passing the rejection criteria.
[c] Number of aliquots used for D_e determination and age calculation after applying the age model of Fuchs & Lang (2001).
[d] For dose rate calculation an a-value of 0.07 ± 0.01 was adopted from Kreutzer (2014).
[e] For dose rate calculation an a-value of 0.04 ± 0.01 was adopted from Kreutzer (2014).

Steinach River. They tried to draw geomorphologic conclusions out of palynological studies, conducted by Ertl (1987). She was able to extract a 158 cm thick pollen profile, in which 14 different pollen segments were identified and correlated to the well established pollen zones Ib/c to Xa after Firbas (Firbas, 1949, 1952). Thus, the pollen profile of the Lindau Moor spans the period between the Bölling interstadial (ca. 15,600 to 13,900 cal BP) and the Subatlanticum (later than ca. 2,800 cal BP).

Based on this pollen profile, Zöller et al. (2007) argued that the clay and peat layers, building up the fen, could only accumulate under predominant slack water conditions. Relying on the assumption that the Lindau Basin had been eroded by a meander of the primary Steinach River, as suggested by the terrace levels observed in the basin, such slack water conditions should not have prevailed in that area until the primary Steinach River had abandoned the Trebgast Valley. With respect to the oldest dated clay layers, Zöller et al. (2007) concluded that this final deflection should at least have occurred before the onset of the Bölling interstadial.

Furthermore relying on the traditional explanation of fluvial terraces to be landscape features typically accumulated during cold phases of glacial periods (e.g., Kleber & Stingl, 2000), a time frame for the final deflection of the primary Steinach River was deduced, spanning from the LGM to the Bölling interstadial (Zöller et al., 2007).

Both, the luminescence and radiocarbon dating results in the presented study as well as the morphostratigraphical findings at the Crottendorf site, are in conflict with this previous age estimation. With the slope sediments being post-deflective, overlying the gravels of the T2 level and being older than the Younger Dryas, the time frame for the deposition of the cover sediments would just range from the LGM to the Younger Dryas, if the age estimation of Zöller et al. (2007) was correct. With this time frame merely comprising a period of not more than 2 to 8 thousand years in maximum, the thickness of the post-deflective slope detritus can hardly be explained to have accumulated in such a short time, unless by a landslide. For a landslide, however, no evidence has been found so far (Zöller et al., 2012b).

Furthermore, the OSL dating results, supported by the AMS ^{14}C dating, clearly show sedimentation ages of approximately 19.4 ± 1.2 ka for the youngest up to 30.7 ± 1.1 ka for the oldest lens of loess-like material, respectively. As the oldest

gleyed loess lens within the periglacial cover sediments is underlain by 6 meter of slope sediments on top of the underlying gravels, the gravels of the T2 level were deposited quite a long time before the onset of the loess derivate's deposition.

Therefore, the obtained OSL and ^{14}C-data indicate a significantly older age for the aggradation of the T2 gravel and point to intense fluvial geomorphodynamics during the Lower and Middle Pleniglacial rather than during the Upper Pleniglacial.

The discrepancy between the results of previous studies and those presented in this paper needs to be further discussed. In order to cope with the problem, the two above mentioned assumptions of a), the Lindau Moor being a key site for the reconstruction of the landscape evolution in the study area, and b), river terrace formation being a process characteristic for cold stages of glacial periods should be revisited.

The main argument for the opinion that the Lindau Basin was eroded by the Steinach River has to be seen in the fact that terrace levels within the basin correlate to terrace levels in the main part of the valley (e.g., Kleber & Stingl, 2000) and, thus, were interpreted to have been accumulated by the primary Steinach River.

However, first preliminary visual investigations of the surficial basin gravels during field trips clearly showed the composition of the basin gravels to be completely different from that of gravel sites in the main part of the valley. With the basin gravels overall showing a dominant abundance of quartz gravels, they completely lack metamorphic and phyllite gravels and, thus, don't show any gravels indicative for the catchment area of the Steinach River. A great portion of ventifacts have been discovered among the basin gravels, typical for and quite frequent in some layers of the Lower Triassic sandstone formations (the so called '*Kulmbach conglomerate*'), outcropping on the lower slopes of the basin (e.g., Zöller et al., 2012b).

Even though not yet being able to disprove the above described assumption, we now strongly doubt that the primary Steinach River has ever flown through the Lindau Basin. On the contrary, the basin may most likely have been eroded by a small tributary river, originating within the basin itself and depositing gravels comprising of locally reworked material from the very easily to erode Lower Triassic sandstone formations. In that case, the development of the Lindau Moor would completely be decoupled from the final deflection of the Steinach River and, thus, would no longer contradict a significantly higher age for this deflection.

Still, our findings do not match the traditional concepts of river terrace forma-

tion, attributing the forming of gravel beds to be typical of cold stages within glacial periods, and especially they do not agree with regional studies (e.g., Kleber & Stingl, 2000; Zöller et al., 2007) which characterized the T2-terrace as geomorphic feature accumulated during the last glacial maximum. However, previous studies (e.g., Vandenberghe, 2002, 2003, 2008, 2015) have already shown that no simple correlation between climate change and fluvial processes can be assumed. Therefore, we interpret the results of the study in hand to be yet another evidence for the complexity of fluvial system response to palaeoenvironmental changes and for its strong dependency on local conditions, such as size and shape of the catchment area or the specific regional settings of geology, morphology and vegetation.

3.6 Conclusion

Hillslope deposits and fluvial gravel aggradations were used as archives for yielding new information on the fluvial evolution of a small dry valley in the headwaters of the Main River in northern Bavaria, Germany. Besides qualitative petrographic analyses and investigations of a fossil terrestrial mollusk assemblage, luminescence dating techniques and AMS ^{14}C dating were applied to date the sediments.

Qualitative petrographic analyses were used as a tool to identify the origin of fluvial terrace gravels and to draw conclusions on the genesis of the particular terrace aggradation. Based on these analyses, the findings of previous studies could partially be confirmed and additional evidence for a very complex landscape evolution, characterized by a minimum twofold river deflection, could be found. However, our results also prove the necessity of further petrographic analyses and a great need for a more detailed map of the terrace levels, based on a high resolution digital terrain model (DTM) of the study area.

The results from the malacological analysis showed a unique community of fossil terrestrial mollusks with a surprising variety of species, so far not reported for the region of northern Bavaria. The analyzed mollusk fauna provides valuable palaeoecological information and indicate a very complex landscape setting characterized by generally cold and dry conditions in the near surroundings as well as by distinct more humid conditions for the actual sampling site.

The calculated luminescence and ^{14}C ages are clearly in conflict with age estimates for the accumulation of the Würmian T2-terrace proposed by previous stud-

ies. The presented results for the dated hillslope detritus point to an older age of the underlying fluvial gravels (T2 terrace) and, thus, suggest a much earlier deflection of the primary Steinach River. They, thereby, indicate very intense fluvial geomorphodynamics during the Lower and Middle Pleniglacial rather than during the Upper Pleniglacial. However, this study has, so far, just been able to present indirect evidence for this conclusion. Hence, further investigations are needed. Direct dating of sand lenses embedded into the gravel beds of the T2 level are carried out at the moment and will directly yield sedimentation ages for the gravel aggradation. Not till then, we will be able to give a final answer to the question of the timing of the T2 terrace formation. But even now, the results of the study in hand indicate that traditional concepts of fluvial terrace aggradation should carefully be reconsidered. They generally raise questions concerning climatic conditions during the Lower and Middle Pleniglacial and their specific impacts on the timing and the processes of fluvial terrace formation. They also point to the fact that fluvial systems have always to be analyzed as individuals, responding in a very specific way to externally and/or internally driven changes in environmental conditions and reflecting the unique local and regional settings of the particular catchments.

Acknowledgements

Our research has generously been funded by the 'Oberfrankenstiftung' since 2011. The engineering company 'Piewak & Partner' (Bayreuth) is acknowledged for yielding stratigraphic plots and photos of boreholes near the village of Crottendorf. We also thank the Bavarian Department for Environment (Bayerisches Landesamt für Umwelt) for providing the high resolution digital terrain model and other maps and data. Heiko Lang (Bayreuth/Hamburg) kindly designed the layout of the basemaps used for Figure 3.5 and parts of the petrographic analyses used for this study have been performed by Julian Brindel (Bayreuth). Finally, we would like to thank the two anonymous reviewers for their constructive comments that significantly improved the quality of the manuscript.

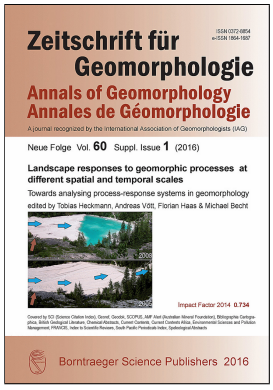

4

Study Two: Deciphering fluvial landscape evolution by luminescence dating of river terrace formation: a case study from Northern Bavaria, Germany

Thomas Kolb, Markus Fuchs & Ludwig Zöller

Zeitschrift für Geomorphologie, Vol. 60 (2016), Suppl. 1, 29-48
published online September 2015
published in print March 2016

Deciphering fluvial landscape evolution by luminescence dating of river terrace formation: a case study from Northern Bavaria, Germany

Thomas Kolb, Markus Fuchs & Ludwig Zöller

Zeitschrift für Geomorphologie, Vol. 60 (2016), Suppl. 1, 29-48
with 5 figures and 3 tables

Summary

Fluvial terraces are widespread geomorphic features, which formed dominantly during the Quaternary. Besides tectonics, the formation of Quaternary fluvial terraces is related to palaeoclimatic changes and corresponding changes in fluvial discharge and sediment load. However, within the Pleistocene, the exact timing and the palaeoenvironmental conditions for terrace formation are still under debate and traditional concepts are questioned.

To shed light on the Pleistocene environmental conditions for terrace formation, we investigate their timing by establishing a local terrace chronostratigraphy based on numerical dating. The study is located in a small valley in northern Bavaria, Germany. Here, within a former interconnection between two headwater streams of the Main River, five Pleistocene terraces are distinguished. The terraces are interpreted as the result of a complex landscape evolution, which is characterized by an at least twofold river deflection. Fluvial and periglacial slope sediments are still widely preserved and can be used as sediment archives.

The study is focused on dating the Upper Pleistocene terrace (T2 level). Following traditional explanations, this terrace level has so far been interpreted as a Würmian (Weichselian) formation, developed during the last glacial maximum (LGM). Optically stimulated luminescence (OSL) ages obtained for fluvial deposits and hillslope sediments, however, indicate a significantly older age for the gravel accumulation. The correctness of the OSL ages is supported by radiocarbon AMS dating.

These results point to significant Würmian (Weichselian) fluvial morphodynamics during early stages of the last glacial cycle (ca. 90 – 80 ka) as well as during the Lower and Middle Pleniglacial (ca. 64 – 30 ka). Furthermore, the results indicate that the response of fluvial systems to environmental changes is complex and strongly de-

pends on local conditions, such as morphology and lithology, the regional hydrological setting in general or the alignment of river courses and the possibility of river deflection in particular.

Keywords: fluvial geomorphology, river terrace, river deflection, OSL, luminescence dating, Quaternary, Northern Bavaria, Germany

4.1 Introduction

The great importance of river terraces as fundamental archives for Quaternary research has well been recognized ever since Penck & Brückner (1909) used Alpine river terraces to derive their theory of four Pleistocene glaciations. Since then, many studies have proved fluvial deposits to be important terrestrial archives, providing basic information for both, palaeoenvironmental and fluvial dynamic research. Their importance for Quaternary research is due to the fact that river terraces are widespread geomorphic features, known from various landscapes and climates all over the world, enabling their investigation on different temporal (e.g., Gibbard & Lewin, 2009; Westaway et al., 2009; Hobo et al., 2010; Wallinga et al., 2010) and spatial scales (e.g., Bridgland et al., 2007; Bridgland & Westaway, 2008a). Many studies have so far been focused on Pleistocene terrace formations and thus primarily dealt with the fluvial response to changing climatic or tectonic conditions (e.g., Antoine et al., 2007; Bridgland & Westaway, 2008b; Busschers et al., 2008; Vandenberghe, 2008). Other studies used Holocene fluvial sediments to draw conclusions on the increasing anthropogenic impact on landscape evolution and fluvial dynamics caused by the interaction between changing climate conditions and human reactions (e.g., Faust et al., 2004).

Along with colluvial and alluvial sediments (e.g., Fuchs et al., 2004, 2011; Verstraeten et al., 2009), river terraces have successfully been used as archives for geoarchaeological studies, providing information on human occupation and land-use changes (e.g., Mishra et al., 2007; Antoine et al., 2010).

Despite being intensely studied, fluvial systems in general and river terrace formation in particular are still not fully understood. For both types of fluvial terraces, strath and fill terraces (e.g., Leopold et al., 1964), a wide variety of models has been derived to explain the mechanisms of terrace formation (e.g., Mol

et al., 2000; Gibbard & Lewin, 2002; Lewin & Gibbard, 2010; Murton & Belshaw, 2011). However, the timing of incision and accumulation phases within fluvial systems and their driving forces are still under debate (e.g., Vandenberghe, 2008; Bridgland & Westaway, 2008a; Murton & Belshaw, 2011). Therefore, the information gained from fluvial archives and their significance for palaeoenvironmental research strongly depends on a precise understanding of the fluvial architecture (e.g., Houben, 2007; Nichols & Fisher, 2007) and accurate dating of the terrace formation (e.g., Fiebig & Preusser, 2003).

Radiocarbon dating has often been applied to fluvial sediments, but is of limited use when organic material is completely missing or re-worked from older deposits (e.g., Rittenour, 2008). Furthermore, its dating range is normally restricted to the last 40-50 ka. Over the last decade, significantly technical and methodological improvements could be achieved in the field of luminescence dating of quartz and feldspar minerals, providing a dating range that at least spans the last glacial-interglacial cycle. New promising developments even allow Middle Pleistocene sediments to be dated (e.g., Buylaert et al., 2009; Kreutzer et al., 2012a). Optically stimulated luminescence (OSL) techniques have successfully been applied to a wide variety of fluvial deposits (e.g., Rittenour, 2008).

However, using OSL methods for dating fluvial sediments is still challenging due to incomplete resetting of the luminescence signal. When being transported in a turbulent flow, some grains are exposed to sunlight for a sufficiently long time, resulting in a complete resetting of the luminescence signal. For other grains the sunlight exposure may not be of sufficient duration, leaving behind a residual signal when the grains are deposited. Using such incompletely bleached samples for dating purposes is problematic because the measured aliquots comprise of a mixture of well-bleached and poorly-bleached grains. In some exceptional cases even all grains of a sample might be insufficiently bleached. The presence of grains that experienced different levels of signal resetting cause a wide scatter of the equivalent dose (D_e) distribution and, thereby, will lead to a significant age overestimation if no correction is applied.

However, with the importance of incomplete bleaching depending on the portion of the residual signal as part of the total luminescence signal, incomplete bleaching is primarily problematic for younger samples and its significance decreases with increasing sample ages. Moreover, there are various techniques dealing with those

insufficiently bleached samples. Besides single-grain techniques (e.g., Duller, 2008b) and small aliquots containing a limited number of grains (e.g., Fuchs & Wagner, 2003; Rodnight et al., 2006; Cordier et al., 2012), approaches have been proposed isolating the multiple components of the OSL signal in order to use only the most light-sensitive components for dating (e.g., Jain et al., 2005). Furthermore, a wide variety of statistical approaches have successfully been applied to determine the accurate burial dose (e.g., Olley et al., 1998; Lepper et al., 2000; Galbraith et al., 1999). Thus, luminescence dating is a promising tool providing important contributions to shed light on still open questions concerning the complexity of fluvial systems.

In this study, we investigate a river drainage system in Northern Bavaria, Germany, to gain information on its Quaternary evolution in interaction with its palaeoenvironments. Generally controlled by the evolution of two major river systems, those of Danube and the Rhine River, it is characterized by an irregular alignment of river courses, showing various triangular and rectangular changes. This irregular pattern is the result of the enlargement of the Rhine River catchment by stepwise headwater erosion and river deflections (e.g., Eberle et al., 2010; Schirmer, 2010, 2012). The latest of these river deflections took place in a small dry valley called Trebgast Valley, which is located in the headwaters of the Main River, the longest right bank tributary of the Rhine drainage system. Although this valley has been object of intensive scientific research since the beginning of the 20th century (e.g., Reck, 1912; Seefeldner, 1914; Henkel, 1917; Körber, 1962; Ertl, 1987; Veit, 1991; Kleber & Stingl, 2000; Zöller et al., 2007, 2012a,b), there is still a lack of reliable age information. Based on lithological and morphostratigraphic evidence, only age estimates were derived, correlating the five Pleistocene river terraces identified within the valley with different glacial stages (e.g., Kleber & Stingl, 2000; Zöller et al., 2007). However, no chronological framework based on numerical dating has been established so far. Thus, a first step to understand the processes responsible for the present-day drainage system is to establish a precise local chronostratigraphy.

This paper gives an overview of the fluvial history and the Pleistocene evolution of the Trebgast Valley, focusing on OSL dating of fluvial deposits originating from the Upper Pleistocene terrace (T2).

4.2 Study area

With regard to the size of the present day creek, the Trebgast Valley is an oversized valley located in the upper catchment of the Main River in northern Bavaria, Germany (Figure 4.1). The drainage system of the study area is dominated by the White Main River and the Red Main River, with both rivers being headwater streams of the Main River, a tributary to the Rhine River. The Trebgast Valley has been identified as a former interconnection between the White and Red Main Rivers (e.g., Kleber & Stingl, 2000). The river Warme Steinach, a tributary to the Red Main River and hereafter just mentioned as Steinach River, is a third river important for the present-day drainage system as well as for the Pleistocene evolution of the research area (Figure 4.1).

The Trebgast Valley is located in a transition zone between two major geological units which are separated by the so called '*Franconian Lineament*', a major NW to SE striking tectonic fault system. To the east of the fault system, plutonites and metamorphic rocks dominate the lithology, exposed in the crystalline basement area of the Bohemian Massif. To the west of the fault system, the study area is dominated by Mesozoic sedimentary rocks of the Northern Franconian Alb. The lithology of the investigated valley itself is mainly characterized by Triassic sandstone, marl and limestone formations.

Table 4.1: Estimated chronology of the Pleistocene terraces of the research area derived from palaeosol sequences embedded in periglacial slope sediments superimposing the terrace gravels. Modified after Veit (1991).

Terrace level	Number of embedded soils	Estimated time frame
T4-terrace	2 fossil soils & holocene luvisol	Third last glacial period
T3-terrace	1 fossil soil & holocene luvisol	Penultimate glacial period
T2/T1-terrace	holocene luvisol/alluvial soil	Würmian (Weichselian) glacial
Floodplain	alluvial soil	Holocene

Based on petrographic and geomorphologic analyses (e.g., Kleber & Stingl, 2000), five Pleistocene river terraces are identified within the Trebgast Valley (Figure 4.2 & Figure 4.3). The terrace formation is explained by a complex landscape

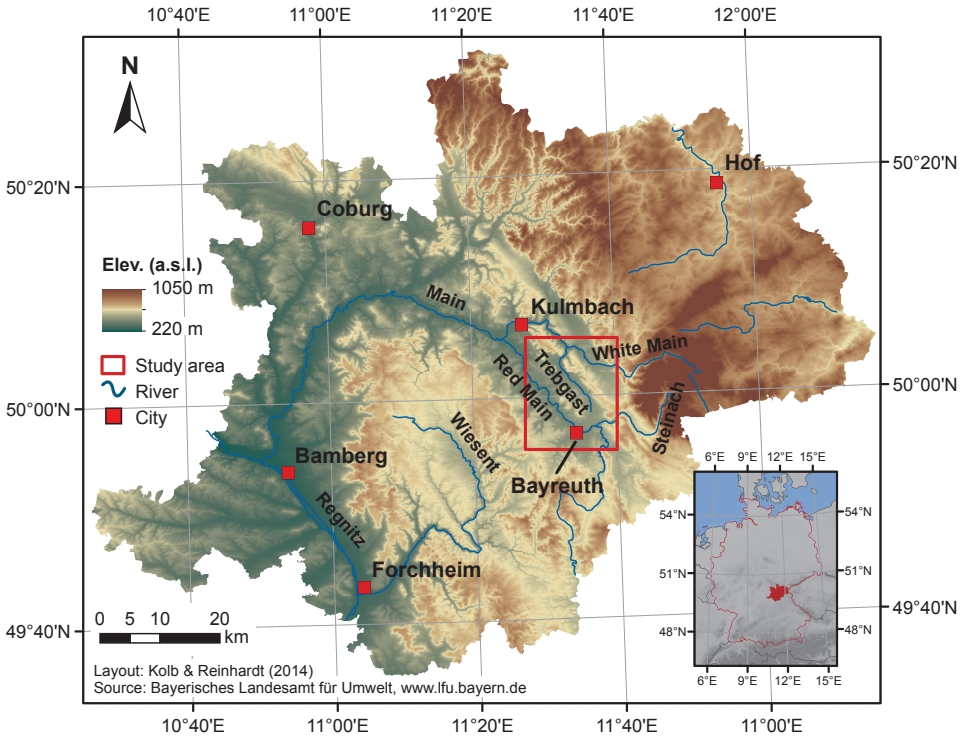

Figure 4.1: Study area. The Trebgast Valley is a small valley located in the Main River catchment in northern Bavaria (Germany). It has been identified as former interconnection between the rivers Red Main and White Main.

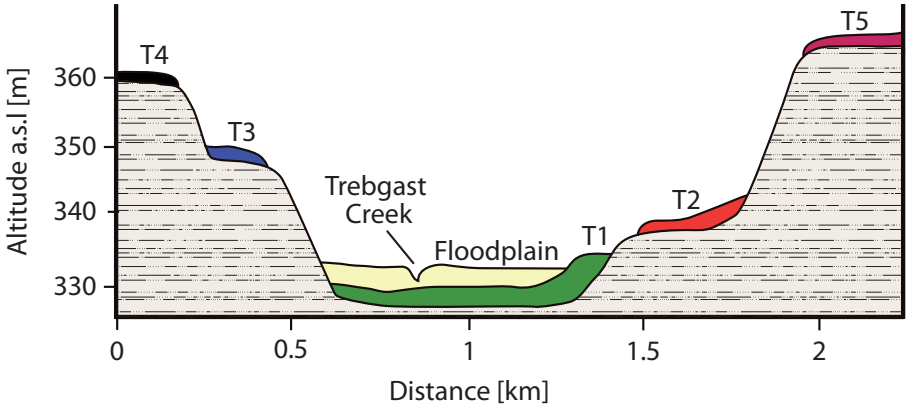

Figure 4.2: Schematic cross-section of the Trebgast Valley showing the five Pleistocene fluvial terraces of the research area. All samples for this study were either directly taken from fluvial sediments of the T2 terrace or originate from hillslope sediments covering the T2 terrace.

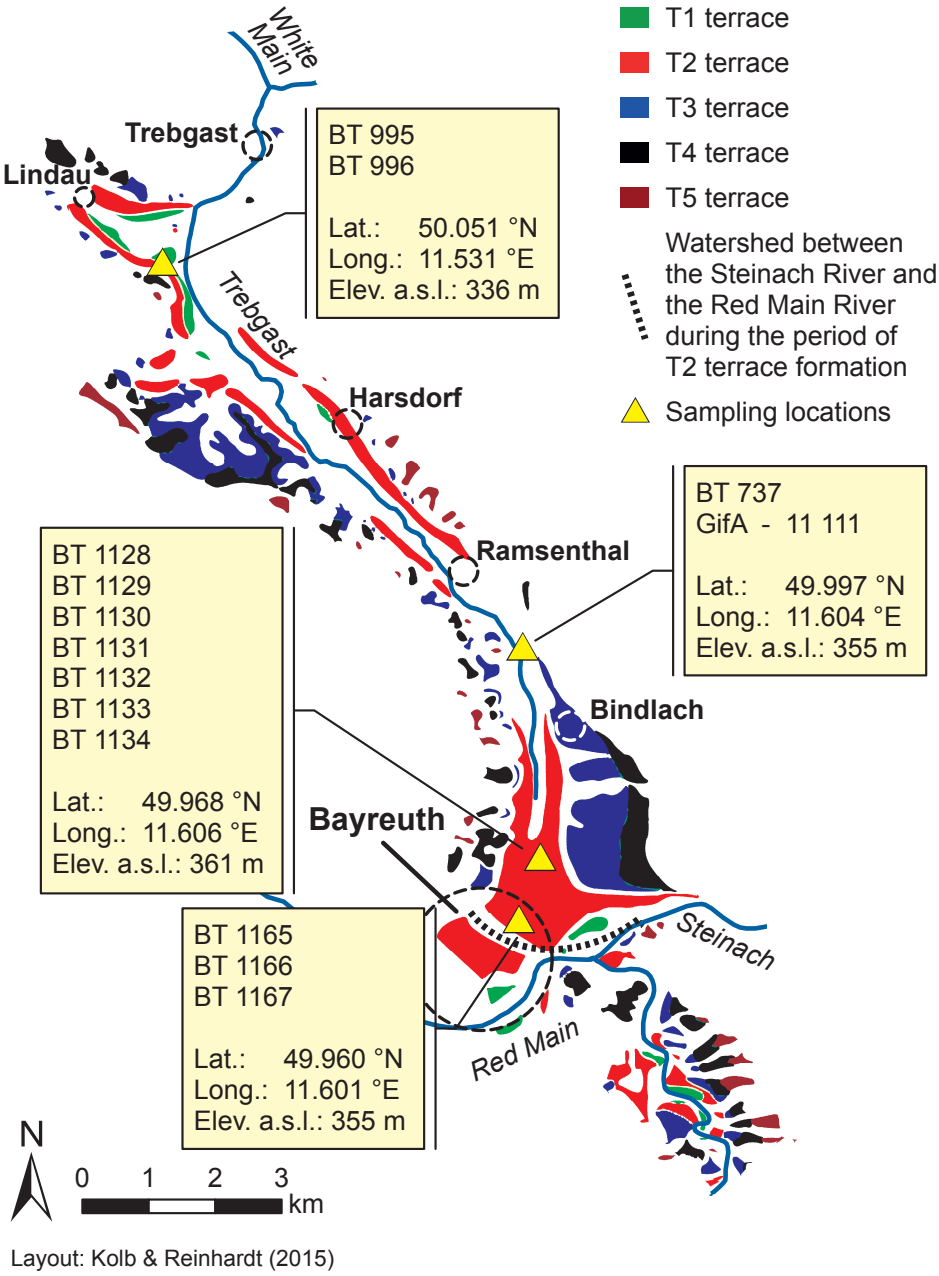

Figure 4.3: The Pleistocene terraces of the study area. Based on petrographic and lithological evidence, five Pleistocene terrace levels have been distinguished. Sampling locations are highlighted by yellow triangles. Modified after Kleber & Stingl (2000).

evolution. Thereafter, at least three evolutionary stages have to be distinguished. In a first stage, both, the rivers Red Main and Steinach, drained the valley. During this period the upper terraces T5 and T4 were formed. After the Red Main River had been deflected to its present-day course, the Steinach River solely used the valley, forming the T3 and T2 terraces. Finally, the Steinach River abandoned the valley as well, leaving behind an oversized valley that was drained by the Trebgast Creek, a small creek originating in the hillslopes of the nearby Middle Triassic limestone cuesta. During this last stage, the youngest Pleistocene fluvial terrace (T1) was deposited, restricted to the lowermost part of the valley.

So far, the chronology of the different evolutionary stages was only based on petrographic and morphostratigraphic findings. Thereby, mainly periglacial slope sediments were used for deriving age information for the terrace formation, determining the numbers of embedded palaeosols as indication of interglacial stages (e.g., Kleber & Stingl, 2000; Veit, 1991). An overview of these previously published age estimations is given in Table 4.1.

4.3 Sampling design

In order to establish a chronological framework for the youngest Pleistocene fluvial terrace of the primary Steinach River (T2), in total 13 samples for luminescence dating were taken from four different locations throughout the Trebgast Valley. The sampling sites were located in the upper, middle and lower section of the valley, respectively (Table 4.3 & Figure 4.3). Except for sample BT 737, all samples were directly taken from fluvial deposits of the T2 terrace. Due to a lack of suitable exposures of the gravel beds in the middle section of the valley, sample BT 737 was taken from a loess-bearing periglacial cover bed, superimposing the T2 terrace gravel with a minimal thickness of ca. 6 meters.

Samples BT 995 and BT 996 originate from sand lenses embedded in the T2 terrace gravels in the lowermost part of the valley. Overlaying deeply weathered Lower Triassic sandstones, the thickness of the gravel bed is only ca. 50 cm. The gravels are covered by a several dm thick layer of sandy loam, showing signs of anthropogenic activity (i.e. bricks and other artifacts).

The samples from the upper reaches (BT 1128 to BT 1134; Figure 4.3) were taken from different palaeochannels within a complex of terrace gravel. These channels

were filled with sand-sized fluvial material. Overlaying Upper Triassic sandstone, the gravel complex showed an average thickness of ca. 2 m and was covered by a mixture of fine and coarse grained material. These surficial deposits were identified as dumped fill, most probably originating from the construction of the nearby motorway during the 1950s. The gravel complex itself and the embedded palaeochannels, however, did not show any sign of human disturbance.

Samples BT 1165, BT 1166 and BT 1167 originate from a construction site in the uppermost part of the valley. Here, close to the present-day watershed between the Trebgast Valley and the Red Main Valley, the investigated gravels are part of a vast alluvial fan, accumulated by the primary Steinach River and reaching far to the west. The gravel deposits overlay sandstone formations of Upper Triassic origin and show an average thickness of ca. 1.5 m.

4.4 Methods

4.4.1 OSL sample preparation and measurement procedure

For OSL measurements the coarse grain quartz fraction (90-200 µm) was used. Following standard procedures, the sample preparation was done in subdued red light (640 ± 20 nm). After wet sieving of the sediment, the samples were treated with HCl and H_2O_2 to remove carbonates and organic remnants. Density separation using sodium polytungstate was applied to separate the quartz from heavy minerals (density > 2.75 g/cm^3) and feldspars (density < 2.62 g/cm^3). In order to remove the alpha irradiated outer layer of the quartz grains and to eliminate any remaining feldspar contamination, the samples were etched in 40% HF for 45 minutes and finally washed in 10% HCl for 30 minutes. The quartz grains were mounted and fixed on aluminum cups by silicon oil, using a 2 mm mask for samples BT 737, BT 995 and BT 996 and a 3 mm mask for all other samples, which approximates a number of 100 – 150 grains per aliquot for the 2 mm mask and about 200 – 300 grains for the 3 mm mask. For each sample more than 40 aliquots were measured (Table 4.3).

All luminescence measurements were carried out at the University of Bayreuth using an automated Risø-Reader TL/OSL-DA-15, equipped with a 90Y/90Sr β-source for artificial irradiation. For OSL stimulation blue LEDs (470 ± 30 nm) were

used. The luminescence signal was detected by a Thorn-EMI 9235 photomultiplier combined with a 7.5 mm U-340 Hoya filter (290-370 nm).

For equivalent dose (D_e) determination the single-aliquot regenerative dose protocol (SAR) proposed by Murray & Wintle (2000) was applied. After measuring the natural luminescence signal, six regeneration cycles were used to define the samples' dose-response. After preheating, the shine-down curves for the natural and regenerated signals as well as for the test dose signals were recorded for 40s at an elevated temperature of 125°C. For every sample an individual preheat temperature was identified by a combined dose recovery and preheat test. Thereby, the aliquots were first artificially bleached for 3 h using a solar lamp (Osram Duluxstar 24 W) and β-irradiated with known doses close to the expected equivalent dose for the respective sample. After that, the D_e was determined using the SAR protocol with five different preheat temperatures of 180-260°C (in steps of 20°C). For each preheat step the mean D_e of three aliquots was determined and the measured-to-given dose ratio was calculated. Based on this ratio, for each sample an individual preheat temperature was chosen for which the given laboratory dose could be reproduced at its best. Dependent on the different locations, the individual preheat temperatures ranged from 200°C to 240°C.

For dose rate ($\dot{D}$) determination, the U- and Th-concentrations were detected by thick source α-counting, the K-contents of the samples were measured by ICP-OES. Cosmic dose-rates were calculated according to Prescott & Hutton (1994). A common water content of 15% was used for all samples. This value was derived using the average value of the possible water content range, based on the porosity of the samples and considering an error, which included the possible water content range (e.g., Fuchs et al., 2010, 2012; Prinz & Strauss, 2011; Scheffer et al., 2011). In order to check the correctness of the chosen value, the in situ water contents of the samples were measured, showing conformity within errors to the chosen water content of 15%. As BT 1128 to BT 1134 clearly showed signs of a significant hydromorphic impact, for those samples a deviant water content of 20% was used.

4.4.2 Luminescence properties and rejection criteria

To ensure their suitability for luminescence dating, all samples had to pass a dose recovery test, in which a given dose in the range of the expected equivalent dose (D_e) could be reproduced within 10% error limits. All samples proved to pass this requirement. Additionally, all aliquots which were not able to pass the rejection criteria for OSL dating were excluded. Thus, only aliquots with a recycling ratio of 0.9-1.1, a recuperation of ≤ 5% of the natural sensitivity corrected signal intensity (Murray & Wintle, 2000) and an IR depletion ratio (Duller, 2003) of 0.9-1.1 were accepted for D_e calculation.

4.4.3 Insufficiently bleached samples and age calculation models

As fluvial deposits are especially prone to incomplete resetting of the luminescence signal, all measurements were carried out on small multiple grain aliquots containing ca. 100 to 300 grains per aliquot (e.g., Fuchs & Wagner, 2003). Thus, aliquots containing insufficiently bleached grains, that would cause an overestimation of the sedimentation age, can be detected and discarded using a sample specific coefficient of variation ν ($\nu = (s/\overline{x}) \cdot 100\%$; s: standard deviation; $\overline{x}$: mean of D_e; Clarke (1996); Clarke et al. (1999); Fuchs & Wagner (2003)). For each sample an individual threshold of ν^* was empirically determined by a 'bleaching and scattering test'. Therefore, ten aliquots of each sample were artificially bleached for three hours using an Osram Duluxstar 24 W solar lamp. These well-bleached subsamples were β-irradiated using doses in the range of the expected equivalent dose. For D_e determination a normal SAR protocol was applied using the same parameters already used for the OSL measurements yielding the age information. Based on the particular D_e distribution, the coefficient of variation was calculated for each of these well-bleached samples. This coefficient was defined as threshold ν^*, which represents the sample specific scatter in D_e distribution that should be expected if the respective sample was well-bleached during deposition. All samples exceeding their particular threshold ν^* are assumed to suffer from incomplete resetting of the luminescence signal.

In order to avoid an age overestimation, it is compulsory to apply an age calculation model that considers the problem of insufficiently bleached samples. In the

field of luminescence dating a wide variety of such statistical methods have been established (e.g., Olley et al., 1998; Galbraith et al., 1999; Galbraith, 2005; Lepper et al., 2000; Fuchs & Lang, 2001). In many studies on fluvial sediments, both, the minimum age model (Galbraith et al., 1999) and the finite mixture model ((Galbraith & Green, 1990), were successfully used (e.g., Olley et al., 2004; Rodnight et al., 2006). However, both statistical methods can only be applied properly when sufficient material is available and a sufficient number of aliquots can be measured. With the age calculation procedure proposed by Fuchs & Lang (2001), there is an approach which can still be applied when the sample quantity is limited. Thereby, the D_e values are sorted in ascending order, stepwise calculating a running mean value. The '*true*' D_e is assumed to be the mean value when the standard deviation first exceeds a critical threshold determined by laboratory tests on well bleached samples. Here, a site-specific critical value of 10% was identified to be typical for samples originating from the study area. This value was derived from the sample specific thresholds determined for the coefficient of variation v^* as described before. In this study, the minimum age model, the finite mixture model and the procedure of Fuchs & Lang (2001) were applied.

4.5 Results – sample characteristics and age calculation

Though all investigated samples passed the dose recovery test and thus were generally suitable for luminescence dating, they proved to be problematic when applying the quality criteria for OSL dating. Especially, many aliquots were not able to meet the threshold defined for the IR depletion ratio, indicating a significant contamination of the measured quartz samples, most probably caused by crystal intergrowth of quartz and feldspar minerals which could not be removed by HF etching. Therefore, a great number of subsamples had to be measured in order to be able to get a sufficient amount of D_e values for OSL age calculation (Table 4.3).

Those aliquots passing the rejection criteria are characterized by bright and fast decaying OSL signals, typical of quartz samples. Using single exponential functions for data fitting, growth curves could be established with high precision. A typical OSL shine-down curve along with a typical growth curve for sample BT 1165 is shown in Figure 4.4a and Figure 4.4b.

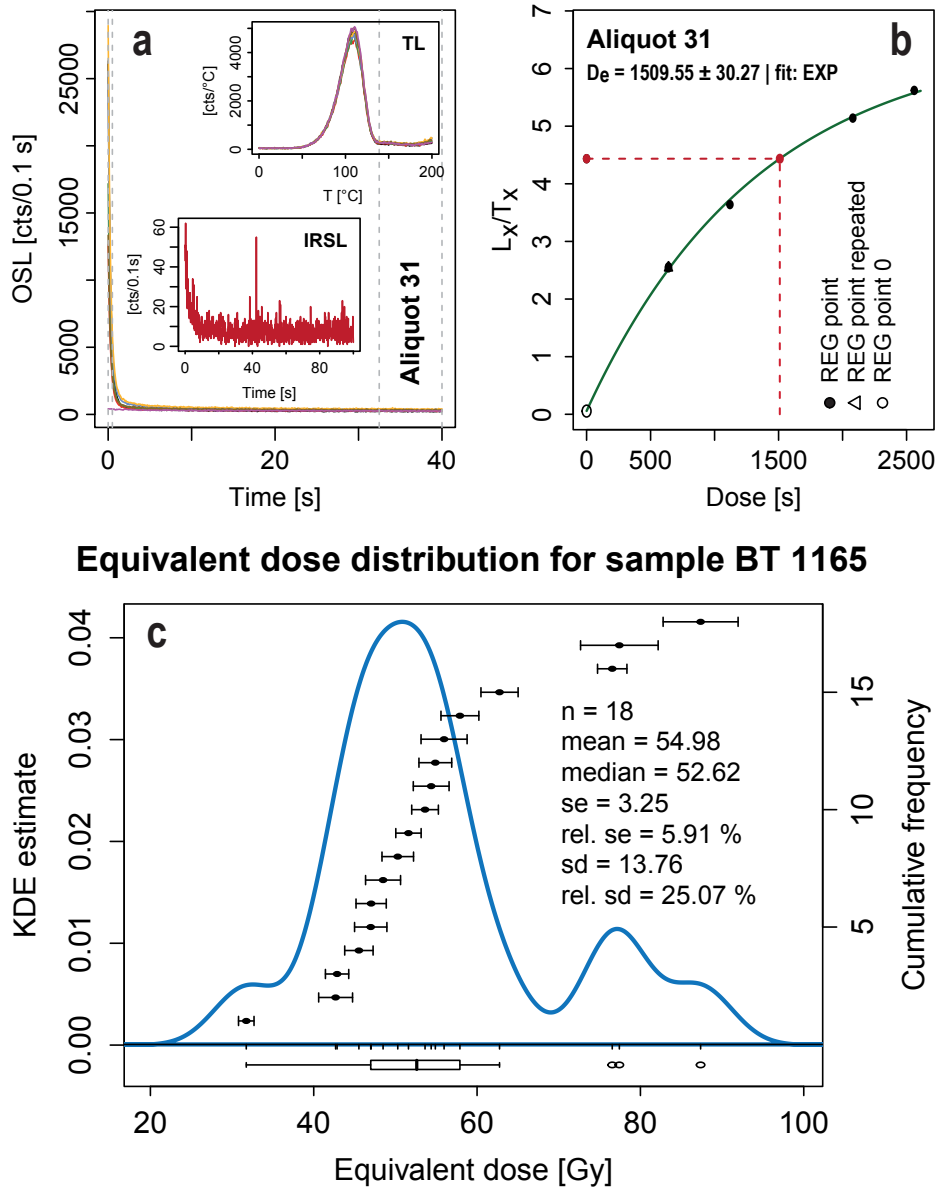

Figure 4.4: Typical OSL shine-down curve (a), growth curve (b) and equivalent dose distribution obtained for sample BT 1165 (c). Aliquots passing the rejection criteria show bright and fast decaying shine-down curves. For all samples a single exponential function was used for data fitting. For sample BT 1165 only 18 out of 48 measured aliquots passed the rejection criteria, showing a wide spread in D_e distribution with a relative standard deviation of ca. 25%.

Characteristic of fluvial deposits (e.g., Stokes et al., 2001; Wallinga, 2002; Jain et al., 2004), all samples show a wide D_e distribution with relative standard deviations > 10% (Table 4.3), ranging from minimum values of 12% (sample BT 1167) to maximum values of 43% (samples BT 1128 and BT 1133). The individual threshold values v^* for well bleached aliquots, which have empirically been determined for each sample, were found to be identical within errors and indicated a scatter of up to 9% for well-bleached samples. Therefore, we decided to give up the sample-specific threshold. In accordance with previous studies (e.g., Clarke, 1996; Clarke et al., 1999; Fuchs & Wagner, 2003; Fuchs et al., 2010), we used a site-specific threshold of 10% to discriminate between well-bleached and insufficiently bleached samples. With relative standard deviations of 12% up to 43%, the coefficient of variation v exceeds this site-specific threshold for all samples, indicating that all investigated samples suffer from incomplete bleaching and request the application of an adequate age calculation model. For BT 1165, the equivalent dose distribution is displayed in Figure 4.4c.

To avoid an overestimation in the calculation of sedimentation ages, the minimum age model (MAM) of Galbraith et al. (1999) considering the annotations made by Cunningham et al. (2011) along with the finite mixture model (FMM) (Galbraith & Green, 1990) were applied. However, due to the restricted number of remaining aliquots, for many samples both age calculation models could not be applied properly and, in these cases, were not able to yield reasonable results. Only the procedure of Fuchs & Lang (2001) could successfully be applied to all investigated samples. Whenever ages could be calculated using the MAM and/or the FMM, these ages were used to check the reliability of the luminescence ages derived from the model of Fuchs & Lang (2001). This cross-check showed good agreement (identical within error margins) for MAM/FMM ages and ages calculated with Fuchs & Lang (2001). As the procedure proposed by Fuchs & Lang (2001) is the model of choice, hereafter only the ages derived from applying this approach are presented (Table 4.3).

For samples BT 995 and BT 996 OSL ages of 88.96 ± 5.92 ka and 84.03 ± 5.61 ka, respectively, could be derived. Samples BT 1128 to BT 1134, taken from different palaeochannels in the upper reaches of the valley, show significantly younger ages. They reach from 33.70 ± 2.29 ka in minimum for sample BT 1131 to a maximum age of 64.11 ± 4.25 ka for sample BT 1133. With OSL ages of 24.58 ± 1.66 ka for

BT 1165, 30.29 ± 2.33 ka for BT 1166 and 20.14 ± 1.26 ka for BT 1167, the youngest sedimentation ages could be derived for samples near the present-day watershed between the Trebgast Valley and the Red Main Valley.

Table 4.2: Radionuclide concentrations, cosmic dose rates and total dose rates.

Sample	Uranium [ppm][a]	Thorium [ppm][a]	Potassium [%][b]	$\dot{D}_{cosmic}$ [Gy/ka][c]	$\dot{D}_{total}$ [Gy/ka][d]
BT 737	4.26 ± 0.21	11.64 ± 0.71	2.53 ± 0.10	0.09 ± 0.01	3.78 ± 0.21
BT 995	2.34 ± 0.21	5.40 ± 0.69	1.92 ± 0.10	0.17 ± 0.01	2.60 ± 0.15
BT 996	1.79 ± 0.19	4.63 ± 0.63	1.92 ± 0.10	0.17 ± 0.01	2.44 ± 0.15
BT 1128	1.66 ± 0.22	5.47 ± 0.74	1.82 ± 0.10	0.14 ± 0.01	2.24 ± 0.14
BT 1129	2.12 ± 0.24	6.01 ± 0.79	2.65 ± 0.10	0.14 ± 0.01	3.03 ± 0.17
BT 1130	3.46 ± 0.28	15.27 ± 0.93	4.22 ± 0.10	0.14 ± 0.01	5.08 ± 0.26
BT 1131	2.00 ± 0.21	7.61 ± 0.71	4.11 ± 0.10	0.14 ± 0.01	4.27 ± 0.22
BT 1132	1.07 ± 0.17	4.71 ± 0.56	3.85 ± 0.10	0.14 ± 0.01	3.72 ± 0.19
BT 1133	1.70 ± 0.19	5.23 ± 0.61	1.60 ± 0.10	0.14 ± 0.01	2.05 ± 0.12
BT 1134	2.49 ± 0.25	8.68 ± 0.81	2.35 ± 0.10	0.14 ± 0.01	3.01 ± 0.17
BT 1165	1.54 ± 0.12	3.19 ± 0.39	1.69 ± 0.10	0.14 ± 0.01	2.08 ± 0.13
BT 1166	1.36 ± 0.17	4.70 ± 0.57	1.55 ± 0.10	0.15 ± 0.01	2.02 ± 0.13
BT 1167	4.33 ± 0.39	16.57 ± 1.31	2.21 ± 0.10	0.15 ± 0.01	3.89 ± 0.23

[a] Determined by thick source α-counting.
[b] Determined by ICP-OES.
[c] Cosmic dose rates were calculated according to Prescott & Hutton (1994).
[d] For dose rate calculation, a water content of 15% (for BT 1128 to BT 1134: 20%) was used.

For sample BT 737 an OSL age of 30.26 ± 1.76 ka was calculated, confirmed by a calibrated radiocarbon age of 30,974-31,500 cal. BP, which could be derived from fragments of mollusk shells from *Pupilla genus* (sample GifA 11 111; Zöller et al., 2012a). The mollusk shells originated from a lens of loess-like material embedded into the hillslope detritus which sample BT 737 was taken from. The radiocarbon age may most probably suffer from a distinct hard water effect and therefore overestimate the sedimentation age by several hundred years. But even without assuming a significant age overestimation, the calculated luminescence age is in agreement with the calibrated ^{14}C age when considering the error margins. The analytic data for dose rate determination and for OSL age calculation are listed in Table 4.2 and 4.3.

Table 4.3: Sample codes, sampling locations, elevation a.s.l., sampling depths, coefficients of variation, equivalent doses and quartz OSL ages.

Sample	Sampling location		Elevation a.s.l. [m]	Sampling depth [cm]	m[a]	n[b]	Without age model		Fuchs & Lang (2001)	
	Latitude [°N]	Longitude [°E]					Mean D_e [Gy][c]	ν[d]	D_e [Gy]	OSL age [ka]
Middle section – periglacial slope sediments covering T2 terrace gravel										
BT 737	49.997	11.604	355	450	94	44	122.53 ± 2.84	15%	114.41 ± 2.12	30.26 ± 1.76
Lower section – sand lens within T2 terrace complex										
BT 995	50.051	11.531	336	80	48	33	305.99 ± 11.7	22%	231.13 ± 6.99	88.96 ± 5.92
BT 996	50.051	11.531	336	90	45	15	212.12 ± 7.22	13%	204.91 ± 6.12	84.03 ± 5.61
Upper section – palaeochannels within T2 terrace complex										
BT 1128	49.968	11.606	361	200	48	32	154.29 ± 11.8	43%	130.02 ± 3.21	58.14 ± 3.82
BT 1129	49.968	11.606	361	200	45	25	168.93 ± 7.60	23%	154.31 ± 3.67	50.99 ± 3.09
BT 1130	49.968	11.606	361	200	43	10	203.52 ± 8.19	16%	203.52 ± 8.19	40.09 ± 2.62
BT 1131	49.968	11.606	361	200	44	13	146.98 ± 11.1	27%	143.87 ± 6.35	33.70 ± 2.29
BT 1132	49.968	11.606	361	200	47	22	178.59 ± 13.0	34%	135.60 ± 4.20	36.49 ± 2.21
BT 1133	49.968	11.606	361	200	45	26	162.93 ± 13.7	43%	131.64 ± 3.47	64.11 ± 4.25
BT 1134	49.968	11.606	361	200	47	20	208.75 ± 17.5	37%	143.84 ± 5.43	47.85 ± 3.23
Uppermost section – alluvial fan										
BT 1165	49.960	11.601	355	200	48	18	54.98 ± 3.25	25%	51.13 ± 1.55	24.58 ± 1.66
BT 1166	49.960	11.601	355	170	48	17	78.17 ± 5.94	31%	61.14 ± 2.66	30.29 ± 2.33
BT 1167	49.960	11.601	355	160	48	19	78.39 ± 1.51	12%	78.39 ± 1.51	20.14 ± 1.26

[a] Number of measured aliquots.
[b] Number of aliquots passing the rejection criteria.
[c] Mean equivalent dose values determined without applying an age model.
[d] Coefficient of variance ν. For all samples an individual threshold ν^* was empirically determined. With the individual thresholds being identical within errors, a common threshold of 10% was used for all samples to identify incompletely bleached samples.

4.6 Discussion

4.6.1 The timing of the T2 terrace formation

In traditional concepts of fluvial terrace formation, river terraces are explained as landscape features typically accumulated during cold phases of glacial periods (e.g., Bryant, 1983; Büdel, 1977; Gibbard, 1985). Following these traditional concepts, previous studies deduced a time frame for the final deflection of the primary Steinach River, spanning from the last glacial maximum (LGM) to the Bölling interstadial (e.g., Kleber & Stingl, 2000; Zöller et al., 2007). Based on morphostratigraphic evidence, the formation of the T2 terrace has so far been interpreted as of upper Würmian (Weichselian) age, with the T2 gravels accumulated by the primary Steinach River during the period of the LGM (e.g., Kleber & Stingl, 2000; Zöller et al., 2007).

However, all samples from the T2 terrace, except for the near present-day watershed samples BT 1165, BT 1166 and BT 1167, show significantly older luminescence ages. Considering the way of fluvial transport and being aware of the problem of incomplete bleaching, these ages have to be interpreted with caution. However, using small aliquots provides a well established tool for identifying incomplete resetting of luminescence signals (e.g., Wallinga, 2002; Fuchs & Wagner, 2003). Thereby, aliquots for which the lowest equivalent doses were obtained are interpreted to contain a dominant amount of well-bleached grains and thus yield the best approximation of the 'true' D_e value. In order to avoid age overestimates and to obtain reliable OSL ages, the approach proposed by Fuchs & Lang (2001) was applied in this study, ensuring that only those aliquots representing the lowest population of the D_e distribution were used for equivalent dose determination and age calculation. Nevertheless, we clearly want to emphasize that even these ages might still be affected by undetected residuals and, thus, suffer from incomplete bleaching causing a possible age overestimation. In particular, this might apply for those samples (e.g., BT 996, BT 1130 and BT 1131) for which only few aliquots were able to pass the strict rejection criteria in this study. However, with increasing ages the effect of such undetected residuals tends to become less important and, therefore, can be assumed to be of little significance for the interpretation of the fluvial terraces in the research area.

The samples from the lowermost part of the valley (BT 995, BT 996) indicate

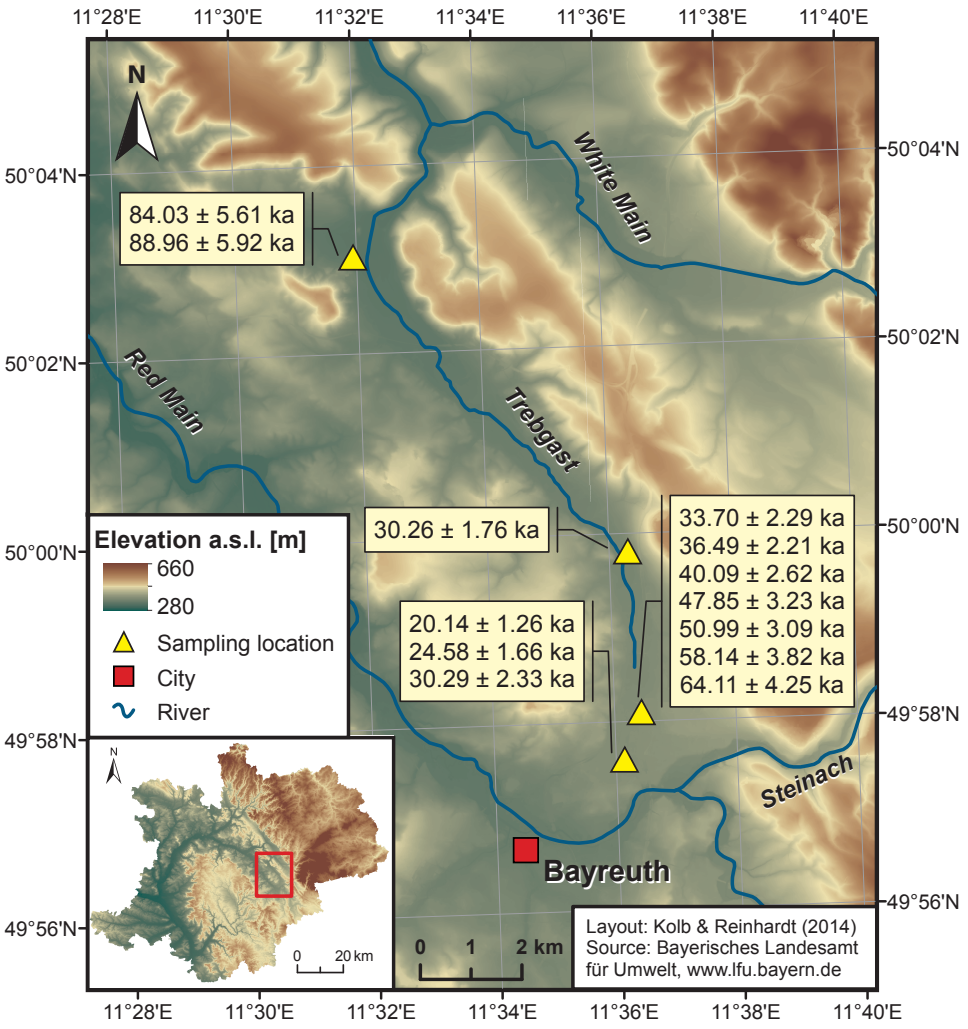

Figure 4.5: The Trebgast Valley. Sampling locations are marked by yellow triangles. For each location the determined quartz OSL ages are displayed.

a period of terrace formation during an early stage of the Würmian (Weichselian) glacial, whereas the samples taken from various palaeochannels located in the upper reaches point to high fluvial activity during the Middle Pleniglacial. Thereby, sample BT 1131 has been identified to be the youngest bed load sediment of the primary Steinach River from within the valley, showing an OSL age of 33.70 ± 2.29 ka.

The luminescence ages obtained for the 9 samples taken from gravel aggradations (BT 995, BT 996 and BT 1128 to BT 1134) are supported by the OSL age obtained for sample BT 737. This sample was collected from a lens of gleyed loess-like material embedded in a periglacial slope detritus. These cover sediments superimpose the T2 terrace with a minimum thickness of ca. 6 meters. Therefore, the obtained OSL ages indicate a significantly older age for the subjacent T2 gravel bed and also point to intense fluvial geomorphodynamics during the Middle or even Lower Pleniglacial.

Our results are in agreement with findings made by other regional studies in Central and Southern Germany. Applying a pIRIR290 approach, Lauer et al. (2014) obtained luminescence ages for feldspar samples which indicated that the Zauschwitz loess sequence in Western Saxony was accumulated during the late Weichselian Pleniglacial. This rather late onset of the loess accumulation is interpreted as a result of an enhanced fluvial activity of the nearby Weisse Elster river prior to ca. 30 ka. For the Upper Rhine Graben Lauer et al. (2010) were able to derive at least three periods of Weichselian fluvial aggradation, with two of them correlating with the Early and the Middle Pleniglacial. Stages of high fluvial activity for the Danube system could be derived by Fiebig & Preusser (2003) for the so called '*High Terrace*' ('*Hochterrasse*'). Using infrared stimulated luminescence dating, they determined sedimentation ages of ca. 75 – 84 ka for the '*Rainer Hochterrasse*' near Münster and of 63 – 75 ka for the '*High Terrace*' of the so called '*Schutter-Donau*' in the region of Ingolstadt. Similar age estimations are, for example, reported by Krömer (2010) for the Danube valley and by Gesslein & Schellmann (2011) for the Lech valley.

In contrast to Kleber & Stingl (2000) and Zöller et al. (2007), no sampling location has so far been found within the Trebgast Valley that provided T2 terrace material, yielding ages which were in accordance with the age estimates of previous studies. With luminescence ages of ca. 20 to 30 ka, only BT 1165, BT 1166

and BT 1167, collected from a vast alluvial fan near the present-day watershed, appear to indicate a significant fluvial activity during the Upper Pleniglacial.

Therefore, the fluvial history of the study area at the end of the Würmian (Weichselian) period may be interpreted in an alternative way. The absence of fluvial deposits of the primary Steinach River within the Trebgast Valley showing ages younger than 30 ka indicates that there was no significant fluvial morphodynamics within the valley at that time. Thus, the primary Steinach River abandoned the valley much earlier than so far assumed. However, it seems very likely that the Steinach River was not immediately deflected to its present day course. In fact, the vast alluvial fan in the southernmost part of the Trebgast Valley suggests that the primary Steinach River was able to reach far to the west.

Having abandoned the main part of the Trebgast Valley and already being a tributary to the Red Main River, the Steinach River still used the southernmost part of the valley, flowing in the Red Main River at a so far unknown location further to the west. The calculated OSL ages for the samples taken from the alluvial fan (BT 1165 to BT 1167) give clear evidence that this evolutionary stage took place during the Upper Pleniglacial. Therefore, the final shift of the primary Steinach River to its present-day course should have taken place later than 20 ka.

4.6.2 Diachronic character of river incision?

An inter-location comparison of the calculated luminescence ages yields the surprising result that the OSL ages of T2 material from the lowermost part of the valley are significantly older than those from the middle section and the upper reaches. This is surprising because the sampling locations have clearly been identified to represent the same terrace level (T2). With the samples from the lowermost part of the valley being older than those from the middle section and the upper reaches, the results presented in this paper show evidence for different luminescence ages of samples originating from the same morphological unit, depending on their particular position within the longitudinal river course.

The reason for this finding is not clear so far. On the one hand, these ages could be seen as ages of deposition, indicating a diachronic accumulation of fluvial sediments within the valley. On the other hand, our findings might also be interpreted as the result of a diachronic river incision, for which the mechanism could be de-

scribed following the concept of backward erosion: at the beginning of a climatically and/or tectonically driven erosion impulse this impulse should be strongest near the base level of erosion. Therefore, it seems likely to assume the initial rate of incision by which a river is able to cut through its previously accumulated deposits to be higher in the lowermost part of a valley than in the middle section or even in the upper reaches. As a result, the river terrace formation (i.e. the abandonment of the former floodplain by lowering the river bed) in the lowermost part of a valley should occur faster than in its upper reaches. When the former floodplain is abandoned and the transformation to a fluvial terrace is finished, the river is not able to relocate the sediments of the abandoned floodplain any more. From the perspective of luminescence dating, this moment is the starting point of luminescence signal growth. As the erosion impulse needs some time to slowly propagate upstream the valley, the luminescence clock at different locations starts at different times, depending on the particular moment when the river has incised sufficiently to abandon its former floodplain.

Similar findings were reported by Rixhon et al. (2011) for $^{10}Be/^{26}Al$ dating of the Main Terrace level in the Ardennian valleys. They concluded that the river incision occurred diachronically along the drainage network and therefore could not have been climatically forced.

However, the question whether a similar interpretation is possible for the results gained in the Trebgast Valley, assuming a climatically and/or tectonically induced erosion impulse to propagate along the stream longitudinal profile, cannot be answered at this moment. Furthermore, we are aware of the fact, that we are not able to decide if our findings just reflect regional or local features strongly affected by the specific hydrological setting of the research area or if a more generalizing interpretation is possible.

Anyway, our findings show the complex character of river systems' response to external forcing and suggest a strong dependency on local and regional conditions. They are in accordance with previous studies that proved a distinct interrelation between the varying geomorphological settings and the particular response of river systems to major changes in climatic conditions (e.g., Mol et al., 2000; Vandenberghe, 2002, 2003). Furthermore, with the determined OSL ages indicating a Lower and Middle Peniglacial period of high fluvial morphodynamics for our research area, our results are in accordance with findings showing that high fluvial

activity is often correlated with glacial-interglacial transition periods or occurred during stages of fast transitions between colder and warmer phases within glacial periods (e.g., Vandenberghe, 1995; Bridgland & Westaway, 2008a). Thus, our results confirm that the interaction between fluvial activity and changing climate conditions is not to be characterized as a simple one-to-one correlation, but has to be interpreted as a complex process-response-system, controlled by various external and internal factors (e.g., Vandenberghe, 2003).

4.7 Conclusion

Fluvial deposits and periglacial slope sediments were used as sedimentary archives for the reconstruction of the fluvial history and palaeoenvironmental evolution in a small dry valley in northern Bavaria, Germany. Focusing on the youngest Pleistocene terrace level and based on luminescence dating of coarse grain quartz samples and AMS ^{14}C dating of mollusk shells, a chronological framework for the fluvial history of the study area during the Würmian (Weichselian) period was derived.

Our results are in conflict with age estimates proposed by previous studies, which were based on traditional concepts of fluvial terrace aggradation (e.g., Kleber & Stingl, 2000; Zöller et al., 2007). Based on a local chronological framework for the T2 terrace formation, a modified regional landscape evolution model is proposed.

The presented luminescence ages point to intense fluvial geomorphodynamics during early stages of the Würmian (Weichselian) glacial as well as during the Lower and Middle Pleniglacial. Evidence for a significant fluvial activity during the Upper Pleniglacial could only be detected for the uppermost part of the study area close to the present-day watershed. Therefore, the obtained OSL ages confirm findings from previous studies showing high fluvial activity to be correlated with stages of fast transition between colder and warmer periods (e.g., Vandenberghe, 1995, 2008). Furthermore, they indicate a complex character of fluvial systems and contradict traditional concepts of river terrace formation based on the simplified one-to-one correlation between fluvial morphodynamics and climate change.

The results presented in this paper suggest a diachronic character of river incision and, hence, point to the complexity of fluvial systems' response to climatically

and/or tectonically forced changes in local and regional palaeoenvironmental conditions.

Acknowledgements

The authors would like to thank the *Bavarian Environment Agency* (*Bayerisches Landesamt für Umwelt - LfU*) for providing the digital terrain model (DTM) and other digital maps of the research area. Many thanks go to the enterprise *Piewak & Partner* (Bayreuth) for generously supporting us with stratigraphic plots and photographs of the boreholes at the Crottendorf site. The *Oberfrankenstiftung* is thanked for partial funding of this study. We also thank the two anonymous reviewers for their constructive and informative reviews, which greatly improved the quality of our manuscript.

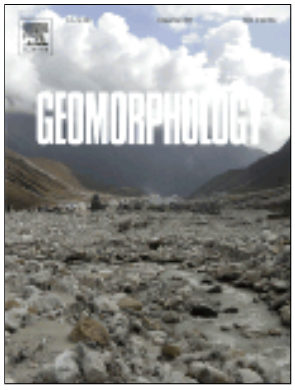

5

Study Three: Luminescence dating of pre-Eemian (MIS 5e) fluvial terraces in Northern Bavaria (Germany) – benefits and limitations of applying a pIRIR$_{225}$-approach

Thomas Kolb & Markus Fuchs

Geomorphology
submitted November 2017

Luminescence dating of pre-Eemian (MIS 5e) fluvial terraces in Northern Bavaria (Germany) – benefits and limitations of applying a $pIRIR_{225}$-approach

Thomas Kolb & Markus Fuchs

Geomorphology – under review
with 9 figures and 5 tables

Summary

Quartz optically stimulated luminescence (OSL) and post-IR IRSL dating of potassium-rich feldspar separates were applied to fluvial sediments which had been supposed to be of pre-Eemian (MIS 5e) age. Our aim was to establish a reliable chronology for a sequence of fluvial terraces in a region of Northern Bavaria (Germany) characterized by a complex Pleistocene fluvial history.

The investigated quartz samples proved to be in dose saturation and the calculated OSL ages could only be interpreted as minimum age estimations. The performance of the used $pIRIR_{225}$-approach was tested by a set of bleaching experiments as well as by dose recovery tests (DRT) and the measurement of sample specific laboratory fading rates. All investigated samples showed excellent dose recovery rates and low residual doses. The phenomenon of 'anomalous fading', however, remained a major problem for age calculation in this study, indicated by rather large g-values determined for our samples despite applying a $pIRIR_{225}$-protocol. At least for the samples investigated in this study, we cannot confirm the promising results of previous studies suggesting that IRSL-signals measured at elevated temperatures following an IR-readout at 50°C provide the potential to reduce 'anomalous fading' to a negligible level that can be considered as laboratory artifact.

Thus, various fading correction methods had to be used. Thereby, only the model proposed by Huntley & Lamothe (2001) could successfully be applied, while the approaches of Lamothe et al. (2003) and Kars et al. (2008) failed due to so far unknown reasons. Overall, the corrected $pIRIR_{225}$-ages were in good agreement with age constraints derived from stratigraphical and sedimentological findings. For some feldspar samples, however, the determined ages were far beyond a realistic age range for a meaningful interpretation when considering the (morpho-)stratigraphical set-

ting. Although the reasons for these significant age overestimations are not clear so far, they might either indicate methodological limitations of the post-IR IRSL approach or point to serious problems attributed to the luminescence properties of the used K-feldspar separates or to the specific regional environmental settings during sample deposition. Despite these problematic findings, the numerical results derived from the post-IR IRSL measurements can be used to establish a preliminary chronological framework for the various evolutionary stages identified in the research area.

Keywords: luminescence, pIRIR, fluvial terrace, fading, pre-Eemian

5.1 Introduction

Fluvial terraces and other fluvial sediments have long been identified to be important archives for palaeoenvironmental research. Thereby, a wide variety of traditional and modern methods is applied in order to derive information on past, present and future fluvial morphodynamics. Besides sedimentological, petrographical, stratigraphical and (micro-)morphological analyses, dating of fluvial sediments is of crucial importance for the interpretation of environmental records. The timing of accumulation and erosion phases may reveal information on changes in palaeoclimatic (e.g., Lauer et al., 2014) or tectonic conditions (e.g., Rixhon et al., 2011; Sohbati et al., 2012) as well as on changes in human occupation and anthropogenic impact on landscape evolution (e.g., Fuchs et al., 2011; Preusser et al., 2016). The importance of fluvial terraces in geomorphology, archaeology and modern river engineering is well documented by a huge and still growing number of studies spanning a wide range of climatic and regional settings including small, medium and large scaled river catchments (e.g., Buch, 1988; Houben, 2003; Knox, 2006; Schirmer, 1983; Schirmer et al., 2005). A major part of these studies, however, seem to have been focusing on either late Pleistocene (i.e. Würmian) or Holocene deposits. There are various reasons for this tendency, including the fact that landforms developed during the last glacial-interglacial cycle are most likely those environmental features best preserved and, thus, dominating the morphology of modern landscapes. But this tendency is also supported by the dating techniques that have so far been available for Quaternary sediments. In the past, radiocarbon dating was the most common method applied to fluvial sediments.

However, its application is strongly hampered by several serious limitations such as the fact that organic material is often completely missing or at least reworked in fluvial environments (e.g., Gillespie et al., 1992; Howard et al., 2009). Furthermore, the dating range of ^{14}C-methods is typically restricted to the last 40 - 50 ka (e.g., Reimer, 2012) and additional uncertainties are introduced by the need of calibration.

Over the last decades, optically stimulated luminescence (OSL) dating has become a widespread tool in palaeoenvironmental research. Despite several methodological challenges (e.g., Wallinga, 2002; Rittenour, 2008), luminescence dating has successfully been applied to a wide range of fluvial sediments in general (e.g., Lauer et al., 2010; Colarossi et al., 2015) and to fluvial terrace material in particular (e.g., Fiebig & Preusser, 2003; Litchfield & Rieser, 2005; Erkens et al., 2009; Rades et al., 2016; Wenske et al., 2012).

Ever since Murray & Wintle (2000) proposed the single aliquot regenerative (SAR) dose protocol, quartz has more and more been the mineral of choice in many of those studies. This preference for quartz dosimeters can be explained by the fact that the fast component of quartz OSL signals is regarded to be rapidly reset even by a short-time sunlight exposure. This easy-to-bleach character of quartz is of special relevance when dating fluvial deposits because solar resetting of waterlain sediments may significantly be limited by attenuation due to either the water column or the suspended load (e.g., Berger & Luternauer, 1987; Berger, 1990).

This advantage of quartz dosimeters, however, is accompanied by severe limitations. Some studies reported on poor luminescence properties of quartz extracts originating from sediments associated with geologically young orogens (e.g., Preusser et al., 2006; Steffen et al., 2009), others were simply confronted with quartz signals showing low luminescence sensitivities as well as considerable medium and slow components (e.g., Lukas et al., 2007). With respect to sediments older than the last glacial-interglacial-cycle, a crucial limitation of quartz minerals is their relatively low saturation dose that is normally regarded to be in a range of approximately 150-200 Gy (e.g., Roberts, 2008), in some exceptional sedimentological settings up to 400 Gy (e.g., Lu et al., 2007; Kemp et al., 2003). Strongly depending on the specific dose rate, this low saturation level considerably restricts the upper dating range of quartz OSL measurements to approximately 50-150 ka (e.g., Timar-Gabor & Wintle, 2013; Chapot et al., 2012).

Infrared stimulated luminescence (IRSL) dating of polymineral samples (fine grain fraction) or of potassium-rich feldspar separates (coarse grain fraction) may offer a suitable approach particularly for older sediments exceeding the upper age range of quartz OSL dating. IRSL signals from feldspars are regularly reported to be very bright and show saturation doses that are an order of magnitude higher than those determined for quartz (e.g., Huntley & Lamothe, 2001; Li et al., 2014). Thus, IRSL-based dating of feldspars, in principle, has the potential for significantly extending the upper age range of luminescence dating. However, feldspar luminescence measurements have long been known to suffer from a phenomenon called 'anomalous fading' (e.g., Wintle, 1973; Aitken, 1985; Spooner, 1994a). This phenomenon can be described as an athermal loss of luminescence signal over time and is – although not yet fully understood – attributed to quantum-mechanical tunnelling of electrons (e.g., Visocekas, 1985; Visocekas et al., 1994; Guérin & Visocekas, 2015).

As this loss of signal will result in serious age underestimations, the major problem of 'anomalous fading' has long prevented feldspar based IRSL measurements from becoming a routine dating approach for Quaternary sediments. In order to correct for fading effects, numerous correction methods have been proposed (e.g., Huntley & Lamothe, 2001; Lamothe et al., 2003; Kars et al., 2008). These approaches, however, are still controversially discussed as they are based on very specific assumptions and, furthermore, require a precise determination of laboratory fading rates. Particular with respect to the still unanswered question whether fading rates determined under experimental conditions can be used as adequate assessments of fading rates over geological periods, there are general concerns about the applicability of correction procedures (e.g., Wallinga et al., 2007; Lowick et al., 2012; Preusser et al., 2014).

Thomsen et al. (2008) were able to prove that laboratory fading-rates could significantly be reduced by applying a two-step post-IR IRSL approach. They suggested using the IRSL-signal measured at elevated temperatures after a low-temperature IRSL-readout to either completely avoid or at least strongly reduce the effects of anomalous fading. Since then, a great variety of different post-IR IRSL protocols have been proposed (e.g., Buylaert et al., 2009; Thiel et al., 2011a; Reimann & Tsukamoto, 2012; Li & Li, 2011) and successfully been tested in many studies indicating that pIRIR-procedures might yield a stable IRSL-signal

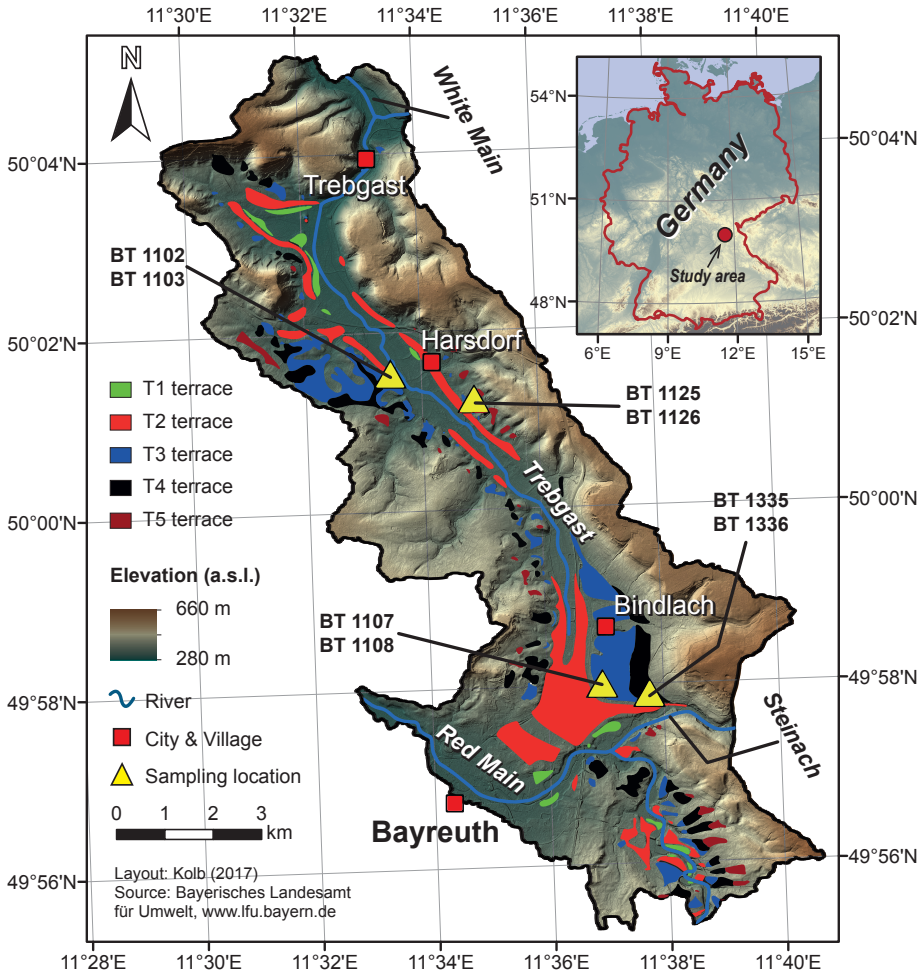

Figure 5.1: Detailed map of the Trebgast Valley. Five Pleistocene fluvial terrace levels have been identified and are indicated in this map by different colours. The sampling locations for luminescence dating are highlighted by yellow triangles.

not or only little affected by fading (e.g., Buylaert et al., 2012b; Li & Li, 2012; Li et al., 2014; Thiel et al., 2011b). These promising results offer the potential that precise and reliable age estimations based on luminescence dating might even be possible for sediments far beyond the last glacial-interglacial-cycle.

The river drainage system in Northern Bavaria, Germany, is characterized by a complex fluvial history (e.g., Eberle et al., 2010; Schirmer, 2010, 2012). With the Main River being one of the most important tributaries to the Rhine system, the irregular, nearly chaotic pattern of its river course reflects the successive enlargement of the Rhine River catchment (e.g., Eberle et al., 2010; Schirmer, 2010, 2012). Many studies about the evolution of the Main River and its headwater streams as well as on adjacent rivers have been published so far, typically focusing either on geological, sedimentological, stratigraphical or historical topics (e.g., Bartz, 1937; Brunnacker, 1973; Körber, 1962; Becker & Schirmer, 1977; Tillmanns, 1980; Peterek et al., 2009; Schirmer, 1983, 2007, 2010, 2014). Apart from a rather limited number of ^{14}C-datings, most of these studies derive chronological conclusions only from sedimentological findings and stratigraphical correlations. With respect to chronological issues there is still a considerable lack of studies providing numerical dating results. This particularly applies to the drainage system in the vicinity of the city of Bayreuth in northern Bavaria, Germany. Here, close to the European drainage divide and near the origins of the Red Main River and the White Main River, two major headwater streams of the Main River, a small valley can be found which reveals a series of fluvial and periglacial hillslope sediments that provide the potential to act as regional palaeoenvironmental archives for reconstructing the Pleistocene and Holocene landscape evolution.

The valley is situated right in the middle of the Upper Franconian Block-Faulted Zone, a geological transition zone separating the Variscian Bohemian Massif in the east from the adjacent South German Block with its Permo-Mesozoic sedimentary cover in the west (e.g., Duyster et al., 1995). Nowadays drained by the small Trebgast Creek, the Trebgast Valley was originally part of the Red Main/Steinach drainage system indicated by five different Pleistocene fluvial terraces within the valley (e.g., Kleber & Stingl, 2000; Zöller et al., 2007). Although the valley and its history have been discussed among geoscientists for more than a century (e.g., Reck, 1912; Seefeldner, 1914; Henkel, 1917, 1920; Stadelmann, 1924), the knowledge about the timing of the different evolutionary stages is still limited.

While several older studies (e.g., Kleber et al., 1988; Veit, 1991; Kleber & Stingl, 2000; Zöller et al., 2007) could only derive age information from the interpretation of sedimentological and stratigraphical findings, recently published studies were able to apply modern luminescence dating methods to terrace deposits and hillslope sediments from the valley (e.g., Kolb et al., 2016, 2017). Using quartz based OSL dating, these studies focused on the youngest Pleistocene fluvial terrace in the Trebgast Valley and constrained a timeframe for its accumulation, pointing to a complex terrace formation during the early Würmian (Weichselian) glacial as well as during the Lower and Middle Pleniglacial (e.g., Kolb et al., 2016, 2017).

The purpose of this study is to apply luminescence dating techniques to fluvial terrace deposits in the headwater area of the Main River drainage system that have been supposed to be of pre-Eemian (MIS 5e) age. We aim at testing the applicability of post-IR IRSL approaches to old samples originating from sediment aggradations being identified as the result of a complex fluvial history. Furthermore, we intend to establish a chronological framework for the oldest Pleistocene terrace levels identified in our research area, for which only weak age estimations have so far been derived from stratigraphical findings.

5.2 Study area and sampling locations

The Trebgast creek is a small tributary of the White Main River, which is one of the most important headwater streams of the Main River. The catchment is located in the north-eastern part of Bavaria, Germany, near the city of Bayreuth approximately 70 km north-east of Nuremberg (Figure 5.1). Showing a total of five Pleistocene fluvial terraces, the valley has been identified to represent a former interconnection between the Red Main Valley and the White Main Valley (e.g., Kleber et al., 1988; Kleber & Stingl, 2000). With both rivers being major headwater streams of the Main River, they still dominate the present-day drainage system of the study area. Based on lithological analyses, the two oldest terrace levels of the Trebgast Valley (T5- and T4- terrace) were identified to have been accumulated by the Red Main River and the Steinach River, the latter representing a local river originating in the nearby crystalline basement area of the Fichtel Mountains ('Fichtelgebirge') east of our study area. With the Red Main River not participating in the

sedimentation of the T3- and T2-terrace any more, these terrace levels were classified as pure Steinach River terraces, indicated by a significant change in the lithological gravel composition. The youngest Pleistocene terrace (T1-level), which was accumulated by the Trebgast Creek after the Steinach River abandoned the valley, is restricted to the lowermost section of the valley and consists of local material as well as reworked T2-terrace gravels (see Figure 5.1).

Based on lithological, pedological and morphostratigraphical evidence, Kleber & Stingl (2000) were able to derive a complex landscape evolution model including three distinct evolutionary stages. This model is discussed in detail by Kolb et al. (2016) who were able to modify and refine the model by adding a fourth evolutionary stage and by determining an OSL-based chronological framework for the T2-accumulation period, which was surprisingly characterized by a diachronic river incision.

Showing a wide and flat valley bottom, the Trebgast Valley is bordered by slightly inclined, only sometimes steep slopes developed in sandstone and limestone formations of Triassic origin. The lithology of the nearby surroundings is characterized by the dichotomy of plutonites and metamorphic rocks exposed in the crystalline basement of the Bohemian Massif to the east and Mesozoic sedimentary rocks dominating the Northern Franconian Alp to the west. For a detailed description of both, the valley morphology as well as the geological setting of the region, the reader is referred to Kolb et al. (2017), with additional background information on the long lasting and controversial research history.

For luminescence dating, a total of 8 samples were collected at four different locations (Figure 5.1 & 5.2). Thereby, two sites assigned to the T3-terrace level and one location for the T4- and the T5-terrace level, respectively, were sampled. Details on the sampling locations are summarized in Table 5.1 and Figure 5.2. The sampling situation at various outcrops is furthermore illustrated by the photos of Figure 5.3.

The first T3-terrace site was an outcrop under forest in a former sand pit situated in the middle section of the valley. With a thin (only ~10 cm) layer of brown forest soil covering a layer of coarse-grained sand intercalated with fluvial gravels, the gravel bed itself showed a total thickness of 60-70 cm. Both samples (BT 1102 and BT 1103) were taken with considerable distance to the upper and lower boundary of the gravel bed in order to avoid contamination with either older or younger material.

Table 5.1: Basic information on sampling locations, sampling methods, dosimeters and applied measurement protocols.

Laboratory code	Field code	Sampling location		Elevation a.s.l. [m]	Depth [cm]	Sampling method[a]	Used dosimeter[b]	Measurement protocols[c]
		Latitude [°N]	Longitude [°E]					
T3-terrace samples								
BT 1102	PE_1 – 40	50.0239	11.5550	354	40	NT	Q & FS	SAR-OSL & $pIRIR_{225}$
BT 1103	PE_2 – 50	50.0239	11.5550	354	50	NT	Q & FS	SAR-OSL & $pIRIR_{225}$
BT 1107	Bind-Log_1	49.9666	11.6124	369	400	DL	Q & FS	SAR-OSL & $pIRIR_{225}$
BT 1108	Bind-Log_2	49.9666	11.6124	369	150	DL	Q & FS	SAR-OSL & $pIRIR_{225}$
T4-terrace samples								
BT 1335	Bin-HF_1	49.9642	11.6292	379	480	DL	FS	$pIRIR_{225}$
BT 1336	Bin-HF_2	49.9642	11.6292	379	410	DL	FS	$pIRIR_{225}$
T5-terrace samples								
BT 1125	PA-T5_2	50.0183	11.5783	363	70	NT	FS	$pIRIR_{225}$
BT 1126	PA-T5_3	50.0183	11.5783	363	110	NT	FS	$pIRIR_{225}$

[a] NT = night time sampling using opaque bags; DL = daylight sampling using light-tight cylinders.
[b] Q = quartz minerals; FS = potassium-rich feldspar separates.
[c] SAR-OSL = single aliquot regenerative dose protocol using blue-light stimulation; $pIRIR_{225}$ = modified elevated temperature post-IR-IRSL procedure.

The T3-terrace samples BT 1107 and BT 1108 originate from a construction site in the southern part of the Trebgast Valley close to the present day drainage divide. Here, the gravel bed showed a thickness of more than 5 m. The base of the terrace gravel was identified in a depth of approximately 5.7 m below the present-day surface. Both samples were taken from sand lenses embedded into the coarsely clastic gravels. While BT 1107 was situated near the base of the excavation pit, BT 1108 was close to the upper boundary of the gravel bed.

Nearby this location, samples BT 1335 and BT 1336 could be collected at a temporary outcrop of T4-terrace gravels. Although the base of the terrace was not yet reached, several meters (~4 m) of strongly compacted fluvial gravels were exposed, covered by periglacial hillslope sediments showing an average thickness of 1.5-2 m. The gravels were intercalated with several sand lenses which the luminescence samples were taken from.

For samples BT 1125 and BT 1126 we dug a several meters long and about 1.5-2 m deep trench on farmland situated on top of a Lower Triassic sandstone complex. The terrace sediments revealed a thickness of 1.3-1.5 m and were covered by a thin (~30-40 cm) soil layer, which was affected by bioturbation and intense human cultivation. The gravel bed itself was just weakly compacted and contained a large amount of coarse-grained sand. In order to minimize the risk of a contamination with younger material we decided not to take samples close to the upper boundary of the terrace. With a sampling depth of 110 cm, BT 1126 was situated slightly above the base of the gravel bed; BT 1125 was sampled in a depth of 70 cm below the surface and originates from the center of the terrace sediments.

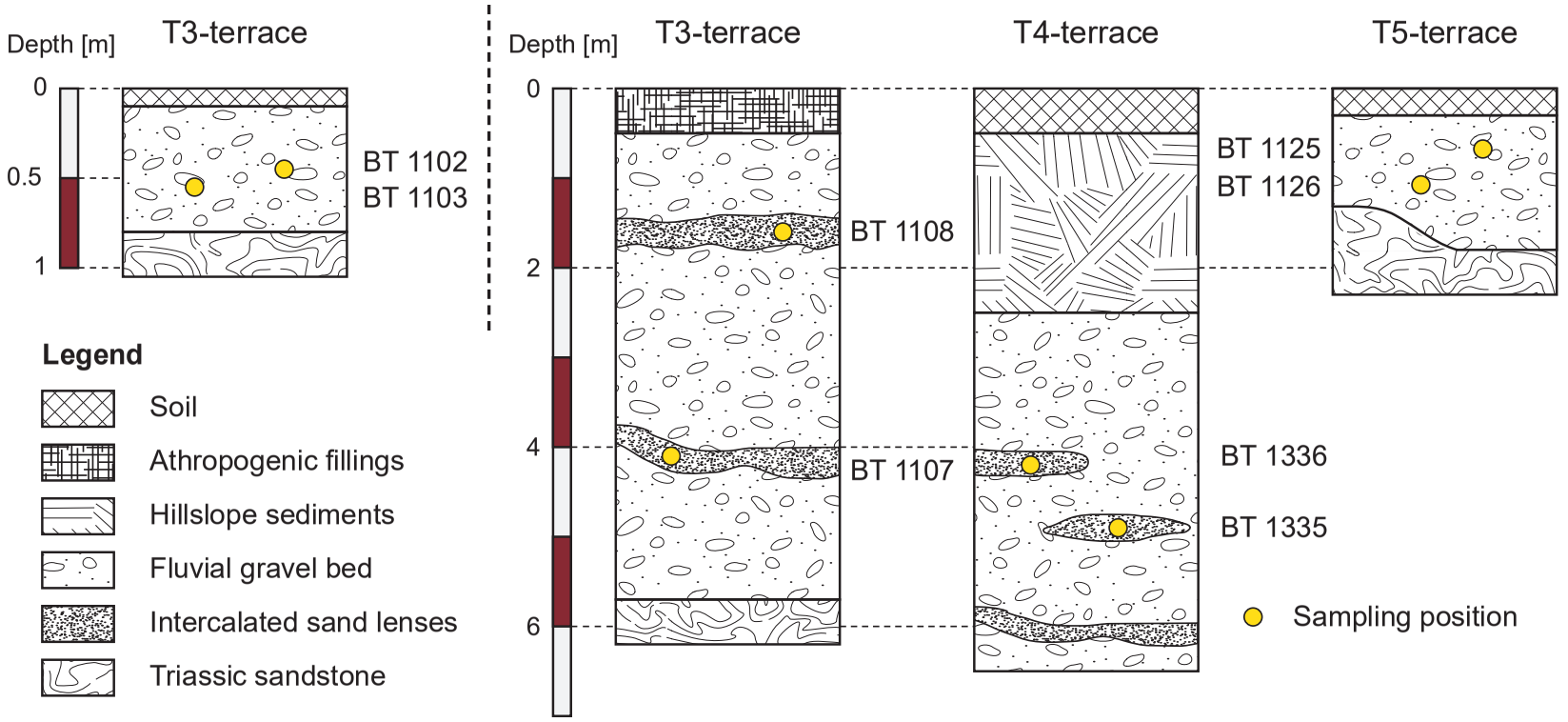

Figure 5.2: Stratigraphic logs of the sampling sites. The exact positions of the luminescence samples are indicated by yellow circles. Please note the different scale for the T3-terrace site on the left!

Figure 5.3: Photos of the sampling sites. (5.3a) Upper part of the T3-terrace outcrop in the southern part of the valley (BT 1107 & BT 1108); (5.3b) T4-terrace near Bindlach (BT 1335 & BT 1336); (5.3c) T5-terrace site (BT 1125 & BT 1126).

5.3 Methodology

5.3.1 Sample preparation and instrumental facilities

All samples were collected either under daylight conditions using light-tight cylinders from stainless steel or at night-time, storing the sampled material in light-tight black bags. Sample preparation was done under subdued red-light conditions (640 ± 20 nm) at the luminescence laboratory of the University of Bayreuth following standard procedures (e.g., Fuchs et al., 2010). After wet sieving to various grain size fractions, the coarse grain fraction (90-200 µm) was treated with 10% HCl and 10% H_2O_2 to remove carbonates and organic matter. In order to gain pure quartz and feldspar separates, the remaining material was subjected to density separation using sodium polytungstate solutions of various densities (2.70 g cm^{-3} and 2.62 g cm^{-3} to separate quartz from heavy minerals and feldspars and subsequently 2.58 g cm^{-3} and 2.53 g cm^{-3} to obtain the potassium-rich feldspar fraction). For the potassium-rich feldspar fraction the heavy liquid density separation was repeated at least three times in order to increase the purity of the separates. The quartz separates were etched in 40% HF for 50 min to remove the alpha-irradiated outer rim and finally washed in 10% HCl for 30 min. The purity of the resulting quartz samples was checked by IR stimulation, determining the IR depletion ratio (Duller, 2003) and by visual inspection of the TL curve shape, i.e. the 110°C TL peak (e.g., Mauz & Lang, 2004). With respect to the problems concerning the application of normal etching procedures for feldspar samples using 10% HF which have been reported by previous studies (e.g., Porat et al., 2015), we decided not to etch the feldspar extracts at all.

For measurement, grains were mounted on aluminium cups and fixed with silicon spray, using a 1 mm mask for the feldspar and a 2 mm mask for the quartz samples. This procedure restricted the number of grains to approximate 20-50 and 50-100 grains per cup, respectively. All luminescence measurements were carried out on automated Risø-Reader TL/OSL-DA-20 systems, equipped with built-in $^{90}Y/^{90}Sr$ β-source for artificial irradiation, providing dose rates of 0.119 ± 0.010 Gy s^{-1} and 0.033 ± 0.002 Gy s^{-1}, respectively. While the OSL stimulation for quartz samples was done by blue LEDs (470 ± 30 nm), infrared light LEDs (875 ± 80 nm) were used to stimulate the feldspar samples. The luminescence signals were detected by a Thorn-EMI 9235 photomultiplier equipped with filter combinations,

centering the detection windows to the dominant emission wavelength of quartz and K-feldspars, respectively. Therefore, the photomultiplier was combined with a 7.5 mm U-340 Hoya filter for the quartz samples (ultra-violet detection window: 290 - 370 nm) and with a 3 mm Chroma Technology D410/30x interference filter, restricting the detection window to the blue-violet wavelength band characteristic for K-feldspar samples.

5.3.2 Measurement protocols and setup for equivalent dose determination

OSL measurements for the quartz samples followed the single aliquot regenerative dose (SAR) protocol proposed by Murray & Wintle (2000), applying the same preheat temperatures to regenerative dose and test dose measurements. Shine-down curves were recorded at a temperature of 125°C for a total of 40 s. The signal used for growth curve construction was obtained from the first 0.6 s of the recorded OSL signal after a background was subtracted that had been derived from the last 7.5 seconds.

For the IRSL measurements of the K-feldspar samples a modified post-IR IRSL 225°C protocol was applied. In principle following the procedure proposed by Buylaert et al. (2009), we recorded both, the IR_{50} signal and the $pIRIR_{225}$ signal, for a prolonged time of 300 s after preheating the samples with a temperature of 250°C for 60 s. The measurement conditions were the same for regenerative dose and test dose steps. The signal used for equivalent dose determination was based upon the integration of the initial 5 s of the recorded $pIRIR_{225}$ signal after subtracting a background that had been averaged over the last 20 s of the respective shine-down curve. Details of the measurement protocols used for this study are summarized in Table 5.2.

Due to high equivalent doses and limited measurement time, $pIRIR_{225}$-measurements had to be restricted to 10 aliquots per feldspar sample (Table 5.5). Thus, no statistical age model (e.g., Galbraith et al., 1999; Galbraith, 2005) could be applied to the equivalent dose data derived from the post-IR IRSL approach. For the quartz separates, OSL measurements were performed on a minimum of 24 up to a maximum of 48 aliquots (Table 5.4). Although applying age models would have been possible, the equivalent dose distributions did not give

Table 5.2: OSL and post-IR IRSL measurement protocols (following Murray & Wintle (2000) and in principle Buylaert et al. (2009)). The $pIRIR_{225}$-protocol proposed by Buylaert et al. (2009) was slightly adjusted by using a prolonged readout time of 300 s for IR_{50}- as well as for IR_{225}-signals. A hot-bleach step was neither applied for the SAR nor for the $pIRIR_{225}$-protocol.

OSL-SAR			$pIRIR_{225}$		
Step	Treatment	Result	Step	Treatment	Result
1	Dose		1	Dose	
2	Preheat (hold for 10 s)[a]		2	Preheat (250°C for 60 s)	
3	OSL at 125°C for 40 s	L_x	3	IRSL at 50°C for 300 s	L_x-IR_{50}
4	Test Dose		4	IRSL at 225°C for 300 s	L_x-IR_{225}
5	Cutheat (no holding)[b]		5	Test Dose	
6	OSL at 125°C for 40 s	T_x	6	Preheat (250°C for 60 s)	
			7	IRSL at 50°C for 300 s	T_x-IR_{50}
			8	IRSL at 225°C for 300 s	T_x-IR_{225}

[a] Preheat temperatures were individually determined for each sample based on a combined preheat and dose recovery test using different preheat temperatures in the range of 180–260°C.
[b] Cutheat temperature equaled preheat temperature.

any evidence indicating a significant proportion of insufficiently bleached aliquots that would have required the consideration of such a statistical approach. Therefore, statistical age models were neither applied to the feldspar nor to the quartz samples.

All luminescence data were analyzed using an R-script based on the R-package `'Luminescence', version 0.7.4` (e.g., Kreutzer et al., 2012b, 2016), applying single exponential functions to the construction of the dose response curves. Thereby, all aliquots that were not able to pass the commonly applied rejection criteria for luminescence dating were excluded. Thus, only aliquots with a recycling ratio of 0.9-1.1, a recuperation of ≤ 5% of the natural sensitivity corrected signal intensity (e.g., Murray & Wintle, 2000) and a signal not lower than 3 times the background were accepted for equivalent dose calculation. Additionally, following the suggestion of Wintle & Murray (2006), all aliquots revealing natural signals higher than the so called '$2D_0$-value' were assessed to be unreliable and, thus, not considered for equivalent dose calculation. However, this criterion was only relevant for quartz samples and did not result in eliminating any aliquot measured

with the $pIRIR_{225}$ approach.

As test measurements for two quartz separates suggested that there might still be a significant feldspar contribution to the luminescence signals of these samples that even could not be removed by repeated HF-etching, we decided to use the IR depletion ratio proposed by Duller (2003) as an additional rejection criterion for the investigated quartz samples. Thus, the IR depletion ratio was calculated for each aliquot and used for discarding those aliquots still contaminated by feldspar remnants which we assumed to be indicated by the calculated IR depletion ratio deviating more than 20% from unity.

5.3.3 Fading measurements, dose recovery and bleaching experiments

As already mentioned above, the post-IR IRSL protocol for feldspar and polymineral samples originally was developed to overcome the problem of anomalous fading and to avoid the difficulties associated with the application of fading correction methods. However, several recent studies (e.g., Li et al., 2017a,b; Roskosch et al., 2015; Alappat et al., 2010) clearly indicated that post-IR IRSL measurements may most probably still be affected by fading even if its extent was reported to be strongly reduced. That is particularly true for the post-IR IRSL 225°C approach used in this study. Therefore, fading tests based on repeated L_x/T_x measurements applying various storage times between irradiation and $pIRIR_{225}$ readout were carried out to all feldspar samples in order to estimate the degree of fading. Measurement parameters were the same as for the equivalent dose measurements. Following the recommendation of Auclair et al. (2003), preheats were performed prior to storage. Thereby, three aliquots per sample that have not been used for D_e determination were bleached and irradiated with a dose close to the expected equivalent dose for the respective sample. To quantify the degree of anomalous fading, the g-value was calculated, corresponding to the percentage of signal loss per decade of time (e.g., Aitken, 1985). Thereby, the g-value was deduced from a regression line fitted through the L_x/T_x-values determined after different delay times which had been plotted against the respective times elapsed since irradiation depicted on a log scaled x-axis. All calculations were done using the R function `'analyse_FadingMeasurement' vers. 0.1.5`, provided by the R pack-

age `'Luminescence'` (e.g., Kreutzer et al., 2012b, 2016). As the status of this function was classified as 'BETA' at the time the fading measurements for this study were analysed, all results were cross-checked by individual calculation of g-values for all samples using an R-script independently developed for this purpose and based on Eq. [4] of Huntley & Lamothe (2001). Results which had been derived from the `'analyse_FadingMeasurement'`-function were confirmed.

A crucial point for the reliability of luminescence ages is the ability of the dosimeter to reproduce a given dose prior to heat treatment within a sufficient accuracy. To test the suitability of the quartz and feldspar separates used in this study, a set of dose recovery tests (DRT) was carried out to determine the dose recovery rate and – for the quartz samples – to estimate the optimal preheat temperatures. While the quartz samples were artificially bleached for 3 h using a solar lamp (Osram Duluxstar 24 W), the feldspar samples were exposed to natural daylight for 3 days to erase the luminescence signal. After checking the signal depletion, both, feldspar and quartz aliquots, were β-irradiated with known doses close to the equivalent doses expected for the respective sample. Thereafter, the equivalent dose was determined using the same measurement protocols and parameters applied to the dating measurements. Whereas, the feldspar DRT was restricted to the preheat temperature of 250°C requested by the $pIRIR_{225}$-protocol, the DRT for the quartz samples was performed as combined preheat and dose recovery test applying five different preheat temperatures in the range of 180°C – 260°C in steps of 20°C. For each preheat temperature the mean D_e of three aliquots was determined and the measured-to-given dose ratio was calculated. Based on this ratio, an optimal preheat temperature was chosen for which the given laboratory dose could be reproduced at its best.

Whereas the post-IR IRSL approach seems to be able to overcome or at least reduce the problem of anomalous fading, many studies reported a significant increase in residual signals for combinations of higher preheat and stimulation temperatures (e.g., Buylaert et al., 2011, 2012b; Stevens et al., 2011; Lowick et al., 2012). Although the reasons for this observed increase are still under debate (e.g., Li et al., 2014; Preusser et al., 2014), these residuals might cause a significant age overestimation if no correction was applied. In order to assess the magnitude of residual doses observed for the various samples used in this study, a series of bleaching experiments applying different types of bleaching mechanisms and times was conducted using natural samples. To test the efficiency of artificial

bleaching conditions normally used for quartz samples at the luminescence laboratory of the University of Bayreuth, we selected three feldspar samples and bleached them by using an Osram Duluxstar 24 W solar lamp for three hours. Additionally, a natural sunlight bleaching was applied to all investigated feldspar samples in this study. The samples were stored outside the laboratory within a box covered by a thin plate of acrylic glass to protect the samples from contamination and unwanted atmospheric exposure (e.g., loss of grains by wind). The discs were divided into two different batches, which were exposed to sunlight for a total of three and ten days, respectively. These bleaching experiments were performed by end of March 2017 during a period of stable and sunny weather conditions. After bleaching the samples, the remaining doses were determined using the same measurement setup as described for the dating measurements.

5.3.4 Dosimetry

For dose rate ($\dot{D}$) determination, the U- and Th-concentrations were detected by thick source α-counting, the external K-contents of the samples were measured by ICP-OES. With respect to the K-feldspar separates an internal potassium content of 12.5 ± 0.5% (e.g., Huntley & Baril, 1997) was included and an assumed a-value of 0.07 ± 0.02 (e.g., Preusser et al., 2014, 2016) was used for considering the alpha attenuation for the non-etched samples. Calculations for determining the environmental dose rate were done applying `DRAC v1.2` (Durcan et al., 2015) in combination with the conversion factors given by Guérin et al. (2011). Allowing for large uncertainties, interstitial water contents in a range of 8% to 10% were assumed to be representative for the burial period, individually derived for each sample from measurements of the present day water contents. Cosmic dose rates were calculated according to Prescott & Hutton (1994) using the `'calc_CosmicDoseRate'`-function provided by the R package `'Luminescence'` (e.g., Kreutzer et al., 2012b, 2016).

Table 5.3: Analytic dose rate data: Sample codes, depths below present-day surface, water contents, radionuclide-concentrations, cosmic and total dose rates for quartz and K-feldspar samples. Water contents were assessed by measuring the present-day water contents additionally considering sample specific stratigraphical information and sedimentological properties.

Laboratory code	Depth [cm]	Moisture [wt.%]	Uranium [ppm][a]	Thorium [ppm][a]	Potassium [wt.%][b]	$\dot{D}_{cosmic}$ [Gy/ka][c]	Total dose rate [Gy/ka][d]	
							Quartz	K-feldspar
T3-terrace samples								
BT 1102	40	8.0 ± 5.0	2.19 ± 0.25	7.04 ± 0.84	1.98 ± 0.20	0.23 ± 0.02	2.94 ± 0.19	3.62 ± 0.29
BT 1103	50	8.0 ± 5.0	1.52 ± 0.14	4.00 ± 0.45	1.80 ± 0.18	0.22 ± 0.02	2.44 ± 0.17	3.07 ± 0.27
BT 1107	400	8.0 ± 5.0	2.11 ± 0.21	5.37 ± 0.68	1.55 ± 0.15	0.14 ± 0.01	2.34 ± 0.15	3.00 ± 0.26
BT 1108	150	8.0 ± 5.0	2.41 ± 0.24	7.34 ± 0.81	2.46 ± 0.25	0.19 ± 0.02	3.41 ± 0.23	4.10 ± 0.32
T4-terrace samples								
BT 1335	480	10.0 ± 5.0	2.51 ± 0.17	6.40 ± 0.55	1.87 ± 0.19	0.13 ± 0.01	—	3.26 ± 0.28
BT 1336	410	10.0 ± 5.0	2.85 ± 0.23	12.12 ± 0.77	3.48 ± 0.35	0.14 ± 0.01	—	5.33 ± 0.38
T5-terrace samples								
BT 1125	70	8.0 ± 5.0	4.60 ± 0.30	12.32 ± 1.00	1.81 ± 0.18	0.21 ± 0.02	—	4.40 ± 0.30
BT 1126	110	8.0 ± 5.0	1.73 ± 0.24	6.44 ± 0.80	1.72 ± 0.17	0.20 ± 0.02	—	3.20 ± 0.27

[a] Determined by thick source α-counting.
[b] Determined by ICP-OES.
[c] Cosmic dose rates calculated according to Prescott & Hutton (1994).
[d] Environmental dose rates were calculated applying `DRAC v1.2` (Durcan et al., 2015) in combination with the conversion factors given by Guérin et al. (2011).
[e] An internal potassium content of 12.5 ± 0.5% (e.g., Huntley & Baril, 1997) and an assumed a-value of 0.07 ± 0.02 (e.g., Preusser et al., 2014) were considered.

5.4 Results and discussion

5.4.1 OSL and IRSL properties

All measured quartz samples show bright and fast decaying shine-down curves (Figure 5.4 – upper diagrams). The recuperation values are low for all samples and are depicted in Figure 5.5. Only 6 aliquots out of 191 had to be rejected due to exceeding the recuperation threshold of 5%. For most aliquots (> 94%) the recycling ratios are within the quality range of 0.9 to 1.1, indicating a good performance of the applied SAR protocol (Figure 5.5).

Figure 5.6 shows the results of the combined preheat and dose recovery tests performed for the quartz samples. Although at least one preheat temperature per sample could be determined for which the given dose could be recovered within acceptable accuracy, the dose recovery tests reveal problematic luminescence characteristics for the investigated quartz separates. Large inter-aliquot scatters could be observed for all samples and nearly for all preheat temperatures. Furthermore, a considerable number of aliquots is associated with large individual errors. These aliquots typically show dose response curves for which the given doses were close to saturation level and, therefore, could not be estimated precisely.

For the post-IR IRSL 225°C measurements very bright, but slowly decreasing shine-down curves could be derived showing patterns characteristic for feldspar samples (Figure 5.4 – lower diagrams). Both, the recycling ratios and recuperation values, were within the accepted limits suggesting an excellent performance of the post-IR IRSL 225°C protocol for all investigated aliquots (Figure 5.4 & 5.7). The given-to-measured-dose ratios for all feldspar samples derived from dose recovery tests are presented in Figure 5.7a. Although the given dose is always slightly (< 5%) underestimated, the dose recovery can be characterized as very good. While the individual dose recovery rates for the various aliquots lie within a range of 0.95 to 0.99, the average dose recovery rate was calculated as 0.97 ± 0.002 and is therefore very close to unity. The individual errors and the inter-aliquot scatters are rather low and for sample BT 1107 even almost negligible. All together, these results demonstrate the suitability of the used feldspar separates for luminescence dating as well as the overall good performance of the applied measurement protocol.

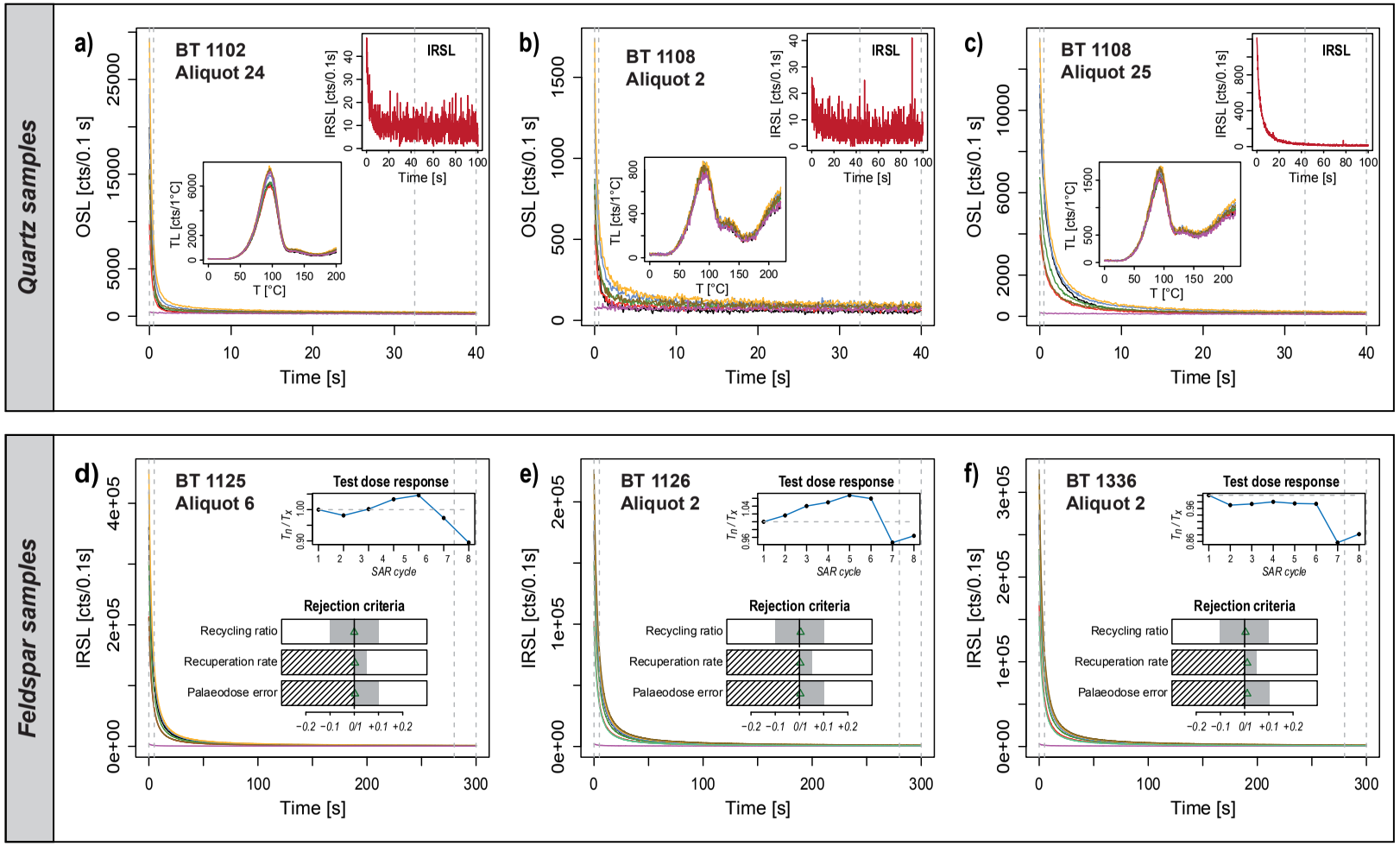

Figure 5.4: Luminescence shine-down curves for quartz (upper part) and feldspar samples ($pIRIR_{225}$-signal; lower part) with additional information characterizing the luminescence properties of the dosimeters. While all feldspar samples show excellent behaviour (Figure 5.4 d-f), the quartz samples are often found to be problematic. When analyzing the TL-curves derived from the preheat step of the test dose measurements, many aliquots revealed rather strange curve shapes not expected and quite exceptional for pure (Figure 5.4a) quartz separates. For some aliquots this can be attributed to feldspar contamination indicated by high IRSL signals (Figure 5.4c). For other aliquots, however, no relevant IRSL signal can be determined (Figure 5.4b).

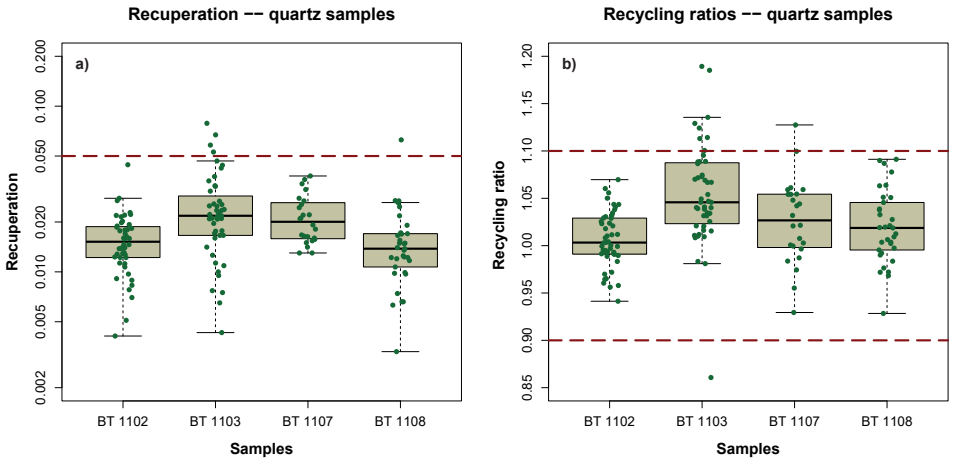

Figure 5.5: Recuperation (Figure 5.5a – note the logarithmic scale used for the y-axis) and recycling ratios (Figure 5.5b) for the investigated quartz samples. Recuperation was generally low and recycling ratios were close to unity for most aliquots.

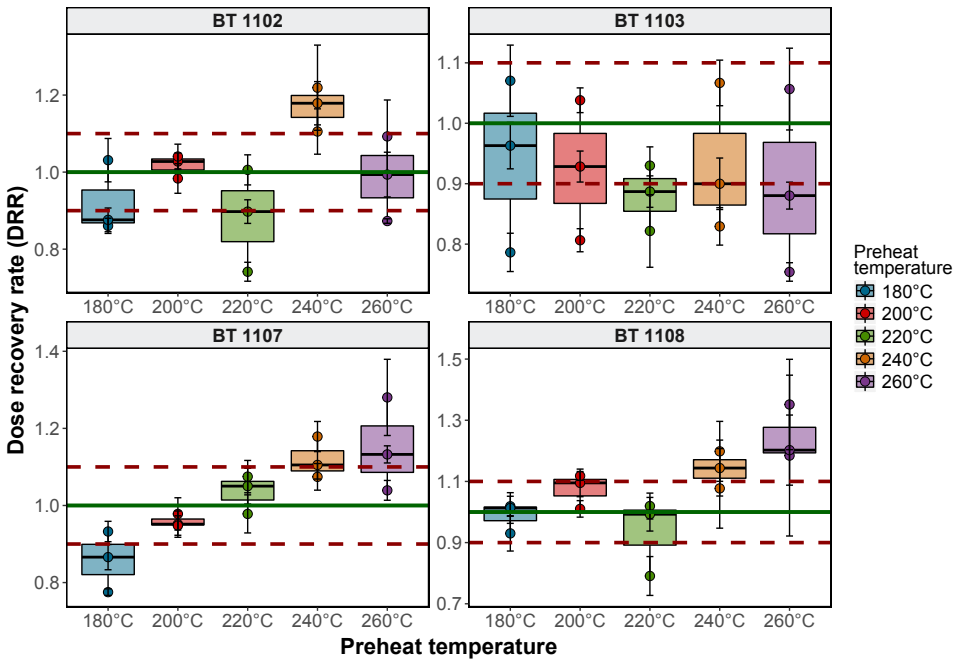

Figure 5.6: Results from combined preheat and dose recovery tests (DRT) for quartz samples. On the whole, the dose recovery is acceptable but not excellent. The large scatter observed for all samples and all preheat temperatures indicate that the samples might be close to saturation and calculated ages require a careful interpretation.

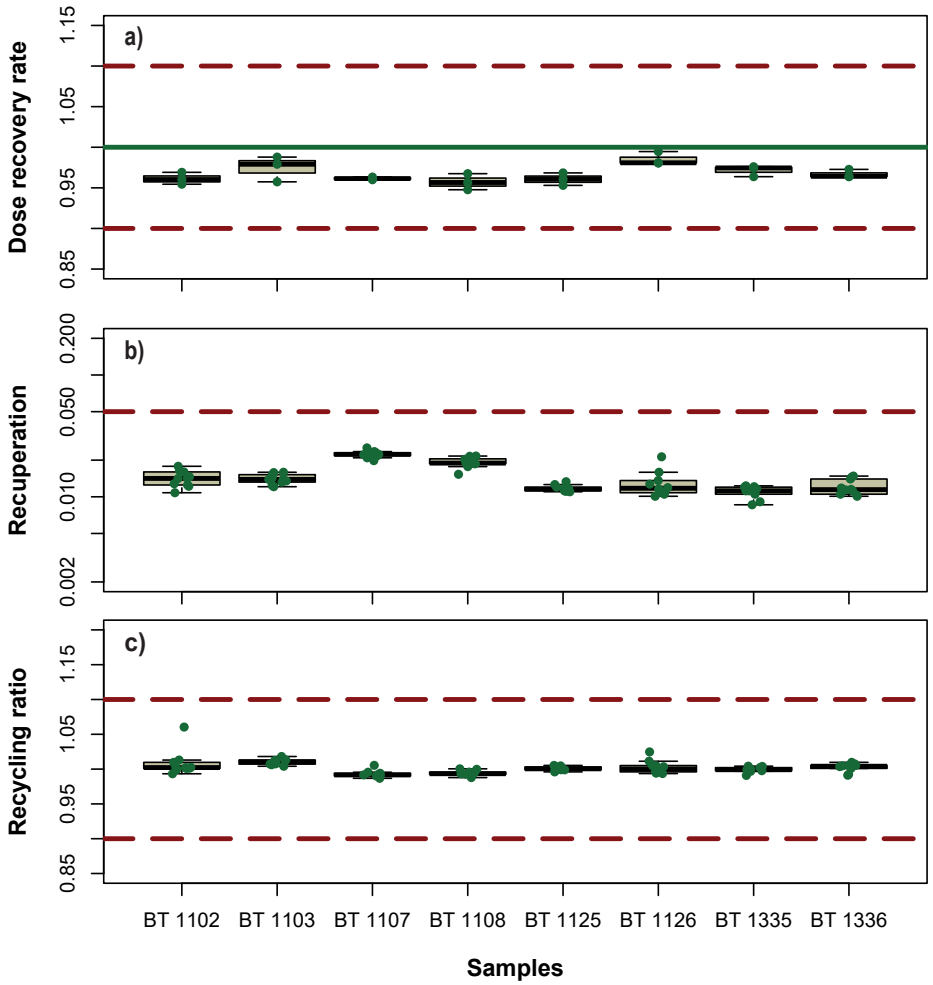

Figure 5.7: Dose recovery tests (DRT), recuperation and recycling ratios for the investigated feldspar samples. Critical threshold values are depicted by the dashed red lines. All samples are able to reproduce the given dose with satisfying accuracy (Figure 5.7a). Recuperation values (Figure 5.7b) are low (note the logarithmic scale of the y-axis) and recycling ratios are close to unity (Figure 5.7c). These findings point to excellent luminescence properties of the used feldspar dosimeters and indicate an overall good performance of the post-IR IRSL protocol.

5.4.2 Dose response curves and equivalent dose distributions

Figure 5.8 is showing abanico plots (Dietze et al., 2016) of equivalent dose distributions and representative dose response curves for a selection of two quartz (upper part) and two feldspar samples (lower part). The equivalent dose distributions gained for the quartz samples are generally characterized by wide kernel density estimate (KDE) plots accompanied by large relative standard deviations of 15% for sample BT 1107 up to maximum values of more than 24% for samples BT 1103 and BT 1108. The individual standard errors associated with the single aliquots show comparatively high values and large variations, represented by the relative positions of the data points plotted on the left side in the abanico plots. With the majority of data points showing relative standard errors in the range of 8-10%, there is a considerable number of aliquots plotting beyond 15% or even close to 20% (for BT 1108 – not shown in the figure). These large individual standard errors correspond to a low precision in equivalent dose estimation for the respective aliquots and again point to the rather problematic luminescence properties of the analyzed quartz separates.

The calculated mean equivalent doses for sample BT 1103 and BT 1107 are well beyond 200 Gy, for sample BT 1102 and BT 1108 even beyond 300 Gy. These equivalent doses are in a dose range that is regularly regarded to be close to the saturation level of typical quartz samples (e.g., Li et al., 2014; Buylaert et al., 2008; Thiel et al., 2011b). Hence, all quartz samples investigated in this study might most probably suffer from distinct saturation effects.

This finding is supported by the shape of many dose response curves. Applying a single saturating exponential function to data fitting often proved to be difficult and was frequently associated with large fitting errors. For quite a substantial number of aliquots the natural sensitivity corrected signal (L_n/T_n) was either in saturation or plotting in the uppermost part of the dose response curve close to saturation level. While for the former aliquots no equivalent doses could be determined at all, the latter yielded equivalent doses associated with large individual errors and often exceeding the $2D_0$-criterion described above. Therefore, quite a large number of aliquots had to be dismissed, i.e. for sample BT 1103 only 25 out of 47 and for sample BT 1108 only 8 out of 33 measured aliquots could be considered for equivalent

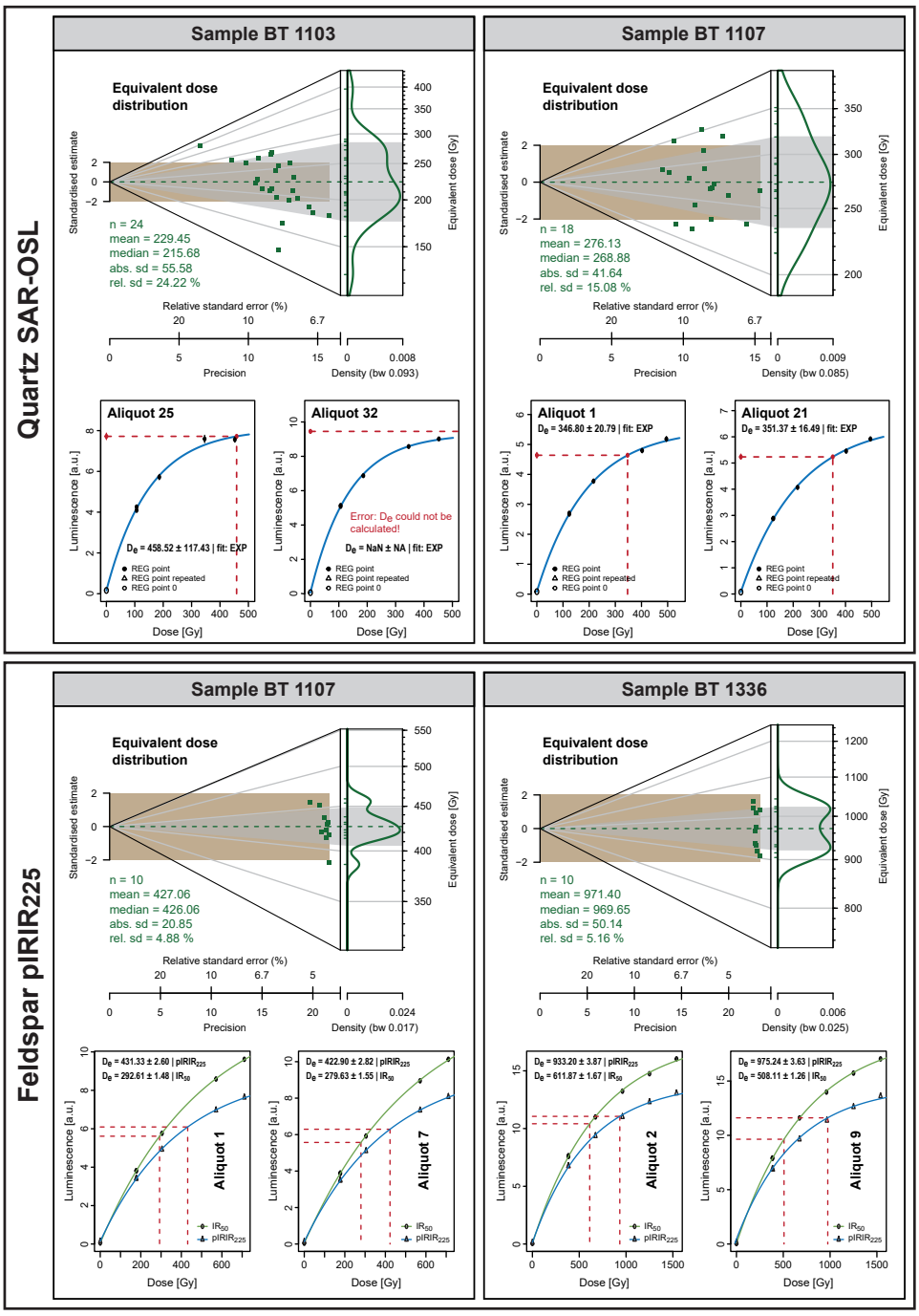

Figure 5.8: Abanico plots and representative dose response curves for two quartz (upper diagrams) and two feldspar (lower diagrams) samples.

dose determination (for details the reader is referred to Table 5.4). In summary, the ages calculated for the quartz samples in this study should be taken with care and can most likely only be interpreted as minimum ages!

The lower part of Figure 5.8 shows typical dose response curves and D_e distributions gained for the feldspar separates analyzed in this study. In contrast to the quartz samples, dose response curve construction using a single saturating function was possible for feldspar samples without any serious problems, indicated by low average fitting errors and always yielding equivalent doses in the exponential but still growing part of the dose response curves, far below the saturation level. The individual standard errors were low for all aliquots and the $2D_0$-criterion never proved to be problematic at all. Thus, nearly all measured aliquots could be used for equivalent dose calculation.

The overall good suitability of the investigated feldspar separates for luminescence dating is supported by the equivalent dose distribution depicted in the abanico plots (Figure 5.8). Apart from samples BT 1125 and BT 1126 containing some outliers, all feldspar separates are characterized by rather narrow distributions with relative standard deviations typically in the range of 4-6%. Maximum relative standard deviations of 13.5% and 9.5% could be determined for samples BT 1125 and BT 1126, respectively. Unfortunately, the KDE plots often show bi- and even multimodal patterns. If showing only one peak, they are at least slightly, but not systematically skewed. For some samples the distribution is shifted to higher equivalent doses, which is expected as typical feature of partially bleached samples, but for other samples the distribution is skewed to lower D_es. These findings make the age calculation, and in particular the subsequent interpretation, considerably more difficult.

5.4.3 Post-IR IRSL residual doses

A fundamental assumption of luminescence dating is that luminescence signals measured in the laboratory should also be completely bleachable under natural sunlight conditions. Otherwise the equivalent dose derived from luminescence measurements would contain an additional inherited signal and, thus, would not represent a reliable estimate of the true palaeodose accumulated in the dosimeter during the burial period under investigation. Incomplete resetting of the luminescence signal during transport might then result in serious age overestimations (e.g., Fuchs et al., 2007).

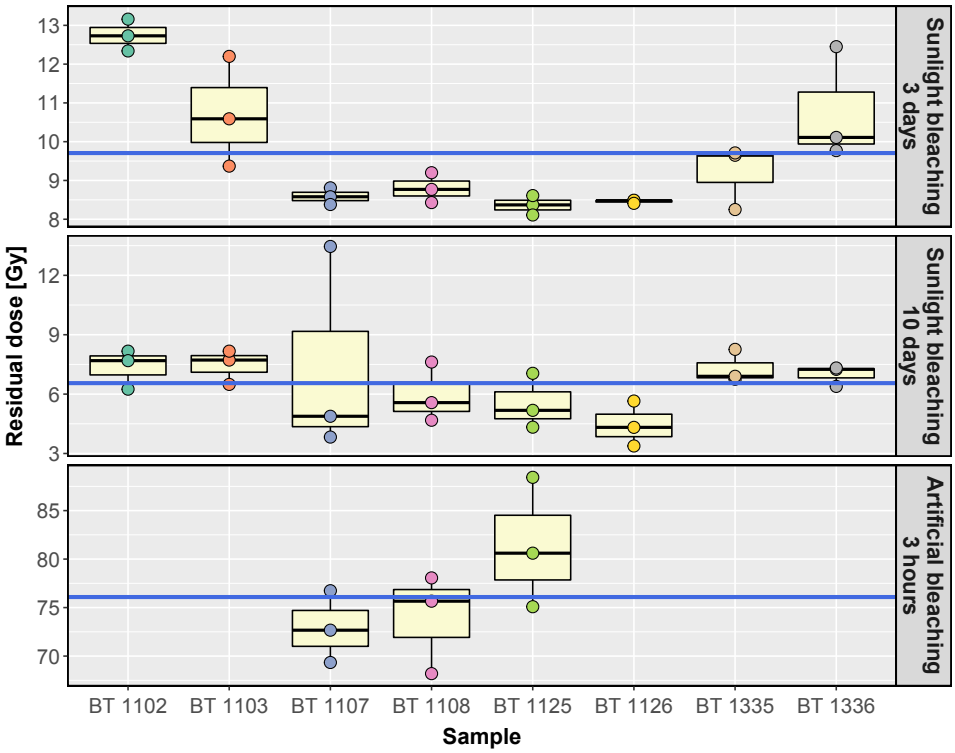

Figure 5.9: Residual doses determined for feldspar samples after a prolonged sunlight bleaching of 3 days, 10 days and after an artificial bleaching of 3 hours. The blue lines indicate the mean residual doses determined for the respective bleaching procedure.

While the harder-to-bleach nature of conventional IRSL-signals derived from feldspar separates have long been known (e.g., Godfrey-Smith et al., 1988; Fuchs et al., 2005) and identified as serious limitation of feldspar dating attempts compared to the fast bleaching OSL signals of quartz samples, a series of studies

was able to prove that post-IR IRSL signals measured at significantly higher stimulation temperatures also consists of components that are more resistant to sunlight bleaching and, thereby, even more difficult to bleach under natural conditions (e.g., Li & Li, 2011; Buylaert et al., 2012b). Moreover, based on the investigation of modern analogues, some studies suggest that there might be a residual dose that is not even erased after a prolonged exposure to sunlight (e.g., Buylaert et al., 2012b; Li et al., 2014). This residual dose is attributed either to a non-bleachable component of the post-IR IRSL signal or to thermal transfer of electrons due to the high preheat temperatures applied in post-IR IRSL protocols (e.g., Buylaert et al., 2012b; Li et al., 2014; Preusser et al., 2014). The magnitude reported for the residual dose by previous studies reach from only a few Gy (e.g., Thomsen et al., 2008; Gaar et al., 2013; Trauerstein et al., 2014) up to significantly higher doses that might seriously affect age calculation even for older samples (e.g., Lowick et al., 2012; Stevens et al., 2011). On the whole, the residual doses reported so far appear to be characterized by large inter-sample variations and may also reflect regional differences (e.g., Li et al., 2014; Preusser et al., 2014).

In order to check the bleachability of the $pIRIR_{225}$-signals, we performed a series of bleaching experiments. The results of these experiments are summarized in Figure 5.9. The samples had been divided into three batches. The lowermost part of Figure 5.9 shows the results for a selection of three samples which had been artificially bleached for 3 h using an Osram Duluxstar 24 W solar lamp. With all samples showing large inter-aliquot scatters, the residual doses determined for individual aliquots range from 68.2 ± 0.3 Gy (sample BT 1108) up to 88.4 ± 0.2 Gy (sample BT 1125). The mean residual dose was calculated as 76.1 ± 2.0 Gy, corresponding to almost 10% up to 18% of the respective equivalent doses. This high average value as well as the considerable dispersion of aliquot specific residual doses clearly indicates that a 3 h artificial bleaching procedure is not sufficient to reset the $pIRIR_{225}$-signal to a level low enough to be negligible for age calculation – at least for the samples analyzed in this study.

However, as already pointed out by previous studies (e.g., Preusser et al., 2014; Sohbati et al., 2012), artificial bleaching under laboratory conditions may not represent an adequate simulation of bleaching conditions in nature. Apart from the fact that natural sunlight differs rather significantly from the spectrum provided by artificial laboratory illumination, experimental settings do not take

into account the specific patterns of geomorphic processes, which are typically characterized by repeated reworking of material for a prolonged time. Especially for long-distance transport, such as fluvial transport processes, the resetting of luminescence signals is caused by the sum of repeated relocation and deposition cycles rather than by a single bleaching event. Thus, the decisive factor is less the duration of a single exposure to sunlight than the total time from the beginning of the transport process to the final deposition of material. As a result, resetting of the hard-to-bleach post-IR IRSL component can be assumed to be more effective in nature than under laboratory conditions.

The upper two diagrams of Figure 5.9 show residual doses determined after a prolonged sunlight bleaching of 3 days and 10 days, respectively. Although these experimental conditions still do not consider repeated relocation cycles, they represent a significantly better model of natural bleaching conditions. For both experimental settings and for all investigated samples, the residual doses are significantly lower than those of the artificial-bleaching experiment. An average residual dose of 9.7 ± 0.3 Gy could be determined for the 3-days-bleaching experiment and an even lower mean value of 6.6 ± 0.4 Gy for the sunlight exposure time of 10 days. Apart from a few exceptions (for 3 days: BT 1103, BT 1335 and BT 1336; for 10 days: BT 1107), the internal variances of residual doses are extremely low for the individual samples. The same applies to the sample-to-sample variation when comparing the mean residual doses determined for the individual samples. In contrast to some previous studies reporting that samples with higher D_e values tend to show higher residual doses (e.g., Buylaert et al., 2012b; Schatz et al., 2012; Sohbati et al., 2012), our data do not give any evidence indicating a correlation between D_e and residual dose.

For a bleaching time of 10 days, the calculated average residual doses correspond to percentages of only 0.7% to 1.5% of the respective equivalent doses (1.0% – 2.2% for a bleaching time of 3 days). These low portions indicate that the residual doses determined for the samples investigated in this study are negligible compared to the measured equivalent doses and, thus, are of little relevance to the age calculation. As the sources of residual doses are only poorly understood and as there is still an ongoing debate on which correction method might be the most appropriate (e.g., Buylaert et al., 2012b; Li et al., 2013, 2014), we decided not to correct for residual doses at all.

5.4.4 Fading rates and fading correction

The effect of anomalous fading of IRSL signals (e.g., Wintle, 1973) has long been identified to be a major issue of luminescence dating using feldspar minerals. If not corrected for, anomalous fading may result in a considerable underestimation of equivalent doses causing incorrect age determinations (e.g., Spooner, 1994a). During past years, various post-IR IRSL approaches have been proposed and tested in order to overcome these problems (e.g., Thomsen et al., 2008; Buylaert et al., 2009; Thiel et al., 2011a; Li & Li, 2011). Ever since, many studies have successfully been applying these approaches showing their potentials to reduce the degree of fading, indicated by significantly lower g-values (e.g., Rades et al. (2016) – g-values of 0.1 ± 0.2 to 1.2 ± 0.2 %$_{decade}$; Colarossi et al. (2015) – all g-values less than 1.5 %$_{decade}$; Trauerstein et al. (2014) – average g-values of 1.1 ± 0.9 to 2.5 ± 0.6 %$_{decade}$; Buylaert et al. (2012b) – average g-value of 1.44 ± 0.03 %$_{decade}$ for postIRIR−290-protocol; Sohbati et al. (2012) – average g-value of 0.94 ± 0.07 %$_{decade}$). Based on the finding that similar g-values could also be determined for quartz samples (e.g., Buylaert et al., 2012b) such low fading rates of approximately 1-1.5 %$_{decade}$ are often regarded as laboratory artifacts (e.g., Thiel et al., 2011a; Buylaert et al., 2012b; Roberts, 2012). As a consequence, luminescence signals derived from post-IR IRSL protocols are interpreted as not affected by anomalous fading and consequently the need for applying a fading correction procedure is questioned (e.g., Colarossi et al., 2015; Trauerstein et al., 2014; Thiel et al., 2011b).

The degrees of fading determined for the feldspar separates analyzed for the study in hand, however, show much higher values for all investigated samples. In order to assess the benefit of applying a post-IR IRSL protocol, post-IR IRSL fading rates are typically compared with those derived from conventional IRSL procedures at 50°C. Due to restricted measurement time we were not able to perform independent IR_{50}-measurements. Thus, g-values for the IR_{50}-signal were derived from the IRSL steps at 50°C performed as part of the $pIRIR_{225}$-measurements prior to the $pIRIR_{225}$-readout (e.g., Buylaert et al., 2012b; Lowick et al., 2012; Preusser et al., 2014). As these $IR_{50/225}$-signals are affected by the specific thermal treatment applied during the $pIRIR_{225}$-measurement, we have to consider that the calculated values may not represent the true g-values that would have been derived from stand-alone IR_{50}-procedures. However, they may at least serve as suit-

able approximation and give a sufficient evaluation of the post-IR IRSL performance.

The determined laboratory fading rates for both, the $IR_{50/225}$-signals and the $pIRIR_{225}$-signals, are summarized in Table 5.5. As the calculated g-value slightly depends on the time between irradiation and IRSL-readout (e.g., Huntley & Lamothe, 2001; Auclair et al., 2003), all g-values in this study were normalized to a delay time of t_c = 2 days to allow inter-sample comparisons.

Laboratory fading rates of the IR_{50}-signals range from 5.75 ± 0.07 %$_{decade}$ for sample BT 1102 to a maximum of 9.46 ± 0.09 %$_{decade}$ for sample BT 1108. For the $pIRIR_{225}$-protocol all calculated g-values are significantly lower, showing a minimum of 2.67 ± 0.17 %$_{decade}$ for sample BT 1335 and maximum values of 4.02 ± 0.12 %$_{decade}$ for sample BT 1108 and 4.05 ± 0.26 %$_{decade}$ for sample BT 1103. Whereas the inter-aliquot scatter is quite low for all investigated samples (indicated by low uncertainties for the mean g-values calculated by averaging the individual g-values of 3 aliquots of the same sample), the mean g-values of different samples are characterized by a large variety not showing any kind of systematic pattern (i.e., high as well as low g-values can be found for both, old and young samples). The fading rates of samples originating from the same outcrop show wide relative differences of up to almost 40% (BT 1102 compared to BT 1103 with both originating from the same T3-location). Overall, these results clearly indicate severe problems in making reliable g-value assessments and thus support the conclusion that measurement protocols are required which avoid the need for a fading correction procedure.

Comparing the g-values of the $IR_{50/225}$- and the $pIRIR_{225}$-signals, the $pIRIR_{225}$-approach at least seems to be able to reduce the impact of anomalous fading for the investigated samples, indicated by the fact that $pIRIR_{225}$ g-values are generally half of those calculated for the $IR_{50/225}$-signals. The laboratory $pIRIR_{225}$ fading rates determined for this study are, nonetheless, still far away from those g-values regarded as measurement artifacts in other studies. Therefore, the determined equivalent doses may most likely still suffer from a distinct loss of luminescence signal and carry the risk of serious age underestimations. Despite the general concerns about the suitability of fading correction procedures (e.g., Wallinga et al., 2007; Lowick et al., 2012; Preusser et al., 2014), we, therefore, decided to calculate fading corrected ages following the approach proposed by Huntley & Lamothe (2001), the dose rate correction (DRC) method of Lamothe et al. (2003) as well

as the procedure introduced by Kars et al. (2008). While the linear correction method of Huntley & Lamothe (2001) yielded comprehensible results for all samples investigated in our study (apart from BT 1102 and BT 1103), the latter two approaches either could not successfully be applied to our datasets at all or provided fading corrected ages that were far beyond the range of a meaningful interpretation of ages when considering the geomorphic and stratigraphic setting. The reasons for this failure in applying the Kars et al. (2008) and Lamothe et al. (2003) models are not clear so far and require further investigation. Thus, only the fading corrected ages following Huntley & Lamothe (2001) are presented in Table 5.5 along with the uncorrected $pIRIR_{225}$-ages.

5.4.5 Luminescence ages

Calculated ages with additional information are summarized in Table 5.5 (feldspar samples) and Table 5.4 (quartz samples). With no specific age model being applied (see section 5.3.2), all luminescence ages are derived from mean equivalent doses divided by the dose rate determined for the specific sample. The dose rate data is compiled in Table 5.3.

5.4.5.1 T3-terrace-level: deviating OSL- and $pIRIR_{225}$-ages

The T3-terrace level is the youngest fluvial terrace investigated in this study. A total of four luminescence samples were taken at two different sites. While samples BT 1102 and BT 1103 were collected from a natural outcrop in the middle section of the valley, samples BT 1107 and BT 1108 came from a construction site close to the present day drainage divide.

Previous regional studies (e.g., Zöller et al., 2012a,b) dealt with Pleistocene cover sediments overlaying the T3-terrace gravels. Findings from these studies and further unpublished data (pers. comm. Ludwig Zöller (2015) about high dose experiments on quartz separates from the study area) suggested the quite exceptional possibility that quartz minerals might be a suitable dosimeter even for fluvial deposits expected to be of pre-Eemian age. Therefore, we decided to apply both, quartz based OSL-dating as well as post-IR IRSL measurements of feldspar separates.

The quartz ages are summarized in Table 5.4. Within errors, all quartz samples reveal identical ages in a range of approximately 92 ka up to 118 ka, indicating a terrace formation at the transition between the Eemian (MIS 5e) interglacial period and the early Würmian (Weichselian). When comparing the ages for the different sampling locations, no significant discrepancies can be identified. As sample BT 1107 was taken at the base of the terrace gravel accumulation and BT 1108 at its top (see sampling depths in Table 5.1), the observed offset of approximately 26 ka between the mean ages of both samples is in good agreement with their specific sampling positions.

These relatively young ages, however, would be contradictory to well documented and repeatedly confirmed (e.g., Kleber & Stingl, 2000; Zöller et al., 2012a,b) findings based on morphostratigraphic investigations pointing to

the T3-terrace being of Rissian (i.e. MIS 6) origin (e.g., Kleber et al., 1988; Veit, 1991). Furthermore, they are in conflict with results of recently published studies (e.g., Kolb et al., 2016, 2017) which were able to constrain a timeframe for the formation of the youngest Würmian terrace (T2 level). Both studies identified stages of pronounced fluvial morphodynamics during the early Würmian phase as well as during the Lower and Middle Pleniglacial and concluded that the accumulation of the T2 terrace in the lowermost part of the valley started at approximately 90 ka. As T2- and T3-terrace levels are developed as clearly distinct geomorphic features divided from each other by a pronounced difference in elevation of more than 10 m, it is hardly conceivable that the beginning of T2-terrace accumulation and the end of T3-terrace forming should have taken place more or less at the same time.

Thus, we strongly doubt that the quartz OSL results give a reliable age estimation of the T3-terrace formation. On the contrary, the above described findings, indicating rather problematic luminescence properties of the quartz separates, suggest that the investigated quartz samples may most likely suffer from distinct saturation effects and that the presented OSL ages have to be interpreted as minimum ages.

Table 5.4: Results for OSL measurements applied on coarse grained quartz separates. Sample codes, number of aliquots, total dose rates, equivalent doses and OSL ages. The ratio of aliquots that could be used for equivalent dose determination to the total number of measured aliquots indicates the rather problematic luminescence properties of the investigated quartz samples.

Sample	n/N[a]	PHT[b]	$\dot{D}_{total}$ [Gy/ka][d]	Equivalent dose D_e [Gy]	Luminescence age [ka][c]
T3-terrace samples					
BT 1102	20/48	200°C	2.94 ± 0.19	307.34 ± 25.98	104.4 ± 11.2
BT 1103	24/47	220°C	2.44 ± 0.17	229.45 ± 20.98	94.1 ± 10.8
BT 1107	18/24	200°C	2.34 ± 0.15	276.13 ± 21.25	118.0 ± 11.9
BT 1108	8/33	220°C	3.41 ± 0.23	314.35 ± 41.40	92.1 ± 13.7

[a] n = number of aliquots passing the rejection criteria and used for equivalent dose determination; N = total number of measured aliquots.
[b] PHT = Preheat temperature. Using the measured-to-given dose ratio, individual preheat temperatures were derived for each sample from a combined preheat and dose recovery test.
[c] OSL ages were calculated using mean D_e values without applying any specific age model.

This interpretation is supported by the uncorrected as well as by the corrected $pIRIR_{225}$-ages depicted in Table 5.5. Both show significantly older ages compared to the quartz based measurements. For samples BT 1107 and BT 1108 the uncorrected $pIRIR_{225}$-ages are slightly higher than those derived from the respective quartz separates. With 106.6 ± 10.6 ka, BT 1108 also underestimates the expected pre-Eemian age by several ten thousand years, whereas the age derived for sample BT 1107 (142.3 ± 14.9 ka) suggests a terrace accumulation during MIS 6. Indicated by relatively large g-values, these uncorrected ages, however, may most likely suffer from anomalous fading. With 193.8 ± 21.7 ka (BT 1107) and 160.2 ± 16.4 ka (BT 1108), the corrected ages are in agreement with the morphostratigraphic findings and point to a T3-terrace accumulation during either MIS 6 or the late MIS 7.

When discussing about the accuracy of this estimation, one has to consider that the applied fading correction model of Huntley & Lamothe (2001) was originally developed for the low dose region. As such, the method is actually limited to relatively young samples with natural signals in the linear part of the dose response curve. Huntley & Lamothe (2001) themselves strongly advise against applying their model to samples older than approximately 20 - 50 ka. On the other hand, Buylaert et al. (2011) successfully used this correction method on samples of Eemian (MIS 5e) age and suggested that it might be able to apply the model to equivalent doses even in the non-linear part of the dose response curve up to 200 Gy. This conclusion is supported by findings for another Eemian site in Northern Russia (Buylaert et al., 2008) for which ages based on the model of Huntley & Lamothe (2001) are in excellent agreement with ages calculated with the DRC approach proposed by Lamothe et al. (2003).

For our samples, problems may arise from the fact that the equivalent doses are higher than 400 Gy and, thus, far beyond the upper limit of 200 Gy mentioned as probably unproblematic in the above cited studies. Therefore, the error introduced by applying the model of Huntley & Lamothe (2001) might most likely be larger for our samples than for those investigated by Buylaert et al. (2011), what on the other hand might partially be compensated by the fact that applying the $pIRIR_{225}$-protcol was able to reduce the g-values needed for the correction in our study (similar idea already mentioned by Sohbati et al. (2012); with references therein). However, this is just an assumption and cannot be verified at this moment. Therefore, we state that the fading correction applied in this study might

be insufficient and, as a result, our corrected ages may still underestimate the true ages. Referring to the encouraging results presented by Buylaert et al. (2008) and Buylaert et al. (2011) and additionally supported by the conformity with the morphostratigraphic findings in our study area, we strongly believe that the corrected ages for samples BT 1107 and BT 1108 can be assessed as reliable estimates that allow constraining a chronological framework for the T3-terrace accumulation.

Although challenging, the samples from the upper reaches of the valley at least yield ages in accordance with findings of previous studies and fit to the landforms identified in the study area. This does not apply to the $pIRIR_{225}$-results gained from the T3-terrace samples of the middle part of the valley. The corrected age of 428 ± 50 ka determined for sample BT 1103 is far beyond a realistic age range for a meaningful interpretation. The same is true for sample BT 1102, at least when considering the stratigraphical and geological settings. The age of 267 ± 27 ka would point to a terrace formation during MIS 8 and would, thus, agree with age estimations expected for the T4-terrace level. If the age of approximately 267 ka for sample BT 1102 was assumed to be correct, the only possible conclusion would be that the classification as T3-terrace location was wrong. Such a misinterpretation might be attributed to the rather small difference in elevation between the T3- and the T4-terrace level of not more than a few meters. If this rather unlikely explanation proved true, the sampling location would need to be re-classified as T4-terrace site. However, this conclusion is clearly disproved by the lithological composition of the respective terrace gravels. Kleber & Stingl (2000) showed that T5- and T4-terrrace gravel can be identified by iron agglutinated gravels indicative of the headwaters of the Red Main River. These so called limonite sandstone gravels are completely missing in samples collected for analyzing the petrographic composition of the controversial location (e.g., Kolb et al. (2017) and supported by field evidence). Thus, the location of samples BT 1102 and BT 1103 is clearly identified as T3-terrace site.

Another striking argument against the reliability of the determined ages for both samples is the large age difference when comparing the samples. With approximately 83 ka, this difference is already obvious for the uncorrected ages and even more pronounced for the corrected ages (161 ka). Considering the fact that BT 1102 and BT 1103 were collected more or less at the same position within the profile (see depths in Table 5.1 and Figure 5.2), this distinct offset cannot be explained only by

different accumulation times.

For the T3-terrace site in the middle section of the valley we, thus, have to summarize that our $pIRIR_{225}$-results are not reliable and that we are not able to draw any meaningful conclusions concerning the age of this landscape feature. The reasons for this failure are not clear so far and require further investigations. However, as the quartz samples do not show a similar overestimation, there might be a serious problem either with the applied $pIRIR_{225}$-protocol or with the used feldspar dosimeter.

5.4.5.2 T4- and T5-terrace – distinct terrace levels or simultaneous accumulation?

Determining the ages for the two oldest Pleistocene terrace levels is both, methodologically challenging and of special importance for the reconstruction of the palaeoenvironmental evolution in the study area. There are no independent age controls for these terrace levels and the morphostratigraphic findings are rather poor. Based on the number of palaeosols embedded into periglacial slope sediments superimposing terrace gravels, Veit (1991) was able to derive a rough chronological estimation for the different terrace levels (e.g., Kolb et al., 2016). Interpreting two fossil soils as indicators of two distinct interglacial stages, he concluded that the T4-terrace must have been accumulated during the '*third-last glacial period*'. Following a similar approach, Kleber & Stingl (2000) were able to derive their landscape evolution model (e.g., Kolb et al., 2016, 2017). Based on analyzing a complex sequence of cover sediments that had already been described by previous studies (Kleber et al., 1988), they suppose the T5-terrace to be of even older age and assigned it to the '*forth-last glacial period*'. However, neither Veit (1991) nor Kleber & Stingl (2000) make a clear statement about its possible age. Thus, we only can assume that '*third-last glacial period*', which is employed for the T4-accumulation stage, should correspond to MIS 8, while the term "*forth-last glacial period*" might be equivalent to MIS 10.

The corrected $pIRIR_{225}$-ages of 250.2 ± 24.2 ka (BT 1336) and 344.4 ± 36.9 ka (BT 1335) determined for the T4-terrace samples are in a range roughly corresponding to MIS 8 and MIS 10, respectively. With both showing rather large standard errors, a precise assignment of the terrace accumulation to either one or the other

marine isotope stage is hardly possible. The mean value for BT 1336 corresponds rather clearly to the glacial maximum of MIS 8 and even when including the errors, sample BT 1336 has most likely to be allocated within this stage. In contrast, sample BT 1335 could either be assigned to the transition period between MIS 9 and MIS 8, to MIS 9 or even to MIS 10, depending on whether the real age is considered to be near the mean value, the lower or the upper error margin. The mean values of both samples differ quite significantly by more than 90 ka. As BT 1335 was taken near the base level and BT 1336 from the middle part of the profile, they represent different phases of terrace accumulation. When looking at the exact sampling positions which only differ by approximately 70 cm, this can only partially explain the observed difference of 90 ka. Similar to the situation described above for the T3-terrace, there might again be a problem with either the feldspar dosimeter or the $pIRIR_{225}$-protocol.

Due to the limited precision of the determined ages, it is extremely difficult to give a final estimation distinctly constraining the T4-terrace formation to a specific marine isotope stage. At least sample BT 1336 points to a terrace accumulation during MIS 8 and is not clearly contradicted by the result obtained for BT 1335. Thus, we conclude that the T4-terrace level is most likely to be associated with MIS 8 or to a transition period between MIS 9 and MIS 8. In this respect, the numerical dating results from this study confirm the morphostratigraphic age estimations for the T4-terrace level made by previous studies.

With values of 262.9 ± 29.0 ka (BT 1125) and 292.8 ± 33.1 ka (BT 1126) the ages determined for the T5-terrace samples are identical within errors. The difference in the mean values may be explained by the fact that BT 1126 originates from the base of the outcrop, while BT 1125 was located slightly higher in the profile. Nevertheless, both samples show rather large errors. Due to these errors, we are once again faced with major difficulties in establishing a precise time frame for the T5-terrace accumulation. If the above made assumption was true that the term '*forth-last glacial period*' is synonymous to MIS 10, ages of approximately 340 ka to 380 ka would be expected. The corrected $pIRIR_{225}$-ages of BT 1125 and BT 1126 do clearly not match to this expected age range. On the contrary, within errors they perfectly agree with the corrected ages determined for the T4-terrace samples and indicate that the T5-terrace formation should have taken place rather during MIS 8 than MIS 10.

Table 5.5: Results for $pIRIR_{225}$-measurements applied on coarse grained K-feldspar samples. Laboratory fading rates are expressed as g-values normalized to 2 days. The g-values determined for the post-IR IRSL approach were found to be approximately half of those derived from the $IR_{50/225}$-signal. However, they were not low enough to treat them as laboratory artifacts.

Laboratory code	n/N[a]	$IR_{50/225}$-fading rate (g_{2days}) [%/decade]	$pIRIR_{225}$-fading rate (g_{2days}) [%/decade]	Total dose rate $\dot{D}$ [Gy/ka]	Equivalent dose D_e [Gy]	Uncorrected $pIRIR_{225}$-age [ka][b]	Corrected $pIRIR_{225}$-age [ka][c]
T3-terrace samples							
BT 1102	9/10	5.75 ± 0.07	2.90 ± 0.05	3.62 ± 0.29	734.84 ± 43.77	202.9 ± 20.3	267.2 ± 27.3
BT 1103	10/10	6.78 ± 0.07	4.09 ± 0.06	3.07 ± 0.27	876.41 ± 60.18	285.6 ± 32.0	427.7 ± 50.2
BT 1107	10/10	8.66 ± 0.12	3.12 ± 0.24	3.00 ± 0.26	427.06 ± 23.94	142.3 ± 14.9	193.8 ± 21.7
BT 1108	10/10	9.46 ± 0.09	4.02 ± 0.16	4.10 ± 0.32	437.29 ± 27.00	106.6 ± 10.6	160.2 ± 16.4
T4-terrace samples							
BT 1335	9/9	6.09 ± 0.03	2.67 ± 0.04	3.26 ± 0.28	864.20 ± 52.49	265.2 ± 27.6	344.4 ± 36.9
BT 1336	10/10	8.25 ± 0.13	3.25 ± 0.12	5.33 ± 0.38	971.40 ± 55.34	182.1 ± 16.7	250.2 ± 24.2
T5-terrace samples							
BT 1125	10/10	6.88 ± 0.09	3.68 ± 0.08	4.40 ± 0.30	797.67 ± 67.29	181.4 ± 19.7	262.9 ± 29.0
BT 1126	9/10	8.97 ± 0.05	2.89 ± 0.06	3.20 ± 0.27	705.74 ± 51.56	220.5 ± 24.8	292.8 ± 33.1

[a] n = number of aliquots passing the rejection criteria and used for equivalent dose determination; N = total number of measured aliquots.
[b] Uncorrected ages were calculated using mean D_e values without applying any age model.
[c] Corrected ages were derived by applying the fading correction procedure proposed by Huntley & Lamothe (2001).

The finding that ages derived from the T5-outcrop cannot be distinguished from those calculated for the T4-samples, suggests different plausible interpretations. First, it seems possible that the so far well established discrimination of the T4- and T5-terrace levels was simply wrong. In that case, different T4- and T5-sites would indeed represent the very same fluvial terrace which was most likely accumulated during MIS 8. This conclusion is supported by the fact that recent studies were not able to identify terrace sequences including both terrace levels at the same time (e.g., Kolb et al., 2017). Despite intensive field work, only sequences including T2-, T3- and T5-accumulations could be found in the lowermost section of the Trebgast valley, while no location could clearly be classified as T4-terrace site. In the upper reaches, the situation seems to be entirely different: with the T5-terrace completely missing, there are several locations only exposing well preserved sequences of T2- up to T4-terrace gravels. Computer based analyses of data gained from a high-resolution digital terrain model (DTM) proved that locations within the Trebgast valley marked as T5- and T4-sites are often only distinguished from each other by slight differences in elevation, typically not exceeding more than a few meters. With respect to the considerable difficulties in following a specific terrace-level over long distances, a misinterpretation of terrace levels at least seems possible. This conclusion, however, is in contrast to findings from the headwaters of the nearby Red Main valley where T4- and T5-terrace levels can both be identified, separated by a pronounced difference in elevation of more than 10 m (e.g., Kleber et al. (1988); Kleber & Stingl (2000); confirmed by results from an unpublished BSc-thesis by Friedl (2014)).

Alternatively, T4- and T5-terrace levels can still be classified as separate terraces of nearly the same age. In principal assigned to the same glacial period (MIS 8), they may represent different accumulation stages during this glacial period that were interjected by a relatively short period of fluvial incision. This interpretation would be in accordance with the stratigraphic findings from the adjacent Red Main valley and would also match to the numerical dating results presented in this study. The large standard errors and the corresponding low precision of the determined sedimentation ages, however, make it impossible to distinguish the individual phases.

Furthermore, the apparent synchronicity in T4- and T5-accumulation might also be attributed to undetected sedimentological problems. The T4-terrace samples were taken from a very compact body of coarse-grained fluvial gravels showing

an average thickness of several meters and covered with approximately 1.5 meters of periglacial hillslope sediments. The T5-terrace site, on the other hand, was characterized by rather loosely deposited gravel sediments located directly underneath the present-day surface. The upper boundary of the fluvial gravels was just covered by a 30-40 cm thick sandy soil. While a significant contamination with younger material due to bioturbation or soil forming processes can be excluded for the T4-terrace site, such a contamination appears to be possible for the T5-terrace gravels. The calculated age would then seriously underestimate the true sedimentation age of the T5-terrace. When using so called small aliquots, such a contamination might be identified by strongly skewed equivalent dose distributions, which have not been determined for the T5-samples under debate. However, Trauerstein et al. (2014) were able to demonstrate that there is an averaging effect when using small aliquots of potassium-rich feldspars. This averaging effect masks the effects of partial bleaching and, thus, makes the identification of a contamination with younger material considerably more difficult if not even impossible. As we can neither deny nor confirm a considerable contamination of the T5-samples, we cannot exclude the possibility of a significant age underestimation. If we assumed such a contamination, the analyzed T5-terrace would be much older than calculated and might even be assigned to MIS 10. However, this is only one possible scenario and so far not supported by any additional evidence. To test this hypothesis, more suitable T5-exposures need to be investigated.

Finally, the unexpected result that T4- and T5-terrace seem to be of the same age might also be explained by unknown methodological problems. Although post-IR IRSL approaches have successfully been applied by numerous studies, it has to be pointed out that significant problems remain unanswered. Far away from being a standard tool for sediment dating, the pIRIR-protocol is still not fully understood and its basic principles are still under debate (e.g., Li et al., 2014). The same is true for the phenomenon of anomalous fading in general and for the various correction methods. Li et al. (2014) summarize that the majority of studies that were successfully applying pIRIR-approaches dealt with relatively young samples between 20 and 100 ka. For older samples associated with higher equivalent doses, post-IR IRSL measurements seem to be less successful. In our study, problems may arise from the fact that all investigated T4- and T5- samples showed equivalent doses of more than 700 Gy and even up to nearly 1000 Gy. While these high equivalent

doses might be the reason for so far unknown problems arising from applying the $pIRIR_{225}$-protocol, they will in any case affect the performance of the applied fading correction method and may most probably introduce large and hard to assess errors.

Regarding the oldest Pleistocene terrace levels, our results indicate a simultaneous accumulation of T4- and T5-terrace during MIS 8. This result partially confirms and partially contradicts morphostratigraphic findings from older studies. However, due to possible methodological problems and with respect to the large uncertainties determined for our ages, the results presented in this study need to be taken with caution. Therefore, this study represents a further step towards the establishment of a chronological framework for the landscape evolution in our study area, but a final age constraint for the older terraces is so far not possible.

5.5 Conclusion

This study applied quartz based OSL dating and $pIRIR_{225}$-measurements performed for potassium-rich feldspar separates to a total of 8 samples, originating from various fluvial terraces expected to be of pre-Eemian (MIS 5e) age. All quartz samples were in or close to saturation and thus yielded no reliable age estimations.

By applying the $pIRIR_{225}$-protocol we were able to considerably reduce the laboratory fading rates determined for the investigated feldspar samples. However, anomalous fading expressed in terms of g-values still remained significant. Thus, fading correction methods had to be applied. Due to so far unknown reasons only the model proposed by Huntley & Lamothe (2001) could successfully be used, whereas the DRC correction after Lamothe et al. (2003) as well as the correction approach of Kars et al. (2008) failed.

The corrected $pIRIR_{225}$-ages partially agree with morphostratigraphic findings of previous studies. They indicate two distinct periods of terrace formation, identifying the T3-terrace level as landscape feature accumulated during MIS 6 and roughly assigning the two oldest fluvial terraces (T4 and T5) to either MIS 8 or to a transition period from MIS 9 to MIS 8. With respect to the T5-terrace level, we were not able to confirm conclusions of previous studies classifying the terrace gravels as fluvial deposits of even older age corresponding to MIS 10. However, the relatively large uncertainties associated with the calculated ages in this study make

the interpretation of results considerably more difficult. Thus, alternative interpretations might be possible. A precise chronological framework, finally constraining the different stages identified for the complex landscape evolution in our study area, requires further investigations including new sampling sites in the Trebgast valley itself as well as within the adjacent Red Main valley.

From a methodological point of view, promising findings of other studies that elevated temperature post-IR IRSL protocols can reduce anomalous fading to a negligible level for which no fading correction is needed any more, cannot be confirmed for the samples analyzed in this study. On the contrary, inconsistencies in the determined ages indicate that the $pIRIR_{225}$-approach used in our study might be limited by either serious methodological problems or problematic luminescence properties of the used feldspar dosimeters. Our results, therefore, point to the necessity of new measurement procedures circumventing the problems associated with anomalous fading and its various correction methods. New technical developments and recent methodological findings with regard to infrared radiofluorescence (IR-RF) of K-feldspar (e.g., Frouin et al., 2017) point to the encouraging possibility that such an approach might be available in the near future.

Acknowledgements

This study was generously funded by the 'Oberfrankenstiftung'. The Bavarian Department of Environment (Bayerisches Landesamt für Umwelt) is thanked for supporting our research by providing a high resolution digital terrain model and other maps and data. We also would like to thank the anonymous reviewers for their helpful comments that significantly improved the quality of our manuscript.

Part III

Synthesis and outlook

6

Synthesis

The studies of Part II summarize the results of scientific investigations performed in an area that has been the subject of geoscientific research for over a century. Despite this long lasting research history, the knowledge about the timing of distinct evolutionary stages and about the dynamics of the regional fluvial system was still insufficient and limited. With respect to chronological problems, the whole region of Upper Franconia and, in particular, the area in the vicinity of the city of Bayreuth are characterized by a remarkable lack of studies applying numerical dating techniques.

Referring to previous studies, our research project aimed at filling this gap and at providing information on the age of fluvial landscape features and on the dynamics of the fluvial evolution in a region dominated by the two headwater streams of the Main drainage system. Over all, the project intended to shed light on the Pleistocene landscape evolution as well as on the increasing human impact on the Holocene development. As an essential part of the research project, the major goal of the presented PhD-thesis was to apply well established and innovative techniques of luminescence dating to challenging environmental archives in order to derive a regional chronological framework for the distinct evolutionary stages of terrace accumulation described for the local drainage system by previous studies (e.g., Kleber & Stingl, 2000; Zöller et al., 2007). Thereby, the individual

studies focus on specific problems, which are reflecting the history and the particular workflow of our research project.

Study 1 (page 79 – 108) represents the starting point of the project. It is focussing on the youngest Pleistocene fluvial terrace accumulated by the primary Steinach River during the Wuermian (Weichselian) period (T2 terrace level). At this point of the project, only a few locations were available from which we could get adequate sample material directly originating from the terrace gravels. Thus, we tried to derive indirect age information on the accumulation of the T2-terrace gravels by dating hillslope sediments superimposing the T2-gravels. With luminescence ages of ~20 ka to ~30 ka for the hillslope sediments, our results pointed to a T2-terrace accumulation period which was much older than expected. As a consequence, our dating results were apparently contradicting the findings of previous studies (e.g., Kleber et al., 1988; Kleber & Stingl, 2000; Zöller et al., 2007), which were attributing the T2-terrace formation to the last glacial maximum (LGM) at ~20 ka.

The correctness of our luminescence ages, however, was confirmed by independent age controls based on radiocarbon dating of whorl fragments of shells from *Pupilla genus*. These shells were sampled from a mollusk assemblage detected in a loess-bearing slope detritus in the middle section of the Trebgast Valley. The malacological analysis of this unique community of fossil terrestrial mollusks, which showed a surprising variety of species, so far not reported for the region of northern Bavaria, revealed additional information on the palaeoenvironmental conditions in the research area.

In this early stage of our project we were strongly concentrating on finding and characterising new exposures, providing suitable material for luminescence dating. Thereby, we were able to investigate the composition of gravels for the various terrace levels by applying qualitative petrographic analyses. These analyses confirmed findings of previous studies (e.g., Kleber et al., 1988; Kleber & Stingl, 2000) and furthermore refined our knowledge about the characteristic petrographic compositions of the various gravel beds, which can be used to distinguish different evolutionary stages.

This is particularly true for the distinct differences between the composition of gravels found in the main valley to those gravels analysed in the Lindau Basin. We were able to show that the basin gravels revealed completely different grain

size distributions and were characterized by a complete lack of metamorphic gravels, which would have been indicative of the Steinach River's catchment area (e.g., Brindel, 2012; Urban, 2013). These new findings allowed us to overcome the apparent discrepancies between our dating results and age estimations made by previous studies (e.g., Zöller et al., 2007). Although the Lindau Basin was correctly identified as key site for the reconstruction of the late Pleistocence and early Holocene evolution of the valley (e.g., Zöller et al., 2007), it has obviously been misinterpreted for several decades (e.g., Steinlein, 1938; Gräbner, 1963, 1985; Kleber & Stingl, 2000). We were able to show that the assumption of the Lindau Basin having been eroded by a meander of the primary Steinach River, which is suggested by the terrace levels observed in the basin (e.g., Kleber & Stingl, 2000), is wrong or at least implausible[1].

If this assumption is wrong and the basin has been eroded by a small tributary river originating within the basin itself, the development of the Lindau Basin is completely decoupled from the final deflection of the Steinach River. Based on this finding, it was possible to overcome the apparent contradiction between our dating results and previous age assessments. As a consequence, we were able to draw the essential conclusion that a significantly higher age for the final deflection of the primary Steinach River could be possible.

In some respect, this conclusion represents the starting point for further investigations summarized in Study 2 (see page 109 - 132). Like Study 1, this study also focused on the youngest Pleistocene Steinach terrace identified within the Trebgast Valley. Luminescence dating was, however, applied on samples directly originating from either natural exposures or temporal outcrops of the T2-terrace gravels. The sampling sites were thereby allocated in all sections of the valley. Therefore, we were able to derive age information for a set of various locations throughout the river's longitudinal course.

From a regional point of view, the essential outcome of our investigations is summarized by the finding that we were not able to identify any T2-terrace material within the main Trebgast Valley that was younger than ~30 ka. Only samples close to the present day watershed in the southernmost part of the valley revealed ages of ~20 ka in minimum. Therefore, we concluded that the primary Steinach River

[1] I would like to point out that even Steinlein (1938) already mentioned that he was not able to detect any gravels within the Lindau Basin that could beyond doubt be attributed to the Steinach River.

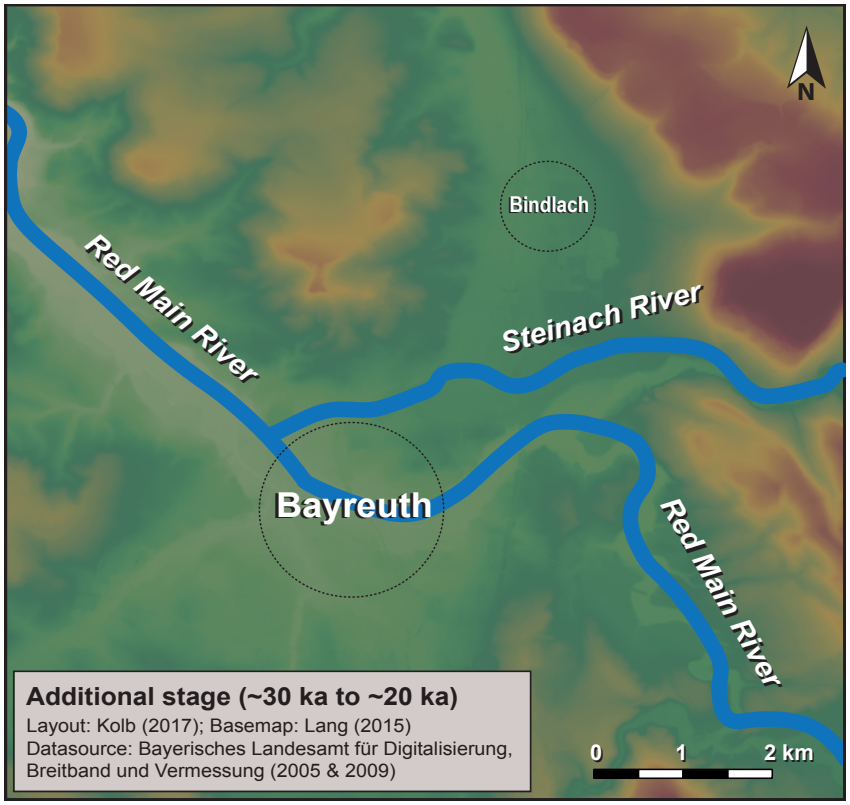

Figure 6.1: Additional evolutionary stage for the local drainage system proposed by Kolb et al. (2016). This intermediate stadium comprised the period from ~30 ka to ~20 ka. Although the primary Steinach River had already abandoned the main part of the Trebgast Valley, it was not yet deflected to its present day course, but used the southernmost part of the Trebgast Valley close to the present-day watershed. This additional stage is suggested by a vast alluvial fan deposited by the Steinach River. Only for these fluvial sediments, which are reaching far to the west, luminescence ages of ~20 ka could be determined.

had abandoned the Trebgast Valley at some time shortly after 30 ka and thus much earlier than assumed by previous studies (e.g., Kleber & Stingl, 2000; Zöller et al., 2007).

Furthermore, the distinctly younger ages for the samples originating from the watershed locations suggested that the primary Steinach River was not immediately deflected to its present day course after it had left the Trebgast Valley, but that there has been an intermediate evolutionary stage. As a result of our findings, we modified the regional landscape model originally proposed by Kleber & Stingl (2000) by introducing an additional evolutionary stage for the period of ~30 ka to ~20 ka. During this relatively short period of time, the primary Steinach River had already abandoned the main part of the Trebgast Valley, but still used the southernmost part close to the present day watershed, flowing into the Red Main River with its mouth at an unknown location further to the west. This configuration of the fluvial alignment prevailed until the final deflection of the Steinach River to its present-day course, which did not take place earlier than ~20-18 ka.

Beyond results of a mere regional interest, Study 2 also revealed findings that bear the potential to be of general significance for fluvial geomorphology and for age estimations of sediments in fluvial systems. Since we took samples from various locations throughout the river longitudinal course, we were able to derive ages for a set of samples that have been found to origin from the very same morphological unit. Surprisingly, luminescence ages of T2-terrace material from the lowermost part of the valley are significantly older than those from the middle section, which in turn are older than those from the upper reaches. Our results suggest a diachronic alignment of sedimentation ages for fluvial deposits, starting with old ages close the mouth of a river and getting progressively younger for locations approaching the upper reaches. In Study 2, these results were attributed to the mechanism of either backward erosion or backward accumulation. If these findings proved true and were not only the result of very specific local conditions, they would indicate the particular importance of careful interpretations of ages derived for fluvial deposits. Then, they might generally be interpreted as evidence for a diachronic rather than a synchronic response of river systems to external or internal forcing, triggering erosion or accumulation processes.

Finally, Study 3 (page 133 – 176) deals with the older terrace levels (T3-, T4- and T5-terrace levels) identified in the study area. As these terrace levels were supposed

to be of pre-Eemian age, innovative techniques of luminescence dating had to be applied. Thereby, we were able to derive a reliable, but still preliminary chronological framework for these older evolutionary stages. However, our analyses also revealed potentially serious methodological problems and indicate that further investigations are required.

From a regional point of view, the age estimations of previous studies (e.g., Kleber et al., 1988; Veit, 1991; Kleber & Stingl, 2000), which were based on morphostratigraphic and lithological evidence, could partially be confirmed. For the older terraces, our dating results clearly indicate two distinct periods of terrace formation. While the T3-terrace could be classified as landscape feature accumulated during MIS 6, a clear attribution of the T4- and T5-terrace to particular marine isotope stages proved to be challenging. Due to the limited precisions of our post-IR IRSL ages[2], they could only be roughly assigned to either MIS 8 or to a transition period from MIS 9 to MIS 8.

Furthermore, it was not beyond doubt possible to confirm that the T4- and the T5-terrace represent two distinct terrace levels, which was assumed by previous studies (e.g., Kleber & Stingl, 2000; Zöller et al., 2007). Although our results, at first glance, indicate a simultaneous accumulation of T4- and T5-terrace during a period comprising MIS 8 and MIS 9, alternative interpretations might be possible and were discussed in Study 3 (see page 173). In general, this PhD-thesis provides an important refinement of knowledge about the timing and the dynamics of the drainage system in the vicinity of the city of Bayreuth, which is summarized in Figure 6.2. With particular respect to the older evolutionary stages however, the local chronological framework established for the Trebgast Valley must still be considered as preliminary.

From a more general point of view, the study is an excellent example for the importance of applying multi-methodological research approaches, especially when working in challenging environmental settings. Only the interplay of modern dating techniques and well-established sedimentological and lithological methods en-

[2] At this point, I would like to emphasize that the relative standard deviations of the calculated pIRIR-ages were in the range of ~10% to ~11%. In general, such variances are not unusual for luminescence dating and with regard to fluvial sediments they might even be interpreted as evidence for a rather good or at least normal precision. However, these relative standard deviations correspond with absolute errors which make it impossible to clearly assign the samples to a distinct marine isotope stage.

hanced by analyses of high-resolution digital terrain models (DTM) made a meaningful interpretation of results possible.

Since the accumulation of the older terrace levels was expected to reveal ages far beyond the upper dating range of standard quartz based OSL methods, we had to shift our attention to modern post-IR IRSL techniques, which are, in principle, providing the opportunity of considerably extending the dating range of luminescence procedures. These innovative measurement protocols, however, are still associated with a substantial number of unanswered theoretical and practical problems. From a methodological point of view, our results revealed some of these problems, which were discussed in Study 3.

With particular respect to the problem of anomalous fading, we have to concede that the post-IR IRSL approach at 225°C, which was used in this study, was only partially successful in reducing the degree of fading for our samples. However, laboratory fading rates were still far away from those values typically regarded as negligible. Therefore, fading correction algorithms had to be applied, which introduced additional uncertainties to our age estimations. Although post-IR IRSL protocols are regularly regarded as not to be affected by anomalous fading at all, this overall promising assumption might not be true for all environmental settings.

In that case, g-value determination will remain important in order to assess the degree of fading and to apply correction procedures, even when using post-IR IRSL approaches. As a result, our findings emphasize the great need for new measurement procedures which are able to circumvent the problems associated with anomalous fading and its various correction methods completely.

With respect to the major research questions formulated in Chapter 1 on page 10, our results can be summarized as follows:

1. Findings of previous studies could only partially be confirmed. Our results point to a much more complex character of the local fluvial history, which was not considered in previous studies.

2. In principle, it seems possible to successfully apply innovative techniques of post-IR IRSL procedures to the older terrace sediments of the research area. However, this PhD-thesis also revealed serious methodological problems that make the interpretation of ages significantly more difficult.

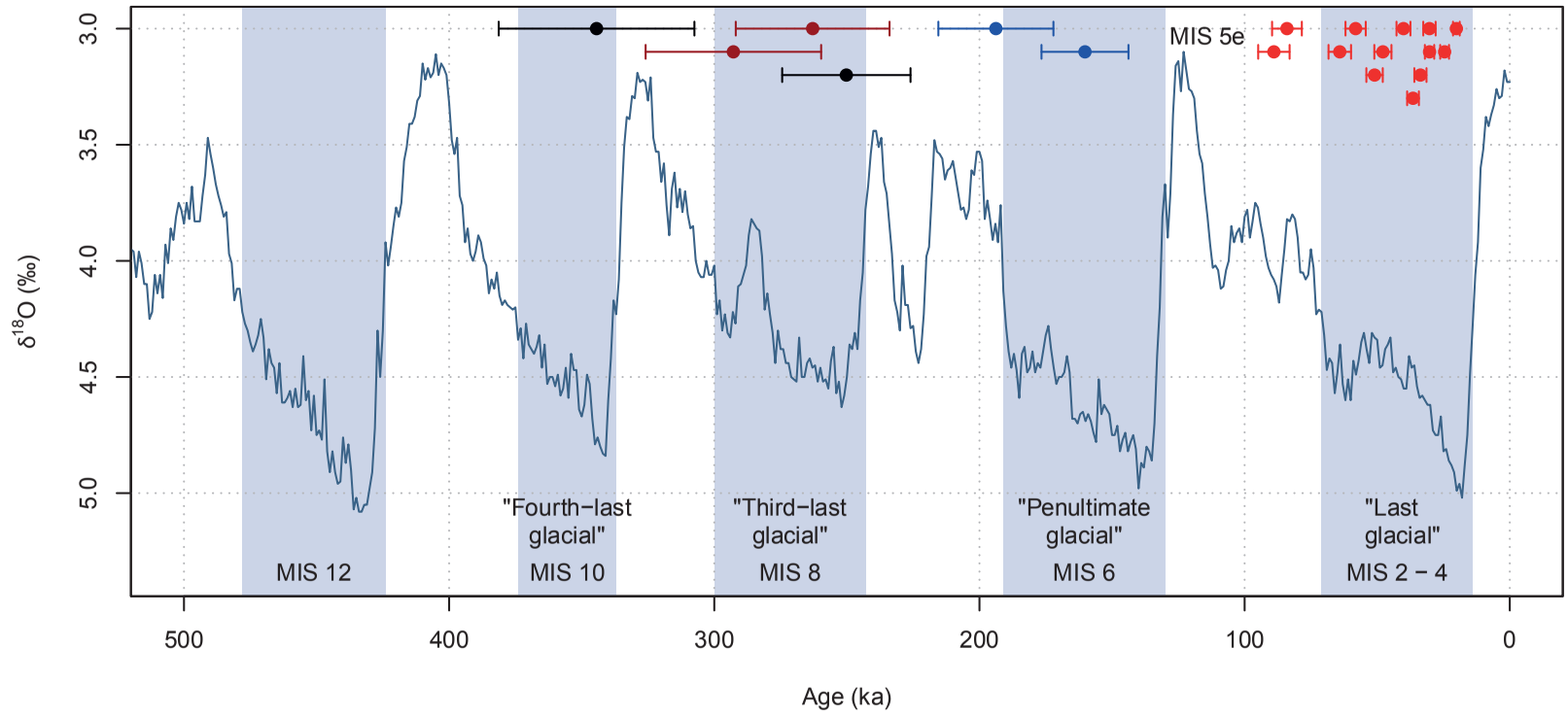

Figure 6.2: Marine isotope stages (MIS) and luminescence ages, summarizing the chronology of fluvial terrace accumulation determined in this PhD-thesis. The figure is based on data from the *LR04 Benthic Stack* of Lisiecki & Raymo (2005) and was plotted using an R-script written by K. Reinhardt. The *LR04 Benthic Stack* comprises the average of 57 globally distributed benthic $\delta^{18}O$ records collected from the scientific literature and spanning a total of ~5.3 million years. For this figure, the data was restricted to the last ~500 ka. Marine isotope stages associated with glacial periods are highlighted by blue rectangles. Luminescence ages are illustrated by filled circles in the upper part of the figure. Their colours correspond to the colours used for the distinct terrace levels in the various maps of this PhD-thesis (red = T2-terrace, blue = T3-terrace, black = T4-terrace, purple = T5-terrace).

7

Outlook

As already mentioned in the preface and in the introduction (Chapter 1), this PhD-thesis was part of a research project which aimed at deriving information on the late Pleistocene and early Holocene landscape evolution in the region of Upper Franconia, Northern Bavaria (Germany). Apart from natural geomorphic processes, also the important role of mankind for landscape evolution dynamics was subject of our scientific investigations. Given the wide range of topics associated with such a research project, this PhD-thesis had to be restricted to a selection of suitable subtopics and is, therefore, focussing on defining a local chronology for the Middle and Upper Pleistocene fluvial evolution, documented by the various terrace levels identified within the Trebgast Valley.

Thus, many data collected in the past years could not be considered for this PhD-thesis. As a consequence, there are several aspects not mentioned in the context of the presented manuscripts at all, like the dating of Holocene floodplain sediments and of colluvial deposits from which we were able to derive new insights into the cultural history and the timing and dynamics of human settlements in our research area. The discussion of other aspects mentioned in the manuscripts may, on the other side, raise new questions, which can act as starting points for further research activities.

One of these aspects is the fact, already emphasized in Study 3, that the chronology for the oldest terrace levels (T4- and T5-level) can still only be referred to as preliminary. The interpretation of our results, which are pointing to more or less equal ages of T4- and T5-terrace remnants, is considerably complicated by the relatively large uncertainties associated with our luminescence ages. These uncertainties may be caused by site specific problems, such as incomplete resetting of luminescence signals due to partial bleaching, the incorporation of older unbleached material from the weak upcoming sandstone rocks – both mechanisms may cause significant age overestimations that could have affected the T4-terrace location – or the contamination of terrace material by younger surficial sediments, which could have happened for the less consolidated terrace material found at the T5-terrace site. An approach to overcome these difficulties may include the strategy to investigate suitable gravel accumulations of fluvial terraces in the upper reaches of the adjacent Red Main Valley that have clearly been identified to correspond to the T4- and T5-terrace levels found in the Trebgast Valley.

As already suggested in the conclusion section (5.5) of Chapter 5, the apparent synchronicity of T4- and T5-terrace accumulation may, however, also be attributed to so far unknown methodological issues of either the applied post-IR IRSL measurement sequence or of the subsequent fading correction procedures. Preliminary findings drawn from fading experiments provided evidence that the performance of fading correction algorithms reacts extremely sensitive to slight changes in the parameters used for the calculations. The determination of these parameters, e.g. laboratory fading rates (g-values) or recombination centre densities (ρ'), strongly depends on the specific settings applied to the fading measurement procedures (e.g., Wallinga et al., 2007; Morthekai et al., 2008; Kars et al., 2012).

Although some advices on how to perform fading measurements have already been proposed (e.g., Auclair et al., 2003), so far there is no commonly applied measurement procedure which includes a standardized sample pre-treatment. In order to assess the influence of different measurement settings and to test if there is an optimum combination of settings, systematic experiments considering a set of varying measurement parameters, such as bleaching time and mechanism, storage time, preheat treatment, administered dose and device specific dose rates, are required.

This time-consuming experiments once again emphasize the great need for alternative measurement procedures which are able to avoid the problems associated with post-IR IRSL protocols. Therefore, IR-radiofluorescence measurements should be applied to current and future samples either originating from the Trebgast Valley or from the adjacent Red Main Valley. First preliminary test measurements on material originating from T3-terrace samples, which were performed in cooperation with Dr. Madhav Murari at the Justus-Liebig-University of Gießen, yielded promising first results.

Overall, the findings and conclusions summarized in this PhD-thesis reveal a rather local character, since they were only derived from sediments originating from a small valley in Upper Franconia. Therefore, at this stage it cannot be excluded that they only reflect the local conditions of the sampling locations within a very specific environmental setting. In order to expand the perspective and to test whether our findings may also allow a more generalizing interpretation, additional regional scaled studies are required.

Particularly, this applies to the diachronic character of river incision proposed in the study of Kolb et al. (2016) (see Chapter 4 on page 129). If this conclusion could be confirmed for other fluvial systems, this might be of great general relevance for geomorphological research in fluvial landscapes and of particular importance for the interpretation of age estimations of fluvial sediments derived from luminescence dating.

After all, similar findings, indicating the possibility of diachronically propagating incision impulses, have so far been reported for $^{10}Be/^{26}Al$ dating of fluvial terraces in the Ardennian valleys by Rixhon et al. (2011). However, additional local and regional studies are indispensable to establish a reliable dataset that allows a more generalizing interpretation of our findings. With a large and still growing number of geomorphological studies, the Main River drainage system as a whole represents a well documented and intensely studied fluvial system, which would certainly be a good starting point for establishing such a dataset.

References

Adamiec, G. & Aitken, M. (1998): Dose-rate conversion factors: update. *Ancient TL*, 16, pp. 37 – 46.

Aitken, M. (1985): *Thermoluminescence dating*. Academic press, London, 359 pp.

Aitken, M. (1998): *An Introduction to Optical Dating – The Dating of Quaternary Sediments by the Use of Photon-stimulated Luminescence*. Oxford University Press, Oxford/New York/Tokyo, 266 pp.

Aitken, M. & Smith, B. (1988): Optical dating: Recuperation after bleaching. *Quaternary Science Reviews*, 7 (3), pp. 387 – 393.

Aitken, M. & Xie, J. (1990): Moisture correction for annual gamma dose. *Ancient TL*, 8, pp. 6 – 9.

Alappat, L., Tsukamoto, S., Singh, P., Srikanth, D., Ramesh, R. & Frechen, M. (2010): Chronology of Cauvery Delta Sediments from Shallow Subsurface Cores Using Elevated-Temperature Post-IR IRSL Dating of Feldspar. *Geochronometria*, 37, pp. 37 – 47.

Anechitei-Deacu, V., Timar-Gabor, A., Fitzsimmons, K., Veres, D. & Hambach, U. (2013): Multi-method luminescence investigations on quartz grains of different sizes extracted from a loess section in Southeast Romania interbedding the Campanian Ignimbrite ash layer. *Geochronometria*, 41 (1), pp. 1 – 14.

Antoine, P., Auguste, P., Bahain, J.J., Chaussé, C., Falguères, C., Ghaleb, B., Limondin-Lozouet, N., Locht, J.L. & Voinchet, P. (2010): Chronostratigraphy and palaeoenvironments of Acheulean occupations in Northern France (Somme, Seine and Yonne valleys). *Quaternary International*, 223 (Supplement C), pp. 456 – 461.

Antoine, P., Lozouet, N.L., Chaussé, C., Lautridou, J.P., Pastre, J.F., Auguste, P., Bahain, J.J., Falguères, C. & Galehb, B. (2007): Pleistocene fluvial terraces from northern France (Seine, Yonne, Somme): synthesis, and new results from interglacial deposits. *Quaternary Science Reviews*, 26 (22), pp. 2701 – 2723.

Auclair, M., Lamothe, M. & Huot, S. (2003): Measurement of anomalous fading for feldspar IRSL using SAR. *Radiation Measurements*, 37 (4), pp. 487 – 492.

Bailey, R. (2000): Circumventing possible inaccuracies of the single aliquot regeneration method for the optical dating of quartz. *Radiation Measurements*, 32 (5), pp. 833 – 840.

Bailey, R. (2001): Towards a general kinetic model for optically and thermally stimulated luminescence of quartz. *Radiation Measurements*, 33 (1), pp. 17 – 45.

Bailey, R., Adamiec, G. & Rhodes, E. (2000): OSL properties of NaCl relative to dating and dosimetry. *Radiation Measurements*, 32 (5), pp. 717 – 723.

Barbouti, A.I. & Rastin, B.C. (1983): A study of the absolute intensity of muons at sea level and under various thicknesses of absorber. *Journal of Physics G: Nuclear Physics*, 9 (12), pp. 1577 – 1595.

Bartz, J. (1937): Die pliocän-diluviale Entwicklung des Mainlaufes. *Zeitschrift der Deutschen Geologischen Gesellschaft*, 89, pp. 328 – 342.

Bayerisches Landesamt für Umwelt (2017a): Hochwassernachrichtendienst Bayern – Statistik Bayreuth/Roter Main. https://www.hnd.bayern.de/pegel/oberer_main_elbe/bayreuth-24123000/statistik? [Online; accessed 30-November-2017].

Bayerisches Landesamt für Umwelt (2017b): Hochwassernachrichtendienst Bayern – Statistik Ködnitz/Weißer Main. https://www.hnd.bayern.de/pegel/oberer_main_elbe/koednitz-24111001/statistik? [Online; accessed 30-November-2017].

Bayerisches Landesamt für Umwelt (2017c): Hochwassernachrichtendienst Bayern – Statistik Trebgast/Trebgast. https://www.hnd.bayern.de/pegel/oberer_main_elbe/trebgast-24114000/statistik? [Online; accessed 30-November-2017].

Bayerisches Landesamt für Umwelt (2017d): Hochwassernachrichtendienst Bayern – Statistik Untersteinach/Warme Steinach. https://www.hnd.bayern.de/pegel/naab_regen/untersteinach-24128004/statistik? [Online; accessed 30-November-2017].

Becker, B. & Schirmer, W. (1977): Palaeoecological study on the Holocene valley development of the River Main, southern Germany. *Boreas*, 6 (4), pp. 303–321.

Berger, G. & Luternauer, J. (1987): Preliminary field work for thermoluminescence dating studies at the Fraser River delta, British Columbia. *Geological Survey of Canada Paper*, 87/IA, pp. 901 – 904.

Berger, G., Mulhern, P. & Huntley, D. (1980): Isolation of silt-sized quartz sediments. *Ancient TL*, 11, pp. 8 – 9.

Berger, G.W. (1990): Effectiveness of natural zeroing of the thermoluminescence in sediments. *Journal of Geophysical Research: Solid Earth*, 95 (B8), pp. 12375–12397.

Brennan, B. (2003): Beta doses to spherical grains. *Radiation Measurements*, 37 (4), pp. 299 – 303.

Brennan, B., Lyons, R. & Phillips, S. (1991): Attenuation of alpha particle track dose for spherical grains. *International Journal of Radiation Applications and Instrumentation. Part D. Nuclear Tracks and Radiation Measurements*, 18 (1), pp. 249 – 253.

Bridgland, D. & Westaway, R. (2008a): Climatically controlled river terrace staircases: A worldwide Quaternary phenomenon. *Geomorphology*, 98 (3), pp. 285 – 315.

Bridgland, D.R., Keen, D. & Westaway, R. (2007): Global correlation of Late Cenozoic fluvial deposits: a synthesis of data from IGCP 449. *Quaternary Science Reviews*, 26 (22), pp. 2694 – 2700.

Bridgland, D.R. & Westaway, R. (2008b): Preservation patterns of Late Cenozoic fluvial deposits and their implications: Results from IGCP 449. *Quaternary International*, 189 (1), pp. 5 – 38.

Brindel, J. (2012): *Qualitative Schotteranalyse im Trebgasttal – Neue Untersuchungen zur Flussgeschichte*. B.Sc. thesis (unpublished), Univ.Bayreuth.

Brunnacker, K. (1973): Gesichtspunkte zur jüngeren Landschaftsgeschichte und zur Flußentwicklung in Franken. *Zeitschrift für Geomorphologie N. F., Supplementbände*, 17, pp. 72 – 90.

Brunnacker, K. & Brunnacker, K. (1956): Die Molluskenfauna einiger Lößprofile im Donautal. *Geologische Blätter für Nordost-Bayern und Angrenzende Gebiete*, 6, pp. 91 – 100.

Bryant, I. (1983): The utilization of arctic river analogue studies in the interpretation of periglacial river sediments from southern Britain. In: K. Gregory (Editor), *Background to Paleohydrology*. Wiley, Chichester, pp. 413 – 431.

References

Buch, M. (1988): Zur Frage einer kausalen Verknüpfung fluvialer Prozesse und Klimaschwankungen im Spätpleistozän und Holozän - Versuch einer geomorphodynamischen Deutung von Befunden von Donau und Main. *Zeitschrift für Geomorphologie N.F., Supplementary Issues*, 70, pp. 131 – 162.

Busschers, F., van Balen, R., Cohen, K., Kasse, C., Weerts, H., Wallinga, J. & Bunnik, F. (2008): Response of the Rhine–Meuse fluvial system to Saalian ice-sheet dynamics. *Boreas*, 37 (3), pp. 377–398.

Buylaert, J., Murray, A. & Huot, S. (2008): Optical dating of an Eemian site in Northern Russia using K-feldspar. *Radiation Measurements*, 43 (2), pp. 715 – 720.

Buylaert, J., Murray, A., Thomsen, K. & Jain, M. (2009): Testing the potential of an elevated temperature IRSL signal from K-feldspar. *Radiation Measurements*, 44 (5), pp. 560 – 565.

Buylaert, J.P., Huot, S., Murray, A.S. & van den Haute, P. (2011): Infrared stimulated luminescence dating of an Eemian (MIS 5e) site in Denmark using K-feldspar. *Boreas*, 40 (1), pp. 46–56.

Buylaert, J.P., Jain, M., Murray, A., Thomsen, K. & Lapp, T. (2012a): IR-RF dating of sand-sized K-feldspar extracts: A test of accuracy. *Radiation Measurements*, 47 (9), pp. 759 – 765.

Buylaert, J.P., Jain, M., Murray, A.S., Thomsen, K.J., Thiel, C. & Sohbati, R. (2012b): A robust feldspar luminescence dating method for Middle and Late Pleistocene sediments. *Boreas*, 41 (3), pp. 435–451.

Bøtter-Jensen, L., McKeever, S. & Wintle, A. (2003): *Optically stimulated luminescence dosimetry*. Elsevier, Amsterdam, 355 pp.

Büdel, J. (1977): *Klima-Geomorphologie*. Gebrüder Bornträger, Stuttgart/Berlin, 304 pp.

Chapot, M., Roberts, H., Duller, G. & Lai, Z. (2012): A comparison of natural- and laboratory-generated dose response curves for quartz optically stimulated luminescence signals from Chinese Loess. *Radiation Measurements*, 47 (11), pp. 1045 – 1052.

Charlton, R. (2008): *Fundamentals of fluvial geomorphology*. Routledge, London, 234 pp.

Chen, R. & Pagonis, V. (2011): *Thermally and optically stimulated luminescence – a simulation approach*. Wiley, Chichester, 419 pp.

Clarke, M. (1996): IRSL dating of sands: Bleaching characteristics at deposition inferred from the use of single aliquots. *Radiation Measurements*, 26 (4), pp. 611 – 620.

Clarke, M.L., Rendell, H.M. & Wintle, A.G. (1999): Quality assurance in luminescence dating. *Geomorphology*, 29 (1), pp. 173 – 185.

Colarossi, D., Duller, G., Roberts, H., Tooth, S. & Lyons, R. (2015): Comparison of paired quartz OSL and feldspar post-IR IRSL dose distributions in poorly bleached fluvial sediments from South Africa. *Quaternary Geochronology*, 30 (Part B), pp. 233 – 238.

Cordier, S. (2010): Optically stimulated luminescence dating: procedures and applications to geomorphological research in France. *Géomorphologie : relief, processus, environnement*, 16 (1), pp. 21 – 40.

Cordier, S., Bridgland, D. & Benito, G. (2015): Research on fluvial archives: from diversity to multidisciplinarity. *Quaternaire*, 26 (1), pp. 3 – 11.

Cordier, S., Harmand, D., Lauer, T., Voinchet, P., Bahain, J.J. & Frechen, M. (2012): Geochronological reconstruction of the Pleistocene evolution of the Sarre valley (France and Germany) using OSL and ESR dating techniques. *Geomorphology*, 165 (Supplement C), pp. 91 – 106.

Cunningham, A., J.W. & Minderhoud, P. (2011): Expectations of scatter in equivalent-dose distributions when using multi-grain aliquots for OSL dating. *Geochronometria*, 38 (4), pp. 424 – 431.

Degering, D. & Krbetschek, M. (2007): Dating of interglacial sediments by luminescence methods. In: F. Sirocko, M. Claussen, M.F.S. Goñi & T. Litt (Editors), *The Climate of Past Interglacials*, Developments in Quaternary Sciences. Elsevier, pp. 157 – 171.

Demoulin, A., Mather, A. & Whittaker, A. (2017): Fluvial archives, a valuable record of vertical crustal deformation. *Quaternary Science Reviews*, 166 (Supplement C), pp. 10 – 37.

Demtröder, W. (2016): *Experimentalphysik 3 – Atome, Moleküle und Festkörper*. Springer Spektrum, Berlin, 586 pp.

Demtröder, W. (2017): *Experimentalphysik 4 – Kern-, Teilchen- und Astrophysik*. Springer Spektrum, Berlin, 497 pp.

Dietze, M., Kreutzer, S., Burow, C., Fuchs, M.C., Fischer, M. & Schmidt, C. (2016): The abanico plot: Visualising chronometric data with individual standard errors. *Quaternary Geochronology*, 31 (Supplement C), pp. 12 – 18.

Duller, G. (1991): Equivalent dose determination using single aliquots. *International Journal of Radiation Applications and Instrumentation. Part D. Nuclear Tracks and Radiation Measurements*, 18 (4), pp. 371 – 378.

Duller, G. (1995): Luminescence dating using single aliquots: Methods and applications. *Radiation Measurements*, 24 (3), pp. 217 – 226.

Duller, G. (2003): Distinguishing quartz and feldspar in single grain luminescence measurements. *Radiation Measurements*, 37 (2), pp. 161 – 165.

Duller, G. (2008a): *Luminescence Dating – Guidelines on using luminescence dating in archaeology*. English Heritage, Swindon, 43 pp.

Duller, G. (2008b): Single-grain optical dating of Quaternary sediments: why aliquot size matters in luminescence dating. *BorFuchs eas*, 37 (4), pp. 589–612.

Duller, G., Bøtter-Jensen, L. & Murray, A. (2000): Optical dating of single sand-sized grains of quartz: sources of variability. *Radiation Measurements*, 32 (5), pp. 453 – 457.

Durcan, J.A., King, G.E. & Duller, G.A. (2015): DRAC: Dose Rate and Age Calculator for trapped charge dating. *Quaternary Geochronology*, 28 (Supplement C), pp. 54 – 61.

Duyster, J., Kontny, A., de Wall, H. & Zulauf, G. (1995): Post-variszische Krustenstapelung am Westrand der Böhmischen Masse. *Geowissenschaften*, 13 (4), pp. 135 – 141.

Eberle, J., Eitel, B., Blümel, W. & Wittmann, P. (2010): *Deutschlands Süden vom Erdmittelalter bis zur Gegenwart*. Spektrum Akademischer Verlag, Heidelberg, 192 pp.

Emmert, U. (1977): *Erläuterungen zur Geologischen Karte von Bayern 1:25000, Bl. 6035 Bayreuth*. Bayerisches Geologisches Landesamt, München.

Emmert, U. & Weinelt, W. (1962): *Erläuterungen zur Geologischen Karte von Bayern 1:25.000, Bl. 5935 Marktschorgast*. Bayerisches Geologisches Landesamt, München.

Erfurt, G. (2003): Infrared luminescence of Pb+ centres in potassium-rich feldspars. *physica status solidi (a)*, 200 (2), pp. 429–438.

Erfurt, G. & Krbetschek, M. (2003a): IRSAR - A single-aliquot regenerative-dose dating protocol applied to the infrared radiofluorescence (IR-RF) of course-grain K-feldspar. *Ancient TL*, 21, pp. 35 – 42.

Erfurt, G. & Krbetschek, M. (2003b): Studies on the physics of the infrared radioluminescence of potassium feldspar and on the methodology of its application to sediment dating. *Radiation Measurements*, 37 (4), pp. 505 – 510. Proceedings of the 10th international Conference on Luminescence and Electron-Spin Resonance Dating (LED 2002).

Erkens, G., Dambeck, R., Volleberg, K.P., Bouman, M.T., Bos, J.A., Cohen, K.M., Wallinga, J. & Hoek, W.Z. (2009): Fluvial terrace formation in the northern Upper Rhine Graben during the last 20000 years as a result of allogenic controls and autogenic evolution. *Geomorphology*, 103 (3), pp. 476 – 495.

Ertl, U. (1987): Pollenstratigraphie von Talprofilen im Main-Regnitz-Gebiet. *Berichte Naturwissenschaftliche Gesellschaft Bayreuth*, 19, pp. 45 – 123.

Falkner, G., Obrdlik, P., Castella, E. & Speight, M. (2001): *Shelled Gastropoda of Western Europe*. Verlag der Friedrich-Held-Gesellschaft, München, 265 pp.

Faust, D., Zielhofer, C., Escudero, R.B. & del Olmo, F.D. (2004): High-resolution fluvial record of late Holocene geomorphic change in northern Tunisia: climatic or human impact? *Quaternary Science Reviews*, 23 (16), pp. 1757 – 1775.

Fiebig, M. & Preusser, F. (2003): Das Alter fluvialer Ablagerungen aus der Region Ingolstadt (Bayern) und ihre Bedeutung für die Eiszeitenchronologie des Alpenvorlandes. *Zeitschrift für Geomorphologie, NF*, 47 (4), pp. 449–467.

Firbas, F. (1949): *Spät- und nacheiszeitliche Vegetationsgeschichte Mitteleuropas nördlich der Alpen – Band I: Allgemeine Waldgeschichte*. Fischer, Jena, 480 pp.

Firbas, F. (1952): *Spät- und nacheiszeitliche Vegetationsgeschichte Mitteleuropas nördlich der Alpen – Band II: Waldgeschichte der einzelnen Landschaften*. Fischer, Jena, 256 pp.

Friedl, A. (2014): *Terrassenrekonstruktion des oberen Rotmaintals mittels DGM*. B.Sc. thesis (unpublished), Univ.Bayreuth.

Frouin, M., Huot, S., Kreutzer, S., Lahaye, C., Lamothe, M., Philippe, A. & Mercier, N. (2017): An improved radiofluorescence single-aliquot regenerative dose protocol for K-feldspars. *Quaternary Geochronology*, 38 (Supplement C), pp. 13 – 24.

Frouin, M., Huot, S., Mercier, N., Lahaye, C. & Lamothe, M. (2015): The issue of laboratory bleaching in the infrared-radiofluorescence dating method. *Radiation Measurements*, 81 (Supplement C), pp. 212 – 217.

Fryirs, K. & Brierley, G. (2013): *Geomorphic analysis of river systems – an approach to reading the landscape*. Wiley-Blackwell, Oxford, 345 pp.

Fu, X., Li, B. & Li, S.H. (2012): Testing a multi-step post-IR IRSL dating method using polymineral fine grains from Chinese loess. *Quaternary Geochronology*, 10 (Supplement C), pp. 8 – 15.

Fu, X. & Li, S.H. (2013): A modified multi-elevated-temperature post-IR IRSL protocol for dating Holocene sediments using K-feldspar. *Quaternary Geochronology*, 17 (Supplement C), pp. 44 – 54.

Fuchs, M., Fischer, M. & Reverman, R. (2010): Colluvial and alluvial sediment archives temporally resolved by OSL dating: Implications for reconstructing soil erosion. *Quaternary Geochronology*, 5 (2), pp. 269 – 273.

Fuchs, M., Kreutzer, S., Fischer, M., Sauer, D. & Sørensen, R. (2012): OSL and IRSL dating of raised beach sand deposits along the southeastern coast of Norway. *Quaternary Geochronology*, 10 (Supplement C), pp. 195 – 200.

Fuchs, M. & Lang, A. (2001): OSL dating of coarse-grain fluvial quartz using single-aliquot protocols on sediments from NE Peloponnese, Greece. *Quaternary Science Reviews*, 20 (5), pp. 783 – 787.

Fuchs, M. & Lang, A. (2009): Luminescence dating of hillslope deposits – A review. *Geomorphology*, 109 (1), pp. 17 – 26.

Fuchs, M., Lang, A. & Wagner, G.A. (2004): The history of Holocene soil erosion in the Phlious Basin, NE Peloponnese, Greece, based on optical dating. *The Holocene*, 14 (3), pp. 334–345.

Fuchs, M., Straub, J. & Zöller, L. (2005): Residual luminescence signals of recent river flood sediments: A comparison between quartz and feldspar of fine- and coarse-grain sediments. *Ancient TL*, 23 (1), pp. 25 – 30.

Fuchs, M. & Wagner, G. (2003): Recognition of insufficient bleaching by small aliquots of quartz for reconstructing soil erosion in Greece. *Quaternary Science Reviews*, 22 (10), pp. 1161 – 1167.

Fuchs, M., Will, M., Kunert, E., Kreutzer, S., Fischer, M. & Reverman, R. (2011): The temporal and spatial quantification of Holocene sediment dynamics in a meso-scale catchment in northern Bavaria, Germany. *The Holocene*, 21 (7), pp. 1093–1104.

Fuchs, M., Woda, C. & Bürkert, A. (2007): Chronostratigraphy of a sediment record from the Hajar mountain range in north Oman: Implications for optical dating of insufficiently bleached sediments. *Quaternary Geochronology*, 2 (1), pp. 202 – 207.

Gaar, D., Lowick, S. & Preusser, F. (2013): Performance of different luminescence approaches for the dating of known-age glaciofluvial deposits from northern Switzerland. *Geochronometria*, 41 (1), pp. 65 – 80.

Gaft, M., Nagli, L., Panczer, G., Waychunas, G. & Porat, N. (2008): The nature of unusual luminescence in natural calcite $CaCO_3$. *American Mineralogist*, 93 (1), pp. 158–167.

Galbraith, R. & Green, P. (1990): Estimating the component ages in a finite mixture. *International Journal of Radiation Applications and Instrumentation. Part D. Nuclear Tracks and Radiation Measurements*, 17 (3), pp. 197 – 206.

Galbraith, R.F. (2005): *Statistics for Fission Track Analysis*. Chapman and Hall, London, 240 pp.

Galbraith, R.F., Roberts, R.G., Laslett, G.M., Yoshida, H. & Olley, J.M. (1999): Optical dating of single and multiple grains of quartz from Jinmium Rock Shelter, Northern Australia: Part I, Experimental design and statistical models. *Archaeometry*, 41 (2), pp. 339–364.

Gesslein, B. & Schellmann, G. (2011): Jungquartäre Flussterrassen am mittleren Lech zwischen Kinsau und Klosterlechfeld - Erste Ergebnisse. *Quaternary Science Journal (Eiszeitalter & Gegenwart)*, 60 (4), pp. 400 – 413.

Gibbard, P. & Lewin, J. (2002): Climate and related controls on interglacial fluvial sedimentation in lowland Britain. *Sedimentary Geology*, 151 (3), pp. 187 – 210.

Gibbard, P. & Lewin, J. (2009): River incision and terrace formation in the Late Cenozoic of Europe. *Tectonophysics*, 474 (1), pp. 41 – 55.

Gibbard, P.L. (1985): *Pleistocene history of the Middle Thames Valley*. Cambridge University Press, Cambridge, 155 pp.

Gillespie, R., Prosser, I.P., Dlugokencky, E., Sparks, R.J., Wallace, G. & Chappell, J.M.A. (1992): AMS Dating of Alluvial Sediments on the Southern Tablelands of New South Wales, Australia. *Radiocarbon*, 34 (1), pp. 29 – 36.

Godfrey-Smith, D., Huntley, D. & Chen, W.H. (1988): Optical dating studies of quartz and feldspar sediment extracts. *Quaternary Science Reviews*, 7 (3), pp. 373 – 380.

Gregory, K.J., Benito, G., Dikau, R., Golosov, V., Johnstone, E.C., Jones, J.A.A., Macklin, M.G., Parsons, A.J., Passmore, D.G., Poesen, J., Soja, R., Starkel, L., Thorndycraft, V.R. & Walling, D.E. (2006): Past hydrological events and global change. *Hydrological Processes*, 20 (1), pp. 199–204.

References

Gräbner, W. (1963): Das Trebgasttal. Eine geologische Studie. *Berichte Naturwissenschaftliche Gesellschaft Bayreuth*, 11, pp. 87 – 188.

Gräbner, W. (1985): Das Trebgasttal aus erdgeschichtlicher Sicht. In: Gemeinde Trebgast (Editor), *950 Jahre Trebgast*. Trebgast, pp. 50 – 87.

Grün, R. (1989): *Die ESR-Altersbestimmungsmtheode*. Springer, Berlin/Heidelberg, 132 pp.

Grün, R. (2001): Trapped charge dating (ESR, TL, OSL). In: D. Brothwell & A. Pollard (Editors), *Handbook of Archaeological Sciences*. Wiley, Chichester and New York, pp. 47 – 62.

Guérin, G., Mercier, N. & Adamiec, G. (2011): Dose-rate conversion factors: update. *Ancient TL*, 29, pp. 5 – 8.

Guérin, G., Mercier, N., Nathan, R., Adamiec, G. & Lefrais, Y. (2012): On the use of the infinite matrix assumption and associated concepts: A critical review. *Radiation Measurements*, 47 (9), pp. 778 – 785.

Guérin, G. & Visocekas, R. (2015): Volcanic feldspars anomalous fading: Evidence for two different mechanisms. *Radiation Measurements*, 81 (Supplement C), pp. 218 – 223.

Henkel, L. (1917): Das Urflußtal zwischen Bayreuth und Trebgast. *Dr. A. Petermanns Mitteilungen aus Justus Perthes' Geographischer Anstalt*, 63, pp. 88 – 89.

Henkel, L. (1920): Die Terrassen des Maintals bis zum Eintritt in die oberrheinische Tiefebene. Beitrag zur Entwicklungsgeschichte des fränkischen Flußnetzes. *Geologische Rundschau*, 10, pp. 137 – 155.

Henshilwood, C.S., d'Errico, F., Yates, R., Jacobs, Z., Tribolo, C., Duller, G.A.T., Mercier, N., Sealy, J.C., Valladas, H., Watts, I. & Wintle, A.G. (2002): Emergence of Modern Human Behavior: Middle Stone Age Engravings from South Africa. *Science*, 295 (5558), pp. 1278–1280.

Herget, J., Dikau, R., Gregory, K.J. & Vandenberghe, J. (2007): The fluvial system — Research perspectives of its past and present dynamics and controls. *Geomorphology*, 92 (3), pp. 101 – 105.

Hobo, N., Makaske, B., Middelkoop, H. & Wallinga, J. (2010): Reconstruction of floodplain sedimentation rates: a combination of methods to optimize estimates. *Earth Surface Processes and Landforms*, 35 (13), pp. 1499–1515.

Houben, P. (2003): Spatio-temporally variable response of fluvial systems to Late Pleistocene climate change: a case study from central Germany. *Quaternary Science Reviews*, 22 (20), pp. 2125 – 2140.

Houben, P. (2007): Geomorphological facies reconstruction of Late Quaternary alluvia by the application of fluvial architecture concepts. *Geomorphology*, 86 (1), pp. 94 – 114.

Howard, A.J., Gearey, B.R., Hill, T., Fletcher, W. & Marshall, P. (2009): Fluvial sediments, correlations and palaeoenvironmental reconstruction: The development of robust radiocarbon chronologies. *Journal of Archaeological Science*, 36 (12), pp. 2680 – 2688.

Huntley, D.J. & Baril, M.R. (1997): The K content of the K-feldspars being measured in optical dating or in thermoluminescence dating. *Ancient TL*, 15, pp. 11 – 13.

Huntley, D.J. & Lamothe, M. (2001): Ubiquity of anomalous fading in K-feldspars and the measurement and correction for it in optical dating. *Canadian Journal of Earth Sciences*, 38 (7), pp. 1093–1106.

Huot, S., Frouin, M. & Lamothe, M. (2015): Evidence of shallow TL peak contributions in infrared radiofluorescence. *Radiation Measurements*, 81 (Supplement C), pp. 237 – 241.

Jain, M. & Ankjærgaard, C. (2011): Towards a non-fading signal in feldspar: Insight into charge transport and tunnelling from time-resolved optically stimulated luminescence. *Radiation Measurements*, 46 (3), pp. 292 – 309.

Jain, M., Murray, A. & Bøtter-Jensen, L. (2003): Characterisation of blue-light stimulated luminescence components in different quartz samples: implications for dose measurement. *Radiation Measurements*, 37 (4), pp. 441 – 449.

Jain, M., Murray, A., Bøtter-Jensen, L. & Wintle, A. (2005): A single-aliquot regenerative-dose method based on IR (1.49eV) bleaching of the fast OSL component in quartz. *Radiation Measurements*, 39 (3), pp. 309 – 318.

Jain, M., Murray, A.S. & Bøtter-Jensen, L. (2004): Optically stimulated luminescence dating: How significant is incomplete light exposure in fluvial environments? *Quaternaire*, 15, pp. 143 – 157.

Jain, M. & Singhvi, A. (2001): Limits to depletion of blue-green light stimulated luminescence in feldspars: implications for quartz dating. *Radiation Measurements*, 33 (6), pp. 883 – 892.

References

Kars, R., Busschers, F. & Wallinga, J. (2012): Validating post IR-IRSL dating on K-feldspars through comparison with quartz OSL ages. *Quaternary Geochronology*, 12 (Supplement C), pp. 74 – 86.

Kars, R., Wallinga, J. & Cohen, K. (2008): A new approach towards anomalous fading correction for feldspar IRSL dating — tests on samples in field saturation. *Radiation Measurements*, 43 (2), pp. 786 – 790.

Kars, R.H., Poolton, N.R., Jain, M., Ankjærgaard, C., Dorenbos, P. & Wallinga, J. (2013): On the trap depth of the IR-sensitive trap in Na- and K-feldspar. *Radiation Measurements*, 59 (Supplement C), pp. 103 – 113.

Kars, R.H., Reimann, T., Ankjærgaard, C. & Wallinga, J. (2014): Bleaching of the post-IR IRSL signal: new insights for feldspar luminescence dating. *Boreas*, 43 (4), pp. 780–791.

Kemp, R., Toms, P., Sayago, J., Derbyshire, E., King, M. & Wagoner, L. (2003): Micromorphology and OSL dating of the basal part of the loess–paleosol sequence at La Mesada in Tucumán province, Northwest Argentina. *Quaternary International*, 106-107, pp. 111 – 117.

Kerney, M., Cameron, R. & Jungbluth, J. (1983): *Die Landschnecken Nord- und Mitteleuropas - ein Bestimmungsbuch für Biologen und Naturfreunde*. Parey, Hamburg & Berlin, 384 pp.

Kim, J., Roberts, H., Duller, G., Lee, Y. & Yi, S. (2009): Assessment of diagnostic tests for evaluating the reliability of SAR De values from polymineral and quartz fine grains. *Radiation Measurements*, 44 (2), pp. 149 – 157.

Kittel, C. (2005): *Introduction to Solid State Physics*. Wiley, Hoboken, NJ, 680 pp.

Klasen, N., Fiebig, M., Preusser, F. & Radtke, U. (2006): Luminescence properties of glaciofluvial sediments from the Bavarian Alpine Foreland. *Radiation Measurements*, 41 (7), pp. 866 – 870.

Kleber, A. & Stingl, H. (2000): Zur Flußgeschichte des Trebgasttals nördlich von Bayreuth. Eine zweiphasige Talverlegung im Rotmainsystem. In: H. Becker (Editor), *Beiträge zur Landeskunde Oberfrankens. Festschrift zum 65. Geburtstag von Bezirkstagspräsidenten Edgar Sitzmann*, Bamberger Geographische Schriften, Sonderheft Nr. 6. Selbstverlag Universität Bamberg, Bamberg, pp. 191 – 208.

Kleber, A., Stingl, H. & Veit, H. (1988): Quartäre Talentwicklung in der Bruchschollenzone um Bayreuth. In: K. Hüser & H. Stingl (Editors), *Deutscher Arbeitskreis für Geomorphologie. 15. Tagung in Bayreuth 1988. Exkursionsführer Oberfranken*. Bayreuth, pp. 37 – 64.

Knox, J.C. (2006): Floodplain sedimentation in the Upper Mississippi Valley: Natural versus human accelerated. *Geomorphology*, 79 (3), pp. 286 – 310.

Kolb, T., Fuchs, M., Moine, O. & Zöller, L. (2017): Quaternary river terraces and hillslope sediments as archives for paleoenvironmental reconstruction: new insights from the headwaters of the Main River, Germany. *Zeitschrift für Geomorphologie, Supplementary Issues*, 61 (1), pp. 53 – 76.

Kolb, T., Fuchs, M. & Zöller, L. (2016): Deciphering fluvial landscape evolution by luminescence dating of river terrace formation: a case study from Northern Bavaria, Germany. *Zeitschrift für Geomorphologie, Supplementary Issues*, 60 (1), pp. 29–48.

Krbetschek, M., Trautmann, T., Dietrich, A. & Stolz, W. (2000): Radioluminescence dating of sediments: methodological aspects. *Radiation Measurements*, 32 (5), pp. 493 – 498.

Kreutzer, S. (2014): *Luminescence based chronologies on Late Pleistocene loess-palaeosol sequences: an applied-methodological study on quartz separates*. Ph.D. thesis, University of Bayreuth, Bayreuth.

Kreutzer, S., Dietze, M., Burow, C., Fuchs, M., Schmidt, C., Fischer, M., Friedrich, J., Mercier, N., Smedley, R., Durcan, J. & King, G. (2016): Luminescence: Comprehensive Luminescence Dating Data Analysis CRAN version 0.7.3. Technical report, http://CRAN.R-project.org/package=Luminescence.

Kreutzer, S., Fuchs, M., Meszner, S. & Faust, D. (2012a): OSL chronostratigraphy of a loess-palaeosol sequence in Saxony/Germany using quartz of different grain sizes. *Quaternary Geochronology*, 10 (Supplement C), pp. 102 – 109.

Kreutzer, S., Lauer, T., Meszner, S., Krbetschek, M., Faust, D. & Fuchs, M. (2014): Chronology of the Quaternary profile Zeuchfeld in Saxony-Anhalt / Germany a preliminary luminescence dating study. *Zeitschrift für Geomorphologie, Supplementary Issues*, 58 (1), pp. 5–26.

Kreutzer, S., Schmidt, C., Fuchs, M.C., Dietze, M., Fischer, M. & Fuchs, M. (2012b): Introducing an R package for luminescence dating analysis. *Ancient TL*, 30, pp. 1 – 8.

Krömer, E. (2010): Fluviale Geomorphodynamik der Donau im Bereich des Rückstaus durch das Isarmündungsgebiet bei Deggendorf (Niederbayern) und Aussagen zur späthochglazialen und spätglazialen Entwicklung. In: G. Schellmann (Editor), *Bamberger physisch-geographische Studien 2002 – 2007. Studien zur quartären Talgeschichte von Donau und Lech*, Bamberger Geographische Schriften 24. Selbstverlag Universität Bamberg, Bamberg, pp. 79 – 87.

References

Körber, H. (1962): *Die Entwicklung des Maintals*. Würzburger geographische Arbeiten, Band 10. Geographisches Institut der Universität Würzburg, Würzburg, 170 pp.

Lamothe, M., Auclair, M., Hamzaoui, C. & Huot, S. (2003): Towards a prediction of long-term anomalous fading of feldspar IRSL. *Radiation Measurements*, 37 (4), pp. 493 – 498.

Lauer, T., Frechen, M., Hoselmann, C. & Tsukamoto, S. (2010): Fluvial aggradation phases in the Upper Rhine Graben—new insights by quartz OSL dating. *Proceedings of the Geologists' Association*, 121 (2), pp. 154 – 161.

Lauer, T., Krbetschek, M.R., Frechen, M., Tsukamoto, S., Hoselmann, C. & Weidenfeller, M. (2011): Infrared radiofluorescence (IR-RF) dating of middle pleistocene fluvial archives of the Heidelberg Basin (Southwest Germany). *Geochronometria*, 38 (1), pp. 23 – 33.

Lauer, T., Von Suchodoletz, H., Vollmann, H., Meszner, S., Frechen, M., Tinapp, C., Goldmann, L., Müller, S. & Zielhofer, C. (2014): Landscape aridification in Central Germany during the late Weichselian Pleniglacial - results from the Zauschwitz loess site in western Saxony. *Zeitschrift für Geomorphologie, Supplementbände*, 58 (1), pp. 27 – 50.

Leopold, L.B., Wolman, M.G. & Miller, J.P. (1964): *Fluvial Processes in Geomorphology*. Freeman, San Francisco, 522 pp.

Lepper, K., Larsen, N.A. & McKeever, S.W. (2000): Equivalent dose distribution analysis of Holocene eolian and fluvial quartz sands from Central Oklahoma. *Radiation Measurements*, 32 (5), pp. 603 – 608.

Lewin, J. & Gibbard, P. (2010): Quaternary river terraces in England: Forms, sediments and processes. *Geomorphology*, 120 (3), pp. 293 – 311.

Li, B., Jacobs, Z., Roberts, R. & Li, S.H. (2014): Review and assessment of the potential of post-IR IRSL dating methods to circumvent the problem of anomalous fading in feldspar luminescence. *Geochronometria*, 41 (3), pp. 178 – 201.

Li, B. & Li, S.H. (2011): Luminescence dating of K-feldspar from sediments: A protocol without anomalous fading correction. *Quaternary Geochronology*, 6 (5), pp. 468 – 479.

Li, B. & Li, S.H. (2012): Luminescence dating of Chinese loess beyond 130 ka using the non-fading signal from K-feldspar. *Quaternary Geochronology*, 10 (Supplement C), pp. 24 – 31.

Li, B., Li, S.H., Wintle, A.G. & Zhao, H. (2007): Isochron measurements of naturally irradiated K-feldspar grains. *Radiation Measurements*, 42 (8), pp. 1315 – 1327.

Li, B., Li, S.H., Wintle, A.G. & Zhao, H. (2008): Isochron dating of sediments using luminescence of K-feldspar grains. *Journal of Geophysical Research: Earth Surface*, 113 (F2), pp. n/a–n/a.

Li, B., Roberts, R.G. & Jacobs, Z. (2013): On the dose dependency of the bleachable and non-bleachable components of IRSL from K-feldspar: Improved procedures for luminescence dating of Quaternary sediments. *Quaternary Geochronology*, 17 (Supplement C), pp. 1 – 13.

Li, Y., Tsukamoto, S., Frechen, M. & Gabriel, G. (2017a): Timing of fluvial sedimentation in the Upper Rhine Graben since the Middle Pleistocene: constraints from quartz and feldspar luminescence dating. *Boreas*, pp. n/a–n/a.

Li, Y., Tsukamoto, S., Hu, K. & Frechen, M. (2017b): Quartz OSL and K-feldspar post-IR IRSL dating of sand accumulation in the Lower Liao Plain (Liaoning, NE China). *Geochronometria*, 44 (1), pp. 1 – 15.

Liritzis, I., Singhvi, A., Feathers, J., Wagner, G., Kadereit, A., Zacharias, N. & Li, S.H. (2013a): *Luminescence Dating in Archaeology, Anthropology, and Geoarchaeology*. Springer International Publishing, Heidelberg, 70 pp.

Liritzis, I., Stamoulis, K., Papachritodoulou, C. & Ioannides, K. (2013b): A re-evaluation of radiation dose-rate conversion factors. *Mediterranean Archaeology and Archaeometry*, 12 (3), pp. 1 – 15.

Lisiecki, L.E. & Raymo, M.E. (2005): A Pliocene-Pleistocene stack of 57 globally distributed benthic δ18O records. *Paleoceanography*, 20 (1), pp. n/a–n/a.

Litchfield, N.J. & Rieser, U. (2005): Optically stimulated luminescence age constraints for fluvial aggradation terraces and loess in the eastern North Island, New Zealand. *New Zealand Journal of Geology and Geophysics*, 48 (4), pp. 581–589.

Lomax, J. (2009): *Palaeodunes as archives of environmental change - A case study from the western Murray Basin (South Australia) based on optically stimulated luminescence (OSL) dating of single and multiple grains of quartz*. Ph.D. thesis, Universität zu Köln, Köln.

Ložek, V. (1964): Quartärmollusken der Tschechoslowakei. *Rozpravy Ústredního ústuvu geologického*, 31, pp. 1 – 374.

Lowick, S.E., Trauerstein, M. & Preusser, F. (2012): Testing the application of post IR-IRSL dating to fine grain waterlain sediments. *Quaternary Geochronology*, 8 (Supplement C), pp. 33 – 40.

Lu, Y., Wang, X. & Wintle, A. (2007): A new OSL chronology for dust accumulation in the last 130,000 yr for the Chinese Loess Plateau. *Quaternary Research*, 67 (1), pp. 152 – 160.

Lukas, S., Spencer, J.Q., Robinson, R.A. & Benn, D.I. (2007): Problems associated with luminescence dating of Late Quaternary glacial sediments in the NW Scottish Highlands. *Quaternary Geochronology*, 2 (1), pp. 243 – 248.

Maddy, D., Demir, T., Bridgland, D.R., Veldkamp, A., Stemerdink, C., van der Schriek, T. & Schreve, D. (2007): The Pliocene initiation and Early Pleistocene volcanic disruption of the palaeo-Gediz fluvial system, Western Turkey. *Quaternary Science Reviews*, 26 (22), pp. 2864 – 2882.

Madsen, A., Buylaert, J. & Murray, A. (2011): Luminescence dating of young coastal deposits from New Zealand using feldspar. *Geochronometria*, 38 (4), pp. 379 – 390.

Mahan, S. & Kay, J. (2012): Building on previous OSL dating techniques for gypsum: A case study from Salt Basin playa, New Mexico and Texas. *Quaternary Geochronology*, 10 (Supplement C), pp. 345 – 352.

Mahesh, K., Weng, P. & Furetta, C. (1989): *Thermoluminescence in solids and its applications*. Nuclear Technology Publishing, Ashford, 306 pp.

Mauz, B., Bode, T., Mainz, E., Blanchard, H., Hilger, W., Dikau, R. & Zöller, L. (2002): The luminescence dating laboratory at the University of Bonn: Equipment and procedures. *Ancient TL*, 20, pp. 53 – 61.

Mauz, B. & Lang, A. (2004): Removal of the feldspar-derived luminescence component from polymineral fine silt samples for optical dating applications: evaluation of chemical treatment protocols and quality control procedures. *Ancient TL*, 22, pp. 1 – 8.

McKeever, S. (1985): *Thermoluminescence of solids*. Cambridge University Press, Cambridge, 376 pp.

Mejdahl, V. (1979): Thermoluminescence dating: beta-dose attenuation in quartz grains. *Archaeometry*, 21 (1), pp. 61 – 72.

Mishra, S., White, M., Beaumont, P., Antoine, P., Bridgland, D., Limondin-Lozouet, N., Santisteban, J., Schreve, D., Shaw, A., Wenban-Smith, F., Westaway, R. & White, T. (2007): Fluvial deposits

as an archive of early human activity. *Quaternary Science Reviews*, 26 (22), pp. 2996 – 3016.

Moine, O. (2003): *Analyse des changements rapides de l'environnement à l'aide des faunes de mollusques terrestres durant la dernière période glaciaire en domaine continental européen*. Ph.D. thesis, University of Montpellier II.

Moine, O. (2008): West-European malacofauna from loess deposits of the Weichselian Upper Pleniglacial: compilation and preliminary analysis of the database. *Quaternaire*, 19 (1), pp. 11 – 29.

Moine, O., Antoine, P., Deschodt, L. & Sellier-Segard, N. (2011): Enregistrements malacologiques à haute résolution dans les lœss et les gleys de toundra du Pléniglaciaire weichselien supérieur : premiers exemples du nord de la Franc. *Quaternaire*, 22 (4), pp. 307 – 325.

Moine, O., Rousseau, D.D. & Antoine, P. (2008): The impact of Dansgaard–Oeschger cycles on the loessic environment and malacofauna of Nussloch (Germany) during the Upper Weichselian. *Quaternary Research*, 70 (1), pp. 91 – 104.

Mol, J., Vandenberghe, J. & Kasse, C. (2000): River response to variations of periglacial climate in mid-latitude Europe. *Geomorphology*, 33 (3), pp. 131 – 148.

Morthekai, P., Jain, M., Cunha, P., Azevedo, J. & Singvhi, A. (2011): An attempt to correct for the fading in million year old basaltic rocks. *Geochronometria*, 38 (3), pp. 223 – 230.

Morthekai, P., Jain, M., Murray, A., Thomsen, K. & Bøtter-Jensen, L. (2008): Fading characteristics of martian analogue materials and the applicability of a correction procedure. *Radiation Measurements*, 43 (2), pp. 672 – 678.

Müller, G. (1964): *Sediment-Petrologie 1 – Methoden der Sedimentuntersuchung*. Schweizerbart, Stuttgart, 303 pp.

Murray, A. & Wintle, A. (2000): Luminescence dating of quartz using an improved single-aliquot regenerative-dose protocol. *Radiation Measurements*, 32 (1), pp. 57 – 73.

Murray, A. & Wintle, A. (2003): The single aliquot regenerative dose protocol: potential for improvements in reliability. *Radiation Measurements*, 37 (4), pp. 377 – 381.

Murton, J.B. & Belshaw, R.K. (2011): A conceptual model of valley incision, planation and terrace formation during cold and arid permafrost conditions of Pleistocene southern England. *Quaternary Research*, 75 (2), pp. 385 – 394.

Nichols, G. & Fisher, J. (2007): Processes, facies and architecture of fluvial distributary system deposits. *Sedimentary Geology*, 195 (1), pp. 75 – 90.

Novothny, A., Frechen, M., Horváth, E., Krbetschek, M. & Tsukamoto, S. (2010): Infrared stimulated luminescence and radiofluorescence dating of aeolian sediments from Hungary. *Quaternary Geochronology*, 5 (2), pp. 114 – 119.

Olley, J., Caitcheon, G. & Murray, A. (1998): The distribution of apparent dose as determined by Optically Stimulated Luminescence in small aliquots of fluvial quartz: Implications for dating young sediments. *Quaternary Science Reviews*, 17 (11), pp. 1033 – 1040.

Olley, J.M., Pietsch, T. & Roberts, R.G. (2004): Optical dating of Holocene sediments from a variety of geomorphic settings using single grains of quartz. *Geomorphology*, 60 (3), pp. 337 – 358.

Penck, A. & Brückner, E. (1909): *Die Alpen im Eiszeitalter*. Tauchnitz, Leipzig, 1199 pp.

Peterek, A., Schunk, R. & Zapf, H. (2009): Geologie und Landschaftsgeschichte in der Umrahmung der Craimoosweihers. *Berichte der Naturwissenschaftlichen Gesellschaft Bayreuth*, 26, pp. 63 – 76.

Pigati, J.S., Quade, J., Shahanan, T.M. & Haynes, C. (2004): Radiocarbon dating of minute gastropods and new constraints on the timing of late Quaternary spring-discharge deposits in southern Arizona, USA. *Palaeogeography, Palaeoclimatology, Palaeoecology*, 204 (1), pp. 33 – 45.

Pigati, J.S., Rech, J.A. & Nekola, J.C. (2010): Radiocarbon dating of small terrestrial gastropod shells in North America. *Quaternary Geochronology*, 5 (5), pp. 519 – 532.

Piégay, H., Kondolf, G.M., Minear, J.T. & Vaudor, L. (2015): Trends in publications in fluvial geomorphology over two decades: A truly new era in the discipline owing to recent technological revolution? *Geomorphology*, 248 (Supplement C), pp. 489 – 500.

Poolton, N., Bøtter-Jensen, L. & Johnsen, O. (1995): Thermo-optical properties of optically stimulated luminescence in feldspars. *Radiation Measurements*, 24 (4), pp. 531 – 534.

Poolton, N., Bøtter-Jensen, L., Ypma, P. & Johnsen, O. (1994): Influence of crystal structure on the optically stimulated luminescence properties of feldspars. *Radiation Measurements*, 23 (2), pp. 551 – 554.

Poolton, N.R.J., Ozanyan, K.B., Wallinga, J., Murray, A.S. & Bøtter-Jensen, L. (2002a): Electrons in feldspar II: a consideration of the influence of conduction band-tail states on luminescence processes. *Physics and Chemistry of Minerals*, 29 (3), pp. 217–225.

Poolton, N.R.J., Wallinga, J., Murray, A.S., Bulur, E. & Bøtter-Jensen, L. (2002b): Electrons in feldspar I: on the wavefunction of electrons trapped at simple lattice defects. *Physics and Chemistry of Minerals*, 29 (3), pp. 210–216.

Porat, N., Faerstein, G., Medialdea, A. & Murray, A.S. (2015): Re-examination of common extraction and purification methods of quartz and feldspar for luminescence dating. *Ancient TL*, 33, pp. 22 – 30.

Prescott, J. & Hutton, J. (1988): Cosmic ray and gamma ray dosimetry for TL and ESR. *International Journal of Radiation Applications and Instrumentation. Part D. Nuclear Tracks and Radiation Measurements*, 14 (1), pp. 223 – 227.

Prescott, J. & Hutton, J. (1994): Cosmic ray contributions to dose rates for luminescence and ESR dating: Large depths and long-term time variations. *Radiation Measurements*, 23 (2), pp. 497 – 500.

Preusser, F., Chithambo, M.L., Götte, T., Martini, M., Ramseyer, K., Sendezera, E.J., Susino, G.J. & Wintle, A.G. (2009): Quartz as a natural luminescence dosimeter. *Earth-Science Reviews*, 97 (1), pp. 184 – 214.

Preusser, F., Degering, D., Fuchs, M., Hilgers, A., Kadereit, A., Klasen, N., Krbetschek, M., Richter, D. & Spencer, J.Q. (2008): Luminescence dating: basics, methods and applications. *Quaternary Science Journal (Eiszeitalter und Gegenwart)*, 57 (1-2), pp. 95 – 149.

Preusser, F., May, J.H., Eschbach, D., Trauerstein, M. & Schmitt, L. (2016): Infrared stimulated luminescence dating of 19th century fluvial deposits from the upper Rhine River. *Geochronometria*, 43 (1), pp. 131 – 142.

Preusser, F., Muru, M. & Rosentau, A. (2014): Comparing different post-IR IRSL approaches for the dating of Holocene coastal foredunes from Ruhnu Island, Estonia. *Geochronometria*, 41 (4), pp. 342 – 351.

Preusser, F., Ramseyer, K. & Schlüchter, C. (2006): Characterisation of low OSL intensity quartz from the New Zealand Alps. *Radiation Measurements*, 41 (7), pp. 871 – 877.

Preusser, F., Schmitt, L., Delile, H. & Grosprêtre, L. (2011): Optically Stimulated Luminescence (OSL) dating of the sedimentation history of the Yzeron Basin (Chaudanne sub-catchment), Rhône Valley, France. *Quaternaire*, 22 (1), pp. 73 – 83.

Prinz, H. & Strauss, R. (2011): *Ingenieurgeologie*. Spektrum Akademischer Verlag, Heidelberg, 738 pp.

Puisségur, J.J. (1976): Mollusques continentaux quaternaires de Bourgogne. Significations stratigraphiques et climatiques. Rapports avec d'autres faunes boréales de France. In: *Mémoires géologiques de l'Université de Dijon*, volume 3. pp. 1 – 241.

Rades, E.F., Fiebig, M. & Lüthgens, C. (2016): Luminescence dating of the Rissian type section in southern Germany as a base for correlation. *Quaternary International*.

Reck, H. (1912): Die morphologische Entwicklung der süddeutschen Schichtstufenlandschaft im Lichte der Davis'schen Cyclustheorie. *Zeitschrift der Deutschen Geologischen Gesellschaft*, 64, pp. 81 – 232.

Reimann, T., Thomsen, K.J., Jain, M., Murray, A.S. & Frechen, M. (2012): Single-grain dating of young sediments using the pIRIR signal from feldspar. *Quaternary Geochronology*, 11 (Supplement C), pp. 28 – 41.

Reimann, T. & Tsukamoto, S. (2012): Dating the recent past (<500 years) by post-IR IRSL feldspar – Examples from the North Sea and Baltic Sea coast. *Quaternary Geochronology*, 10 (Supplement C), pp. 180 – 187.

Reimann, T., Tsukamoto, S., Naumann, M. & Frechen, M. (2011): The potential of using K-rich feldspars for optical dating of young coastal sediments – A test case from Darss-Zingst peninsula (southern Baltic Sea coast). *Quaternary Geochronology*, 6 (2), pp. 207 – 222.

Reimer, P., Baillie, M., Bard, E., Bayliss, A., Beck, J., Blackwell, P., Ramsey, C.B., Buck, C., Burr, G., Edwards, R., Friedrich, M., Grootes, P., Guilderson, T., Hajdas, I., Heaton, T., Hogg, A., Hughen, K., Kaiser, K., Kromer, B., McCormac, F., Manning, S., Reimer, R., Richards, D., Southon, J., Talamo, S., Turney, C., van der Plicht, J. & Weyhenmeyer, C. (2009): IntCal09 and Marine09 Radiocarbon Age Calibration Curves, 0-50,000 Years cal BP. *Radiocarbon*, 51 (4), pp. 1111 – 1150.

Reimer, P.J. (2012): Refining the Radiocarbon Time Scale. *Science*, 338 (6105), pp. 337–338.

Rhodes, E. (2000): Observations of thermal transfer OSL signals in glacigenic quartz. *Radiation Measurements*, 32 (5), pp. 595 – 602.

Rhodes, E. & Bailey, R. (1997): The effect of thermal transfer on the zeroing of the luminescence of quartz from recent glaciofluvial sediments. *Quaternary Science Reviews*, 16 (3), pp. 291 – 298.

Rittenour, T.M. (2008): Luminescence dating of fluvial deposits: applications to geomorphic, palaeoseismic and archaeological research. *Boreas*, 37 (4), pp. 613–635.

Rixhon, G., Braucher, R., Bourlès, D., Siame, L., Bovy, B. & Demoulin, A. (2011): Quaternary river incision in NE Ardennes (Belgium)–Insights from 10Be/26Al dating of river terraces. *Quaternary Geochronology*, 6 (2), pp. 273 – 284.

Roberts, H.M. (2008): The development and application of luminescence dating to loess deposits: a perspective on the past, present and future. *Boreas*, 37 (4), pp. 483–507.

Roberts, H.M. (2012): Testing Post-IR IRSL protocols for minimising fading in feldspars, using Alaskan loess with independent chronological control. *Radiation Measurements*, 47 (9), pp. 716 – 724.

Rodnight, H., Duller, G., Wintle, A. & Tooth, S. (2006): Assessing the reproducibility and accuracy of optical dating of fluvial deposits. *Quaternary Geochronology*, 1 (2), pp. 109 – 120.

Roskosch, J., Tsukamoto, S. & Frechen, M. (2015): Luminescence Dating of Fluvial Deposits from the Weser Valley, Germany. *Geochronometria*, 42 (1), pp. 126 – 138.

Rousseau, D.D. (1987): Paleoclimatology of the Achenheim series (middle and upper pleistocene, Alsace, France) A. malacological analysis. *Palaeogeography, Palaeoclimatology, Palaeoecology*, 59 (Supplement C), pp. 293 – 314.

Rémillard, A., Buylaert, J.P., Murray, A., St-Onge, G., Bernatchez, P. & Hétu, B. (2015): Quartz OSL dating of late Holocene beach ridges from the Magdalen Islands (Quebec, Canada). *Quaternary Geochronology*, 30 (Part B), pp. 264 – 269.

Schatz, A.K., Buylaert, J.P., Murray, A., Stevens, T. & Scholten, T. (2012): Establishing a luminescence chronology for a palaeosol-loess profile at Tokaj (Hungary): A comparison of quartz OSL and polymineral IRSL signals. *Quaternary Geochronology*, 10 (Supplement C), pp. 68 – 74.

Scheffer, F., Blume, H.P., Brümmer, G., Horn, R., Kandeler, E., Kögel-Knabner, I., Kretzschmar, R., Stahr, K., Wilke, B.M., Thiele-Bruhn, S. & Welp, G. (2011): *Lehrbuch der Bodenkunde*. Spektrum Akademischer Verlag, Heidelberg, 569 pp.

Schirmer, W. (1983): Die Talentwicklung an Main und Regnitz seit dem Hochwürm. *Geologisches Jahrbuch*, A71, pp. 11 – 43.

References

Schirmer, W. (1984): Moenodanuvius – ein uralter Fluß auf der Frankenalp. *Hollfelder Blätter*, 9 (2), pp. 29 – 32.

Schirmer, W. (2007): Geschichte und Bau des Maintals am Beispiel des Obermains. *Bayreuther Geographische Arbeiten*, 28, pp. 102 – 119.

Schirmer, W. (2010): Die Geschichte von Moenodanuvius und Main in Oberfranken. In: G. Dippold (Editor), *Streifzüge durch Franken. Band 1*. Colloquium Historicum Wirsbergense, Lichtenfels, pp. 9 – 24.

Schirmer, W. (2012): River history of the Upper Main River area from Tertiary to Holocene. In: L. Zöller & A. Peterek (Editors), *From Paleozoic to Quaternary. A field trip from the Franconian Alb to Bohemia*, DEUQUA Excursions. Geozon Science Media, Greifswald, pp. 25 – 42.

Schirmer, W. (2014): Moenodanuvius – Flussweg quer durch Franken. *Natur und Mensch*, Jahresmitteilungen 2013 der Naturhistorischen Gesellschaft Nürnberg, pp. 89 – 146.

Schirmer, W., Bos, J., Dambeck, D., Hinderer, M., Preston, N., Schulte, A., Schwalb, A. & Wessels, M. (2005): Holocene fluviatile processes and valley history in the River Rhine catchment. In: J. Herget & R. Dikau (Editors), *Natural and Human Impacts in the River Rhine Catchment*. Bonn, pp. 199 – 215.

Schmidt, C. (2013): *Luminescence dating of heated silex - Potential to improve accuracy and precision and application to Paleolithic sites*. Ph.D. thesis, Universität zu Köln, Köln.

Schoorl, J. & Veldkamp, A. (2003): Late Cenozoic landscape development and its tectonic implications for the Guadalhorce valley near Álora (Southern Spain). *Geomorphology*, 50 (1), pp. 43 – 57.

Schulte, L., Julià, R., Burjachs, F. & Hilgers, A. (2008): Middle Pleistocene to Holocene geochronology of the River Aguas terrace sequence (Iberian Peninsula): Fluvial response to Mediterranean environmental change. *Geomorphology*, 98 (1), pp. 13 – 33.

Seefeldner, E. (1914): *Morphogenetische Studien aus dem Gebiete des Fränkischen Jura*. Forschungen zur deutschen Landes- und Volkskunde 21,3. Engelhorns Nachf., Stuttgart, 77 pp.

Smith, B., Wheeler, G., Rhodes, E. & Spooner, N. (1991): Luminescence dating of zircon using an imaging photon detector. *International Journal of Radiation Applications and Instrumentation. Part D. Nuclear Tracks and Radiation Measurements*, 18 (1), pp. 273 – 278.

Sohbati, R., Murray, A.S., Buylaert, J.P., Ortuño, M., Cunha, P.P. & Masana, E. (2012): Luminescence dating of Pleistocene alluvial sediments affected by the Alhama de Murcia fault (eastern Betics, Spain) – a comparison between OSL, IRSL and post-IRIRSL ages. *Boreas*, 41 (2), pp. 250–262.

Spooner, N. (1992): Optical dating: Preliminary results on the anomalous fading of luminescence from feldspars. *Quaternary Science Reviews*, 11 (1), pp. 139 – 145.

Spooner, N. (1994a): The anomalous fading of infrared-stimulated luminescence from feldspars. *Radiation Measurements*, 23 (2), pp. 625 – 632.

Spooner, N. (1994b): On the optical dating signal from quartz. *Radiation Measurements*, 23 (2), pp. 593 – 600.

Stadelmann, W. (1924): *Das obermainische Schollenland: eine morphogenetische Studie*. Ph.D. thesis, Ludwigs-Maximilians-Universität München, Munich.

Steffen, D., Preusser, F. & Schlunegger, F. (2009): OSL quartz age underestimation due to unstable signal components. *Quaternary Geochronology*, 4 (5), pp. 353 – 362.

Steinlein, H. (1938): *Das Bundsandsteingebiet zwischen Kulmbach und Bayreuth*. Abhandlungen der Preußischen Geologischen Landesanstalt – Neue Folge, Heft 180. Preußische Geologische Landesanstalt, Berlin, 90 pp.

Stevens, T., Marković, S.B., Zech, M., Hambach, U. & Sümegi, P. (2011): Dust deposition and climate in the Carpathian Basin over an independently dated last glacial–interglacial cycle. *Quaternary Science Reviews*, 30 (5), pp. 662 – 681.

Stokes, S. (1994): The timing of OSL sensitivity changes in a natural quartz. *Radiation Measurements*, 23 (2), pp. 601 – 605.

Stokes, S., Bray, H. & Blum, M. (2001): Optical resetting in large drainage basins: tests of zeroing assumptions using single-aliquot procedures. *Quaternary Science Reviews*, 20 (5), pp. 879 – 885.

Strebler, D. (2013): *Use of Minerals other than Quartz and Feldspars for Luminescence Dating*. Msc thesis, University of Oxford.

Syers, J., Chapman, S., Jackson, M., Rex, R. & Clayton, R. (1968): Quartz isolation from rocks, sediments and soils for determination of oxygen isotopes composition. *Geochimica et Cosmochimica Acta*, 32 (9), pp. 1022 – 1025.

Thiel, C. (2011): *On the applicability of post-IR IRSL dating to different environments*. Ph.D. thesis, Freie Universität Berlin, Berlin.

Thiel, C., Buylaert, J.P., Murray, A., Terhorst, B., Hofer, I., Tsukamoto, S. & Frechen, M. (2011a): Luminescence dating of the Stratzing loess profile (Austria) – Testing the potential of an elevated temperature post-IR IRSL protocol. *Quaternary International*, 234 (1), pp. 23 – 31.

Thiel, C., Buylaert, J.P., Murray, A. & Tsukamoto, S. (2011b): On the applicability of post-IR IRSL dating to Japanese loess. *Geochronometria*, 38 (4), pp. 369 – 378.

Thomsen, K., Murray, A., Jain, M. & Bøtter-Jensen, L. (2008): Laboratory fading rates of various luminescence signals from feldspar-rich sediment extracts. *Radiation Measurements*, 43 (9), pp. 1474 – 1486.

Thomsen, K.J., Murray, A., Jain, M. & Buylaert, J.P. (2012): Re 'Luminescence dating of K-feldspar from sediments: a protocol without anomalous fading correction' by Bo Li and Sheng-Hua Li. *Quaternary Geochronology*, 8 (Supplement C), pp. 46 – 48.

Tillmanns, W. (1980): Zur plio-pleistozänen Flußgeschichte von Donau und Main in Nordostbayern. *Jahresberichte und Mitteilungen des oberrheinischen geologischen Vereins, N. F.*, 62, pp. 199 – 205.

Timar-Gabor, A. & Wintle, A. (2013): On natural and laboratory generated dose response curves for quartz of different grain sizes from Romanian loess. *Quaternary Geochronology*, 18, pp. 34 – 40.

Trauerstein, M., Lowick, S.E., Preusser, F. & Schlunegger, F. (2014): Small aliquot and single grain IRSL and post-IR IRSL dating of fluvial and alluvial sediments from the Pativilca valley, Peru. *Quaternary Geochronology*, 22 (Supplement C), pp. 163 – 174.

Trauerstein, M., Lowick, S.E., Preusser, F. & Veit, H. (2017): Testing the suitability of dim sedimentary quartz from northern Switzerland for OSL burial dose estimation. *Geochronometria*, 44, pp. 66 – 76.

Trautmann, T., Krbetschek, M., Dietrich, A. & Stolz, W. (1998): Investigations of feldspar radioluminescence: potential for a new dating technique. *Radiation Measurements*, 29 (3), pp. 421 – 425.

Trautmann, T., Krbetschek, M., Dietrich, A. & Stolz, W. (2000): The basic principle of radioluminescence dating and a localized transition model. *Radiation Measurements*, 32 (5), pp. 487 – 492.

Tsukamoto, S., Denby, P., Murray, A. & Bøtter-Jensen, L. (2006): Time-resolved luminescence from feldspars: New insight into fading. *Radiation Measurements*, 41 (7), pp. 790 – 795.

Urban, T. (2013): *Qualitative Schotteranalysen quartärer Ablagerungen im Lindauer Kessel*. B.Sc. thesis (unpublished), Univ.Bayreuth.

van Es, H., den Hartog, H., de Meijer, R., Venema, L., Donoghue, J. & Rozendaal, A. (2000): Assessment of the suitability of zircons for thermoluminescence dating. *Radiation Measurements*, 32 (5), pp. 819 – 823.

van Gorp, W., Veldkamp, A., Temme, A., Maddy, D., Demir, T., van der Schriek, T., Reimann, T., Wallinga, J., Wijbrans, J. & Schoorl, J. (2013): Fluvial response to Holocene volcanic damming and breaching in the Gediz and Geren rivers, western Turkey. *Geomorphology*, 201 (Supplement C), pp. 430 – 448.

Vandenberghe, J. (1995): Timescales, climate and river development. *Quaternary Science Reviews*, 14 (6), pp. 631 – 638.

Vandenberghe, J. (2002): The relation between climate and river processes, landforms and deposits during the Quaternary. *Quaternary International*, 91 (1), pp. 17 – 23.

Vandenberghe, J. (2003): Climate forcing of fluvial system development: an evolution of ideas. *Quaternary Science Reviews*, 22 (20), pp. 2053 – 2060.

Vandenberghe, J. (2008): The fluvial cycle at cold–warm–cold transitions in lowland regions: A refinement of theory. *Geomorphology*, 98 (3), pp. 275 – 284.

Vandenberghe, J. (2015): River terraces as a response to climatic forcing: Formation processes, sedimentary characteristics and sites for human occupation. *Quaternary International*, 370 (Supplement C), pp. 3 – 11.

Veit, H. (1991): Das Bindlacher Schotterfeld und seine Deckschichten. Ein Beitrag zur Quartärstratigraphie in Oberfranken. *Geologische Blätter NO-Bayern*, 41, pp. 1 – 14.

Verstraeten, G., Lang, A. & Houben, P. (2009): Human impact on sediment dynamics — quantification and timing. *CATENA*, 77 (2), pp. 77 – 80.

Visocekas, R. (1985): Tunnelling radiative recombination in labradorite: Its association with anomalous fading of thermoluminescence. *Nuclear Tracks and Radiation Measurements (1982)*, 10 (4), pp. 521 – 529.

Visocekas, R., Spooner, N., Zink, A. & Blanc, P. (1994): Tunnel afterglow, fading and infrared emission in thermoluminescence of feldspars. *Radiation Measurements*, 23 (2), pp. 377 – 385.

Viveen, W., Schoorl, J., Veldkamp, A., van Balen, R., Desprat, S. & Vidal-Romani, J. (2013): Reconstructing the interacting effects of base level, climate, and tectonic uplift in the lower Miño River terrace record: A gradient modelling evaluation. *Geomorphology*, 186 (Supplement C), pp. 96 – 118.

Wagner, G. (1998): *Age Determination of Young Rocks and Artifacts. Physical and Chemical Clocks in Quaternary Geology and Archaeology*. Springer, Berlin & Heidelberg, 466 pp.

Wagner, G.A., Krbetschek, M., Degering, D., Bahain, J.J., Shao, Q., Falguères, C., Voinchet, P., Dolo, J.M., Garcia, T. & Rightmire, G.P. (2010): Radiometric dating of the type-site for Homo heidelbergensis at Mauer, Germany. *Proceedings of the National Academy of Sciences*, 107 (46), pp. 19726–19730.

Walker, M. (2005): *Quaternary dating methods*. Wiley, Chichester, 286 pp.

Wallinga, J. (2002): Optically stimulated luminescence dating of fluvial deposits: a review. *Boreas*, 31 (4), pp. 303–322.

Wallinga, J., Bos, A.J., Dorenbos, P., Murray, A.S. & Schokker, J. (2007): A test case for anomalous fading correction in IRSL dating. *Quaternary Geochronology*, 2 (1), pp. 216 – 221.

Wallinga, J., Hobo, N., Cunningham, A.C., Versendaal, A.J., Makaske, B. & Middelkoop, H. (2010): Sedimentation rates on embanked floodplains determined through quartz optical dating. *Quaternary Geochronology*, 5 (2), pp. 170 – 175.

Wallinga, J., Murray, A. & Wintle, A. (2000): The single-aliquot regenerative-dose (SAR) protocol applied to coarse-grain feldspar. *Radiation Measurements*, 32 (5), pp. 529 – 533.

Wallinga, J., S. Murray, A. & Bøtter-Jensen, L. (2002): Measurement of the Dose in Quartz in the Presence of Feldspar Contamination. *Radiation Protection Dosimetry*, 101 (1-4), pp. 367–370.

Wenske, D., Frechen, M., Böse, M., Reimann, T., Tseng, C.H. & Hoelzmann, P. (2012): Late Quaternary river terraces in the Central Mountain Range of Taiwan: A study of cover sediments across a terrace section along the Tachia River. *Quaternary International*, 263 (Supplement C), pp. 26 – 36.

Westaway, R., Bridgland, D.R., Sinha, R. & Demir, T. (2009): Fluvial sequences as evidence for landscape and climatic evolution in the Late Cenozoic: A synthesis of data from IGCP 518. *Global and Planetary Change*, 68 (4), pp. 237 – 253.

Wikimedia Commons (2016): File:Alpha Decay.svg – Wikimedia Commons, the free media repository. https://commons.wikimedia.org/w/index.php?title=File:Alpha_Decay.svg&oldid=215592965 [Online; accessed 20-November-2017].

Wikimedia Commons (2017a): File:Beta-minus Decay.svg — Wikimedia Commons, the free media repository. https://commons.wikimedia.org/w/index.php?title=File:Beta-minus_Decay.svg&oldid=268273522 [Online; accessed 20-November-2017].

Wikimedia Commons (2017b): File:Gamma Decay.svg – Wikimedia Commons, the free media repository. https://commons.wikimedia.org/w/index.php?title=File:Gamma_Decay.svg&oldid=262321665 [Online; accessed 20-November-2017].

Wintle, A. (1973): Anomalous Fading of Thermo-luminescence in Mineral Samples. *Nature*, 245, pp. 143 – 144.

Wintle, A. & Murray, A. (2006): A review of quartz optically stimulated luminescence characteristics and their relevance in single-aliquot regeneration dating protocols. *Radiation Measurements*, 41 (4), pp. 369 – 391.

Wintle, A.G. (1997): Luminescence dating: laboratory procedures and protocols. *Radiation Measurements*, 27 (5), pp. 769 – 817.

Wolf, D., Seim, A. & Faust, D. (2014): Fluvial system response to external forcing and human impact – Late Pleistocene and Holocene fluvial dynamics of the lower Guadalete River in western Andalucía (Spain). *Boreas*, 43 (2), pp. 422–449.

Yukihara, E. & McKeever, S. (2011): *Optically stimulated luminescence – Fundamentals and applications*. Wiley, Chichester, 362 pp.

Zhao, H. & Li, S.H. (2002): Luminescence Isochron Dating: A New Approach with Different Grain Sizes. *Radiation Protection Dosimetry*, 101 (1-4), pp. 333–338.

Zimmerman, J. (1971): The radiation-induced increase of the 100 C thermoluminescence sensitivity of fired quartz. *Journal of Physics C: Solid State Physics*, 4 (18), pp. 3265 – 3276.

Zöller, L., Hambach, U., Kleber, A., Kolb, T. & Moine, O. (2012a): Quaternary valley and slope development in the headwaters of the River Main, Upper Franconia – puzzling ancient stream courses and sedimentary archives. In: D. Sauer (Editor), *From the northern ice shield to the Alpine glaciations: a quaternary field trip through Germany*, DEUQUA Excursions. Geozon Science Media, Greifswald, pp. 47 – 65.

Zöller, L., Hambach, U., Kolb, T., Moine, O. & Kühn, P. (2012b): Landscape development in the Trebgast Valley north of Bayreuth and its surroundings (Upper Franconia): ongoing research. In: L. Zöller & A. Peterek (Editors), *From Paleozoic to Quaternary: a field trip from the Franconian Alb to Bohemia*, DEUQUA Excursions. Geozon Science Media, Greifswald, pp. 6 – 24.

Zöller, L. & Pernicka, E. (1989): A note on overcounting in alpha-counters and its elimination. *Ancient TL*, 7, pp. 11 – 14.

Zöller, L., Stingl, H. & Kleber, A. (2007): Das Trebgasttal – Tal- und Landschaftsentwicklung nahe der Europäischen Hauptwasserscheide im Raum Bayreuth. *Bayreuther Geographische Arbeiten*, 28, pp. 79 – 101.

Part IV

Appendix

A

Radionuclide conversion factors

The following table presents three commonly applied systems of conversion factors to calculate dose rate components based on radionuclide concentrations. In this table the conversion factors introduced by Adamiec & Aitken (1998), Guérin et al. (2011) and Liritzis et al. (2013b) are depicted as summarized on the `Dose Rate and Age Calculator` (`DRAC`) homepage[1]. For this PhD-thesis only the conversion factors of Guérin et al. (2011) were used, which are depicted in the third column of the table.

[1] https://www.aber.ac.uk/en/dges/research/quaternary/luminescence-research-laboratory/dose-rate-calculator/?show=datatables&datatableid=1.

Table A.1: Radionuclide conversion factors – alpha, beta and gamma dose rate components [Gy ka^{-1}] produced per unit of the parent radionuclide. As summarized on the DRAC-homepage[a], the respective values are given for 1 ppm uranium, 1 ppm thorium, 1 ppm rubidium and 1% potassium.

Dose component	Adamiec & Aitken (1998)	Guérin et al. (2011)	Liritzis et al. (2013b)
U_{α}	2.78 ± 0.011	2.795 ± 0.011	2.793 ± 0.011
Th_{α}	0.732 ± 0.003	0.738 ± 0.003	0.738 ± 0.003
U_{β}	0.146 ± 0.0004	0.146 ± 0.0004	0.146 ± 0.0004
Th_{β}	0.027 ± 0.001	0.028 ± 0.001	0.028 ± 0.001
K_{β}	0.782 ± 0.007	0.798 ± 0.007	0.801 ± 0.007
Rb_{β}	0.00038 ± 8.216E-6	0.00037 ± 8.0E-6	0.00037 ± 8.0E-6
U_{γ}	0.113 ± 0.0002	0.112 ± 0.0002	0.112 ± 0.0002
Th_{γ}	0.048 ± 0.0002	0.048 ± 0.0002	0.048 ± 0.0002
K_{γ}	0.243 ± 0.005	0.249 ± 0.005	0.25 ± 0.005

[a] https://www.aber.ac.uk/en/dges/research/quaternary/luminescence-research-laboratory/dose-rate-calculator/?show=datatables&datatableid=1;
accessed 2017-11-20.

B

Attenuation factors

B.1 Grain size attenuation factors

The following tables contain shortened versions of the attenuation factor datasets for alpha and beta particles provided on the homepage of the `Dose Rate and Age Calculator` (`DRAC`)[1]. These datasets were calculated based on the data published by Brennan et al. (1991) and Brennan (2003). Thereby, Durcan et al. (2015) used smoothed spline functions for data fitting to generate datasets for grain size ranges of 1-1000 µm. The tables are restricted to those grain sizes relevant for this PhD-thesis and contain two different correction factors. The *attenuation factor* 1-Φ(D) is used to correct external doses, while the *absorption factor* Φ(D) is applied to internal doses (Durcan et al., 2015). Thereby, `DRAC` considers attenuation factors from the minimum and maximum grain sizes provided by the user. Based on these values, mean attenuation and absorption factors are calculated which are then applied to the dose rate determination (e.g., Durcan et al., 2015).

[1] https://www.aber.ac.uk/en/dges/research/quaternary/luminescence-research-laboratory/dose-rate-calculator/?show=datatables&datatableid=2; https://www.aber.ac.uk/en/dges/research/quaternary/luminescence-research-laboratory/dose-rate-calculator/?show=datatables&datatableid=3.

Table B.1: Grain size attenuation factors for alpha particles according to Brennan et al. (1991). The table is a shortened version of the dataset on the DRAC-homepage[b], restricted to those grain sizes relevant for this PhD-thesis. Φ(D) = *absorption factor*; 1-Φ(D) = *attenuation factor*.

Grain size (μm)	Uranium		Thorium		Combined	
	Φ(D)	1-Φ(D)	Φ(D)	1-Φ(D)	Φ(D)	1-Φ(D)
...	...	...	...	...	...	...
4	0.083	0.917	0.072	0.928	0.077	0.923
5	0.105	0.895	0.089	0.911	0.097	0.903
6	0.126	0.874	0.106	0.894	0.116	0.884
7	0.148	0.852	0.124	0.876	0.136	0.864
8	0.169	0.831	0.141	0.859	0.155	0.845
9	0.191	0.809	0.159	0.841	0.174	0.826
10	0.212	0.788	0.176	0.824	0.194	0.806
11	0.234	0.766	0.193	0.807	0.213	0.787
...	...	...	...	...	...	...
90	0.840	0.160	0.800	0.200	0.819	0.180
91	0.841	0.159	0.802	0.198	0.821	0.179
92	0.842	0.158	0.804	0.196	0.823	0.177
93	0.844	0.156	0.806	0.194	0.824	0.176
94	0.845	0.155	0.808	0.192	0.826	0.174
95	0.846	0.154	0.810	0.190	0.827	0.172
...	...	...	...	...	...	...
195	0.918	0.082	0.911	0.089	0.914	0.086
196	0.918	0.082	0.911	0.089	0.914	0.085
197	0.919	0.081	0.912	0.088	0.915	0.085
198	0.919	0.081	0.912	0.088	0.915	0.084
199	0.920	0.080	0.913	0.087	0.916	0.084
200	0.920	0.080	0.913	0.087	0.916	0.084
...	...	...	...	...	...	...

[b] https://www.aber.ac.uk/en/dges/research/quaternary/luminescence-research-laboratory/dose-rate-calculator/?show=datatables&datatableid=2; accessed 2017-11-20.

Table B.2: Grain size attenuation factors for beta particles according to Brennan (2003). The table is a shortened version of the dataset on the DRAC-homepage[c], restricted to those grain sizes relevant for this PhD-thesis. Φ(D) = *absorption factor*; 1-Φ(D) = *attenuation factor*.

Grain size (μm)	Uranium		Thorium		Potassium		Combined	
	Φ(D)	1-Φ(D)	Φ(D)	1-Φ(D)	Φ(D)	1-Φ(D)	Φ(D)	1-Φ(D)
...	...	...	...	...	...	...	...	...
4	0.009	0.991	0.011	0.989	0.001	0.999	0.006	0.994
5	0.011	0.989	0.014	0.986	0.002	0.998	0.007	0.993
6	0.013	0.987	0.017	0.983	0.002	0.998	0.009	0.991
7	0.015	0.985	0.019	0.981	0.003	0.997	0.010	0.99
8	0.017	0.983	0.022	0.978	0.003	0.997	0.012	0.988
9	0.019	0.981	0.024	0.976	0.003	0.997	0.013	0.987
10	0.021	0.979	0.026	0.974	0.004	0.996	0.014	0.986
11	0.022	0.978	0.029	0.971	0.004	0.996	0.015	0.985
...	...	...	...	...	...	...	...	...
90	0.09	0.910	0.125	0.875	0.034	0.966	0.072	0.928
91	0.091	0.909	0.126	0.874	0.034	0.966	0.073	0.927
92	0.092	0.908	0.127	0.873	0.034	0.966	0.073	0.927
93	0.092	0.908	0.128	0.872	0.035	0.965	0.074	0.926
94	0.093	0.907	0.129	0.871	0.035	0.965	0.074	0.926
95	0.093	0.907	0.129	0.871	0.035	0.965	0.075	0.925
...	...	...	...	...	...	...	...	...
195	0.148	0.852	0.199	0.801	0.074	0.926	0.125	0.875
196	0.148	0.852	0.199	0.801	0.074	0.926	0.126	0.874
197	0.149	0.851	0.200	0.800	0.075	0.925	0.126	0.874
198	0.149	0.851	0.201	0.799	0.075	0.925	0.127	0.873
199	0.150	0.850	0.201	0.799	0.075	0.925	0.127	0.873
200	0.150	0.850	0.202	0.798	0.076	0.924	0.128	0.872
...	...	...	...	...	...	...	...	...

[c] https://www.aber.ac.uk/en/dges/research/quaternary/luminescence-research-laboratory/dose-rate-calculator/?show=datatables&datatableid=3;
accessed 2017-11-20.

B.2 Etch depth attenuation factors according to Brennan (2003)

The following table shows etch attenuation factors that take into account the change in beta induced dose rates caused by chemical etching. Based on the dataset originally reported by Brennan (2003), the provided values have been recalculated by applying a smoothing spline function (Durcan et al., 2015) and are used in DRAC to further attenuate the $\dot{D}_\beta$.

Table B.3: Etch depth attenuation factors for beta particles according to Brennan (2003). The table is a shortened version of the dataset on the DRAC-homepage[d], restricted to those etch depths relevant for this PhD-thesis. Please note that the etch attenuation factors have been recalculated by Durcan et al. (2015) and are given as *'secondary etch attenuation factors'*. For details see main text of the original publication of Durcan et al. (2015). Φ(D) = *absorption factor*; 1-Φ(D) = *attenuation factor*.

Etch depth (μm)	Uranium		Thorium		Potassium		Combined	
	Φ(D)	1-Φ(D)	Φ(D)	1-Φ(D)	Φ(D)	1-Φ(D)	Φ(D)	1-Φ(D)
...	...	...	...	...	...	...	...	...
10	1.081	0.991	1.083	0.987	1.081	0.997	1.081	0.993
11	1.087	0.990	1.089	0.986	1.088	0.997	1.088	0.992
12	1.093	0.990	1.095	0.985	1.094	0.997	1.094	0.992
13	1.098	0.989	1.101	0.984	1.101	0.996	1.100	0.991
14	1.103	0.989	1.107	0.983	1.107	0.996	1.106	0.991
15	1.108	0.988	1.112	0.983	1.113	0.996	1.111	0.990
16	1.113	0.988	1.117	0.982	1.119	0.996	1.117	0.990
17	1.118	0.987	1.122	0.981	1.125	0.995	1.122	0.990
18	1.122	0.987	1.127	0.980	1.131	0.995	1.127	0.989
19	1.127	0.986	1.131	0.980	1.137	0.995	1.132	0.989
20	1.131	0.986	1.136	0.979	1.142	0.995	1.137	0.988
...	...	...	...	...	...	...	...	...

[d] https://www.aber.ac.uk/en/dges/research/quaternary/luminescence-research-laboratory/dose-rate-calculator/?show=datatables&datatableid=4;
accessed 2017-11-20.

B.3 Water content attenuation factors according to Aitken & Xie (1990)

The following table contains attenuation factors for considering the effect of soil moisture to dose rates as given on the homepage of DRAC[2]. This values were derived from the publication of Aitken & Xie (1990).

Table B.4: Water content attenuation factors.

Dose component	Attenuation factor
Alpha	1.49
Beta	1.25
Gamma	1.14

[2] https://www.aber.ac.uk/en/dges/research/quaternary/luminescence-research-laboratory/dose-rate-calculator/?show=datatables&datatableid=5.

C

Radioactive decay chains

The following diagrams show various radioactive decay processes which are the main source of naturally occurring ionizing radiation either originating from within the mineral grains (internal dose rate) or from the surrounding sediments (external dose rate).

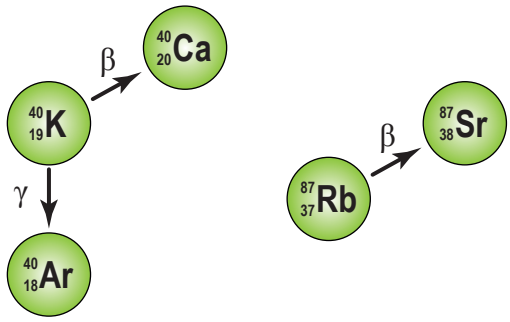

Figure C.1: Radioactive decay schemes of potassium-40 and rubidium-87. While ^{87}Rb is a pure β-emitter, ^{40}K shows two distinct types of radioactive decay. Approximately 89.5% decay to ^{40}Ca by emitting a beta-particle associated by an antineutrino. ~10.5% decay to ^{40}Ar due to an initial electron capture, followed by gamma ray emission (e.g., Aitken, 1985). As the electron capture itself is not associated with a release of energy which could contribute to the accumulation of luminescence signals, only the gamma emission is depicted in the figure.

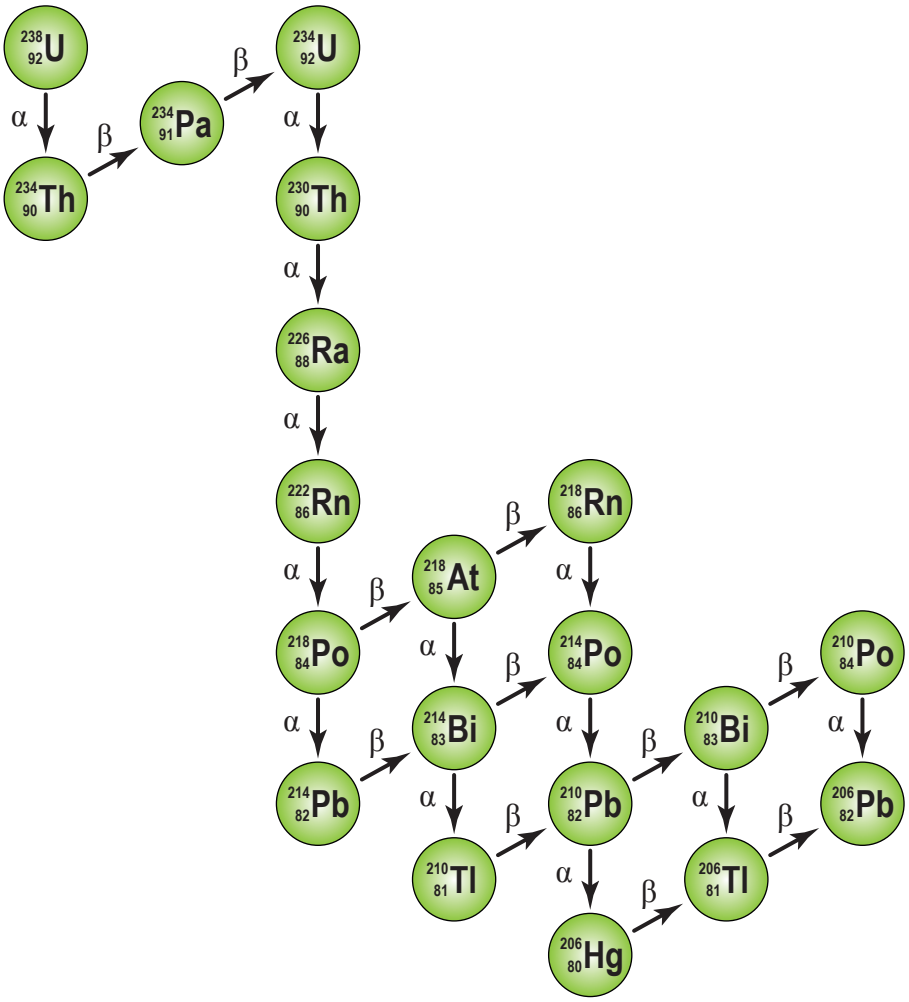

Figure C.2: Decay scheme for the ^{238}U radioactive series. Vertical arrows indicate alpha decays, diagonal arrows represent beta decays.

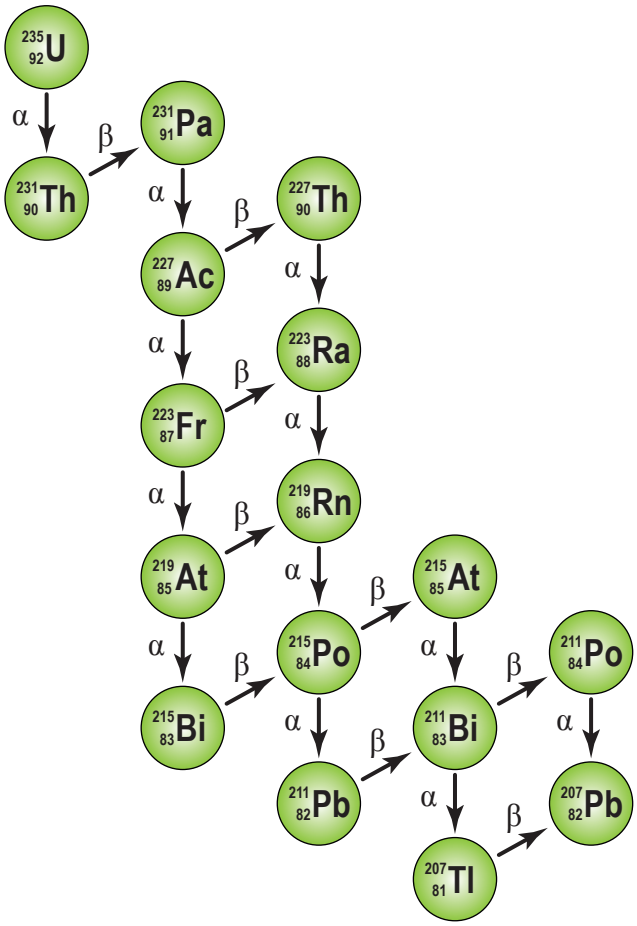

Figure C.3: Decay scheme for the ^{235}U radioactive series. Vertical arrows indicate alpha decays, diagonal arrows represent beta decays.

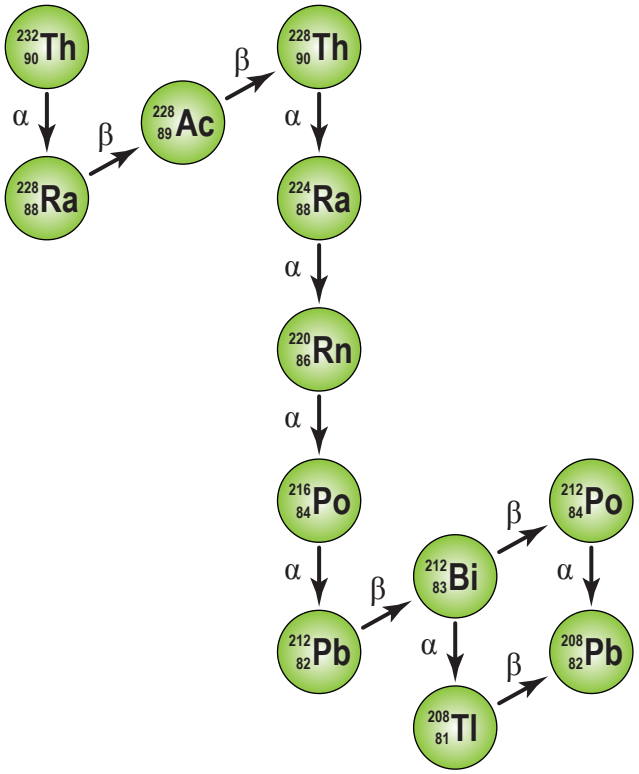

Figure C.4: Decay scheme for the ^{232}Th radioactive series. Vertical arrows indicate alpha decays, diagonal arrows represent beta decays.

D

List of publications and presentations

Only publications and presentations related to the present thesis are listed below.

D.1 Scientific articles

1. Kolb, T. & Fuchs, M. (2018): Luminescence dating of pre-Eemian (MIS 5e) fluvial terraces in Northern Bavaria (Germany) – benefits and limitations of applying a $pIRIR_{225}$-approach. *Geomorphology*, submitted.

2. Kolb, T., Fuchs, M., Moine, O. & Zöller, L. (2017): Quaternary river terraces and hillslope sediments as archives for paleoenvironmental reconstruction: new insights from the headwaters of the Main River, Germany. *Zeitschrift für Geomorphologie, Supplementary Issues*, 61 (1), pp. 53 – 76.

3. Kolb, T., Fuchs, M. & Zöller, L. (2016): Deciphering fluvial landscape evolution by luminescence dating of river terrace formation: a case study from Northern Bavaria, Germany. *Zeitschrift für Geomorphologie, Supplementary Issues*, 60 (1), pp. 29–48.

4. Zöller, L., Hambach, U., Kleber, A., Kolb, T. & Moine, O. (2012a): Quaternary valley and slope development in the headwaters of the River Main, Upper Franconia – puzzling ancient stream courses and sedimentary archives. In: D. Sauer (Editor), *From the northern ice shield to the Alpine glaciations: a quaternary field trip through Germany*, DEUQUA Excursions. Geozon Science Media, Greifswald, pp. 47 – 65.

5. Zöller, L., Hambach, U., Kolb, T., Moine, O. & Kühn, P. (2012b): Landscape development in the Trebgast Valley north of Bayreuth and its surroundings (Upper Franconia): ongoing research. In: L. Zöller & A. Peterek (Editors), *From Paleozoic to Quaternary: a field trip from the Franconian Alb to Bohemia*, DEUQUA Excursions. Geozon Science Media, Greifswald, pp. 6 – 24.

D.2 Conference talks

1. Kolb, T., Fuchs, M. & Zöller, L. (2009): Eine günstige Versuchsanordnung der Natur zur Lumineszenzdatierung hoch- und spätglazialer Hangsedimente im Taltorso des Tregbasttales bei Bayreuth. Conference talk at the annual German Luminescence and ESR Meeting 2009 in Hannover.

2. Kolb, T., Fuchs, M. & Zöller, L. (2012b): Neue Erkenntnisse zur pleistozänen und frühholozänen Entwicklung des Trebgasttales bei Bayreuth. Conference talk at the AK Geomorphologie Annual Conference 2012 in Freising.

3. Kolb, T., Fuchs, M. & Zöller, L. (2013): Die Datierung von Flussterrassen – Neue Befunde zur zeitlichen Entwicklung von Flusslaufverlagerungen: Das Fallbeispiel Trebgasttal bei Bayreuth. Conference talk at the AK Geomorphologie Annual Conference 2013 in Eichstätt.

4. Kolb, T., Fuchs, M. & Zöller, L. (2014a): Die Datierung (prä-)würmzeitlicher Flussterrassen – Neue Befunde zur zeitlichen Entwicklung von Flusslaufverlagerungen: Das Fallbeispiel Trebgasttal bei Bayreuth. Conference talk at the AK Geomorphologie Annual Conference 2014 in Kiel.

5. Kolb, T., Fuchs, M. & Zöller, L. (2014b): The timing of river terrace formation – A case study from the headwaters of the River Main. Conference talk at the annual German Luminescence and ESR Meeting 2014 in Giessen.

6. Kolb, T., Moldenhauer, K.M., Jäger, P., Schmidt, C. & Zöller, L. (2016b): Auensedimente und kolluviale Ablagerungen als Umweltarchive: Versuch einer Landschaftsrekonstruktion für das mittelalterliche Oberfranken. Conference talk at the AK Geomorphologie Annual Conference 2016 in Jena.

D.3 Invited talks

1. Kolb, T., Fuchs, M. & Zöller, L. (2012a): Main oder nicht Main: Das Trebgasttal und seine Entwicklung – Projektvorstellung und erste Ergebnisse. Invited public talk at the Geographical Colloquium of the University of Bayreuth.

2. Kolb, T., Fuchs, M. & Zöller, L. (2015a): Main oder nicht Main – Neue Erkenntnisse zur zeitlichen Stellung von Flusslaufverlagerungen im Nordosten Bayerns. Invited talk at the Geographical Colloquium of the Technische Universität Dresden.

3. Kolb, T., Fuchs, M. & Zöller, L. (2015b): Paläoumweltforschung in Oberfranken – Neue Ergebnisse zur Landschaftsgeschichte des Trebgasttales. Invited public talk at the Colloquium Historicum Wirsbergense.

4. Kolb, T., Fuchs, M. & Zöller, L. (2016a): Vor Prof. Stingls Haustüre: Neueste Ergebnisse zur Landschaftsgeschichte des Trebgasttales. Invited public talk at the Scientific Colloquium on the occasion of Prof. Dr. H. Stingl's 80th birthday celebration.

D.4 Conference posters

1. Kolb, T., Fuchs, M. & Zöller, L. (2012a): Landschafts- und Kulturgeschichte Oberfrankens – Das Trebgasttal und seine Entwicklung. Poster presentation at the AK Geoarchäologie Annual Conference 2012 in Leipzig.

2. Kolb, T., Fuchs, M. & Zöller, L. (2012b): Neue Erkenntnisse zur pleistozänen und frühholozänen Entwicklung des Trebgasttales bei Bayreuth. Poster presentation at the DEUQUA meeting 2012 in Bayreuth.

3. Kolb, T., Fuchs, M. & Zöller, L. (2013a): New evidence for the complexity of river terrace formation in Northern Bavaria. Poster presentation at the annual German Luminescence and ESR Meeting 2013 in Freiberg.

4. Kolb, T., Fuchs, M. & Zöller, L. (2013b): New evidence for the complexity of river terrace formation in Northern Bavaria. Poster presentation at the EGU General Assembly 2013 in Vienna.

5. Kolb, T., Fuchs, M. & Zöller, L. (2014a): The timing of river terrace formation – a case study from the headwaters of the River Main, Northern Bavaria, Germany. Poster presentation at the 14th edition of the Luminescence and Electron Spin Resonance Dating conference (LED) 2014 in Montreal.

6. Kolb, T., Fuchs, M. & Zöller, L. (2014b): The timing of river terrace formation – possibilities and challenges of luminescence dating methods: a case study from Northern Bavaria, Germany. Poster presentation at the EGU General Assembly 2014 in Vienna.

7. Kolb, T., Fuchs, M. & Zöller, L. (2015): Luminescence dating of river terrace formation – methodological challenges and complexity of result interpretation: a case study from the headwaters if the River Main, Germany. Poster presentation at the EGU General Assembly 2015 in Vienna.

E

Declarations – (Eidesstattliche) Versicherungen und Erklärungen gemäß der Promotionsordnung der Fakultät für Biologie, Chemie und Geowissenschaften der Universität Bayreuth in der Fassung vom 15. September 2017

Declarations

The following declarations are required by the examination regulations for achieving the academic degree of Doctor of Natural Sciences (Dr. rer. nat.) of the Faculty of Biology, Chemistry and Geosciences at the University of Bayreuth. By signing these declarations the author confirms that

- he has written this PhD-thesis himself, only using literature sources and other auxiliaries that have clearly been marked in the thesis,
- he has not previously tried to achieve an academic degree by submitting the present thesis,
- he has not taken advantage of commercial promotion consultants or similar service providers nor will ever do so in future.

Furthermore, the author consents to

- the electronic version of this PhD-thesis being subject to a separate review,
- investigations of internal university facilities of scientific self-control if there were any evidence of scientifically inappropriate behaviour.

As the official language of the examination regulations is German, these declarations are written in German.

(Eidesstattliche) Versicherungen und Erklärungen

§ 8 Satz 2 Nr. 3 PromO Fakultät

Hiermit versichere ich eidesstattlich, dass ich die Arbeit selbständig verfasst und keine anderen als die von mir angegebenen Quellen und Hilfsmittel benutzt habe (vgl. Art. 64 Abs. 1 Satz 6 BayHSchG).

§ 8 Satz 2 Nr. 3 PromO Fakultät

Hiermit erkläre ich, dass ich die Dissertation nicht bereits zur Erlangung eines akademischen Grades eingereicht habe und dass ich nicht bereits diese oder eine gleichartige Doktorprüfung endgültig nicht bestanden habe.

§ 8 Satz 2 Nr. 4 PromO Fakultät

Hiermit erkläre ich, dass ich Hilfe von gewerblichen Promotionsberatern bzw. -vermittlern oder ähnlichen Dienstleistern weder bisher in Anspruch genommen habe noch künftig in Anspruch nehmen werde.

§ 8 Satz 2 Nr. 7 PromO Fakultät

Hiermit erkläre ich mein Einverständnis, dass die elektronische Fassung der Dissertation unter Wahrung meiner Urheberrechte und des Datenschutzes einer gesonderten Überprüfung unterzogen werden kann.

§ 8 Satz 2 Nr. 8 PromO Fakultät

Hiermit erkläre ich mein Einverständnis, dass bei Verdacht wissenschaftlichen Fehlverhaltens Ermittlungen durch universitätsinterne Organe der wissenschaftlichen Selbstkontrolle stattfinden können.

Bayreuth, Dezember 2017

Thomas Kolb